Frontispiece. Mottled and variegated alluvial plain red beds of the Aztec Siltstone at A1, units 11 to 14. The massive red siltstone and claystone unit is interpreted as an overbank deposit, and has been overlain by a channel sandstone with an erosional, scoured lower surface. The overbank sediment contains calcareous nodules (kankar), vein networks, and burrows, all of which are interpreted as soil features. Post-depositional reduction has produced the drab mottled and variegated zones, and these relate to the reducing influence of sandstone horizons, these include the overlying channel sandstone and the thin interbeds of sandstone which core the drab horizons that run through the massive red unit.

THE AZTEC SILTSTONE : AN UPPER DEVONIAN ALLUVIAL PLAIN

RED BED SEQUENCE, SOUTHERN VICTORIA LAND, ANTARCTICA

JOHN GORDON McPHERSON

Submitted for the Degree of Doctor of Philosophy

in Geology at the Victoria University of Wellington

October 1975.

THE AZTEC SILTSTONE : AN UPPER DEVONIAN ALLUVIAL PLAIN
RED BED SEQUENCE, SOUTHERN VICTORIA LAND, ANTARCTICA

TABLE CAPTIONS

FIGURE CAPTIONS

ABSTRACT

The Aztec Siltstone (Late Devonian) crops out for 150 km
along the Transantarctic Mountains, between the Mawson and
Mulock Glaciers of southern Victoria Land, Antarctica. It is
the uppermost formation of the Taylor Group, the lower of the
two subdivisions of the Beacon Supergroup of southern Victoria
Land. The formation consists largely of fine to medium-
grained sandstone, and greyish red (1OR 4/2), grey (N5), and
greenish grey (5G 6/1) siltstone and claystone. Other
lithologies include carbonaceous siltstone and claystone,
limestone and intraformational conglomerate. Conchostracans,
fish fossils, plant fragments, and gypsum lenses are present
also.

Cross-stratification, horizontal stratification, channelling,
and "fining-upwards" cycles indicate deposition from shallow,
high sinuosity (tortuous), meandering streams that migrated
laterally across a broad alluvial plain. The sandstone beds
are laterally accreted channel deposits, whereas the siltstone
and claystone beds represent overbank deposition by vertical
accretion in the interchannel areas of the floodbasin. Other
floodbasin deposits include lacustrinal sediments from pluvial
ponds and ox-bow lakes, and palustrinal sediments from the
backswamps. Overbank deposition of bed load material formed
levees, and stream avulsion and crevassing during flood stage
produced crevasse-splay deposits.

The sandstone beds are quartzarenites, with detrital grains
consisting largely of plutonic quartz; other grains include
chert, feldspar, metamorphic quartz and a trace of heavy minerals.
Sandstone textures average fine-grained and well sorted, although
sandstone with textural inversion is common. Compositional and
textural characteristics indicate that the sandstone is a
product of the reworking of older quartzarenite in the source
area.

Subaerial exposure was a feature of the fine-grained
floodbasin sediments; the evidence includes the abundance of

mudcracks, and a variety of soil features. The latter include extensive kankar ('caliche') horizons, pseudo- or wavey bedding structures, a compositional and textural similarity to modern soils, vein networks (considered to be a product of deep cracking in the unconsolidated substratum), burrowing, and root horizons with in some cases associated plant fragments. The kankar ('caliche') suggests that there was a period of prolonged subaerial exposure and soil development which followed the deposition of fine-grained, fine member lithologies of the "fining upwards" cycles. This period was probably in the range 5,000 to 50,000 years.

The Aztec Siltstone is a typical "variegated" red-bed sequence, containing interbedded red and drab fine-grained lithologies. The fine-grained drab lithologies consist of quartz grains set in a matrix of green illitic and chloritic clay. The colour in the interbedded red and grey siltstone and claystone results from a haematite pigment, which in the red samples is present in a concentration sufficient to completely mask the green colour of the clay matrix. The reddening is believed to have been a penecontemporaneous process that took place in the floodbasin sediments during their prolonged subaerial exposure under a hot and seasonally wet and dry (savanna) climate. The haematitic pigment was derived from the *in situ* and progressive dehydration of detrital amorphous and poorly crystalline brown hydrated ferric oxide in those sediments which maintained an oxidizing environment and were above the ground-water table during the dehydration process. Sediments which remained in a water-logged state, below the water table, and in association with organic matter, were invariably reduced and lost their iron oxide in solution. Later post-depositional reduction of some red lithologies produced reduction spheres and channels, reduced burrows and vein networks, and the reduced layers immediately underlying the scoured surface at the base of the channel sandstones. Some chemical redistribution of iron contributed to the variegated and mottled horizons of the formation.

The mineral composition of adjacent red and drab lithologies is essentially the same except for the haematite constituent. The red average 5.86 (σ = 1.09) percent total Fe (as Fe_2O_3), of which 3.01 (σ = 0.63) percent is as haematite pigment, 1.57 percent Fe_2O_3 is in a combined form (probably as ferric silicates), and 1.14 (σ = 0.57) percent is as FeO. The green average 3.65 (σ = 1.81) percent total Fe (as Fe_2O_3) of which approximately 0.27 percent is as haematite pigment, approximately 1.4 percent Fe_2O_3 is in a combined form, and 1.77 (σ = 1.37) percent is as FeO. In the majority of the green lithologies the free ferric oxide (as haematite or hydrated ferric oxide) was removed in solution during reduction, and at the same time minor amounts of clay matrix were also leached out.

ACKNOWLEDGEMENTS

oxygen isotope analyses, and to Mr Raymond Soong of
Geological Survey, D.S.I.R. for the infrared spectro-
photometric analyses.

. Last but by no means least, this study would not
have been possible but for the generosity of my parents
and Mr Cliff K. McPherson.

CHAPTER 1

INTRODUCTION

Regional Setting

Although the total area of the Antarctic Continent above present day sea level is 13,000,000 km^2, only 1 percent of this is exposed rock, the rest being permanently covered by ice to an average depth of 4,000 metres. A large portion of exposed bed-rock lies within a high (exceeding 5,000 m) narrow mountain range, the Transantarctic Mountains. This 3,000 km-long range stretches from the Weddell Sea to northern Victoria Land. In south Victoria Land, all exposed rock except for the Cenozoic volcanic islands is part of the range. The high peaks slope to the west beneath the ice of the South Polar Plateau, and end on the eastern margin with the Ross Sea (Fig. 1.1).

The rocks of the Transantarctic Mountains are similar throughout their length. A Precambrian and Lower Palaeozoic basement is overlain by a thick (up to 3,500 m) flat-lying non-marine clastic sequence, the Beacon Supergroup (Barrett, 1972), from Devonian or older to Jurassic in age. These strata are intruded and overlain by Jurassic Ferrar Group dolerites and volcaniclastics (Fig. 1.2).

The Beacon Supergroup (Ferrar, 1907; Barrett, 1972) in south Victoria Land, the area of this study, consists of up to 2,300 m of flat-lying non-marine clastics of from Devonian or older to Jurassic in age. It has been subdivided into the Taylor and Victoria Groups (Harrington, 1965), the division being at the disconformity produced by the Permo-Carboniferous glaciation (Maya Erosion Surface), (Fig. 1.2). The Taylor Group sediments rest unconformably on the Kukri peneplain (Gunn & Warren, 1962) developed on the Basement Complex of metavolcanic, metasedimentary, and plutonic rocks. They are composed of up to 1,100 m of quartzose sandstone with thin red beds near the base, middle, and top (Fig. 1.2).
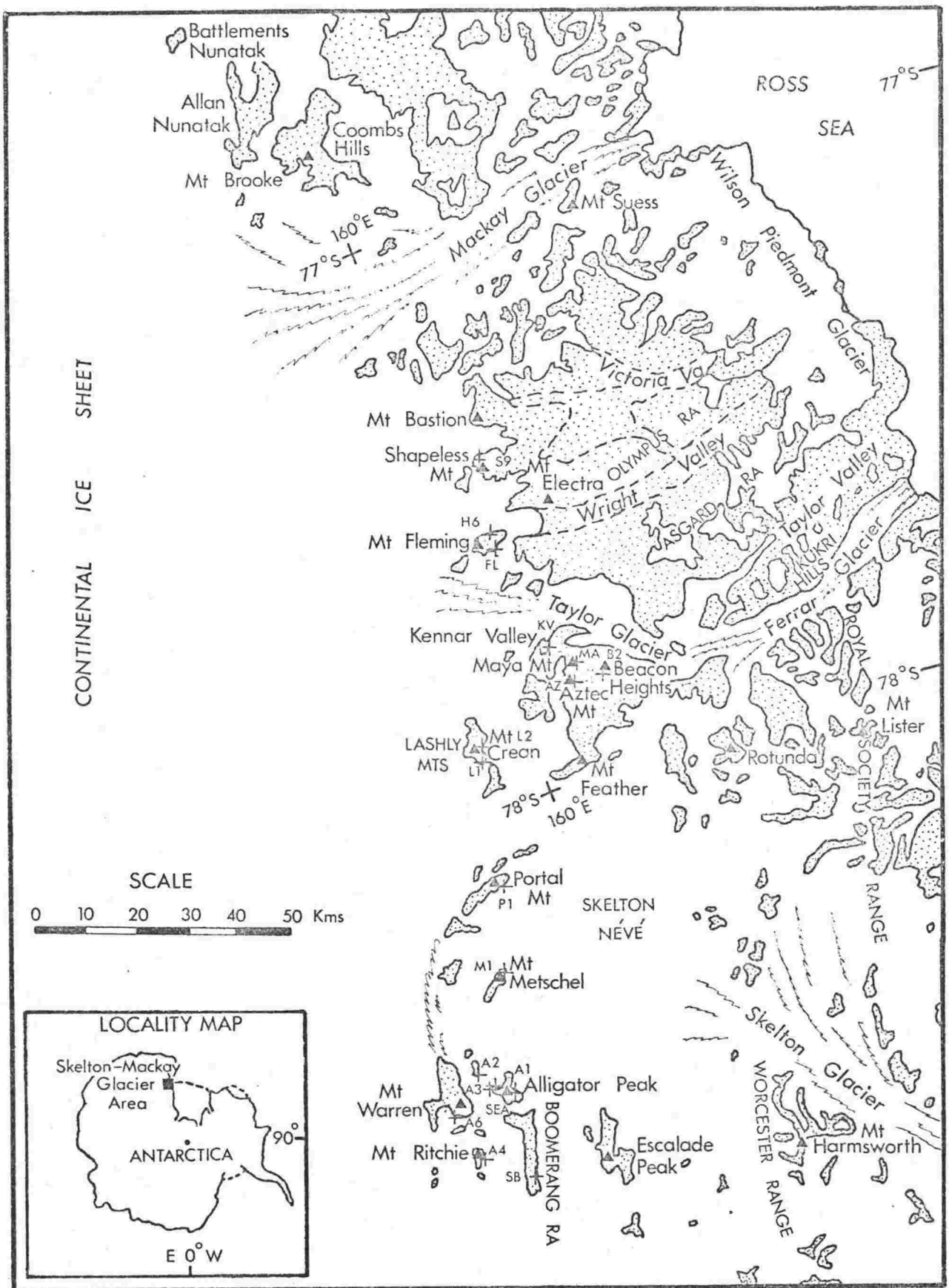
Fig. 1.1.   Map of southern Victoria Land, Antarctica.

Approx. Time in Millions of Years

JURASSIC

180

TRIASSIC

Coal

Dicroidium

230

PERMIAN

Coal & Logs
Glossopteris
Gangamopteris

270 — PYRAMID E.S.

350 — MAYA E.S.

Fish & Soils
Plants & Roots

PREDEVONIAN(?) TO UPPER DEVONIAN

— HEIMDALL E.S.

?440

500 — KUKRI E.S.

P.E. — CAMB.

>600

FERRAR GROUP	Kirkpatrick Basalt (?m)	
	Ferrar Dolerite (?m)	
	Mawson Formation (123 m)	
VICTORIA GROUP	Lashly Formation (520 m)	Member D
		Member C
		Member B
		Member A
	Feather Formation (250 m)	Fleming Member (100 m)
	Weller Coal Measures (254 m)	
	Metschel Tillite (70 m)	
	Aztec Siltstone (217 m)	
TAYLOR GROUP	Beacon Heights Orthoquartzite (350 m)	
	Arena Sandstone (360 m)	
	Altar Mountain Formation (285 m)	Odin Arkose (50 m)
	New Mountain Sandstone (351 m)	Terra Cotta Siltstone (80 m) Boreas Subgreywacke (117 m) Windy Gully Sandstone (48 m)
	Basement Complex	

BEACON SUPERGROUP

METRES
700
500
300
100
0

Legend

Sandstone

Siltstone and Claystone

Basalt and Dolerite

Tillite

Volcaniclastics

Metavolcanic, Metasedimentary, & Plutonic Rocks

Conglomerate

Erosion Surface

Fig. 1.2. Generalized stratigraphic column of the rocks of the Beacon Supergroup of southern Victoria Land, Antarctica.

The Taylor Group sediments are largely unfossiliferous
except for the two uppermost formations, the Beacon Heights
Orthoquartzite, which contains rare *Haplostigma* impressions,
and the Aztec Siltstone, which contains abundant fish remains,
plant leaf and stem impressions,and conchostracans. Hence the
age of the basal formations is speculative. The sequence is
considered to be largely non-marine, at least above the
Heimdall Erosion Surface, and numerous mudcrack horizons
and red beds record subaerial exposure from time to time.
The clastics are thought to have been derived from continental
areas of low relief on both sides of the present Transantarctic
Mountains, and deposited on broad low-lying alluvial plains
(Barrett, 1972; Barrett and Kohn, 1975).

The Victoria Group is a heterogeneous assemblage of rocks
including glacial beds, alluvial plain sediments, and
volcaniclastics, ranging in age of from Early Permian to
Late Triassic (Kyle, 1975) and reaching a maximum thickness
in south Victoria Land of 1,200 m (Fig. 1.2). The formations
contain an abundant micro- and macrofossil flora, and include
coal seams at a number of horizons. The sediments are more
feldspathic, not as well sorted and hence sedimentologically
less mature than those of the underlying Taylor Group. They
are considered to have been eroded from a less mature cratonic
highland to the east in the vicinity of the present Ross Ice
Shelf (Barrett and Kohn, 1975).

The purpose of this study was to determine the palaeogeo-
graphy and environment of deposition of a single formation, the
Aztec Siltstone, within the Beacon Supergroup in south Victoria
Land. The Aztec Siltstone is a flat lying, interbedded sequence
of sandstone, siltstone and claystone, and is a typical red-bed
formation in that the fine-grained sediments are red and green.
It was the aim of the author to interpret from the stratigraphy,
the sedimentation pattern, and the petrography, the types of
processes which were involved in the deposition of the formation,
and the processes and conditions which affected the sediments
after deposition. The origin of the red sediments was of
particular interest in the study.

Field Activities

During the austral summers of 1968-69, 1970-71, 1971-72, and 1973-74, the 13th, 15th, 16th, and 18th expeditions from Victoria University investigated the geology of the Beacon Supergroup, including the Aztec Siltstone, in south Victoria Land, Antarctica. Detailed accounts of the expedition were published in the Immediate Report after each field season (Webb, 1969; Barrett and Kohn, 1971; Askin et al. 1972; Allis et al. 1973; Crump et al. 1974).

Areas visited by the expeditions ranged from the Darwin Mountains in the south, to Allan Nunatak in the north (Fig. 1.1). Air support was provided by the United States Navy, using C-130 Hercules transport aircraft and helicopters; ground travel was by motor toboggan, man-hauling, and walking.

All but the 18th expedition were involved in a geological reconnaissance and regional mapping program in south Victoria Land. Sections of Aztec Siltstone were measured, described, and sampled in considerable detail at the localities shown in Figure 1.1. A 1.5 m long staff and abney level were used for measuring most sections. The information gathered has been published as an Antarctic Data Series (Askin et al. 1971; Barrett and Webb, 1973) and it is from here that all information regarding the sections used in this thesis, is taken. The data on each section includes the names of those who carried out the measurement and description of the section.

Some sections were re-examined during the 18th expedition (Crump et al. 1974) and include Shapeless Mountain (S9), the Lashly Mountains (L1 and L2), Aztec Mountain (AZ-17, 18, 19), Mount Metschel (M1 and M2), and Alligator Peak (A1, A2, and A3). The author spent a total of 5 months in the field as a member of the 15th and 18th expeditions.

Fossil fish remains were collected from many localities in the areas visited during the 15th expedition, by two Australian vertebrate palaeontologists Dr A. Ritchie (Curator of Fossils, Australian Museum, Sydney), and Mr G. C. Young (Curator of Fossils, Bureau of Mineral Resources, Canberra).

Field study in Antarctica is carried out only during the austral summer months (November to February), and has the advantages of 24 hours of daylight and a lack of weathering on outcrops. However, this is somewhat compensated by the low temperatures ($0^{o}C$ to $-20^{o}C$), the widely spaced outcrops, and the remoteness of the area. Only a limited number of the sections were able to be re-visited by the author.

Previous Investigations

The Aztec Siltstone was collected and studied early in the history of geological investigation of Antarctica. This early interest was not petrological, but palaeontological, for the formation contained a rich Devonian fish fossil fauna. Debenham (1921) writes of fossil fish remains from a moraine on the MacKay Glacier, "these occur in pieces of shale and shaly sandstone which are identical in outward appearance with the bands of shale that are found in the lower layers of the Beacon Sandstone. In one case the fish scales are in a finely laminated shale, but generally they are in irregular pieces of rock which has no definite cleavage and contains a good deal of rather coarse sand".

The first report of the formation *in situ* was by McKelvey and Webb (1959) (Table 1.1). They recorded 18.5 m of mixed siltstone (red and green) and sandstone (white and green), approximately 470 m above the base of the Beacon Sandstone at Aztec Mountain in the Beacon Valley. The unit was assigned Member B of the Beacon sediments, and later termed a "red-green siltstone facies" (McKelvey and Webb, 1961). Gunn and Warren (1962) made the first collection of *in situ* fossil fish remains, and extended the known outcrops to the Boomerang Range, the Lashly Mountains, and Mount Feather. A fresh-water environment of deposition was invoked by them on the basis of the fossil fish, after comparison with similar species thought to be fresh water from the Old Red Sandstone of Great Britain. Webb (1963) proposed the name Aztec Siltstone for the sequence

Table 1.1   Previous investigations of the Aztec Siltstone

Worker	Date	Locality	Results of Investigation
Woodward	1921	MacKay Glacier moraines	Fish fossils dating the host as Upper Devonian.
McKelvey & Webb	1959	Beacon Valley	First *in situ* description of the formation.
" "	1961	" "	Proposed the formation as a "red-green siltstone facies" in the Beacon Group sediments. Member B status.
Gunn & Warren	1962	Boomerang Ra., Lashly Mts, Mt Feather	First *in situ* fossil fish remains collected. Fresh water environment of deposition suggested on the basis of the fossil fish being considered non-marine.
Webb	1963	Aztec Mt	Proposed the name Aztec Siltstone and gave a type section on Aztec Mt. Considered as a non-marine and specifically a shallow lacustrine or paludal basin environment of deposition, with some fluviatile sedimentation.
Harrington	1965	Beacon Heights area	Defined the Maya Erosion Surface, and correlated the Aztec Siltstone with fish bearing Witteberg Shales of South Africa, and the Bluff Cove beds of the Falkland Is.
Matz & Hayes	1966	Ferrar Gl.-MacKay Gl.	S.E. to N. palaeocurrent directions.
White	1968	Allan Nunatak-MacKay Gl.	Identified fish and proposed an upper Middle Devonian age.
McElroy	1969	Beacon Heights area	Suggested a shallow water fluviatile and deltaic environment of deposition.
Helby & McElroy	1969	Aztec Mt	Micro-flora gave an Upper Devonian (Frasnian) age compared to the Australian sequence.
Ritchie	1969	Boomerang Ra.-Olympus Ra.	Upper Devonian age based on the fossil fish.
McKelvey et al.	1970a	Boomerang Ra.-Olympus Ra.	Thickest section in the south and thinning to the north.
Matz et al.	1972	Ferrar Gl.-MacKay Gl.	Suggested a shallow marine environment of deposition.

and gave a type locality at Aztec Mountain. He compared the formation to other red bed deposits of the Rocky Mountains region of North America, and concluded "a shallow lacustrine or paludal basin within a large piedmont valley flat" to be the environment of deposition. The sandstones he interpreted as coarse channel detritus from a flood channel within the basin.

The investigations of the formation in the years after 1963 extended the known outcrop localities (Matz and Hayes, 1966; McElroy, 1969; McKelvey *et al.* 1970a), supported an Upper Devonian age (Helby and McElroy, 1969; Ritchie, 1969), and defined the disconformity which truncates the Aztec Siltstone as the glacial Maya Erosion Surface (Harrington, 1965; McKelvey *et al.* 1970a). McElroy (1969) suggested a dominantly shallow water, fluviatile and deltaic system as the depositional environment for the formation, and gave Lake Eyre in Central Australia as a possible modern analogy.

CHAPTER 2

STRATIGRAPHY

Definition

The Aztec Siltstone was defined by Webb (]963) as the red
and green siltstone sequence overlying the Beacon Heights
Orthoquartzite and underlying the Weller Sandstone. The type
section given was Aztec Mountain (77° 47' S : 160° 28' E)
on the west wall of Beacon Valley in the upper Taylor Glacier
region. Subsequent work by McKelvey, Webb, Kohn, and Gorton
in the 1968-69 season showed the formation to be 56 m thick at
the type section on Aztec Mountain (77° 49' S. : 160° 40' E),
conformably overlying the Beacon Heights Orthoquartzite, and
disconformably (Maya Erosion Surface) underlying the Metschel
Tillite (McKelvey *et al*. 1970a).

The formation is a flat lying, interbedded sequence, in
places cyclic, of lenticular channel and sheet sandstone, and
greyish red (10R 4/2), grey (N5), and greenish grey (5G 6/1)
siltstone and claystone (McPherson, 1973). Thickness of beds
is from 10 cm to 15 m. Locally it contains beds of carbonaceous
siltstone and claystone, thin limestone, and intraformational
conglomerates. Conchostracans, fish fossils, plant fragments,
and gypsum lenses are present also. Burrows, desiccation
cracks, kankar ('caliche') deposits, and ripple marks are
common features in the formation.

Distribution and Thickness

The Aztec Siltstone can be traced from the southern part
of the Boomerang Range, 150 km north as far as Shapeless Mountain,
and possibly further to Mount Bastion. The most westerly extent
of the formation is in the vicinity of Mount Ritchie, on the edge
of the Polar Plateau, and the most easterly is at Beacon Heights.
To the north of Mount Bastion the Aztec Siltstone appears to be

completely absent, and the Beacon Heights Orthoquartzite
(Razorback Formation, Mirsky *et al.* 1965; Fortress Sandstone,
Allen, 1962) is overlain disconformably by Permian coal measures.
Nevertheless, sandstone fragments containing fish fossil remains
were recorded in moraine at Mount Suess, in the lower Mackay
Glacier, by Debenham (1921), Gunn and Warren (1962), and the
author. It is probable therefore, that these fragments were
eroded from presently unknown outcrops at the head of the Mackay
Glacier in the vicinity of the North Willett Range.

The formation has not been recognized south of the Mulock
Glacier, although the nearest and most probable localities,
the Cook Mountains and Conway Range, have not yet been explored.
Further south, in the Darwin Mountains, the Darwin Tillite, a
correlative of the Metschel, is in some places, a grey, greyish-
red and greenish-grey siltstone, very similar to the Aztec
Siltstone (Barrett and Kyle, 1975). They suggested that the
red colour is inherited, and results from Permian glacial erosion
of Aztec Siltstone north of the Darwin Mountains.

Recent erosion has removed the Aztec Siltstone east of
Beacon Heights, where the uppermost formation is the Beacon
Heights Orthoquartzite. The removal of younger beds has been
aided by the gentle westerly dip of the Beacon Supergroup along
the east coast of south Victoria Land.

Stratigraphic columns have been draughted to give a
diagrammatic representation of the strata of the formation
(Fig. 2.1). The sections are keyed, where possible, to a single
datum plane, the contact between the Beacon Heights Orthoquartzite
and the Aztec Siltstone. Correlation between sections or beds on
the basis of single persistent units is rare, due to their
lensing and interdigitating character. Palaeontological
correlation, on the basis of the fish fossils, is not possible
because the fish show insufficient evolutionary variation
(G. C. Young pers. comm.). Some correlations have been made
and are shown on the columns (Fig. 2.1) and explained in
Chapter 3, p. 15.

Thicknesses for complete sections vary considerably from
217 m, a maximum at Mount Ritchie, to 42 m, a minimum at Maya

Mountain. A projection of the geographic positions of the
sections onto an approximate north-south line was carried out
so as to be able to compare relative thickness with relative
geographic position (Fig. 2.2). The figure shows an apparent
linear thinning trend for the Aztec Siltstone, from south to north.
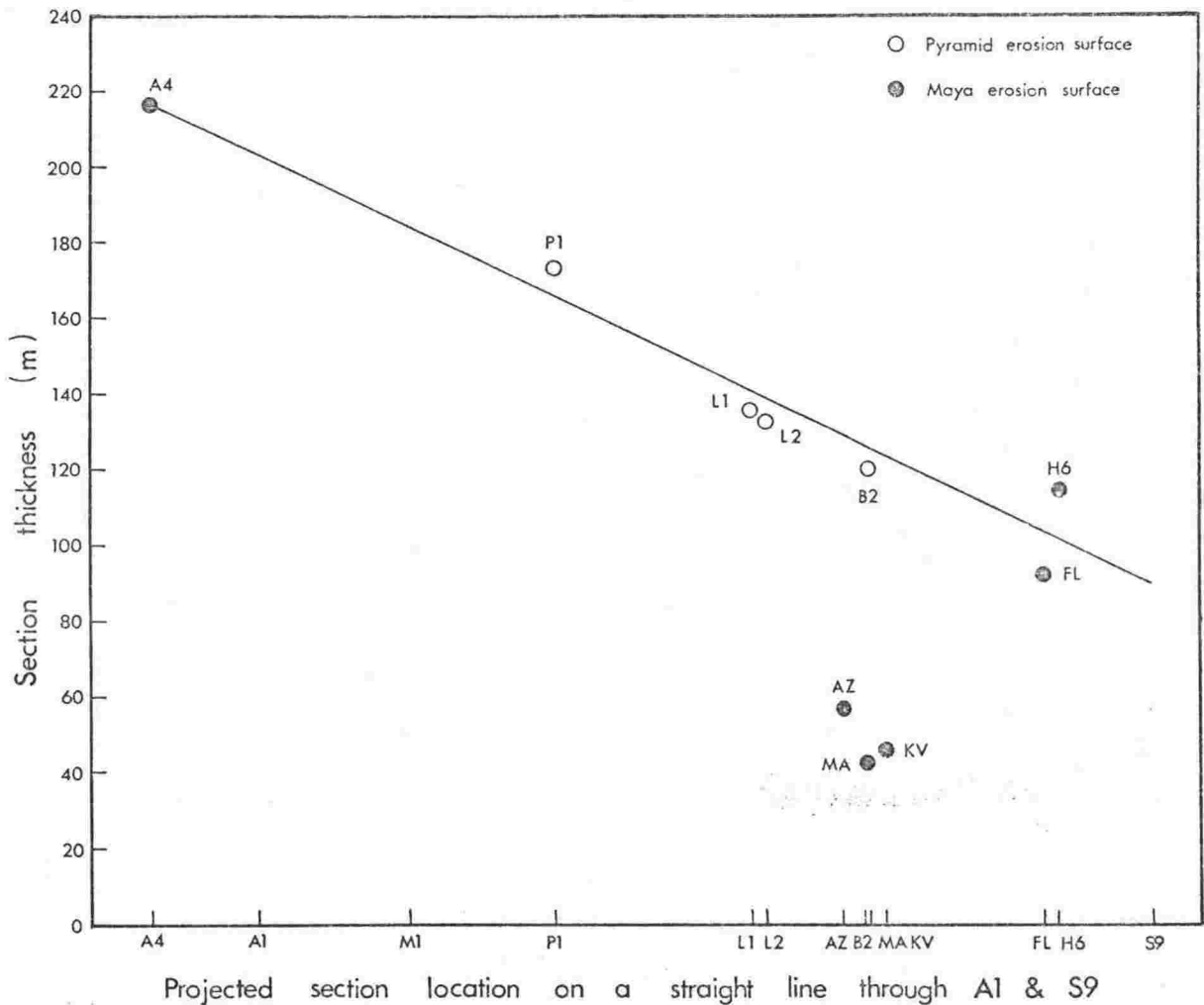
Fig. 2.2 Variations in thickness of Aztec Siltstone in complete
          sections lying on an approximate north-south line.

The thinning may have been a depositional feature, reflecting
the palaeoslope of a basin of deposition for the formation, or

it may be a product of bevelling by the Permo-Carboniferous continental ice sheet, which produced the upper erosional surface of the Aztec Siltstone. If the thinning is a depositional feature then it would be expected that the proportion of fine-grained sediments would increase to the north. However, the trend is the reverse (Fig. 3.12). It is considered most probable that the northeast thinning of the Aztec resulted from bevelling by the Permo-Carboniferous continental ice sheet.

The three sections near Beacon Valley (Aztec Mountain, AZ; Maya Mountain, MA; Kennar Valley, KV) (Fig. 2.1) do not conform to the thinning relationship (Fig. 2.2). They all lie within an 8 km radius and have approximately 70 m of Aztec Siltstone less than expected for a linear thinning trend. This local thinning is attributed to glacial erosion of a local valley within the Aztec Siltstone of the region.

Known outcrops of Aztec Siltstone not included here as measured sections, are at the N.E. Warren Range (Barrett and Webb, 1973), Mount Weller (Webb, 1963), and Mount Feather (Gunn and Warren, 1962). Aztec Siltstone has been reported at Mount Bastion by Barrett and Webb (1973), but this is tentative. The characteristic siltstone units are absent from the section, as are features such as desiccation cracks, burrows, ripple marks, and calcareous nodules.

Nature of Upper and Lower Contacts

The Aztec Siltstone has a conformable lower contact with the Beacon Heights Orthoquartzite, a thick, mature, orthoquartzitic sandstone, readily recognized by its massive bluff or cliff and ledge forming structure. The transition to the Aztec Siltstone is gradational, normally over 5 to 20 m. Thin siltstone and claystone beds and lenses appear (Figs 2.1 and 3.13), becoming thicker and more common upwards, giving rise to slope forming units. There is also an accompanying change in the character of the sandstones. Those of the Beacon Heights Orthoquartzite are generally wholly quartz cemented, whereas those in the Aztec

Siltstone commonly have some clay or calcite matrix or cement (Chapters 5 and 6).

The Metschel Tillite disconformably overlies the Aztec Siltstone where it has not been eroded by the subsequent Pyramid Erosion Surface at the base of the Weller Coal Measures (McKelvey et al. 1970a). In many areas e.g. Aztec Mountain, Mount Fleming, and Maya Mountain, the tillite is preserved only in the hollows of the glacial Maya Erosion Surface. In areas where tillite is absent, i.e. where Weller Coal Measures lie directly on the Aztec Siltstone e.g. at P1, L1, and L2, it is common to find clasts of tillite in recent moraines. It is evident therefore that the Pyramid erosion cycle has removed much or all of the Metschel Tillite, but, due to the low relief of the Maya Erosion Surface (3.7 m, McKelvey et al. 1970a; 1-2 m, Barrett et al. 1971) has nowhere greatly eroded the Aztec Siltstone.

At the localities of Mount Metschel, Shapeless Mountain, and the Lashly Mountains, the basal part of the Metschel Tillite is lithologically similar to the underlying Aztec Siltstone and the contact between the two appears gradational (Fig. 2.3). At Mount Metschel (M1), and the Lashly Mountains (section adjoining L2), the tillite contains beds of greyish red siltstone showing greenish grey reduction zones (Barrett and Kyle, 1975) (Fig. 2.4) very similar to those of the Aztec Siltstone. On close examination of the contact zone between the two formations, the tillite can only be distinguished by the presence of scattered clasts. It is thought that in these cases, the basal units of the Metschel Tillite are eroded products of underlying red Aztec Siltstone lithologies which have undergone a patchy, in situ, postdepositional reduction.
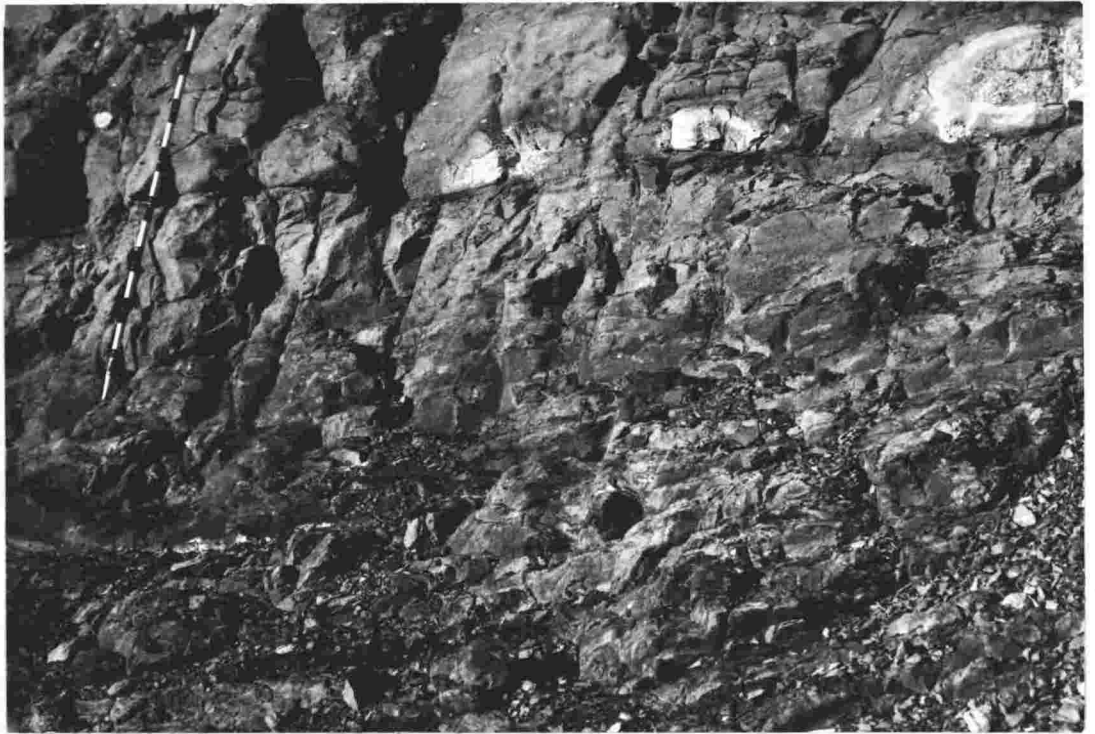
Fig. 2.3.   The gradational contact (at level of base of staff)
            between the Aztec Siltstone and the overlying
            Metschel Tillite at section M1.   Staff in dm.

Fig. 2.4.   Basal units of the Metschel Tillite made up of red,
            haematitic matrix eroded from the underlying Aztec
            Siltstone.   Local green reduction spots and lenses
            are present also.   Granitic clasts are incorporated
            in the tillite;   a 6 cm clast lies to right of scale,
            which is in cm.

15.

CHAPTER 3

LITHOLOGY

The Aztec Siltstone consists predominantly of fine to
medium grained sandstone (50%), and siltstone and claystone
(50%), but also includes rare conglomerate and thin limestone
beds.

Siltstones and Claystones

The textural classification of Picard (1971) (Fig. 5.9)
has been employed in this thesis. It was found from thin section
analysis that the field named siltstones are more clay rich than
was at first suspected, and therefore fall into domains
intermediate between true siltstones and claystones; that is,
clayey siltstones, silty claystones or even claystones. True
siltstones are uncommon, as are mudstones. Because of the
similar petrology of all these lithologies they are generally
discussed together and referred to as "siltstones and claystones",
"fine-grained beds", or "fine member units".

The massive and unbedded fine-grained beds of the formation
which constitute roughly one third of the fine-grained beds
(Fig. 4.1), commonly weather to form bluffs, with minor blocky
or flaky partings. The more abundant thin bedded or laminated
siltstones weather by slabbing and form platy low angle slopes.
The siltstones and claystones in general do not show a weathering
coating on the surface and are very fresh and highly indurated.

Siltstone and claystone beds are extremely variable in
thickness, from less than 10 cm to 15 m. Individual beds are
commonly lense-shaped, and may wedge out over distances of
from 3 m to 500 m depending on the bed thickness. However,
most have a lateral extent greater than the outcrop width.
the only fine-grained bed that could be positively correlated
between two sections, was an 8 to 9 m thick, massive, nodular,
red and green siltstone in the sections at Aztec Mountain
(AZ-17, AZ-18) and Maya Mountain (MA) (Fig. 2.1). This unit

could be traced visibly for the 2 km between these two sections, as a resistant bluff among predominantly slope forming lithologies. At Alligator Peak, unit 22 of section A1 is probably equivalent to unit 6 of A3, 1000 m away (Fig. 2.1), for they have a similar lithology, colour, and bed form, more particularly a distinct wavy or pseudobedding character described in Chapter 4 under Stratification. Sections P1, L1, and L2, which are as much as 20 km apart (Fig. 2.1), have a similar lacustrinal bed, approximately 5 m thick, containing gypsum lenses, conchostracans, and fish remains.

The colour of the fine-grained lithologies of the formation, is the most distinctive property. The predominant colours as determined from the Geological Society of America Rock-Color Chart (Goddard et al. 1963) are light greenish-grey (5GY 7/1 or 8/1) or greenish-grey (5GY 6/1 or 5G 6/1) and greyish-red (10R 4/2). The light greenish-grey and greenish-grey beds will simply be referred to as green, and the greyish-red as red, for the purpose of this thesis. Drab is used as a collective term for the green and grey lithologies.

Remarkable consistency in colour was a feature of all measured sections. A colour chart was not used by McKelvey et al., when measuring sections of Aztec Siltstone during the 1968-69 expedition (Barrett and Webb, 1973) but the colours of beds described by them are assumed to be comparable with those measured by the author. This was checked by the author at some of their sections during the 1973-74 expedition.

Red beds constitute 30 percent of the fine-grained sediments of the formation, or 15 percent of the entire formation as determined from complete sections (Table 3.1), and the colours are found to be almost identical to those in most other red bed sequences throughout the world, e.g. the Catskill facies (Devonian) of the Appalachians (Friend, 1966), the Chugwater (Triassic) Formation of Wyoming (Picard, 1965) and the Juniata and Bald Eagle Formations (Upper Ordovician) of Pennsylvania (Thompson, 1970).

Another colour of importance in the fine-grained lithologies was medium grey (N5). Although it applies to only a small volume

of sediment it is a colour generally present as a transitional
zone at red-green boundaries, where it has a thickness roughly
proportional to the thickness of the adjoining coloured beds,
from a few millimetres in width (Fig. 3.5) up to 0.5 m. It is
always present in this red-green association.

Some siltstones and claystones have a light olive-grey
(5Y 5/2 or 6/1) or olive-grey (5Y 4/1) colour, but these
constitute only a minor percentage of the total green beds
of the formation.

Greyish-purple (5P 4/2) or greyish-red-purple (5RP 4/2)
fine-grained beds are common in the Mount Metschel (M1 and M2)
sections. An explanation for their colour is given in Chapter
5, p.   along with an explanation for the origin of the red
and green lithologies.

Dark grey (N3) and black (N1) carbonaceous siltstones and
claystones are present in the sections at the Lashly Mountains
(L1 and L2), Mount Fleming (F1 and H6) and Shapeless Mountain
(S9) (Fig. 2.1). At L1 units 8 and 10, and L2 unit 3, these
black beds contained veins and lenses of gypsum (Chapter 5,
Table 5.7) up to 3 mm thick. The beds hosting gypsum were
laminated, and contained symmetrical ripples, conchostracans,
and thin interbeds of fine-grained sandstone. They are
considered to be shallow lake sediments. There are two
possible sources for the gypsum:

(1) It could be an early precipitate from evaporating saline
lake waters. Laboratory experiments by Usiglio (1849; in Clark,
1924) showed that evaporating saline waters will first precipitate
small amounts of $CaCO_3$ and when evaporated to about one fifth
original volume, gypsum is precipitated. Later stages of
evaporation produce halite, sulphates and chlorides of magnesium,
and halides of sodium and potassium. The gypsiferous Aztec
Siltstone beds also contain calcite as a matrix but no halite,
and this suggests that, if this process took place, then
precipitation stopped at gypsum.

(2) The gypsum may be a product of the oxidation of sulphides
which were formed in a euxinic lake environment.

$$2FeS_2 + 15/2O_2 + 4H_2O \rightarrow Fe_2O_3 + 4SO_4^= + 8H^+$$
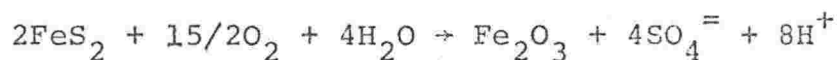
The reaction is catalyzed by bacteria which make use of the energy released (Krauskopf, 1967 p.275). In arid regions where calcium concentrations in surface and subsurface waters is high, the sulphate generated by the reaction may combine to form gypsum.

A study of the variability of colour in the formation (Fig. 3.1) shows that there is little ordered variability in a section, with the geographic location of that section. A weak trend is shown by sections in the middle of the outcrop area (Fig. 1.1) which tend to have the highest percentages of red siltstones and claystones.

A plot of the percentage of red fine-grain sediment against the total percentage of fine-grained lithology in the section (Fig. 3.2) shows no ordered trend.

Red-green variations within individual sections were plotted by graphing the percentage red siltstone and claystone for 10 m intervals up the section (Fig. 3.3). The figure shows little consistent trend in red-green variation either within a section or between sections. However, there is a weak trend towards increasing percentages of green siltstone and claystone in the uppermost metres of these lithologies in many of the sections, suggesting that non-oxidising conditions became more common for the youngest fine-grained deposits of the Aztec Siltstone.

The colour of the fine-grained sediments in the main, conforms to bedding, but local differences in colour, either red in a green host or green in a red host, are very common. Zones of green, as irregular patches, mottles, spheres, veins, and stringers, are very common in massive red beds (Figs. 3.4, 3.5, 3.6 and the frontispiece). In most cases e.g. the spheres, they had been produced from the red, but in some others they may be relics of a former green unit as seen in Figure 4.5. A substantial number of massive green units were found on

19.
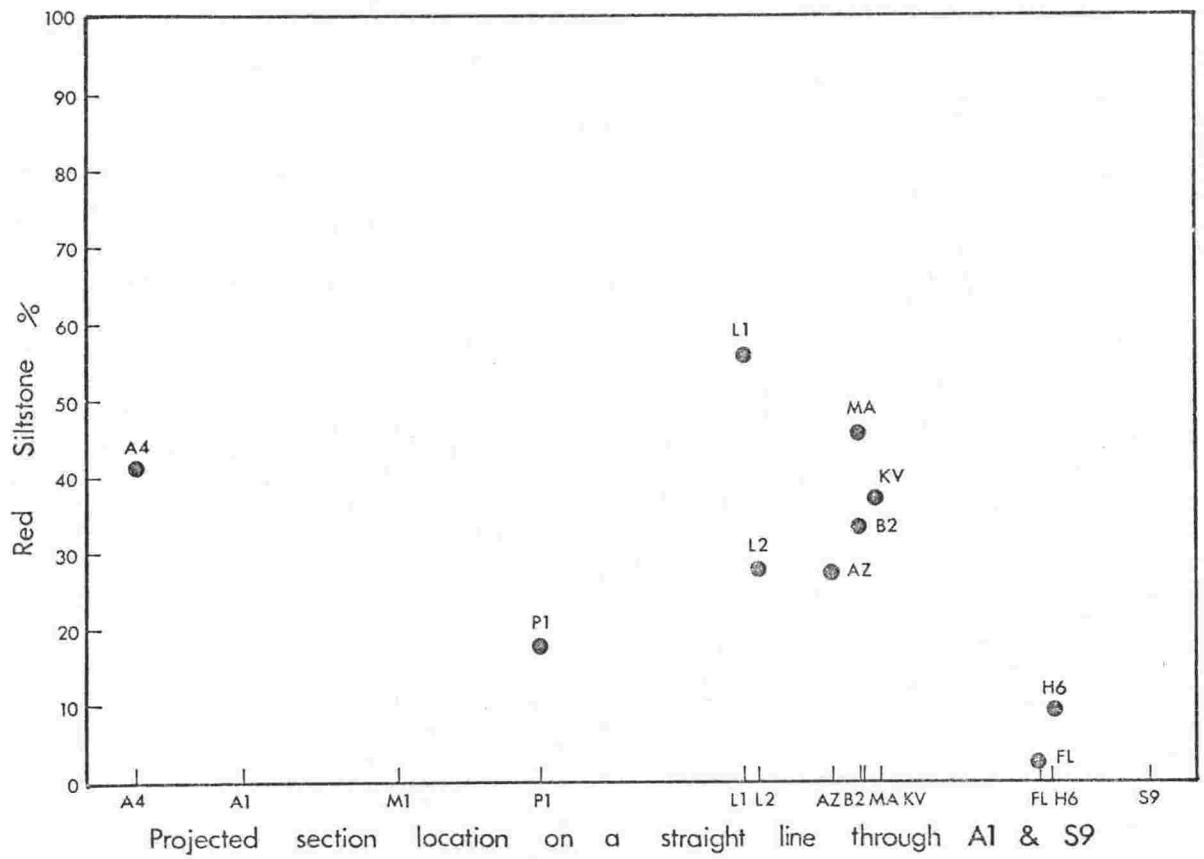
Fig. 3.1. Variations in the total thickness of red siltstone as
a percentage of the total siltstone of complete sections
of Aztec Siltstone lying on an approximate north-south
line.
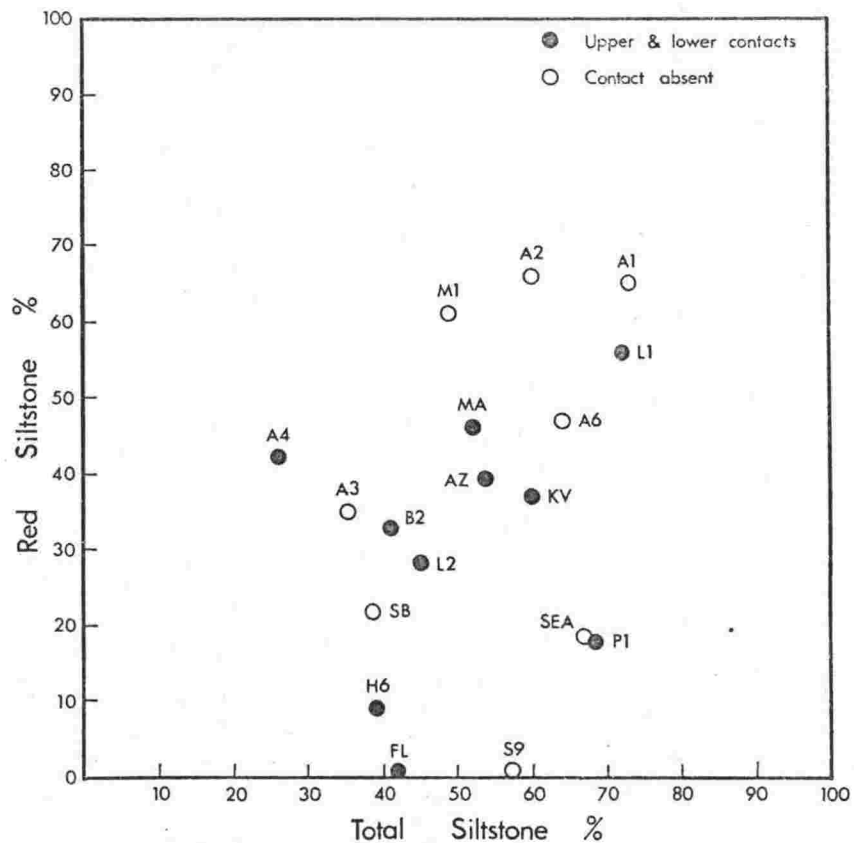
Fig. 3.2. Variations in the thickness of red siltstone plotted
against the total siltstone content in sections of
Aztec Siltstone.
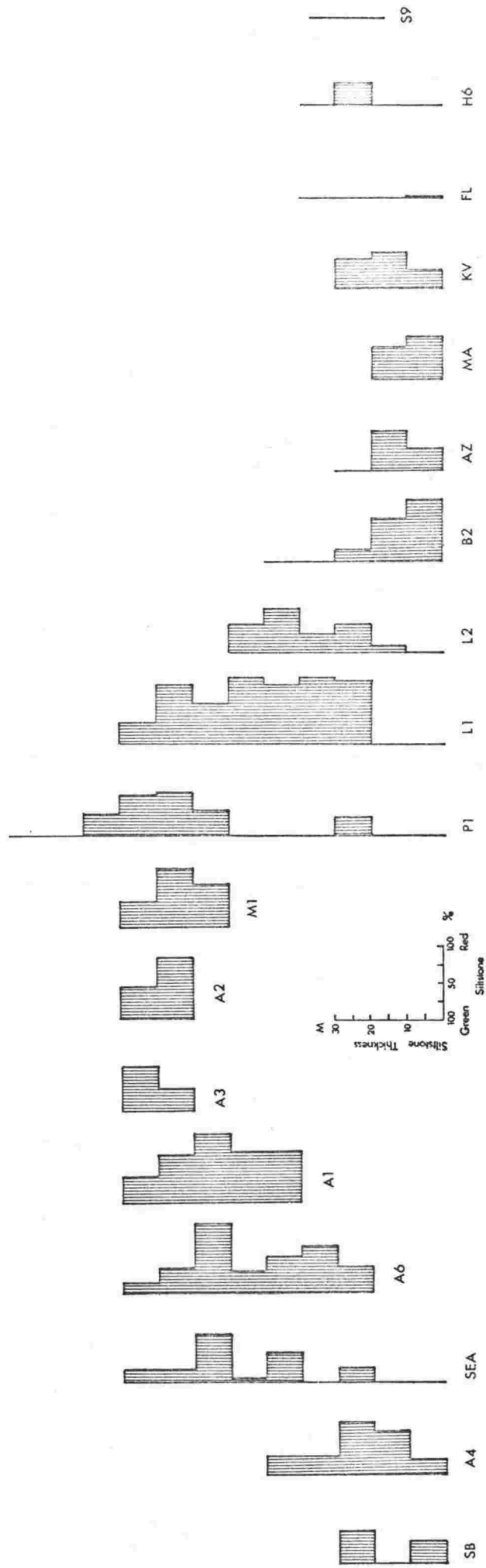
Fig. 3.3. Red-green siltstone variations within sections of the Aztec Siltstone. Sandstones were removed from the column for the purpose of the calculation, and where it was found that there was insufficient siltstone and claystone (by less than or equal to 5 m) to make up the last 10 m interval, the top 10 m of siltstone and claystone was used. If more than 5 m was missing then the last interval was ignored. The 10 m interval was selected as it was large with respect to the thickness of individual units (the mean fine member thickness is 3.9 m, Fig. 7.10), and yet small with respect to the total thickness of siltstone and claystone in the section.
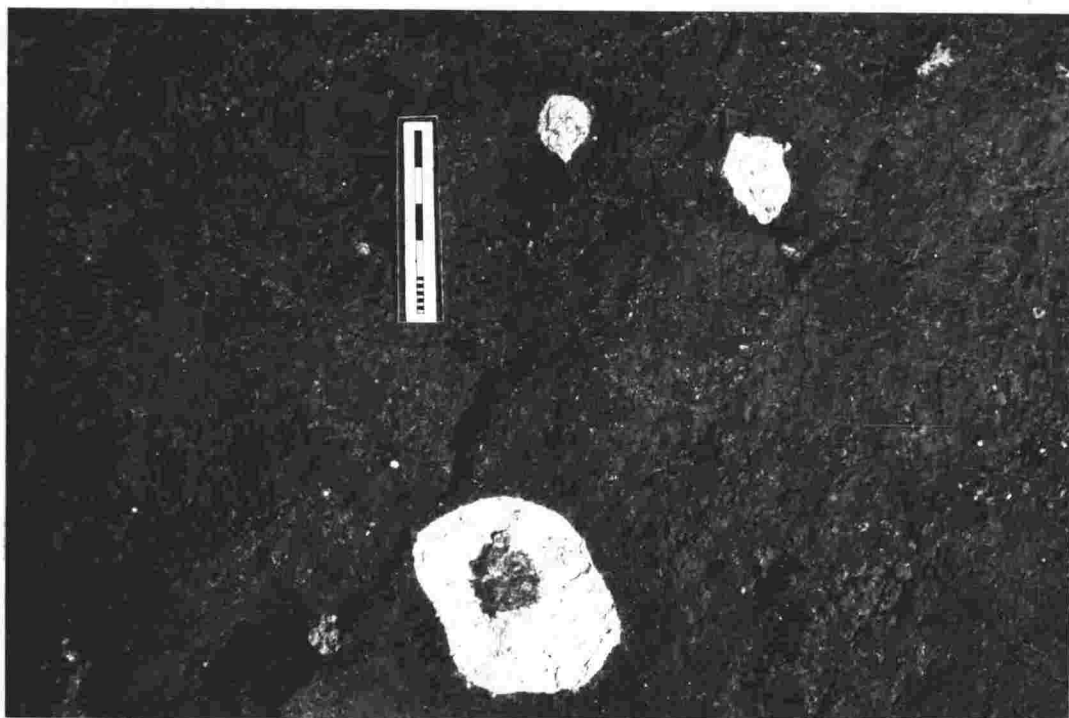
Fig. 3.4. Green reduction spheres within a massive red claystone
unit at A1, unit 22. Scale in cm and mm.
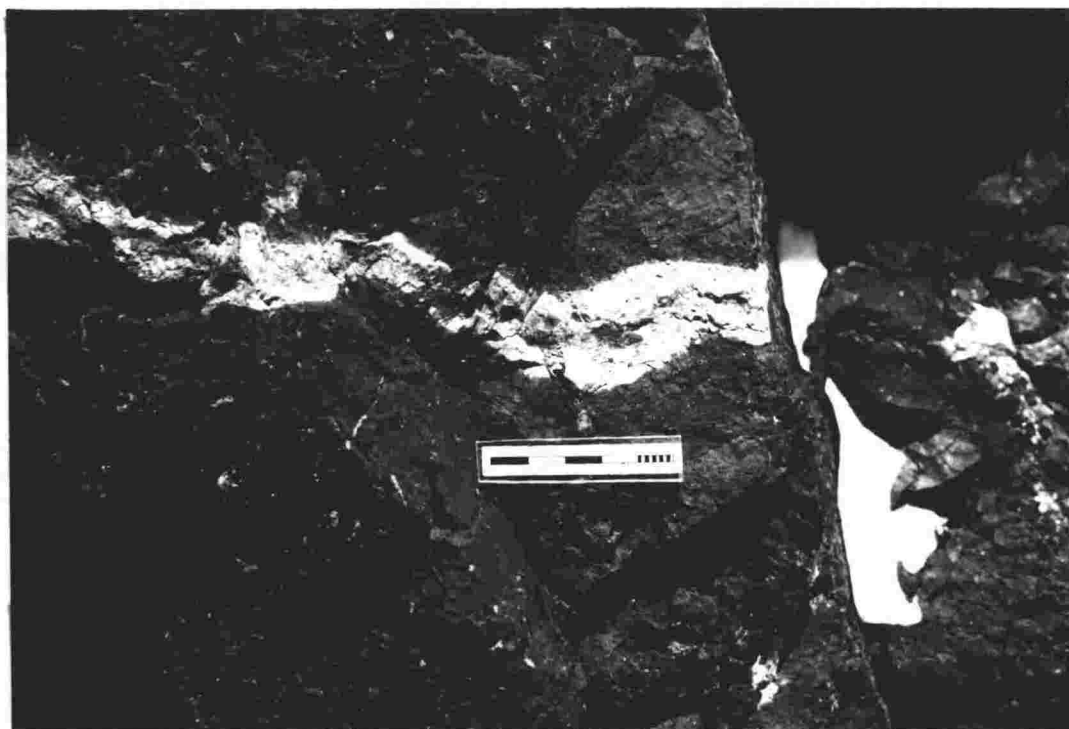
Fig. 3.5. Green reduction channels within a massive red claystone
unit at A1, unit 22. The channel has a grey (N5)
margin. Scale in cm and mm.

Fig. 3.6. Mottled and streaked green reduction pattern developed
in a red unit at Al, units 16 to 22. This is caused .
by a fluctuating ground-water table and reducing
solutions migrating through more permeable horizons.
Section heights approx. 3 m (see also Fig. 7.9).   .

very close inspection, in some cases microscopic, to contain small relic zones of red, indicating that the unit was most probably a former red unit.

Almost invariably, red siltstone or claystone in association with coarser-grained beds, showed green contacts (Figs 4.13, 4.26 and 4.30). Red fine-member siltstone and claystone beds underlying coarse-member channel sandstones, had a green or grey zone at the upper contact in almost every case. In many cases the zone was gradational from green at the contact, down through grey to red. The width of these zones was proportional to the thickness of the coarse-member sandstone.

Some fine-grained units consisted of alternating, thin (less than]0 cm), red and green beds. It was observed in a number of examples that this colour change, in large part, corresponded to small grain-size variations in the lithologies; the green beds were the coarser grained sediments.

Close inspection of green beds which ran through the middle of red units (Frontispiece) revealed that they were cored by sandstone or coarse siltstone in almost every case.

Colour variations closely correspond to early post-depositional features such as mudcracks, vein networks, root structures, burrows, nodules, and concretions, and details of these are discussed in Chapter 4.

The general distribution of red and green fine-grained lithologies is analysed and discussed in this chapter under Bulk Variability p. 29, and in Chapter 7.

Sandstones

Fine to medium-grained sandstones constitute 50 percent by volume of the Aztec Siltstone (Table 3.1), and are fairly evenly distributed generally in a cyclic form throughout the entire formation. The detailed distribution is discussed in this chapter under Bulk Variability p. 29. Individual beds are from 0.1 to 15 m thick, and are commonly tabular or lenticular in shape. Beds commonly extend laterally for

distances greater than the outcrop widths and are assumed to persist for distances in the order of 100's of metres. This is particularly true of thick tabular bodies which are composed of more than one cycle of channel sand deposition, and probably extend for distances in the order of kilometres as was observed in the Aztec Mountain sections, particularly AZ-18.

Contacts with siltstones and claystones were either gradational (regular or irregular), interfingering, sharp, or erosional. The former occurred on the upper contacts of sandstone bodies when part of a "fining-upwards" cycle, and the latter case when there had been scouring of the underlying unit immediately prior to deposition of the sandstone.

The present day weathering of outcrops produces bluffs, platforms, and ledges of sandstone as a result of their massive splitting character (Table 4.4). The sandstone varies in induration depending largely on the proportion of clay matrix, and this is reflected in the form of the outcrop. Sandstone in the Aztec Siltstone is normally less indurated than sandstone of the underlying Beacon Heights Orthoquartzite. Present day surface weathering in sandstone commonly produces an iron stain coating up to 10 cm in thickness.

The colour of sandstone beds is most commonly white (N9) light greenish-grey (5GY 8/1), yellowish-grey (5Y 8/1), or shades of grey. No red sandstones were observed in the formation, although there are some greyish-orange-pink (10R 8/2) beds in A1. Even thin lenses of sandstone present in the middle of thick, red, fine-grained units are green, grey, or white.

Units of gritty (quartzose) sandstone are rare in the formation. Where present they are normally accompanied by quartz pebbles, as at A4 and H6.

Conglomerates

Conglomerates in the Aztec Siltstone are intraformational
in character. They are most common in the coarse-member units,
concentrated in sandstone in troughs immediately overlying the
erosion or scoured surface (Figs. 3.7 and 3.8; see also
Chapters 4 and 7 for a description of scoured surfaces and
facies relationships). These "channel lag" deposits are
primarily composed of siltstone and claystone clasts and are
considered to have been derived from the underlying fine-
member lithologies by subaqueous stream erosion immediately
prior to the depositional phase of the overlying and more
coarse bed (Allen, 1962a, 1965b). The clasts range widely
in size from a few millimetres up to 4 cm (Fig. 3.8, 3.9),
and are generally set in a matrix of medium to coarse-grained
sand. Clasts are highly angular and of low sphericity (Fig.
3.9). Their lack of rounding suggests that they can have
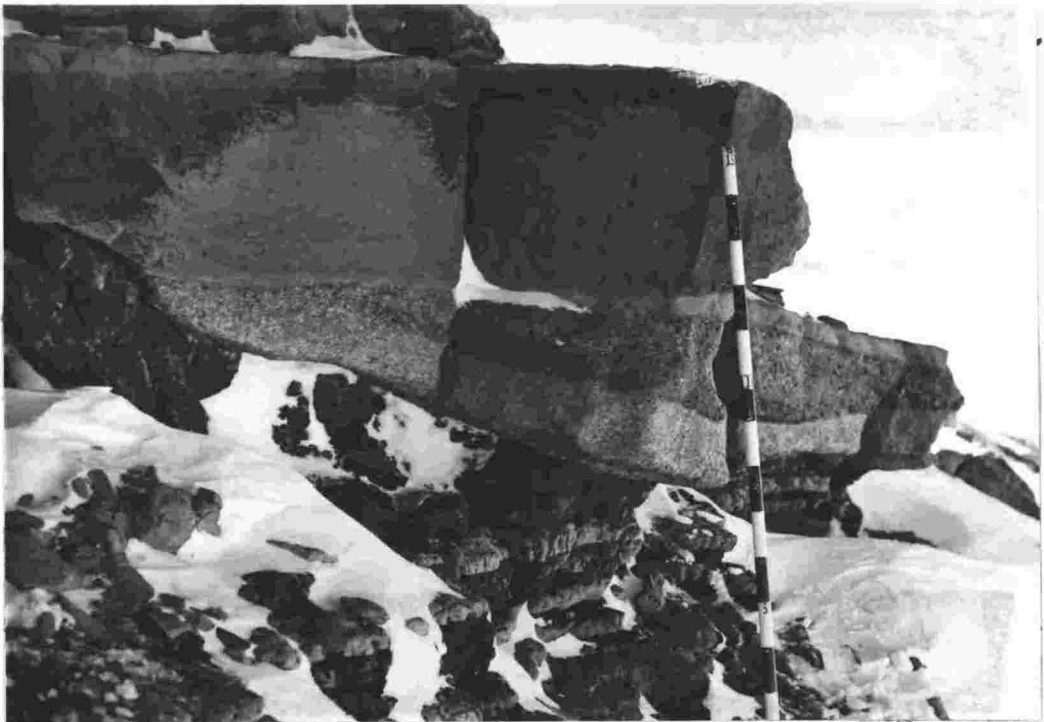
Fig. 3.7. Intraformational conglomerate filling a channel in a
a scoured surface cut into the upper part of a fine-
grained, fine member portion of an alluvial cycle (L1,
unit 29) by the erosive powers of the migrating stream.
Staff in dm.

Fig. 3.8. Intraformational conglomerate (a closer view of that in
           in Fig. 3.7) consisting of clasts of red siltstone and
           claystone eroded from the underlying fine member. The
           fact that the clasts are red suggests that the red
           haematite pigment or precursory mineral must have been
           present in the fine-grained sediment prior to deposition
           of the overlying cycle. Some of the red clasts have green
           reduction rims. Scale in cm and mm.
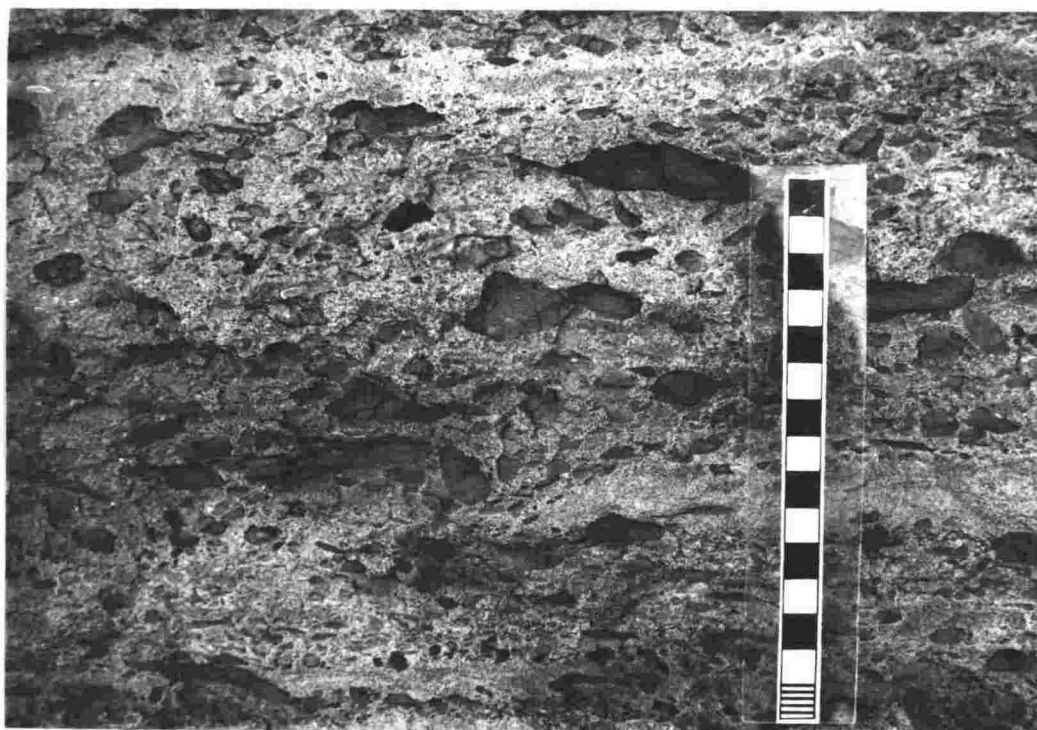
Fig. 3.9. Intraformation conglomerate consisting of clasts of green
           siltstone and claystone eroded from fine-grained, fine member
           lithologies by channel cutting, and incorporated into basal
           channel sandstone. Location L2, unit 10. Scale in cm and mm.

travelled not more than a few hundred metres from their site
of origin (Smith, 1972).

Intraformational conglomerate was commonly present in thin
(less than 0.2 m) beds, lenses, or pockets, throughout "multi-
storey" sandstone bodies (Chapter 7, Fig. 7.11). This suggests
that there was continuous local corrasion of fine-member beds
during coarse-member deposition.

Imbrication of the clasts was noted at some localities
e.g. L1, unit 22.

Conglomerate clasts may have resulted in part from the
erosion of mudcurls (Chapter 4, Mudcracks) as the incidence of
mudcracking during the deposition of the Aztec Siltstone was
very high (Fig. 2.1). Air-dried mudcurls would be rapidly
destroyed during transportation however. Probably the bulk of
the clasts were eroded and transported in a wet plastic state,
as suggested by Smith (op.cit.).

Red siltstone or claystone clasts are common in conglomerate
(e.g. Fig. 3.8) and establish that red fine-grained beds were
present locally during deposition of the Aztec Siltstone. Where
red clasts had been incorporated into green units, reduction at
the clast margins has taken place (Fig. 3.8).

Intraformational conglomerates contain concentrations of
reworked and thus generally disarticulated, fish plate material
(Figs. 4.14 and 7.7). In some cases this has resulted in a
breccia of bone plates (A4, unit 62; P1, unit 20).

Limestones

Limestones are a very minor lithology of the Aztec Siltstone,
even although calcium carbonate is a very common matrix constit-
uent of fine-grained units, and is present as a cement in many
sandstones. In some beds, calcite in the form of ·nodules was
present in a percentage which exceeded the non-calcite fraction,
and so by definition these beds formed true limestones. Their
morphology and genesis is however that of nodules and, as such,
they are described in Chapter 4.

The only other true limestone was an oolitic limestone at
Portal Mountain (P1, unit 12), and this occurred as thin beds
and lenses in a 2.3 m-thick laminated to very thin bedded,
massive, green siltstone. In thin section (Fig. 3.10) the
limestone consisted of spherical or subspherical oöids averaging
1 mm in size, composed largely of microcrystalline (0.01 to
0.2 mm) calcite and in some cases containing 20 micron grains
of largely authigenic quartz. The oöids "float" in a matrix
of macrocrystalline (greater than 1 mm) calcite. The matrix
contains some very fine-grained (less than 1 micron) haematite
in lenses within the calcite. X-ray diffraction analysis of
the oolite (Table 5.7) confirmed the calcite and quartz
composition.
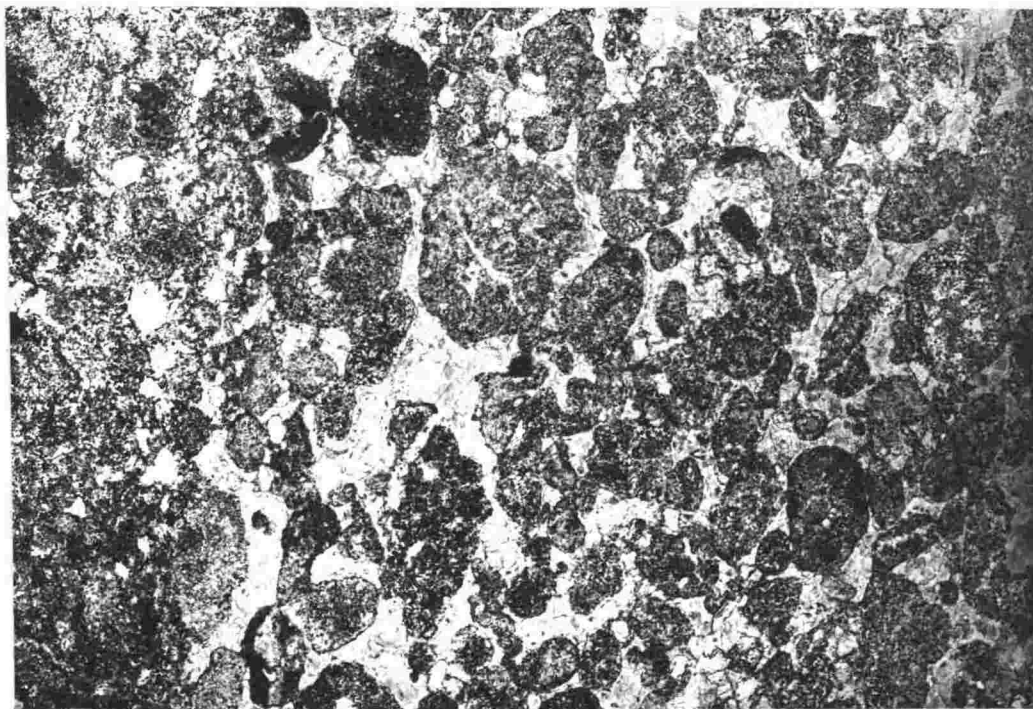
Fig. 3.10. Oolitic limestone (23306). The ooids are "floated" in
a matrix of macrocrystalline calcite which also contains
haematite pigment. Plain light. Scale 5 cm = 4.7 mm.

The oöids did not show the radial grain orientation commonly found in oöids and thought to be a product of diagenesis (Kahle, 1974). This may be due to recrystallization of the calcite during diagenesis possibly aided by contact metamorphism from neighbouring dolerite sills and dykes.

The unit hosting the oolitic limestone, and the associated units (units 10, 11, 13, and 14) are highly calcareous, laminated and very thin bedded, siltstones and claystones, considered to be of a lacustrinal origin (Chapter 7, Fine-member dominated sequences, Fig. 7.12). It is suggested that shallow, calcium carbonate saturated lake waters provided the environment for formation of the oöids, which probably accreted initially about detrital quartz grains in a "free-rolling" environment, probably in the higher energy wave zone of the lake edge (Pettijohn, 1957). Calcium carbonate was widespread in the Aztec Siltstone alluvial plain sediments, especially in the form of kankar (Chapter 4, Nodules) in the floodbasin deposits. It is to be expected that the lake waters would be high in carbonate, both because they have drained through these sediments and because of the seasonally hot and dry climate which would have concentrated it by evaporation. The haematite in the calcite matrix between the oöids is probably a detrital product derived initially from erosion of the reddened overbank sediments by the rivers feeding the lake. The very fine-grained (approximately 1 micron) haematite would be carried in suspension into the lake and deposited with the precipitating oöids.

Pisolitic limestones are present in the formation, and are discussed under the heading of Concretions in Chapter 4.

Bulk Variability

The Aztec Siltstone is the only Taylor Group formation with a large proportion of siltstone and claystone. The average percentage of fine-grained beds for all complete sections measured is 50 percent, with a maximum of 72 percent at Mount
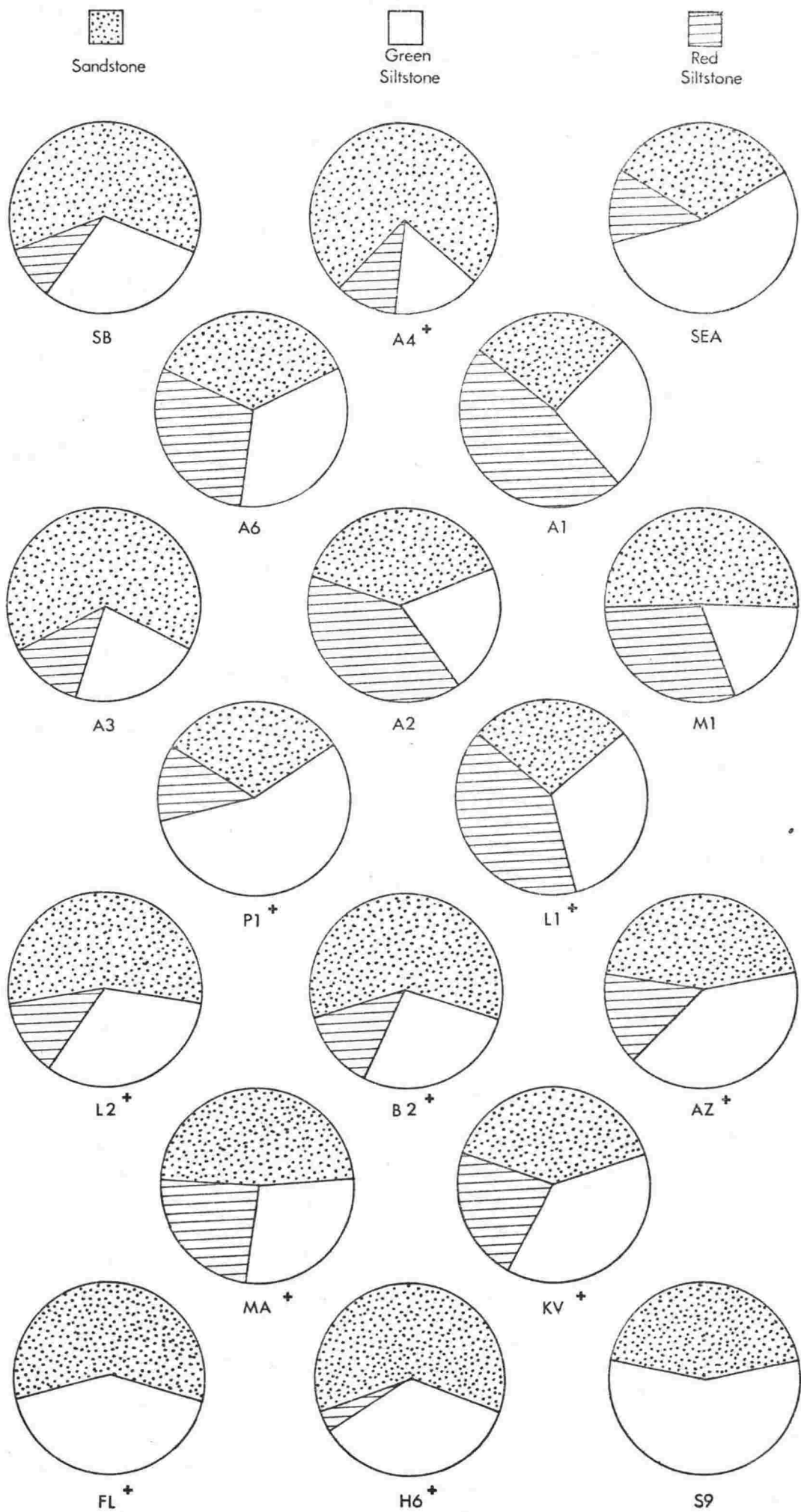
Fig. 3.11. Lithologic proportions of sections of Aztec Siltstone. Data from Table 3.1. (+ indicates complete sections).

Crean (L1) and a minimum of 26 percent at Mount Ritchie (A4),
(Table 3.1, Figs 3.11 and 3.12). The very low value for Mount
Ritchie is attributed to a loss of exposure at the larger scree
and snow slopes which are typically developed on siltstone and
claystone units. A maximum of 39 percent siltstone and clay-
stone is possible if all the unseen units are siltstones and
claystones. Apart from the above mentioned two sections and
Portal Mountain Pl), there is less than 22 percent relative
deviation in siltstone and claystone from the average
(Table 3.1, Fig. 3.11).
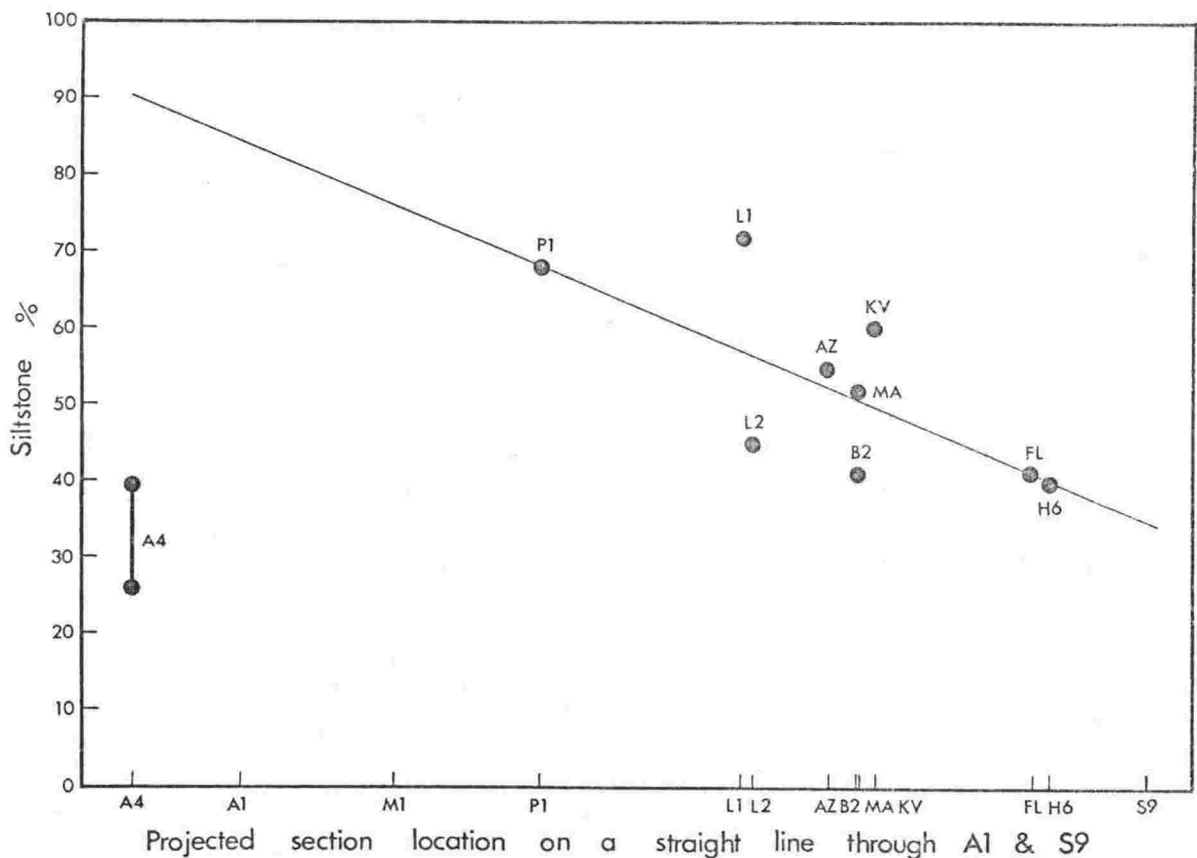
Fig. 3.12. Variations in the siltstone content of complete sections
of Aztec Siltstone lying on an approximate north-south
line.

Figure 3.12 shows a northward trend of decreasing
siltstone and claystone percentage. The anomalous value of
Mount Ritchie (A4) is not completely due to the loss of

Table 3.1   Lithologic content of sections of the Aztec Siltstone.
Values are in percentages.

Section	Sandstone			Siltstone		
	Coarse or gritty	Fine to medium	Very fine to fine	Red	Green	Black
SB	0	61	0	9	30	0
+A4	3	69	2	11	15	0
SEA	0	32	1	13	54	0
A6	0	18	18	29	35	0
A1	0	26	0	48	26	0
A3	0	65	0	12	23	0
A2	0	25	16	38	21	0
M1	0	34	17	30	19	0
+P1	0	26	6	12	56	0
+L1	0	25	3	40	17	15
+L2	0	41	15	12	27	5
+B2	7	39	13	14	27	0
+AZ	1	44	0	15	40	0
+MA	0	48	0	24	28	0
+KV	0	40	0	22	38	0
+FL	0	58	1	0	33	8
+H6	0	58	3	4	26	9
S9	0	43	0	0	43	14
Mean of all sections	1	42	5	18	31	3
Mean of complete sections	1	45	4	15	31	4

+ Complete sections i.e. sections underlain by the Beacon Heights
Orthoquartzite and overlain by the Metschel Tillite or the Weller
Coal Measures.

exposure, because even with the maximum value inserted it is still very low. The trend of increasing sandstone with decreasing latitude is weak, and may not be a depositional characteristic. If the portion of Aztec Siltstone eroded from the top of each section by the Permo-Carboniferous glacial bevelling (Chapter 2, Nature of Upper and Lower Contacts) was not representative of the section as a whole, then the remaining portion is atypical of the deposited sequence.

Siltstone and claystone, to sandstone percentages were calculated over 10 m intervals for all sections, to show lithologic variation within sections of Aztec Siltstone. The graphic representation is shown in Figure 3.13, and has been plotted as overlapping bars to show the 20 m average interval, and shaded over the 10 m central portion of each bar, to show the variation more clearly. A minimum of 30 m of Beacon Heights Orthoquartzite was included at the base of the section, where it existed.

Figure 3.13 clearly denotes the incoming of the Aztec Siltstone by the sudden increase in siltstone and claystone units. There is a trend towards a bimodal distribution of siltstone and claystone in the formation for six of the sections. Those complete sections which do not have bimodal distribution, all lie in the northern sector of the area studied. The erosion of the Aztec Siltstone in the north may account for this. The bimodal tendency may well be due to an allocyclic (Beerbower, 1964) phenomenon e.g. slope increase as the basin of deposition subsided or the source area was uplifted. This would result in a stream discharge increase, and during these periods of higher energy, the streams would have been more confined to the channels, with less overbank deposition and stream migration, resulting in more common sandstone deposition.

MARKOVIAN CHAIN ANALYSIS

From an examination of the sections in the field and the stratigraphic columns of those sections (Fig. 2.1), it is evident that there exists an order in the bedding sequence of

34.
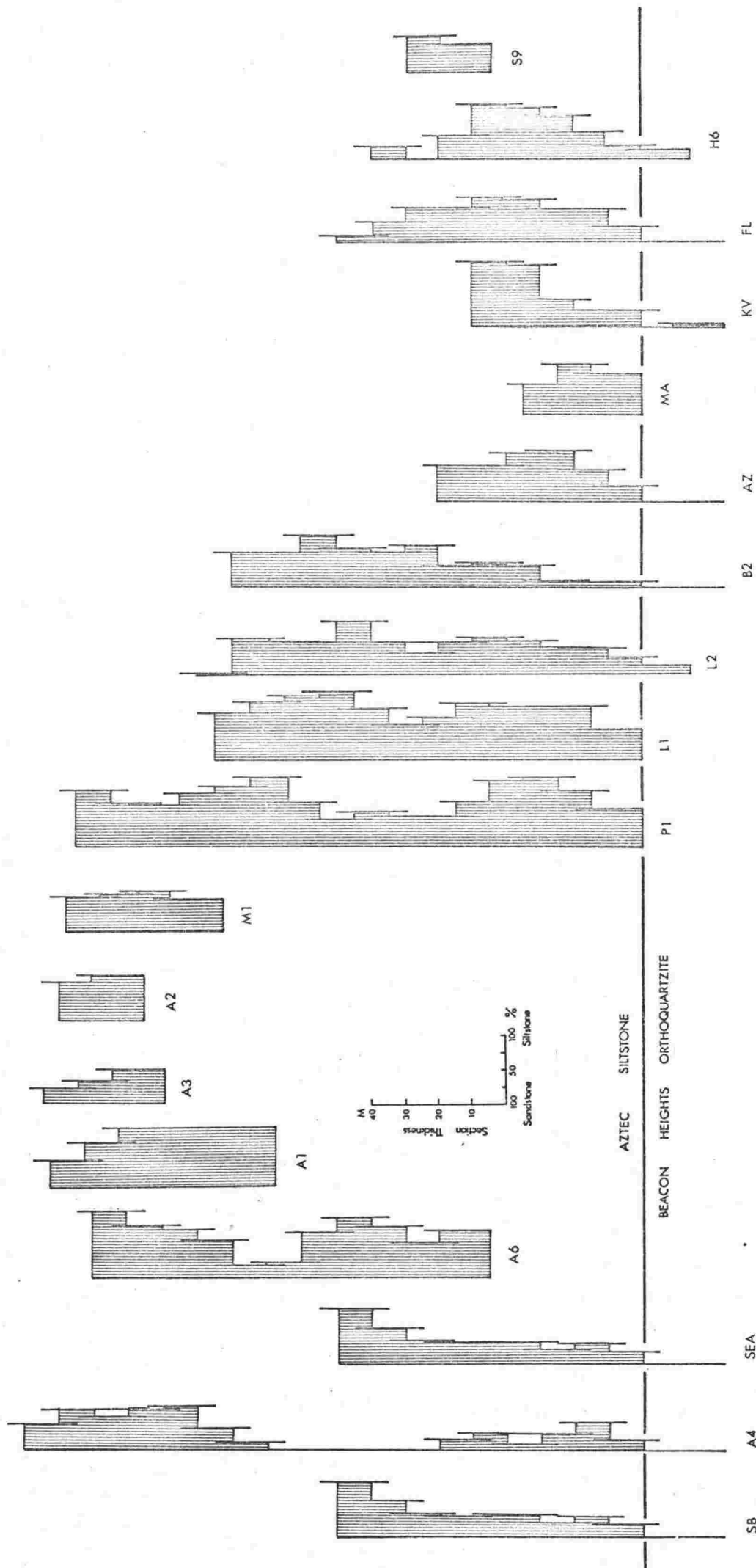
Fig. 3.13.   Siltstone and claystone, to sandstone percentages, calculated over 10 m intervals for all sections of Aztec Siltstone. The 10 m interval was chosen, as it was large with respect to the smallest unit (less than 1 m), and yet small in respect to the total thickness of the section. Other intervals were tried, but with less success. "Moving averages" were calculated for each section to show the major trends. The percentage of sandstone in a 20 m interval was averaged every 10 m up the section. Losses in exposure were completely left out of the averages, and if the last 20 m interval was not filled by less than or equal to 5 m at the top of the section, then a 20 m interval was taken from the top of the section downwards. If more than 5 m was missing, then the last interval was ignored. Mudstone and claystone were incorporated as siltstone.

sandstone and the finer lithologies. To quantitatively and objectively test for the degree of randomness of the bedding sequence of the whole formation, sections were evaluated using the Markovian Chain Analysis (Gingerich, 1969; Krumbein and Dacey, 1969; Selley, 1970; Lumsden, 1971; Miall, 1973).

A Markov chain is "a stochastic process which moves through a finite number of states, and for which the probability of entering a certain state depends only on the last state occupied" (Kemeny and Snell, 1960, p.207). Thus, in a Markov process there is a "memory" of earlier events such that the probability of event B following event A, while not a certainty, is significantly greater or lesser than that predicted by pure chance.

A data array (matrix) is used to facilitate Markovian analysis. Thus, if f_{ij} is the probability of going from state L_i to state L_j, these probabilities can conveniently be arranged as in Table 3.2. If for example in a vertical sequence of rocks, the component L_i is designated as a fine

Table 3.2   Generalized data array

	L_1	L_2	L_3	L_4	L_j	
L_1	f_{11}	f_{12}	f_{13}	f_{14}	..	f_1
L_2	f_{21}	f_{22}	f_{23}	f_{24}	..	f_2
L_3	f_{31}	f_{32}	f_{33}	f_{34}	..	f_3
L_4	f_{41}	f_{42}	f_{43}	f_{44}	..	f_4
L_i	..	..	..	..	f_{ij}	f_i

Total

to medium sandstone and L_3 a red fine-grained bed, then if L_3 overlies L_1 10 times, the element f_{13} will be 10. A matrix of this type is called a Transition Count Matrix (f_{ij}). It is a

two-dimensional array which records the number of times that all possible vertical lithologic transitions occur in a given stratigraphic succession.

For the Aztec Siltstone analysis, transitions were recorded only between different lithologies, and not within a single lithology. This is termed "unit facies" (Lumsden, 1971) or "embedded Markov chain" (Krumbein and Dacey, 1969) analysis. Hence, zeros will appear on the array diagonals. Where transitions between units of the same lithology but differing character are recorded, a "multistorey facies" (Lumsden, 1971) analysis results. In this case the array diagonals will not be zero. This approach was not employed for the Aztec Siltstone because of the difficulty in establishing critera for the recognition of what constitutes a major change within a single lithology.

The lithologies chosen for the analysis of the Aztec Siltstone were fine to medium sandstone (1), very fine to fine sandstone (2), red fine-grained beds (3), and green fine-grained beds (4). The minor carbonaceous fine-grained lithologies of the formation were included with the green fine-grained beds. To have incorporated more components was not possible because they were not recorded in some sections, even though they may be present.

The sections of Aztec Mountain (AZ), Alligator Peak (A3), Kennar Valley (KV), Maya Mountain (MA), Shapeless Mountain (S9), and the south Boomerang Range (SB), could not be evaluated by the Markov analysis because the available section descriptions were not sufficiently complete.

From the Transition Count Matrix (f_{ij}), an Independent Trial Matrix (e_{ij}) can be calculated which shows the chance of occurrence of an event if the pair transitions are a function of random processes. Thus, in Table 3.3, the number of transitions from fine to medium sandstone to an overlying component is 223; in other words, fine to medium sandstone occurs 223 separate times in a total of 815 units present. Thus, there are 592(815-223) possible units that could follow a unit of fine to medium sandstone. Of these 592 units, there

Table 3.3a   Transition count matrix for all sections combined

		Fine to medium sandstone	Very fine to fine sandstone	Red siltstone	Green siltstone	
Fine to medium sandstone	1	0	9	43	171	223
Very fine to fine sandstone	2	8	0	18	41	67
Red siltstone	3	45	15	0	129	189
Green siltstone	4	173	37	126	0	336

$= f_{ij}$

T=815

Table 3.3b   Independent trial matrix for all sections combined
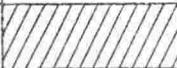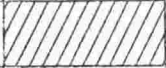
	1	2	3	4
1	/////	0.113	0.319	0.568
2	0.298	/////	0.253	0.449
3	0.356	0.107	/////	0.537
4	0.466	0.140	0.395	/////

$= e_{ij}$

Table 3.3c   Transition probability matrix for all sections combined
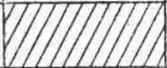
	1	2	3	4
1	/////	0.040	0.193	0.767
2	0.119	/////	0.269	0.612
3	0.238	0.079	/////	0.683
4	0.515	0.110	0.375	/////

$= p_{ij}$

Table 3.3d   Difference matrix for all sections combined

	1	2	3	4
1	/////	-0.073	-0.126	0.199
2	-0.179	/////	0.016	0.163
3	-0.118	-0.028	/////	0.146
4	0.049	-0.030	-0.020	/////

$= d_{ij}$

are 67 of very fine to fine sandstone. Thus, if the vertical lithologic transitions are functions of chance, there is a probability of 0.113(67/592) that fine to medium sandstone will be followed by very fine to fine sandstone; 0.319(189/592) that it will be followed by red siltstone, and 0.568(336/592) that it will be followed by green siltstone.

The Transition Probability Matrix (p_{ij}) reflects the observed probability of occurrence of each event. This matrix is obtained by taking the number of transitions of one component to another, and dividing by the total number of transitions involving the first component. Thus for Table 3.3, fine to medium sandstone occurs 223 times and is followed by red siltstone a total of 43 times; hence, the Transition Probability is 0.193(43/223). The p_{ij} values will reflect the presence of any Markovian dependency relationship.

By applying a chi-square (χ^2) test to the sequence, the probability that the observed Transition Count Matrix (f_{ij}) is the result of a random process operating within the observed frequency of rock types (f_i) is determined (Billingsley, 1961; Gingerich, 1969) (Table 3.5).

$$\chi_v^2 = \sum_{ij} (f_{ij} - f_i e_{ij})^2 / f_i e_{ij}$$

where:
f_{ij} = transition count matrix.
f_i = the frequency distribution of rock types.
e_{ij} = independent trials matrix.
v = degrees of freedom = total number of positive entries in e_{ij} minus the rank of e_{ij}.

The figure of less than 0.05 was taken as the significant probability i.e. a 95 percent confidence level (Table 3.5). Lumsden (1971, p.456) stated that "unit facies" analysis may be regarded as evaluating the lower limit of probability of memory, and that for probabilities in the range of 0.05 and 0.20 suggesting possible significance, there is most likely a significant memory.

A Difference Matrix (d_{ij}) is calculated by subtracting the Independent Trials Matrix (e_{ij}) from the Transition Probability Matrix (p_{ij}).

$$d_{ij} = p_{ij} - e_{ij}$$

Positive values indicate which transitions have occurred with greater than random frequency. The larger the value of the entry, the greater the chance of occurrence. A fully developed cycle in a sedimentary sequence is determined by following the positive difference elements through the matrix. An overlap zone exists in the low positive values (Lumsden, 1971, p.457).

Figures 3.14 and 7.4 show a cyclic sequence obtained by combining data for the whole formation (Table 3.3). It is a typical "fining-upwards" sequence consisting of a basal coarse member of fine to medium sandstone, overlain by green siltstone in turn overlain by a very fine to fine sandstone, followed by green siltstone overlain by red siltstone and a return to green siltstone (Fig. 7.4). Such a sequence has a probability of randomness of less than 0.001. The complete and ideal cycle is not very common, due to either the premature occurrence of the basal sandstone unit of the overlying sequence, or to the absence of one or more medial units. The interpretation for the ideal cycle is given in Chapter 7.

815 units

$\chi_8^2 = 68.65$

$P = {<}0.005$

Red siltstone

(15%)　(16%)

(21%)　(5%)

Fine to medium → Green siltstone ⇄ Very fine to fine
sandstone　　　　　　　　　　　(5%)　　sandstone

(21%)
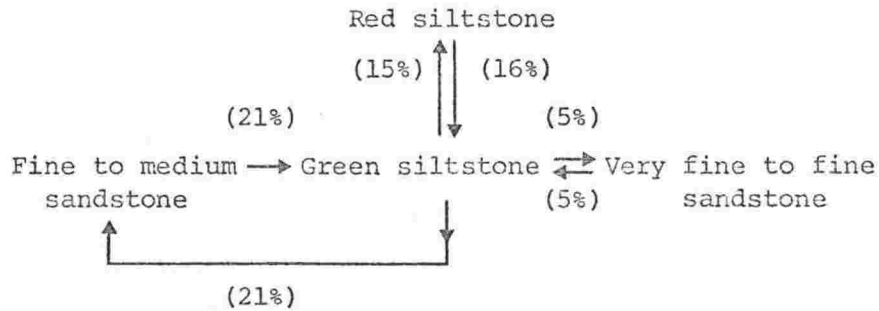
Figure 3.14. The fully developed 'ideal' cycle showing the most
probable upward transitions for the sedimentary
sequence produced by combining all measured sections
of Aztec Siltstone. The relative percentage of
transitions for the respective lithologies are
shown in parentheses.

M1

← VF-F SSt
(20%)　(20%)
→ Gr.　SiSt →
(8%)　(5%)
← Rd.　SiSt ←
(13%)　(15%)
→ F-M　SSt

P1

← Rd. SiSt
(14%)　(14%)
→ Gr.　SiSt →
(7%)
VF-F SSt
(26%)　(28%)
(3%)
← F-M　SSt ←

L2

← Rd. SiSt
(15%)　(15%)
→ Gr.　SiSt →
(6%)
VF-F SSt
(23%)　(30%)
(6%)
← F-M　SSt ←
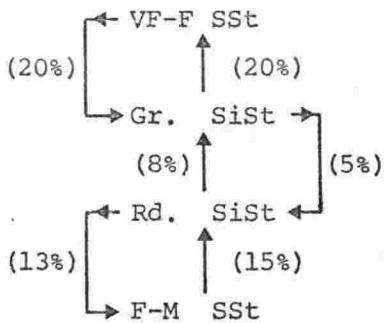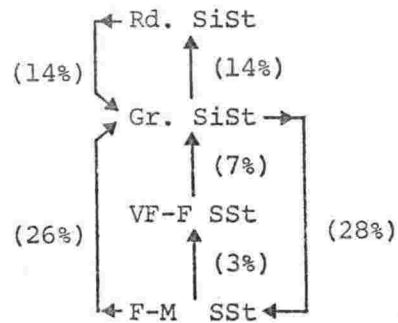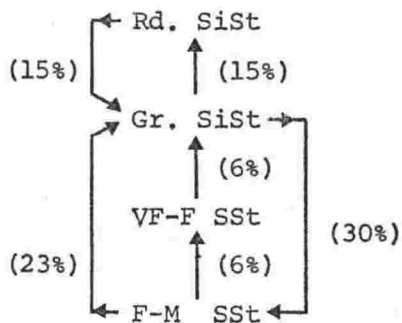
Figure 3.15. Markov chain diagrams showing
the most probable upwards
transitions for sections with a
significant memory in the bedding
sequence. Fully developed cycles
are shown by following the arrows
through the diagram. The relative
percentage of transitions for the
respective lithologies are shown
in parentheses.

Table 3.4   Upward transition probability matrices for those strati-
             graphic sections with a memory and therefore a cyclic
             sequence.

M1

	1	2	3	4
1	////	0.00	0.67	0.33
2	0.00	////	0.11	0.89
3	0.56	0.11	////	0.33
4	0.23	0.62	0.15	////

P1

	1	2	3	4
1	////	0.10	0.00	0.90
2	0.00	////	0.17	0.83
3	0.09	0.00	////	0.91
4	0.59	0.12	0.29	////

L2

	1	2	3	4
1	////	0.21	0.00	0.79
2	0.00	////	0.25	0.75
3	0.00	0.12	////	0.88
4	0.67	0.00	0.33	////

Figure 3.15 illustrates the sequences obtained from the
analysis (Tables 3.4 and 3.5) for stratigraphic sections from
throughout the formation. Sections in the central region of
the outcrop area e.g. Mount Metschel (M1), Portal Mountain (P1),
the Lashly Mountains (L2) show a higher probability of cyclicity.
Section L2 contains the typical "fining-upwards" cycles (Allen,
1965c), initiated by a basal fine to medium sandstone grading
vertically into a very fine to fine sandstone overlain by fine
member units of green siltstone followed by a red siltstone and
a return to a green siltstone. The chi-square value of 16.79
gives a probability (P) of 0.03, indicating there to be 97

Table 3.5.   Tests for the probability of randomness of the deposited
             sequence of Aztec Siltstone in respective sections, based
             on the equation of Billingsley (1961).

	No. units	χ^2	Degrees freedom	Probability of randomness
A4	46	6.92	8	0.5
S.E.A.	83	9.16	8	0.3
A6	79	8.22	8	0.4
A1	43	0.54	5	0.99
A2	18	3.87	8	0.9
M1	40	27.36	8	<0.001
P1	72	16.32	8	0.04
L1	72	9.46	8	0.3
L2	47	16.79	8	0.02
B2	57	8.66	8	0.4
FL	67	4.65	8	0.8
H6	39	2.25	8	0.96

chances in 100 that the sequence is cyclic rather than random.
A sedimentological interpretation of the cycles in the Lashly
Mountain section (L2) is given in Chapter 7.

CHAPTER 4

SEDIMENTARY STRUCTURES

The Aztec Siltstone has a great abundance and variety
of sedimentary structures compared with the other Taylor Group
formations. Grouped together they provide valuable data for
paleogeographic and paleoclimatological interpretation.

The structures are discussed under a modified listing
of Pettijohn (1957 p.158). They are classified as organic
and inorganic with the latter subdivided into mechanical and
chemical. The chemical structures are concretions and nodules
(Pettijohn, 1957, p.200), and they have been further classified
using the Tarr and Twenhofel classification (Twenhofel, 1932)
into syngenetic and epigenetic varieties.

Inorganic Structures

MECHANICAL STRUCTURES

Stratification

Horizontally stratified sandstones are common in the
formation (Table 4.1; Fig. 4.1), and are generally laminated,
very thin bedded, or unbedded (common in the very fine sand-
stones) (Table 4.2). Many of these sandstones have a massive
splitting character (Table 4.4). The horizontally laminated
sandstones (generally very fine to medium grained) are
commonly associated with scour surfaces, cut and fill
structures and intraformational conglomerate, and belong
to the "flat-bedded" facies of Allen (1964b, 1965b, 1970),
and Allen and Friend (1968). Primary current lineation
(Allen, 1964b) is observable in some cases on the parted
lamination planes (Fig. 4.2), and denotes deposition by
unidirectional turbulent flow in the upper flow regime
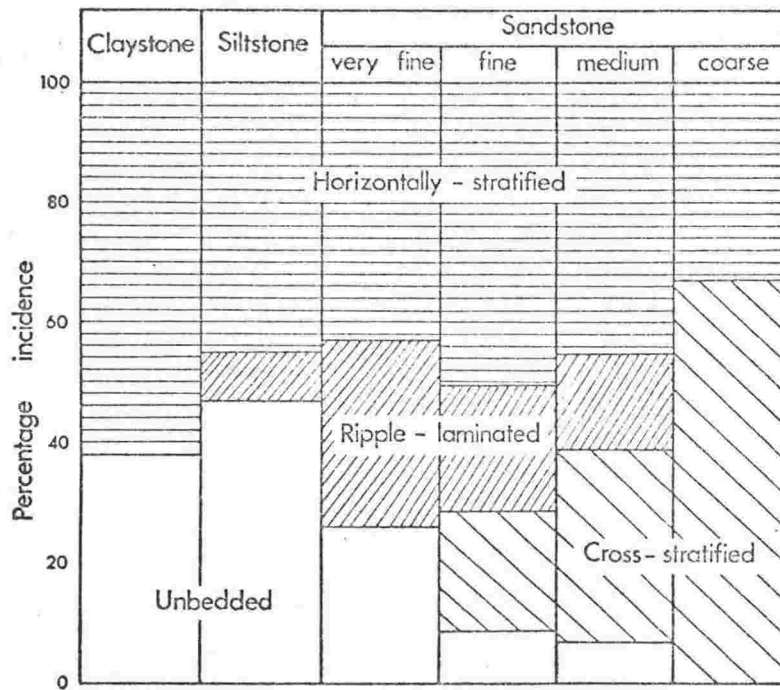
Fig. 4.1. Distribution of stratification structures with respect to size classes. Based on 493 observations.

Table 4.1 Frequency of occurrence of the internal structure of stratified units with respect to size classes.

| Internal primary structure of stratified unit | Percentage | | | | Siltstone | Claystone |
| | Sandstone | | | | | |
	Very fine	Fine	Medium	Coarse		
Horizontally stratified	43	50	45	33	45	62
Ripple laminated	31	21	16	0	8	0
Cross stratified	0	20	32	67	0	0
Unbedded	26	9	7	0	47	38
No. of observations	42	200	62	3	178	8

Table 4.2   Frequency of occurrence of the forms of stratification
             with respect to size classes.

| Horizontal stratification | Percentage | | | | | |
| | Sandstone | | | | Siltstone | Claystone |
	Very fine	Fine	Medium	Coarse		
Unbedded	38	15	12	0	52	38
Thick bedded	7	3	0	0	2	0
Thin bedded	7	8	12	0	7	12
Very thin bedded	24	20	16	0	11	0
Laminated	24	51	60	100	28	25
Thinly laminated	0	3	0	0	1	25
No. of observations	29	118	32	1	163	8

Table 4.3   Frequency of occurrence of the forms of cross-stratification
             with respect to size classes.

| Cross-stratification | Percentage | | | | | |
| | Sandstone | | | | Siltstone | Claystone |
	Very fine	Fine	Medium	Coarse		
Trough cross-beds	0	85	90	100	0	0
Planar cross-beds	0	10	10	0	0	0
Simple cross-beds	0	5	0	0	0	0
No. of observations	0	40	20	2	0	0

Table 4.4   Frequency of splitting characteristics with respect
to size classes.

Splitting property	Percentage					
	Sandstone				Siltstone	Claystone
	Very fine	Fine	Medium	Coarse		
Massive	46	46	48	100	34	0
Blocky	3	8	4	0	1	0
Slabby	6	18	19	0	6	0
Flaggy	0	12	10	0	2	0
Shaly-Platy	33	12	17	0	25	38
Flaky	3	3	0	0	22	8
Papery	3	0	0	0	6	54
Knobbly	6	1	2	0	4	0
No. of observations	33	184	69	3	214	13

(Harms and Fahnestock, 1965;   Allen, 1964b).

Ripple-laminated very fine and fine sandstones are common
(Fig. 4.1, Table 4.1) but ripple-marked surfaces are not so common.
Ripple-drift bedding (Kappa-cross-stratification of Allen, 1963a)
is common (Fig. 4.3), as are micro-cross-laminated (Nu-cross-
stratification of Allen, 1963a) units.   Sets of cross-strata
are of the order of 2 to 3 cm in size, but are grouped into
cosets up to 1 m thick.   Both are generated by the migration of
trains of asymmetrical ripples, the Nu variety resulting from
specifically small-scale linguoid ripple trains.   They are a
product of currents (hydraulically smooth) of the lower flow
regime, just competent to move grains along.

Cross-stratified sandstones (Table 4.1 and Fig. 4.1) are
large scale (greater than 5 cm) and in sets of 0.1 m to 0.4 m
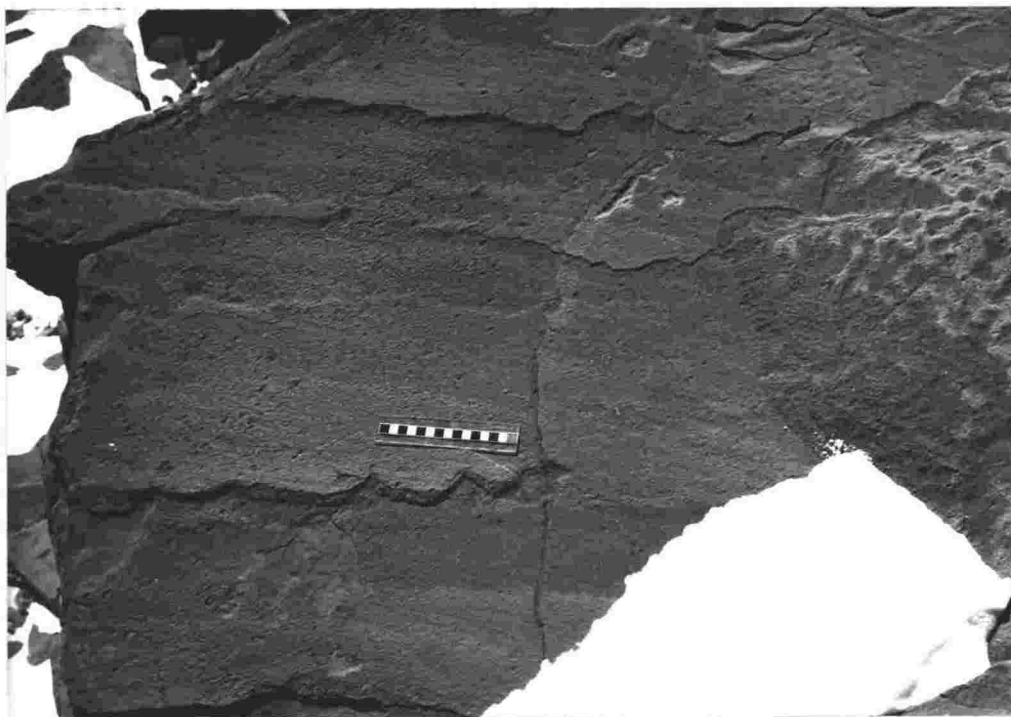
Fig. 4.2. Primary current lineation in a flat-bedded, fine to medium grained, coarse member, channel sandstone at L2, unit 25. Scale in cm.
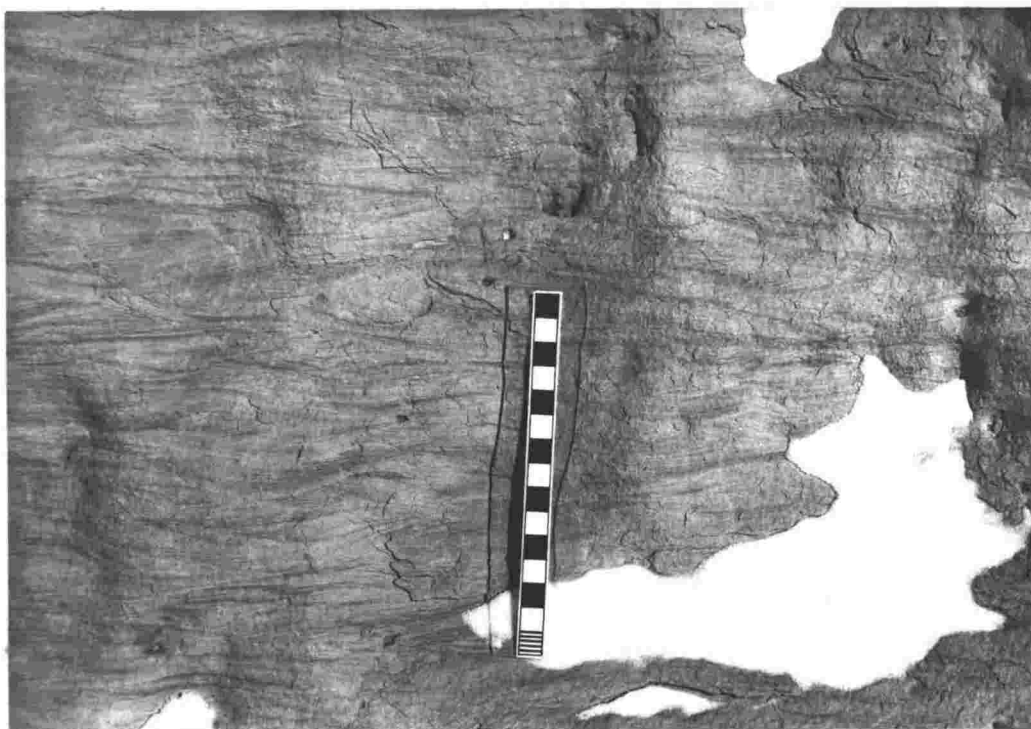
Fig. 4.3. Ripple-drift bedding (Kappa-cross-stratification of Allen, 1963a) in a very fine to fine grained sandstone at L1, unit 33. Scale in cm.

thickness, with a maximum coset thickness in the order of metres. They are largely the trough variety with minor planar cross-beds (Table 4.3). Cosets of cross-strata made up of sets (5 to 10 cm) of tabular or Omikron-cross-stratification (Allen, 1963a, p. 109) (Fig. 4.4) are common.

The large scale cross-stratified sandstones are generated by the migration of trains of large-scale ripples, and dunes, which are products of a turbulent flow in the upper part of the lower flow regime. They represent high flow intensities and high sedimentation rates, and are thus generally products of flood stage conditions on the flood plain.

The siltstones and claystones of the formation are mostly either unbedded (i.e. bedding greater than 100 cm), or are laminated (Tables 4.1 and 4.2; Fig. 4.1). Some thin bedding is present in alternating very fine sandstone and siltstone beds. Bedding is however often indistinct. The unbedded units are massive or flaky in splitting character, whilst the bedded units tend to be flaky or shaly (Table 4.4). Thus, the well laminated units are typically slope-forming, while the massive siltstones and sandstones develop a cliff and ledge topography.

Post-depositional colour changes in some siltstone and claystone units have obscured and clearly destroyed the bedding. This is shown by remnant patches of well-laminated greenish grey siltstone surrounded by uniformly greyish red unbedded siltstone in many units (Fig. 4.5). Here, irregular patches of the laminated greenish grey siltstone units have changed to a uniform greyish red leaving no trace of forming bedding.

Many of the siltstones and claystones show extensive bioturbation (see Chapter 4, Trace Fossils) which has been responsible for the obliteration of former bedding in some of the now massive units (Fig. 4.49). Extensive and repeated mudcracking, nodule growth, and other soil processes have also contributed to the destratification of the beds.

In a number of units of the formation (e.g. A1, unit 22; A2, unit 6), and in particular those associated with kankar ('caliche') deposits (Chapter 4, Nodules), were recorded
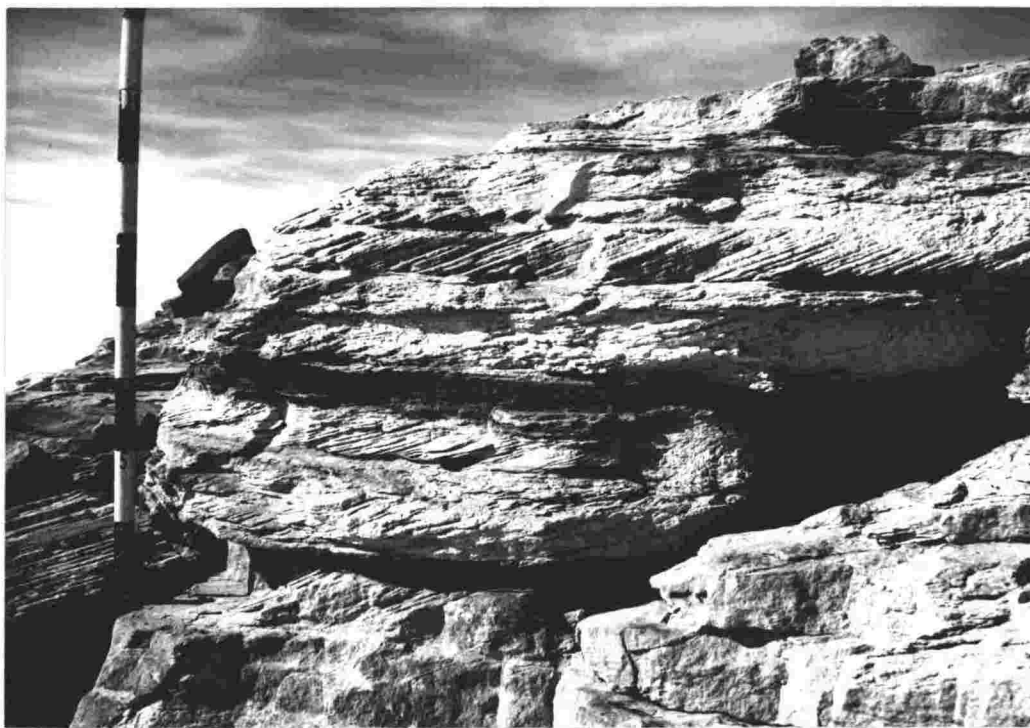
Fig. 4.4.   Cosets of tabular or Omikron-cross-stratification (Allen,
            1963a, p.109) in fine to medium grained sandstone at Al,
            unit 30.   Staff in dm.
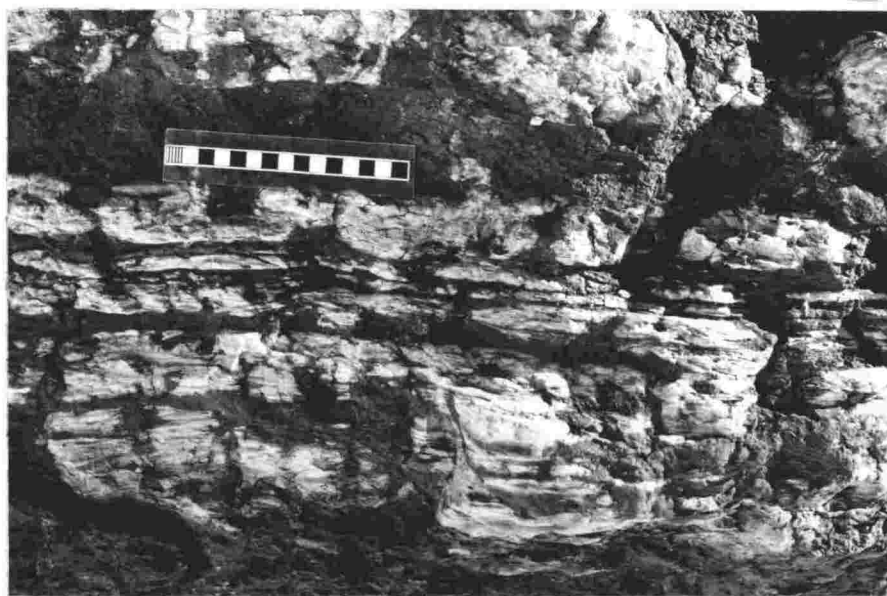
Fig. 4.5.   Spattered reddening which has partially obliterated bedding
            features in a former drab fine grained lithology.   The
            reddening resulted from the localized post-depositional,
            chemical redistribution of iron.   Scale in cm.

Fig. 4.6. Buckle cracks or pseudo-anticlines in a red, kankar nodule-
bearing, fine-grained unit at A2, unit 6. Staff in dm.

Fig. 4.7. Slumped foresets in laminated sandstone-claystone interbeds
at M1, unit 16. Scale in cm.

pseudobedding structures, composed of horizontal, wavy
"buckle cracks" (Fig. 4.6). Similar features in the Old Red
Sandstone have been termed pseudo-anticlines by Allen (1974a,
1974c). They are considered to have been caused by the bowing
and buckling of beds or lenses of sediment due to water loss
(Reeves, 1970, p.359, cf. plates 2A and 2B), and have been
widely recognized in modern kankar deposits, particularly in
playa sediments. Allen (1974a, 1974c) considers that they
are possibly comparable with the gilgai of certain soils of
hot sub-humid to semi-arid regions. Gilgai is the name given
to the wavy or hummocky surface developed on these soils and
is produced by seasonal wetting and drying and consequent
expansion and contraction of deep clayey soils.

Mechanical or gravity deformation structures are uncommon,
except for rare contemporaneous folding and thrusting at some
units displaying, for example, convolute bedding and slumped
foresets in alternating sandstone-claystone units (Fig. 4.7).

Ripple Marks

Asymmetric (including linguoid) and symmetrical ripple
marks are present at most localities but are common at only a
few. Asymmetric ripples are rare. Table 4.5 characterises
the ripple marks of the Aztec Siltstone. They are considered
to have formed in water, and are of both the wave and current
origin, based upon the Ripple Index and Ripple Symmetry Index
diagram of Tanner (1967, p.97, Fig. 1) (Fig. 4.8). The
symmetrical are all wave formed, produced by oscillatory
currents generated most commonly by waves in shallow, standing
bodies of water. The linguoid ripples record a gentle uni-
directional hydrodynamically smooth current in the lower flow
regime.

The symmetrical ripples are commonly found in thin sand-
stone interbeds in laminated siltstone or claystone units
(Fig. 4.9). In many cases, a layer of clay covering the
ripples is extensively mudcracked (Figs. 4.10 and 4.11).
This suggests that conditions altered rapidly within the flood-
plain.

Table 4.5. Characteristics of the ripples of the Aztec Siltstone

Location	Type	Wavelength (λ) cm	Height (h) cm	Ripple Index (λ/h)	Stoss Side (1a) cm	Leg Side (1b) cm	Ripple Symmetry Index (1a/1b)	Grain Size (mm)
A1, unit 26	Symmetrical	4.5	0.2	1:22.5	-	-	-	-
"	"	2.2	0.3	1: 7.3	1.2	0.9	1.3	0.0312 (5φ)
"	"	1.8	0.2	1: 9.0	0.9	0.8	1.1	0.0345 (4.85φ)
L1, unit 3	"	10.0	1.0	1:10.0	-	-	-	-
" unit 10	"	2.4	0.3	1: 8.0	1.2	1.2	1.0	0.0312 (5φ)
"	"	2.1	0.3	1: 7.0	1.1	1.0	1.1	0.0312 (5φ)
"	"	2.0	0.3	1: 6.7	-	-	-	-
"	"	3.0	0.5	1: 6.0	-	-	-	-
"	"	3.0	0.3	1:10.0	-	-	-	-
"	"	8.0	2.0	1: 4.0	-	-	-	-
"	"	12.0	1.0	1:12.0	-	-	-	-
" unit 27	"	4.0	0.5	1: 8.0	2.0	2.0	1.0	0.0740 (3.75φ)
"	"	2.0	0.2	1:10.0	-	-	-	-
L2, unit 11	Asymmetrical (Linguoid)	3.0	0.3-0.5	1:6.0-10.0	-	-	-	-
" unit 12	Symmetrical	3.4	0.3	1:11.3	-	-	1.0	-
"	"	23.8	1.7	1:14.0	12.0	11.8	1.0	0.163 (2.63φ)
" unit 24	"	0.24	0.05	1: 4.8	-	-	1.0	0.0495 (4.33φ)
B2, unit 4	"	3.0	1.0	1: 3.0	-	-	-	-
H6, unit 22	Asymmetrical (Linguoid)	10.0	-	-	-	-	-	-
S9, unit 6	Symmetrical	4.5	1.0	1: 4.5	-	-	-	-
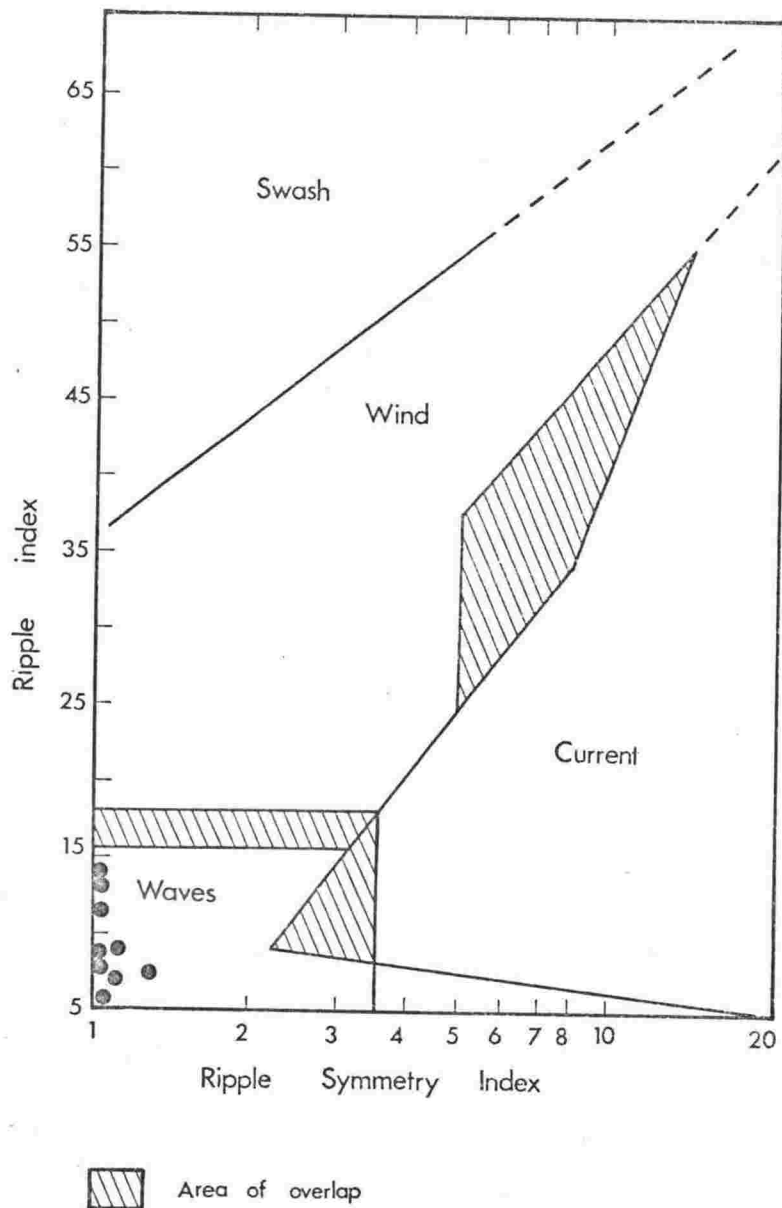
Fig. 4.8. Ripple Index versus Ripple Symmetry Index for the ripples of the Aztec Siltstone. Fields of ripple type are after Tanner (1967).

The palaeoenvironment for the creation of the symmetrical ripples was investigated using equations derived by Tanner (1971). Tanner produced a series of equations relating ripple-mark wavelength to grain size, water wavelength and water depth, with predictive abilities higher than 80 percent. His data
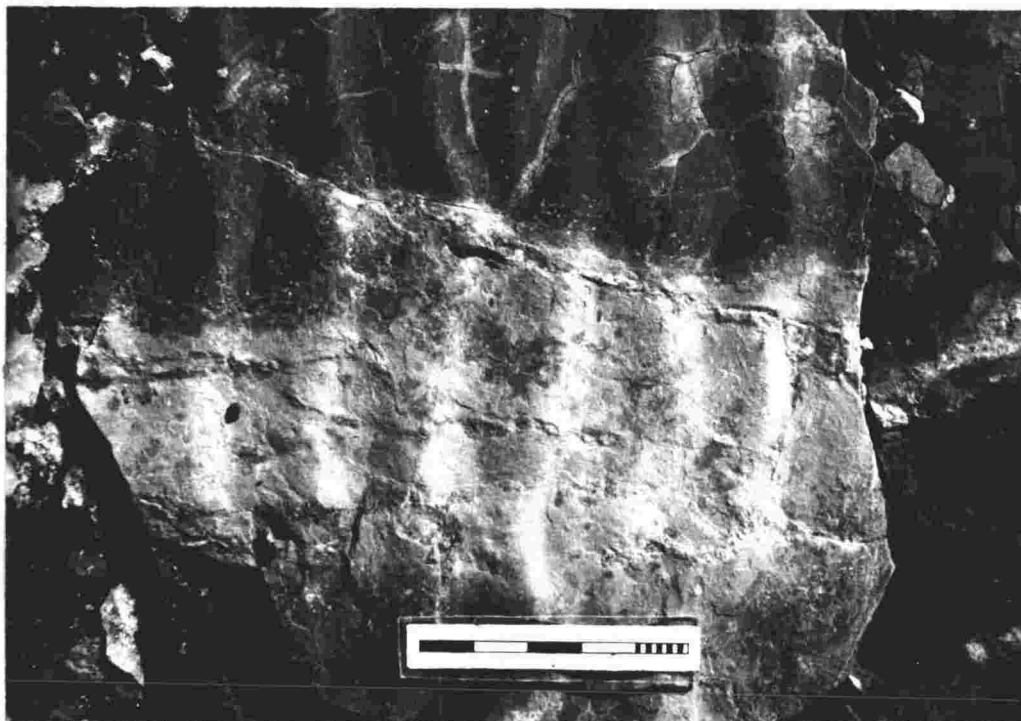
Fig. 4.9.   Symmetrical ripples from Al, unit 26.   Scale in cm and mm.
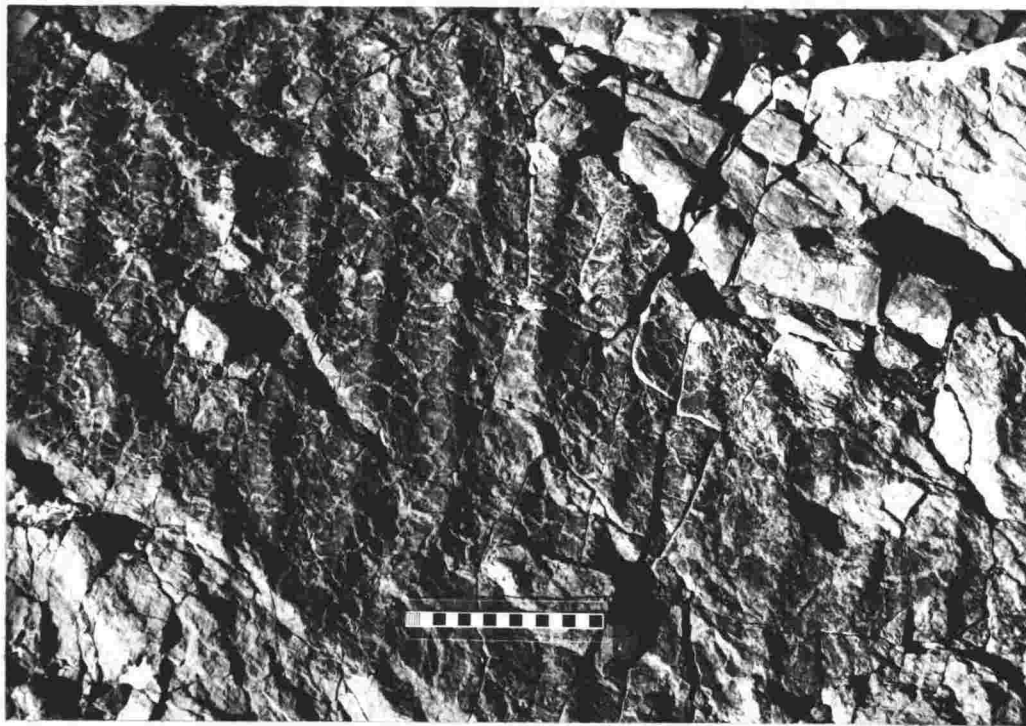
Fig. 4.10.   Symmetrical ripples at M2 which were covered with a veneer of
clay that cracked on drying.   Scale in cm.

Fig. 4.11. Symmetrical ripples at L2, unit 12. Mudcracks have formed
in clay veneer covering the ripples. Scale in cm.

was obtained from a study of modern examples in ponds, lakes
and seas, and an application to an ancient environment.

The equations used are:

For Water Wave Height:

$$H = 38.52 + 1.89s - 7.11 \ln g$$

For Water Depth:

$$\ln h = 22.74 + 0.97s - 3.72 \ln g - 0.41H$$

where

H = water wave height (cm).

s = ripple mark wavelength (cm).

g = grain size of the ripple marks (um).

h = water depth (cm).

The results (Table 4.6) show that the symmetrical ripple
marks in the Aztec Siltstone were produced in a relatively
shallow body of water, approximately 70 cm deep, by wind-induced
waves having a height of approximately 15 cm.

Table 4.6. Palaeoenvironment for the creation of the ripples
of the Aztec Siltstone, based on the equations of
Tanner (1971)

Location of Ripple Field	Wavelength (cm)	Grain Size (μm)	Water Wave Height (cm)	Water Depth (cm)
A1, Unit 26	2.0	33	17	92
L1, Units 3 and 10	2.2	31	18	100
L1, Unit 27	4.0	74	15	71
L2, Unit 24	0.2	50	11	47
Average	2.1	47	15	71

Tanner also showed that symmetrical ripples, which have an
average wavelength of less than about 5 cm, are indicative, with
fairly good reliability, of a highly restricted fetch. Thus, the
small average wavelength for the Aztec ripples (2.1 cm) suggests

that they were generated in a pond or small lake environment.

The symmetrical ripple marks of the Aztec Siltstone are
considered to have been produced in small shallow lakes, by wind-
induced waves approximately 15 cm high.

Rain Impressions

These were recorded on the crests of straight symmetrical
ripples from the Shapeless Mountain section (S9, unit 6)
(Fig. 4.12). They are considered to have formed either while
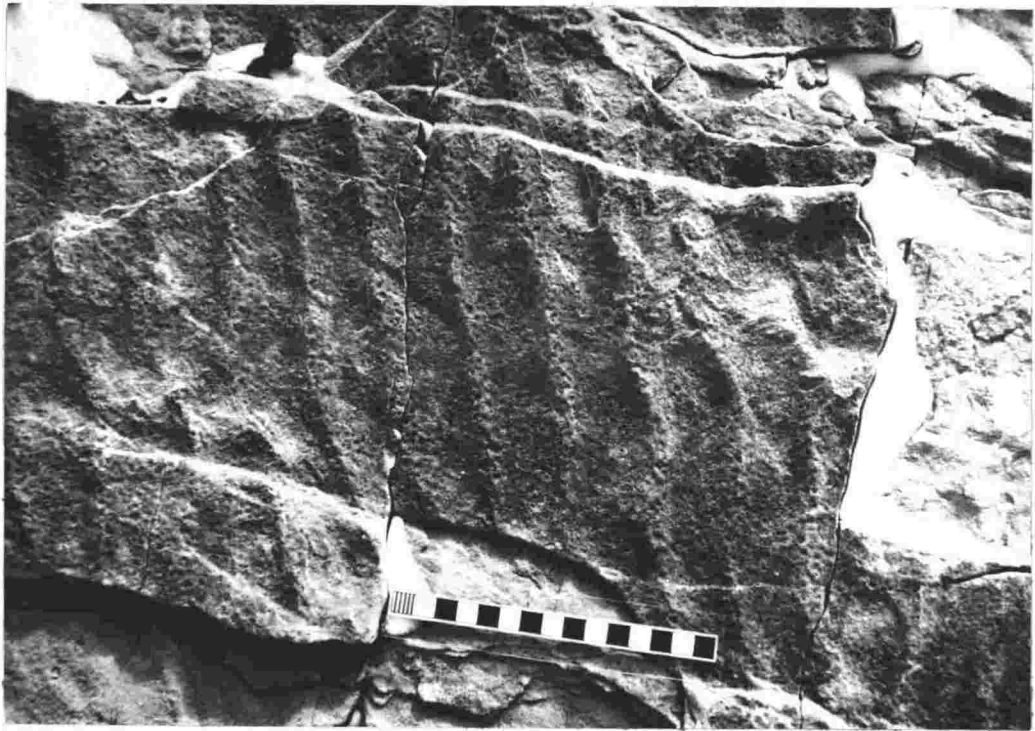
Fig. 4.12. Impressions of rain drops on the crests of straight,
symmetrical ripples at S9, unit 6. Scale in cm.

the troughs were filled with water and only the crests were
subaerially exposed, or when all were exposed, but the rain
filling the troughs obliterated the impressions. Rain

impressions are very common in seasonally arid or semi-arid
regions, and were observed by the author to be abundant
throughout central Australia in the sediments of pluvial ponds
and ephemeral streams.

Scoured Surfaces and Local Channelling

Sharp erosional surfaces between siltstone or claystone,
and overlying sandstone units are common throughout the Aztec
Siltstone (Figs. 2.1 and 4.13). These so called "scoured
surfaces" (Allen, 1962a, 1965b) can be traced laterally for
the extent of the outcrop, normally tens of metres. They
are broadly concordant with bedding, and have a mean local
relief in the order of centimetres, though a number reach
0.5 m. The surfaces locally truncate bedding and other
sedimentary structures (Figs. 3.7 and 4.14). The overlying
sediments are generally fine to medium grained sandstones,
often incorporating clasts of the eroded underlying unit
(Fig. 3.8). The intraformational conglomerate "channel
lag" (Chapter 3 p. 25) so produced is usually concentrated
in local channels, troughs, and lows in the erosion surface.

Scoured surfaces are generated by subaqueous
stream erosion immediately prior to the depositional phase
of the overlying and more coarse bed (Allen, 1962a, 1965b).
The lateral extent of the surface is due to the lateral
migration of the eroding force, i.e. the stream channel.
Such surfaces are a common product of cyclic, fluviatile
deposits, more especially those of high sinuosity stream
deposits, and have been best described for the Old Red Facies
of Great Britain (Allen, 1962a, 1965b), Spitsbergen (Friend,
1965), and the Catskill Facies of the Appalachians (Allen
and Friend, 1968). The cyclic sequences of the Aztec
Siltstone containing repeated scoured surfaces, are described
in Chapters 3 and 7.

Larger scale channeling is often seen developed in
units of the Aztec Siltstone. In some of the more massive
sandstone units, cut-off channels have been observed with
a depth in the order of 0.5 to 3 m, and a maximum width in
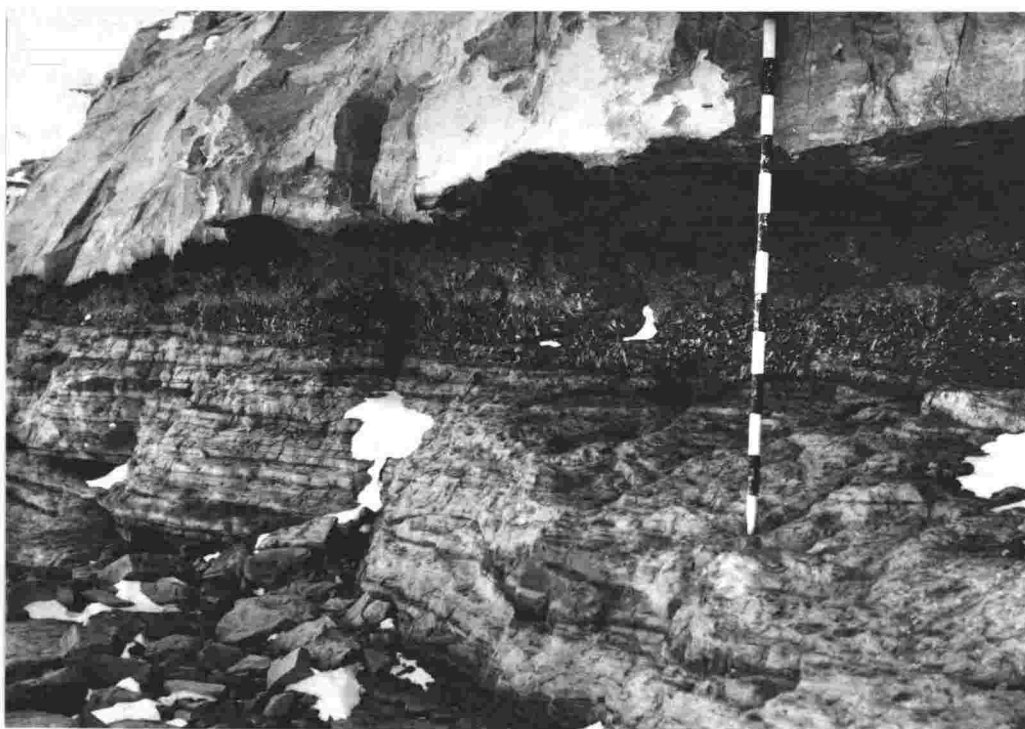
Fig. 4.13. A scoured surface at the base of a coarse member, channel
sandstone, at L2, unit 10. The erosional surface is cut
into a fine member, red, fine-grained unit. Note that the
fine-grained unit in contact with the overlying sandstone
has been reduced and is green. Staff in dm.
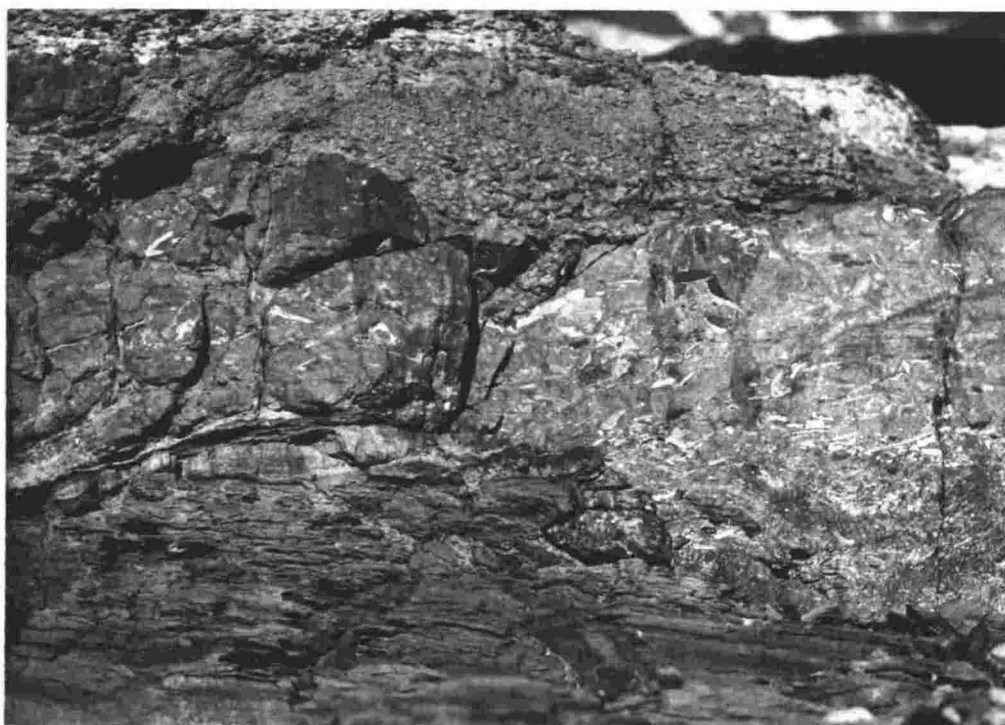
Fig. 4.14. A scoured surface eroded into a thinly laminated green siltstone
unit at M1. The channel sandstone which immediately overlies
the scoured surface contains an intraformational conglomerate,
or channel lag including locally reworked fish plate material.
Scale 5 cm = 0.25 m.

the order of 10's of metres (Fig. 4.15).

Fig. 4.15. A cut-off channel infilled with fine to medium grained
            sandstone, inbedded in a multistorey sandstone body. The
            section appears to be normal to the channel flow direction.
            Staff in dm.

Mudcracks

Polygonal mudcracks are abundant throughout the formation
(Fig. 2.1), in the upper portions of claystone and siltstone units
overlain by coarser grained siltstone, or sandstone. They occur
mostly in alternating claystone and fine sandstone sequences
for example, the Beacon Heights section (B2, unit 22), Aztec
Mountain (AZ, 42 m above the base) and Mount Fleming (FL, 45 m
above the base). They are preserved as coarse grain infillings,
i.e. sand casts (Figs. 4.16 and 4.18), or as tips of sand
fillings tracing out the shape of the polygonal cracks (Figs.
4.17 and 4.18).

Fig. 4.16.   Mudcracks which have been infilled by sand from the overlying
sandstone interbeds, L2, unit 10.   The fine-grained interbeds
are approximately 15 cm thick.
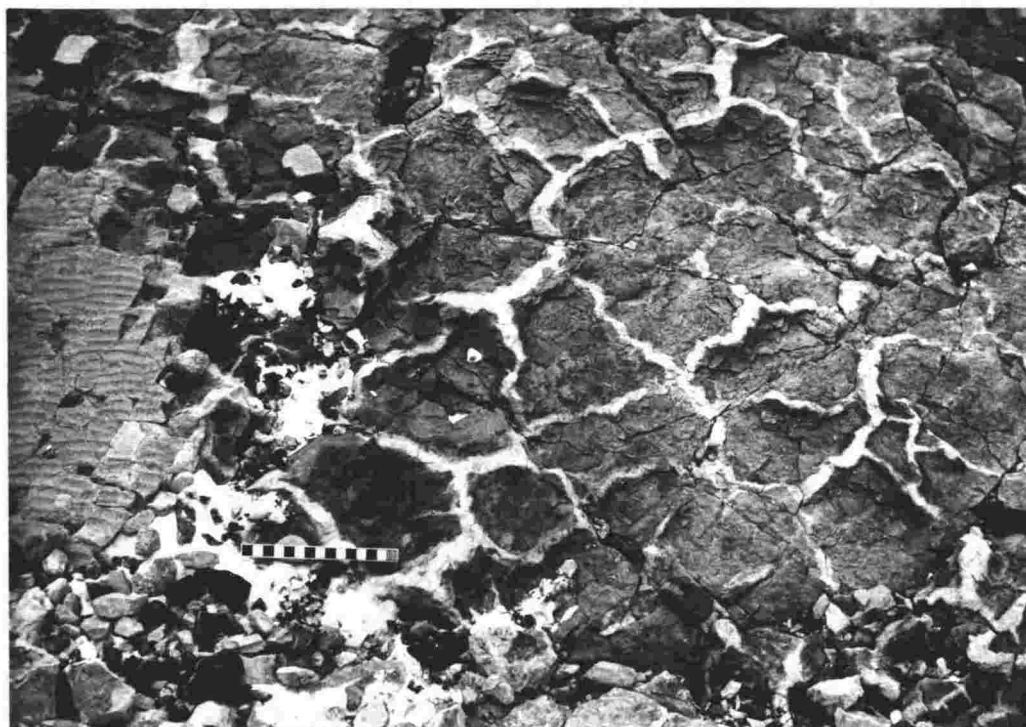
Fig. 4.17.   A mud-cracked pavement at M2.   Some small symmetrical ripples
overlie the mudcracks in the left of the photograph.   Scale
in cm.
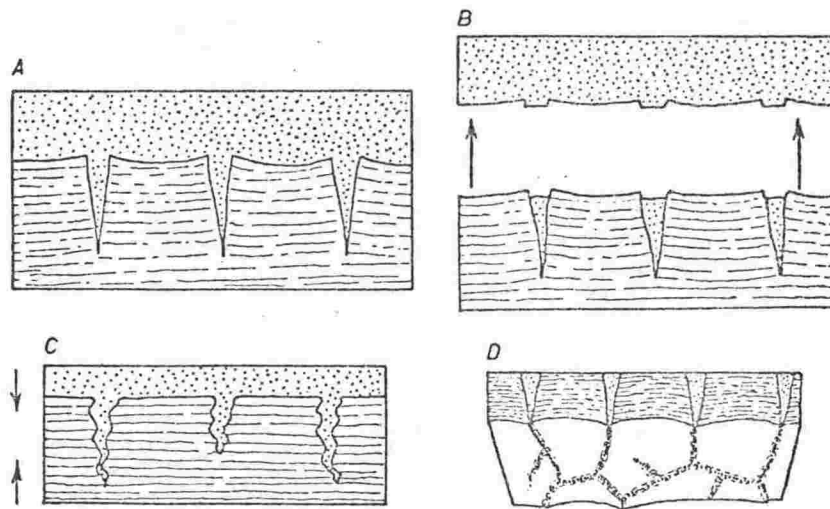
Fig. 4.18. Mudcracks and their infillings (Sherbon-Hills, 1963, p.20).

- A. Mudcracks filled and covered with sand.
- B. Sandstone separated from mudstone, showing broken casts of cracks on base of sandstone.
- C. Compaction of mud causes crumpling of sand-fillings.
- D. Tips of sand-fillings show as polygons on lower surface of mud.

Fig. 4.19. Mudcracks preserved as casts in a sandstone. The cracks are of two sizes; the larger are ½ cm wide and 10 to 15 cm across, whilst the smaller are 2 mm wide and 1 cm across.

The mudcracks mostly range from 1 mm wide and 5 mm across the polygons, to 1 cm wide and 15 cm across the polygons, but Webb (1963 p.373) reported examples with polygon widths up to 0.6 m across. Many show excellent preservation, with little deformation. Two orders of cracks have been noted at several places; the larger are ½ cm wide and 10-15 cm across, whilst the smaller are 2 mm wide and 1 cm across (Fig. 4.19). The smaller scale cracking is not so deep and is considered to have developed later than the larger (Twenhofel, 1932, p.688).

A unit within the Lashly Mountain section (L1, unit 12) shows in side profile, curled edges of mudcracks developed on thin claystone laminae within a massive fine sandstone (Fig. 4.20). An exposed horizontal surface displayed the usual mudcrack pattern. The preservation of such features requires a specific environment of deposition (Twenhofel, 1932, p.690). If a subaqueous deposit overlaid the mudcracks, the curled edges would be likely to rehydrate and collapse on contact with the water, or be destroyed by the erosive nature of the depositing currents. The latter case is the process which generates the mudcurls seen as intraformational conglomerate in many of the coarser grained units. To preserve curled mudcracks, a covering of rapidly deposited aeolian drift sand which could penetrate above and below the curls is required. Excellent modern day examples are reported by Glennie (1970 p.52) from arid and semi-arid regions. They were commonly observed in the process of formation and preservation in sand-bed ephemeral streams of central Australia by the author (Fig. 4.21).

The palaeogeographic implications from mudcracking as extensive as that observed for the Aztec Siltstone are significant. Mudcracks are developed wherever clayey sediments are exposed to the atmosphere for a considerable period of time. The cracking is due to the dehydration and subsequent shrinkage of clays in the deposit when desiccated by exposure. Although mudcracks are common in present day paralic and littoral marine environments, the fossil evidence of soils, nodules,
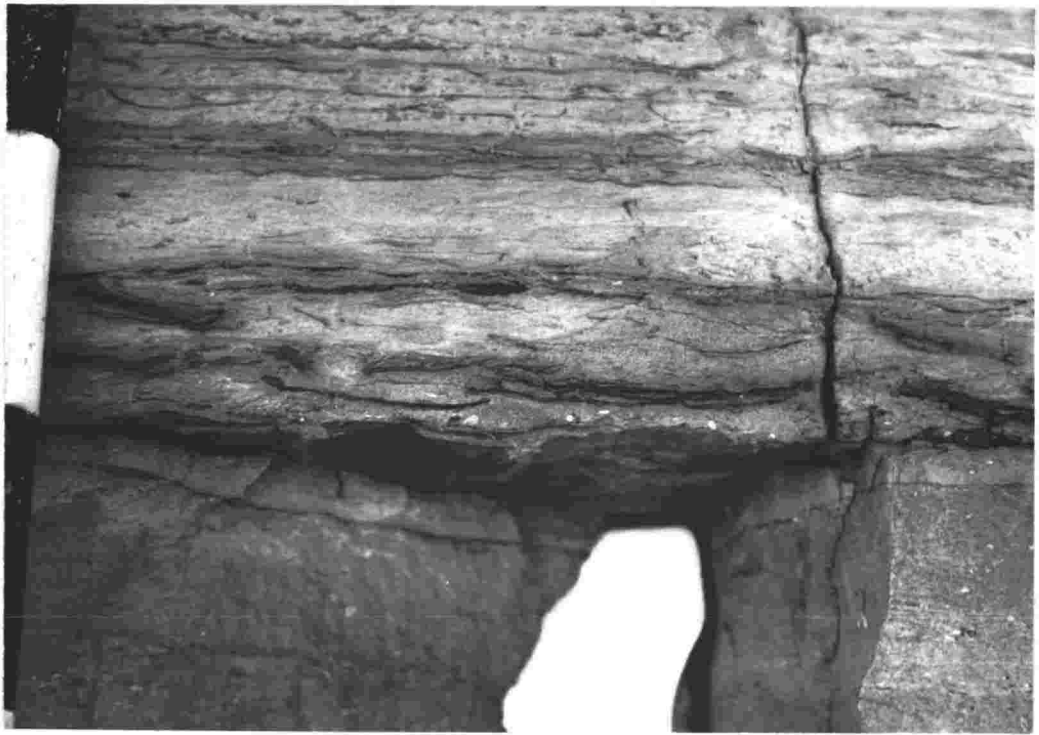
Fig. 4.20. A side profile view of curled edges of mudcracks developed on thin claystone laminae within a massive fine-grained sandstone. The curled edges have been preserved by being covered by aeolian drift sand cf. Fig. 4.21. Scale in dm.

Fig. 4.21. Mudcurls formed in an ephemeral stream bed in central Australia. A veneer of clay that was deposited as suspension load on the sandy stream bed by the 'dying' stream, has been desiccated and curled at the edges. Such structures are commonly covered and hence preserved by aeolian drift sand from within the dry stream bed. Note the hammer for scale.

conchostracans, and fish, and the oxygen, carbon, and strontium isotopes (Chapters 4, 6, 7, 8 and 9) shows that the formation was deposited under non-marine conditions.

Relatively high temperature, indicative of an arid climate was regarded by Kindle (1924) as an important factor in mudcrack formation, but Krynine (1935) showed that formation and preservation under humid climatic conditions was also feasible. Dunbar and Rogers (1957, p.199) noted that if the "mud is more or less calcareous, the $CaCO_3$ tends to set upon exposure to the air". As the finer lithologies of the Aztec Siltstone tend to be high in $CaCO_3$ (Chapters 5 and 6), this may have been an important contributing mechanism for formation.

Mudcracks in general are considered one of the best evidence for non-marine deposition (Dunbar and Rogers, 1957 p.200). Twenhofel (1932, p.691) noted that the best examples of mudcracks were developed on floodplains and deltas following flooding, or in ephemeral lakes of arid regions where the deposited silts and muds are subjected to desiccation upon recession of the depositing waters and consequent exposure to subaerial conditions. He noted that the process is favoured by a lack of vegetation, a medium by which water would be retained, and quoted the flood plain of the Tigris-Euphrates as a modern example. A similar depositional environment is proposed for the Aztec Siltstone.

Subaqueous Shrinkage Cracks

Shrinkage cracks were observed in a 6.2 m thick lacustrinal sequence located at Aztec Mountain (AZ-17, 5.4 m down from the Maya Erosion Surface). The sequence consisted of alternating fine sandstone or siltstone, and claystone units, containing ferruginous concretions, gypsum, black shales, and fossil fish. Shrinkage cracks were found in an alternating and laminated very fine sandstone or siltstone, light grey (N7), and a greyish black (N3) claystone (Fig. 4.22). The cracks are small scale structures (3 to 10 mm deep, and 10 to 25 mm across the top) consisting of vertical cracks in the claystone, infilled by coarse siltstone or very fine sandstone originating from the overlying lamina. Differential compaction accompanied

CM
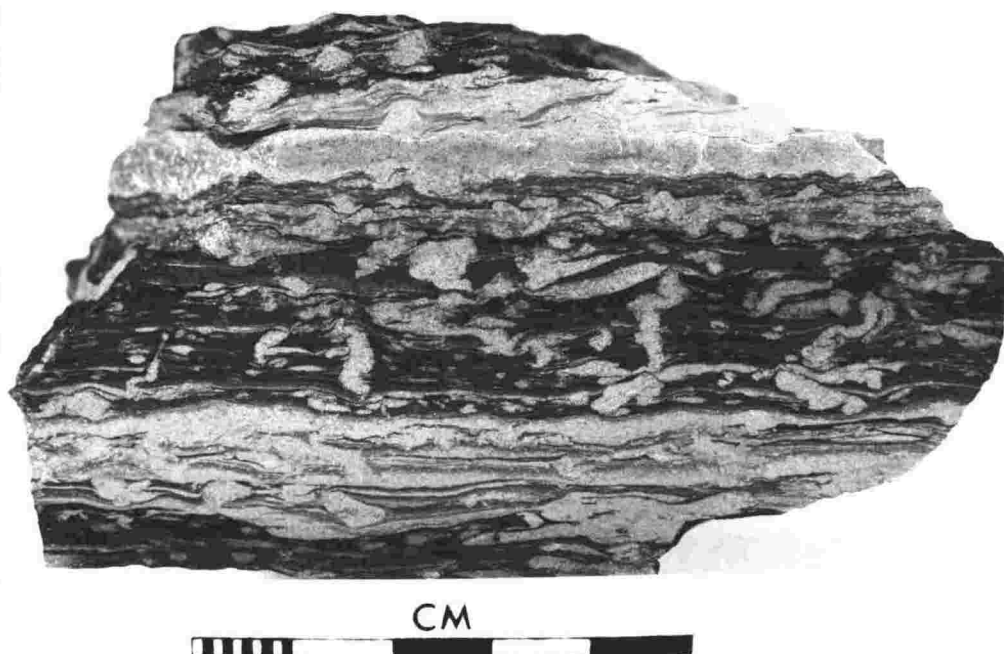
Fig. 4.22. Subaqueous shrinkage cracks in an interlaminated very fine
sandstone and claystone lithology, AZ-17, 30 m from the base.
The cracks have been infilled with coarse silt or very fine
sand, and have been distorted by differential compaction.

by some lateral displacement has folded (ptygmatic folds)
and distorted the cracks, and given rise to the bulbous shape.

The structures are identical in lithology and morphology
to the shrinkage cracks described by Donovan and Foster for
the Middle Devonian Old Red Facies of North East Scotland
(1972, p.309-317). They attribute the structures to
subaqueous shrinkage by a syneresis mechanism, and by
simulation demonstrated that they were developed in a
shallow but relatively large lake. Their formation was
attributed to salinity changes, a conclusion also reached
by Jungst (1934), Van Straaten (1954), and Burst (1965).
Subaqueous syneresis cracks are abundant in the Eocene Green
River Formation (Picard, 1966), and the Triassic Lockatong
Formation (Van Houten, 1964a). Burst (1965) suggested that
salinity changes related to seasonal climatic changes were
important. It is suggested that the Aztec shrinkage-cracks
are due to a syneresis mechanism in a lake that underwent
salinity changes in response to seasonal evaporation.
Marked salinity changes were very probable, for analcime,
which today is precipitated from saline lakewaters (Hay, 1966),

is found in the fine-grained sediments and pisolites of the formation (Chapter 5, Analcime, p.154). During the dry period, the evaporation increased the salinity, resulting in the syneresis of the greyish black claystone. The resultant cracks were then infilled by coarse siltstone or very fine sandstone which was deposited during the high sediment influx as the next wet period began.

Vein Networks

These structures were recorded from throughout the formation but are more abundant from the southern sections, beyond and including those in the Lashly Mountains (Fig. 2.1). They were not recorded by earlier parties, though re-examination of previously described sections has shown that vein networks are present. Vein networks occur almost exclusively in unbedded siltstone or claystone lithologies. Their form is a network of subvertical anastomising veins up to 5 cm wide and 50 cm apart, irregularly penetrating down for 0.3 to 1.5 m from the top of the unit (Figs. 4.23 and 4.24). They typically taper towards the base, and are generally composed of the same material as the overlying unit, commonly a channel sandstone (Chapter 7) (Fig. 4.25). However, in some cases the overlying and host units are of the same lithology and vary only in colour. The veins assume the colour of the overlying bed, generally a greenish grey (5G 6/1) in a greyish red (5R 4/2) host (Fig. 4.24).

Vein networks are generally associated with kankar ('caliche') horizons (Chapter 4, Nodules) and it was found that nodules increased in occurrence within the southern sections as do the vein network horizons. Either they were present together in the same horizon, or more commonly the kankar was found in the same bed but beneath the vein networks (Fig. 4.23).

These structures are thought to be, or to originate from, desiccation cracks, produced by clay contraction as a result of alternate wetting and drying. They are then preserved by infilling during the deposition of the overlying unit, or by reduction induced by solutions migrating down the crack paths from the above unit, or by both processes (Fig. 4.26).

Fig. 4.23. Vein networks in a massive, red, fine-grained unit at L1,
unit 26. Some veins were infilled with sand during
deposition of the overlying channel sandstone, and most have
acted as channels for the downward migration of reducing
solutions derived from the channel sandstone and are therefore
drab in colour. The vein networks are underlain by a horizon
of kankar ('caliche') nodules.
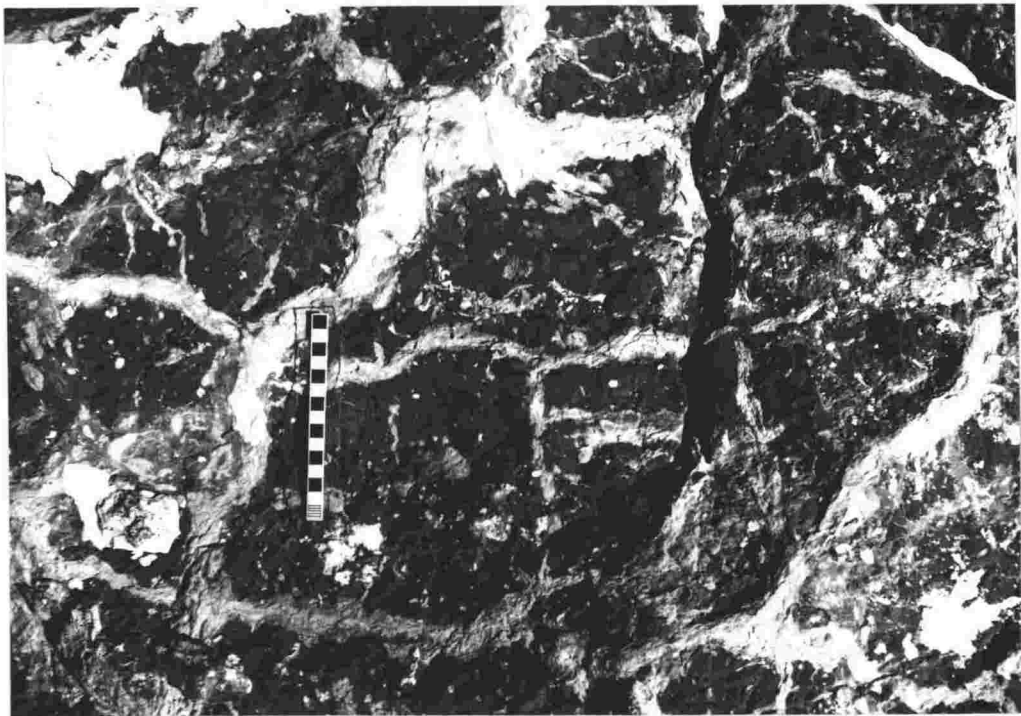
Fig. 4.24. Vein networks from L1, unit 26, close up. The green veins
have grey margins. Scale in cm.
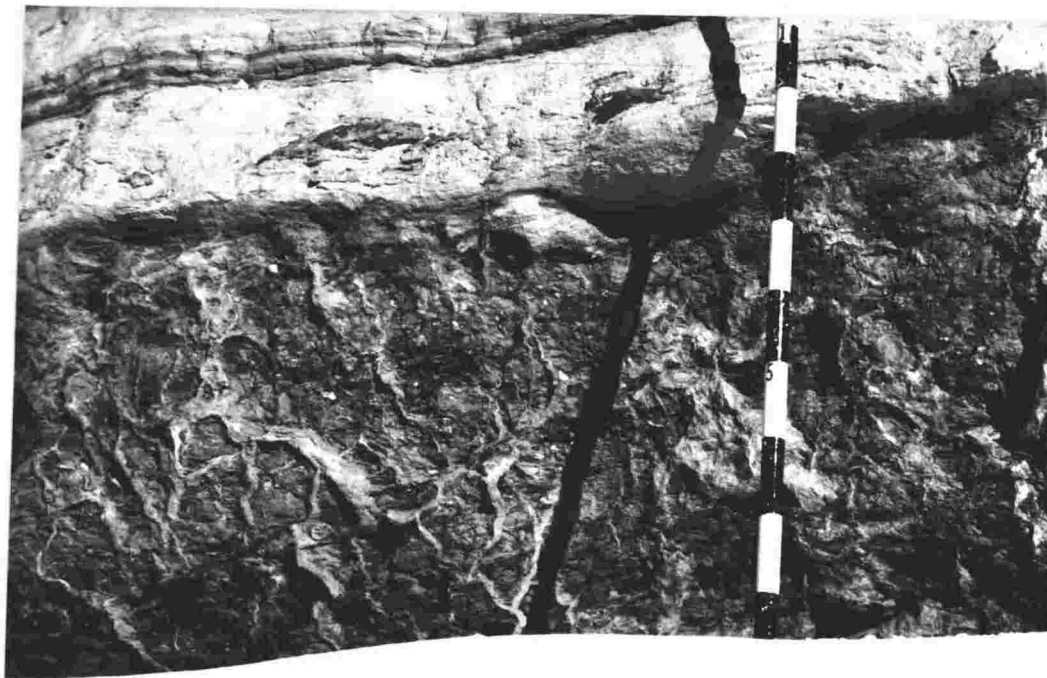
Fig. 4.25. Vein networks in a green siltstone unit, L1, unit 33. These typically taper toward the base and have been infilled with sand from the overlying unit. Staff in dm.
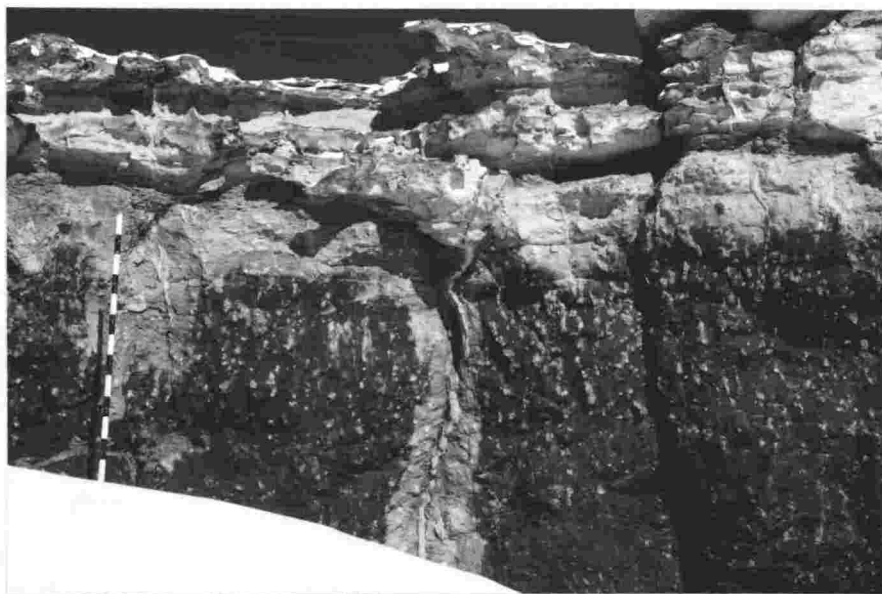
Fig. 4.26. Single veins in a massive, kankar ('caliche')-bearing, fine-grained red (soil) unit at AZ-17, 7 m from the base. The fine-grained unit is overlain (via a scoured surface, 10 cm above the staff) by a channel sandstone which has been the source of vein infilling, and reduction of the veins and adjacent host. Staff in dm.

The more extensive vein networks, are probably due to
repeated cracking as a result of successive periods of wetting
and drying of the deposit.

The rare vein networks in sandstone, are developed only
in units with a clay matrix in excess of approximately 15
percent. This is consistent with the view that the veins
are a desiccation feature.

Vertical cracking of this type is a common feature in the
fine grained deposits, including soils of deltas and flood
plains, in arid or semi-arid (preferably seasonal) regions.
Neal *et al.* (1968, p.70) reported similar desiccation fissures,
penetrating up to 5 m from the surface in former lacustrine
sediments in an arid playa environment. White (1972)
described desiccation fissures in the soil of playa-like
depressions, and observed that cracks of from 1.5 m to 2 m
deep developed in soil from 2 to 3 m thick. He noted that
their characteristics, i.e. size and depth, were determined
by soil texture, depression flooding rate, and depth of drying
and wetting. Also, that major cracks were wider in clay soils
than in coarser-textured soils, and increased in size with
thickness of the soil. The uniformity of spacing between
cracks and the crack width increased with the number of cycles
of wetting and drying the soil had undergone.

Cracking however may or may not be completely a surface-
controlled feature, and it is thought that many of the vein
networks described here are similar to the gammate and
reticulate veins (net-gammate) (Taylor and Pohlen, 1962,
p. 81-82) developed in the clay rich fragipan or B horizons
of Palliform soils (yellow-grey earth, zonal soils) (Figs.
4.27 and 4.28). These structures are produced when the soils
are exposed to a pronounced seasonal drying in sub-humid or
semi-arid areas. The gammate veins are commonly gleyed and
leached of iron, thus assuming a greenish grey reduction colour.
This is the typical colour of the veins of the Aztec Siltstone.

The association of vein networks and kankar horizons is
not unexpected since the conditions for formation of both are
similar, especially climate. Both are products of soils of
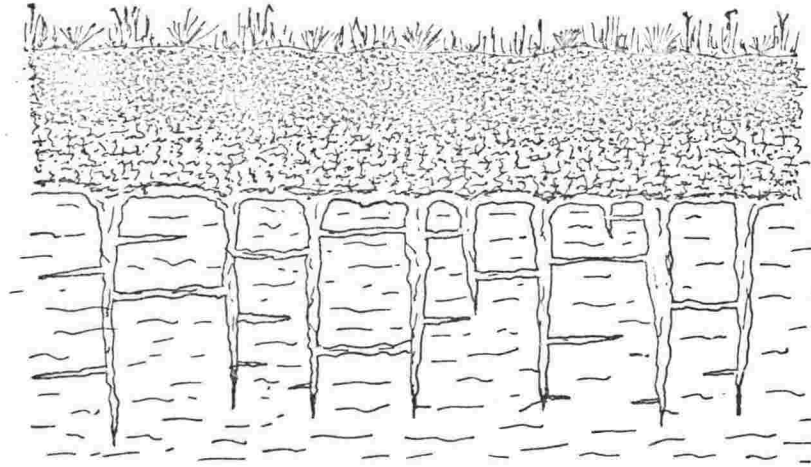
Fig. 4.27. The characteristic form of net-gammate structures (vertical veins surmounted by reticulate veins) in the lower and clay-rich horizons of Palliform soils (yellow-grey earth, zonal soils) which have been subjected to pronounced seasonal drying.
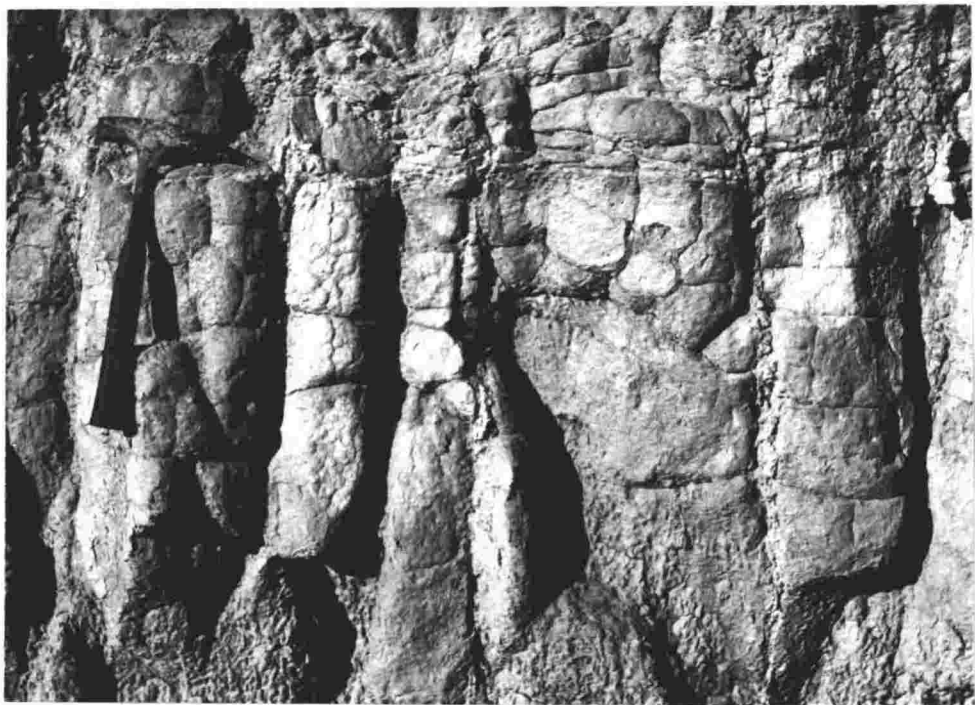
Fig. 4.28. Net-gammate structures in Palliform (yellow-grey earth soils) of the Wairarapa plains, N.Z. Hammer is 33 cm long.

strongly seasonal and generally semi-arid to arid regions
(annual precipitation less than 65 cm) (Chapter 4, Nodules).
Also, cracking is characteristic of the upper portions of
soil profiles, whilst the calcareous nodular horizons are
generally restricted to the lower parts, which is the normal
observed order in the Aztec Siltstone (Fig. 4.23).

Twenhofel (1932, p.691) in discussing structures similar
to vein networks, suggested that repeated cracking and
subsequent infilling by material identical to the host,
would, after several years, knead and mix the deposit so
thoroughly, that a total loss of stratification could result.
This process may have destroyed the bedding in some of the
presently unbedded siltstone or claystone units of the Aztec
Siltstone. However, many of the fine-grained units may never
have had a visible depositional bedding form i.e. they are
unstratified deposits.

CHEMICAL STRUCTURES

A distinction in form is normally made between nodules
and concretions. Both are composed of an aggregate of mineral
matter unlike and generally harder than that of the host rock
in which they occur, but whereas nodules are highly irregular
and tuberous, concretions are more regular i.e. spherical,
spheroidal, or disk-shaped, and commonly accreted about a
nucleus sometimes with a concentric structure (Pettijohn, 1957).
The classification of nodules and concretions used in this
thesis, was proposed by Tarr and Twenhofel (Twenhofel, 1932,
p.705-706), and is based upon the time relations to the
enclosing rock. It is as follows:

Syngenetic:	Nodules and concretions formed contemporaneously with the host i.e. before burial.
Epigenetic:	Nodules and concretions formed after deposition of the host. These are further divided into displacive and replacive varieties, depending upon the state of the host.

Nodules

Nodules are a common and distinctive feature of the
siltstone and claystone lithologies of the Aztec Siltstone.
They are widespread at all levels in the formation, but are
more abundant in sections south of Beacon Heights (Fig. 2.1).
In morphology, they are highly tuberous (Fig. 4.29), and have
a characteristically warty or knobby surface. They impart
this character to weathered rock faces wherever they occur.
The nodules are generally scattered evenly throughout an
entire unit, varying from 1 to 50 percent of the unit by
volume (Figs. 4.30, 4.31). In some cases they are concentrated
into horizons where they may be in a high concentration (up to
80 percent by volume of the bed). In some examples of the
latter case, it can be seen that individual nodules have
coalesced by thin linkages of nodular material, forming a
network. At a unit in the Aztec Mountain section (AZ-17,
unit 5), nodules have developed in vertical stringers (Fig.
4.35)

Nodules have a relationship to vein networks in that they
are commonly found concentrated in horizons directly underlying
extensive vein network systems e.g. Fig. 4.23.   '

Nodules are evenly distributed in both red and drab,
fine-grained lithologies. They do not precisely follow bedding
planes, but in a small number of cases, they show some minor
extension in a direction parallel to bedding, probably due to
a compaction effect.

Compositionally the nodules tend to be consistent within
and between sections (Tables 5.7 and 5.9). All are calcareous,
with a compositional variation arising from a percentage of in-
cluded host material, and in some cases from metamorphic minerals
produced by nearby dolerite intrusion. Most nodules are composed
largely of calcite (Table 5.7) in a disseminated, cryptocrystal-
line (less than 10 microns) form, and dissected by veins of well
crystallized (greater than 50 microns) calcite or crystallaria
(Brewer, 1964, p.284) (Fig. 4.32). Dolomite was not recorded.
The nodules are in some instances bordered by an epidote rich
zone (1/2 to 2 mm thick) (cf. Fig. 4.40), which in the case
of the smaller nodules may be spread throughout. The epidote,
pale yellow-green and in euhedral crystalline form (Fig. 4.33)
is a contact metamorphic product (Chapter 5 p.158). The
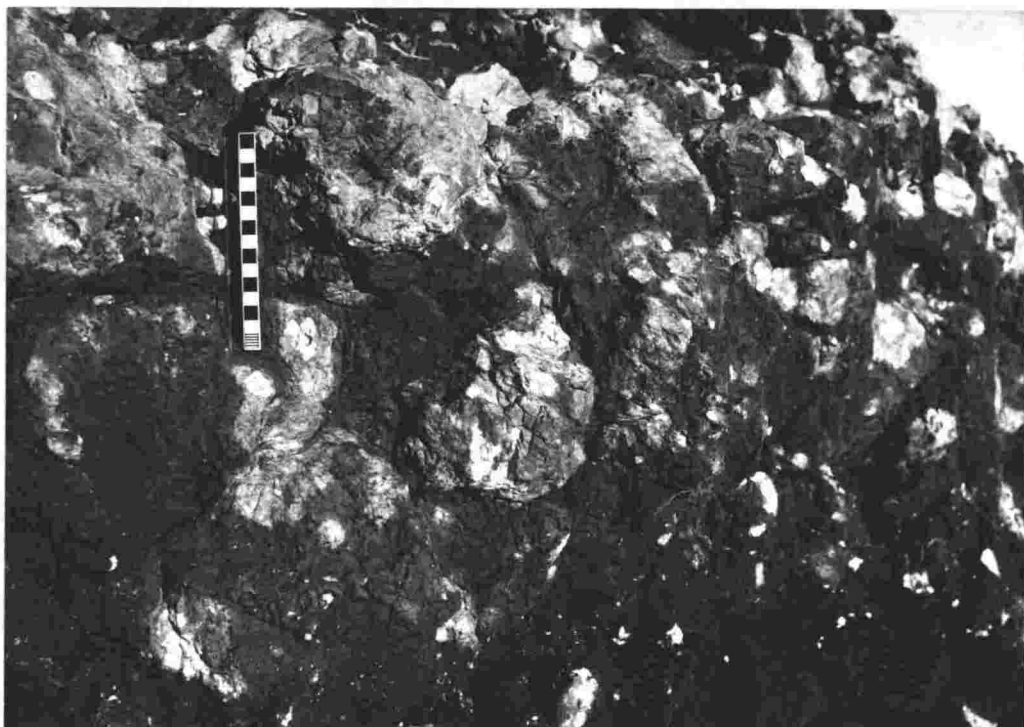
Fig. 4.29. Calcareous nodules (kankar) in a massive red fine-grained
lithology (M1, unit 19), exhibiting their typical tuberous
form. Scale in cm.

Fig. 4.30. Calcareous nodules (kankar) scattered throughout a massive
red fine-grained unit at L2, unit 9.
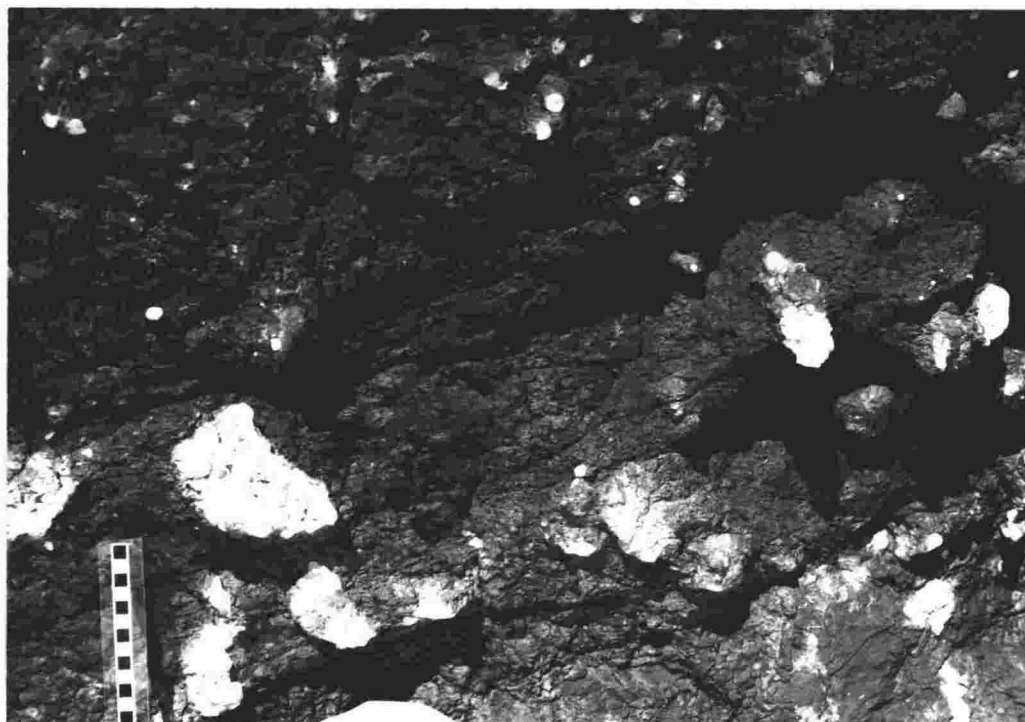
Fig. 4.31. Calcareous nodules in a massive red fine-grained unit at AZ-17, 7 m from the base. Scale in cm.
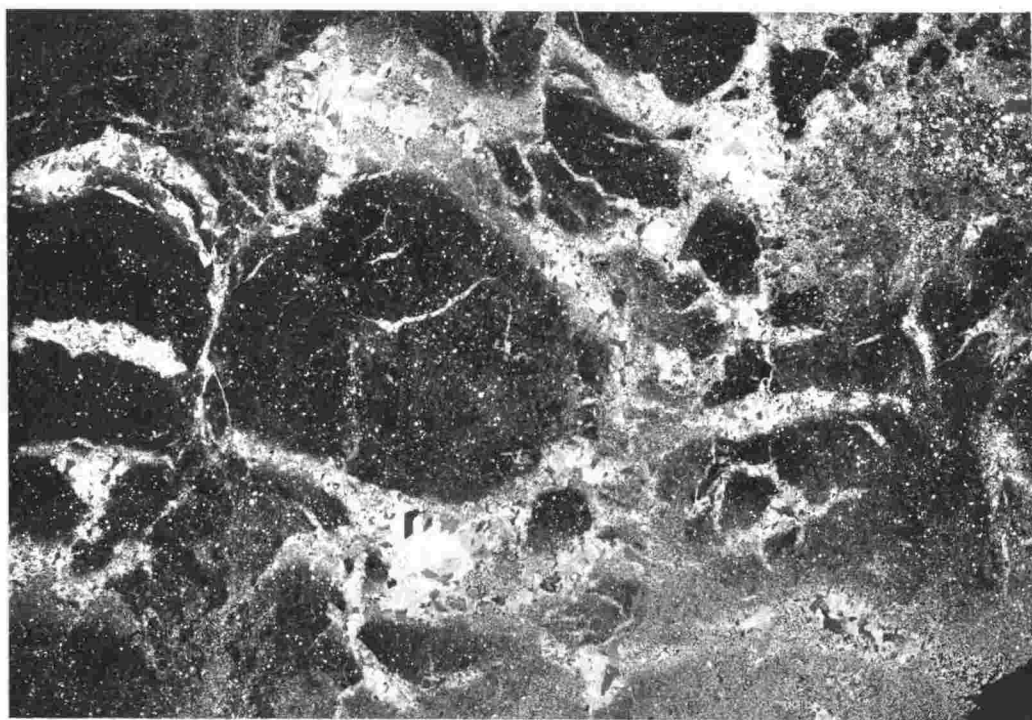
Fig. 4.32. Calcareous nodule (kankar) in thin section, showing zones of cryptocrystalline calcite surrounded and dissected by veins and patches of well crystallized calcite, or crystallaria of Brewer, 1964. The calcite incorporates host material including quartz grains, haematite and clays. Polarized light. Scale 5 cm = 10 mm.

Mount Metschel section (Ml), has undergone more extensive metamorphic alteration because of a 200+ m-thick sill above, and the calcareous nodules there show extensive replacement due to contact metamorphism, with abundant epidote and lesser amounts of prehnite, laumontite, and grossular (Tables 5.7 and 5.9).

Most nodules have incorporated some host material, generally less than 15 percent by volume, with the calcite (Fig. 4.32). This includes haematite pigment, which was present in many nodules contained within drab units. The host material can be identified from the similarities in grain size, shape, and mineralogy, to the surrounding host. The host material, and notably the clastic quartz grains are commonly concentrated around the margin of the nodule. The enclosed quartz grains commonly show corrosion at their margins and replacement by the calcite matrix. In many examples, the included host material (including haematite in some examples) is also concentrated into veins and patches throughout the calcite, suggesting a fissuring of the nodule sometime after formation (samples 23228, 23237, 23436) (Fig. 4.32) but prior to lithification of the surrounding sediment.

The nodules are considered to be epigenetic (Tarr and Twenhofel, 1932, p.706) i.e. formed after deposition of the enclosing sediment. The delicate vertical linkages between nodules, the incorporation of host material, and the fact that the nodules do not precisely follow bedding planes, all indicate that the nodules are not of a syngenetic origin. They probably formed close to the surface of recently deposited sediment. The best evidence comes from a bed at the Alligator Peak section (Al) that is laterally equivalent to unit 22. This bed has nodules that appear abraded and look as though they were deposited along with the enclosing sediment (Fig. 4.34). It is suggested that they were eroded from an earlier overbank deposit in which they had formed pene-contemporaneously, and were deposited as pebbles in the bed in which they are now found.

Other evidence to support this epigenetic origin of nodules is the relatively low percentage (less than 15 percent)

Fig. 4.33. Epidote in thin section, from the epidote-rich border that
surrounds nodules in sample 23233, A1, unit 1. Plain light.
Scale 5 cm = 0.24 mm.

Fig. 4.34. Redeposited calcareous nodules in a fine sandstone unit at
A1 (laterally equivalent to unit 22). Note how the burrows
deviate around the nodules. Scale in cm and mm.

of included host lithology. If the nodules were of a late
epigenetic origin i.e. diagenetic, they would be expected to
incorporate much more of the host as they grew. It is
suggested that the relatively pervious nature of unconsolidated
sediment, and the low load pressure, permit freer diffusion
of the calcareous fluids forming the nodules, and enable the
growing nodule to displace the clastic quartz grains of the
host. They are therefore of the epigenetic and displacive
variety (Tarr and Twenhofel *op.cit.*).

In a few instances, burrows were observed to deviate
around nodules (e.g. A1, units 10 and 11, see also Fig. 4.34)
indicating that the nodules had taken on their present form
while they were within a few tens of centimetres of the
sediment surface.

A unit in the Aztec Mountain section (AZ-18, 20.3 m
up from the base of the Aztec Siltstone) considered to be a
palaeosol on the basis of its unbedded character, vein networks
and calcareous nodules, has nodules (glaebules in the soil
micromorphological terms of Brewer, 1964) which are developed
in vertical stringers (Fig. 4.35). This is the growth form

Fig. 4.35. Calcareous nodules (kankar) developed in vertical stringers
(AZ-17, 7 m from the base) suggesting that they formed from
the vertical migration of calcareous solutions. Scale in
dm and cm.

expected of nodules resulting from the vertical migration of
calcareous solutions, and the characteristic pattern of many
soil nodules.

In summary, the calcareous nodules of the Aztec Siltstone
are pedogenic features. They developed under the influence of
normal weathering and pedogenic processes in subaerially
exposed overbank sediments (Chapter 7) subject to a strongly
seasonally, semi-arid to arid climate. They are commonly
associated with other pedogenic features e.g. vein networks,
extensive burrowing, a typical soil chemistry and micro-
morphology, and root structures, all of which are discussed
in Chapters 4, 5 and 6.

Modern Analogues

The calcareous nodules of the Aztec Siltstone have modern
analogues in the Pedocal soils of many parts of the world. As
pedogenic nodules, both the modern and ancient examples are
best referred to as kankar ('caliche') (Heath, 1965).
'Caliche' is the term used by many North American geologists
to denote soil carbonates, but unfortunately it is also
recognized as a term for the sodium nitrate-rich soils and
deposits of Chile and Bolivia. Calcrete is a term widely used
in Australia and South Africa for calcium carbonate deposits,
but it is not specifically restricted to soil carbonates. The
Hindi work "kankar" is used specifically for pedogenic calcium
carbonate nodules, and is derived from the Sanskrit "karkara"
meaning "hard". It is unfortunate that the term "kunkar" has
been used in South Australia for Quaternary soil carbonates,
as the spelling does not conform to current geological usage
in India from whence the word was imported.

Kankar is formed in a soil profile where upper-zone
solubles are carried downward and precipitated when soil
moisture is removed by evapo-transpiration, some underlying
solubles initially rising with capillary water (Reeves, 1970,
p.354).

$$CaCO_3 + H_2CO_3 \rightleftharpoons Ca^{2+} + 2HCO_3^{2-}$$

soil carbonate $\uparrow\downarrow$

$$H_2O + CO_2$$

rainwater   atmosphere
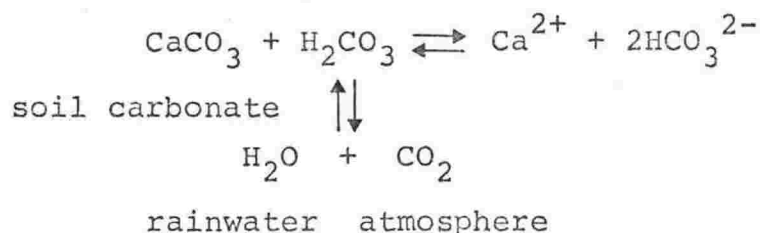
The ideal conditions for this process are those providing relatively high rates of evapo-transpiration, and low precipitation so as not to lose the highly mobile Ca^{2+} ion from the profile. However, there must be sufficient soil water to carry the dissolved products to depths. It is found that the depths below ground surface at which the kankar is formed is proportional to annual precipitation (Jenny, 1941; Krauskopf, 1967, p.200). Reeves (1970) suggested that highly seasonal climates provide the most suitable conditions for formation.

Kankar is most common in modern soils of arid and semi-arid regions of the earth, and is the characteristic product of Pedocal soils. The latter are defined as soils in which, regardless of the presence or absence of lime carbonate in the parent rock, lime carbonate (and/or sulphate) has accumulated in the soil during the process of soil-making and as a result of the soil-forming processes (Marbut, 1951). Pedocals occupy some 43 percent of the present land surface, and are generally confined to regions receiving less than 65 cm of precipitation annually.

Soil carbonate accumulates by illuviation (Buol, 1965; Gile *et al.* 1966; Gile, 1970; Reeves, 1970) and "accretes about skeletal grains as more or less independent domains, leading to separation of the grains, and, necessarily, creation of inter-grain regions of nearly pure carbonate" (Gile *et al.* 1966, p.356). The resultant external morphology and internal fabric of the nodules of modern kankar (Buol, 1965; Gile *et al.* 1966; Gile, 1970; Reeves 1970; Williams and Polach, 1971) is very similar to that seen in the Aztec Siltstone examples; the cryptocrystalline (less than 10 microns) calcite containing veins of well crystallized (greater than 50 microns) calcite,

the similar clastic grain displacements, and the veins and patches of included host (s-matrix, Brewer, 1964).

The kankar of the Aztec Siltstone closely corresponds to stages II and III of the Gile et al. K fabric genetic sequence (Gile, et al. 1966, p.352), and to the late youth and mature stages of Reeves (1970, p.355-357). Both genetic sequences were proposed for modern kankar deposits, and the authors found that an age in excess of 5,000 years is required for the formation of nodules belonging to these stages. Extensive calcareous duricrusts were reported for stage IV (old), and gave ages for formation of at least 50,000 years. Such features were not recorded in the Aztec Siltstone.

The source of carbonate for modern kankar is found to be either a calcium-bearing parent rock, or an aeolian distributed calcareous dust (Gile, et al. 1966; Gile, 1970; Reeves, 1970). Carbonate loess is particularly important in arid environments, as indicated by the presence of thick kankar profiles on the downwind side of the world's major deserts (Reeves, 1970, p.355). Reeves estimated that between 16 and 31 tons of carbonate per acre have fallen around Las Cruces, New Mexico, during the last 10,000 years.

For the Aztec Siltstone, the source could have been either parent rock or loess or both. The original parent rock for the Lower Taylor Group sediments and possibly at least some of the Aztec Siltstone, is a basement complex of plutonic, metasedimentary, and metavolcanic rocks, with a high proportion of Ca feldspars; Koettlitz Marble of Blank et al. 1963. In addition, the soil profiles of the Aztec Siltstone were developed in floodbasin deposits which were subaerially exposed for considerable periods (Chapters 4, 7, 9 and Conclusions), thus presenting likely depositional sites for calcareous loess generated during the more arid times.

The thick, kankar profiles which are very common in the Aztec, are considered to have formed under aggrading soil conditions (Reeves, 1970), with the added sediment derived largely from intermittent overbank floods, but possibly also from the aeolian redistribution of sediment. Under a strongly

seasonal climate, the free-draining subaerially exposed overbank
fines, would undergo carbonate precipitation at depth in the
profile during the hot dry period, and calcite solution and
eluviation during the wetter period, in some cases also
accompanied by further sedimentation.

The kankar of the Aztec Siltstone is closely comparable
with the carbonate palaeosols reported from similar fluviatile
and lacustrinal sequences. They have been described from the
Catskill-Old Red Facies in the central Appalachians by Woodrow
(1968), Allen and Friend (1968), Fletcher and Woodrow (1970)
and Walker (1971); from the Late Devonian Perry Formation of
Maine by Schluger (1971); from the Old Red Sandstone by Burgess
(1961), Allen (1965b, 1974a, 1974c) and Leeder (1973b); from
the Wood Bay Formation of Spitsbergen by Friend and Moody-Stuart
(1970); from the New Red Sandstone by Bruck et al. (1967)
and Steel (1974a, 1974b); and from the Upper Cretaceous-Lower
Eocene of Languedoc (southern France) by Freytet (1973). In
every case, a close analogy with modern kankar ('caliche') can
be drawn.

In summary, therefore, the calcareous nodules of the
Aztec Siltstone are considered to be of a pedogenic origin,
formed by illuviation in soil profiles developed on the inter-
fluve surfaces (aged between 5,000 and 50,000 years) of an
alluvial plain, under the influence of relatively high
temperatures and a moderately low but highly seasonal rainfall.

Concretions

Mineral segregations of this type are more regular in
form than nodules, and commonly nearly spherical or disk shaped.
Examples of such structures are infrequent in the Aztec Siltstone,
and are largely ferruginous in composition. They vary in size
from 2 mm up to 20 cm. Concretions are most common in sections
north of Portal Mountain, especially the Lashly Mountain section
L1 (Fig. 2.1). Ferruginous concretions, commonly with pyrite
cores (Table 5.7), were observed in sections P1, L1, B2, AZ,
FL, and S9 (Fig. 2.1). The concretions were invariably found
in sediments considered to be of a lacustrinal origin (Chapter
7), based upon evidence from bed forms (laminated, with common

oscillation ripples),grain size (fine-grained, siltstones and claystones with thin interbeds of very fine to fine sandstones), fossils (conchostracans, fish remains) and subaqueous syneresis cracks. The sediments are either carbonaceous (Fig. 2.1) and thus black or dark grey in colour, or are greyish yellow green (5GY 7/2) or light olive grey (5Y 5/2), the characteristic colours of strongly reduced deposits of the formation.

The ferruginous concretions can be classified into three basic types. The first consist of pyritic concretions 1 to 3 cm across, scattered in patches throughout alternating siltstone-sandstone sequences e.g. L1, unit 5, 23424. They commonly grow from the sandstone into the overlying green siltstone bed, producing a bulbous or spheroidally aggregated upper surface, with a regular spherical lower surface (Fig. 4.36).

The second type (e.g. 23300) occur as cubic pyrite centres (Table 5.7) to some of the large brownish black (5YR 2/1) reduction mottles present in greenish grey (5GY 6/1), greyish yellow green (5GY 7/2), or light olive grey (5Y 5/2) siltstone and claystone units. The pyrite growth was in most cases observed to have displaced the surrounding host, and given rise to a zone of increased reduction centred on the pyrite and distinguished by the darker green mottles (Fig. 4.37). They are thus considered as epigenetic and displacive concretions.

The third type, best distinguished in thin section, consist of zones rich in amorphous iron oxides (Table 5.7) which have grown outward from a central point, replacing the former clay matrix (e.g. 23440). Bedding and the quartz grain density is largely undisturbed by this process (Fig. 4.38), indicating that they are formed *in situ*, subsequent to deposition of the host sediment. Like the calcareous nodules described on p. 73 ,they are epigenetic, but are replacive rather than displacive, indicating a later time of formation.

A strongly reducing environment during formation is indicated for the ferruginous nodules, on combined evidence of rock colour, the high carbonaceous contents, and the pyrite stability (Krumbein and Garrels, 1952, p.26). The generation
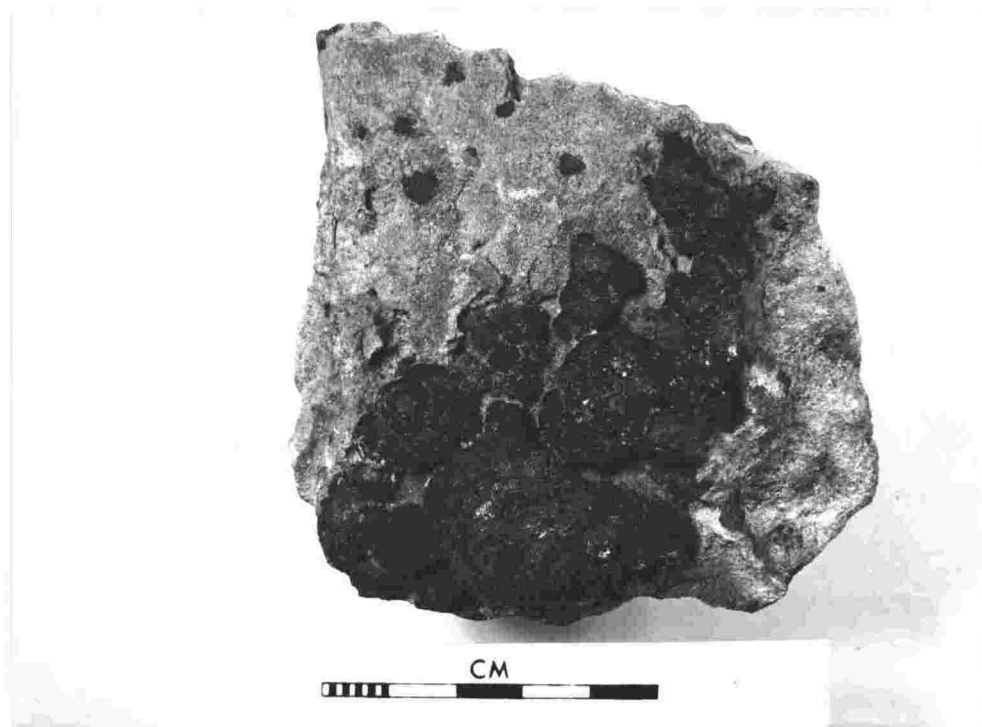
Fig. 4.36. Bulbous shaped pyritic concretions in a sandstone from L1, unit 5.
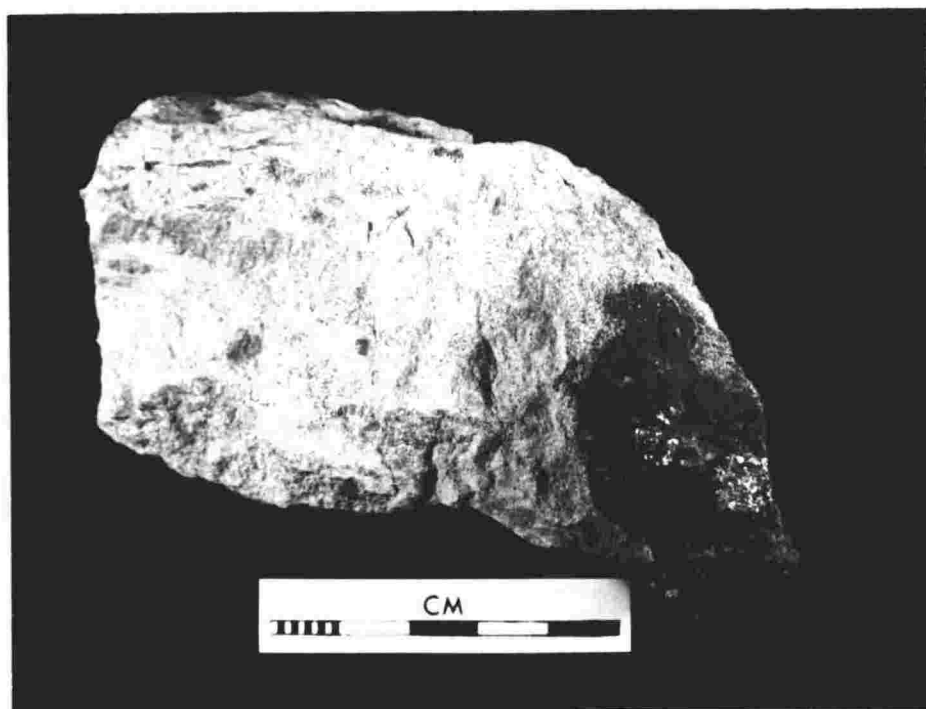
Fig. 4.37. A pyritic concretion in a sandy siltstone from P1, unit 3. The pyrite core is surrounded by a dark green mottled zone.

Fig. 4.38. A replacive, epigenetic, concretion (as seen in thin section) composed of amorphous iron oxide, which has grown outward from a central point while leaving the bedding undisturbed. Sample 23440, L1, unit 33. Plain light. Scale 5 cm = 9 mm.

of such conditions is commonly initiated by bacterial decomposi-
tion of enclosed organic matter under anaerobic conditions in
stagnant lake bottom sediments. It is suggested that the three
types of ferruginous concretions here described, were developed
at three different times under these conditions. The first
type have a structure indicating growth in a manner similar to
that for manganese nodules of the ocean floor; that is
accretion of nodules on the surface of the host bed, before
deposition of the overlying siltstone. This suggestion is
supported by a lack within the concretion of included silt from
the overlying unit. The second type are considered to have
accreted within the enclosing sediment soon after deposition,
because of the observed displacement of host material. The
third type are later stage epigenetic and replacive concretions,
probably growing during early diagenesis under a continuing
reduced environment.

Two types of non-ferruginous concretion were observed in
the Aztec Siltstone. At Portal Mountain (Pl, unit 38, sample
23319) a sandstone contained scattered, preferentially cemented,
spheres, 2 to 10 cm across. The cementing materials for the
host are heulandite and illitic and chloritic clays (Tables
5.7 and 5.9). As concretions, they are epigenetic and replacive,
for the hosted clastic quartz grains do not show displacement in
thin section. It is suggested that they are diagenetic features,
produced by local zeolitization of the fine-grained matrix, under
conditions of raised temperature and pressure, and possibly
associated with the contact metamorphism by neighbouring
dolerite sills and dykes.

The second type of non-ferruginous concretion, is found
at Portal Mountain (Pl, unit 14, sample 23310), and the Lashly
Mountains (L2, unit 3) (Fig. 4.39). The structures are lensoid
in shape, are from 2 to 20 cm long, and are composed largely
of cryptocrystalline (less than 10 microns) calcite (Fig. 4.40).
The Portal Mountain example also contains analcime (Tables
5.7 and 5.9). Most concretions are rimmed by a zone of epidote,
and in some cases hydrated ferric iron oxides. As in the earlier
described epidote-containing nodules (Chapter 4, Nodules), the
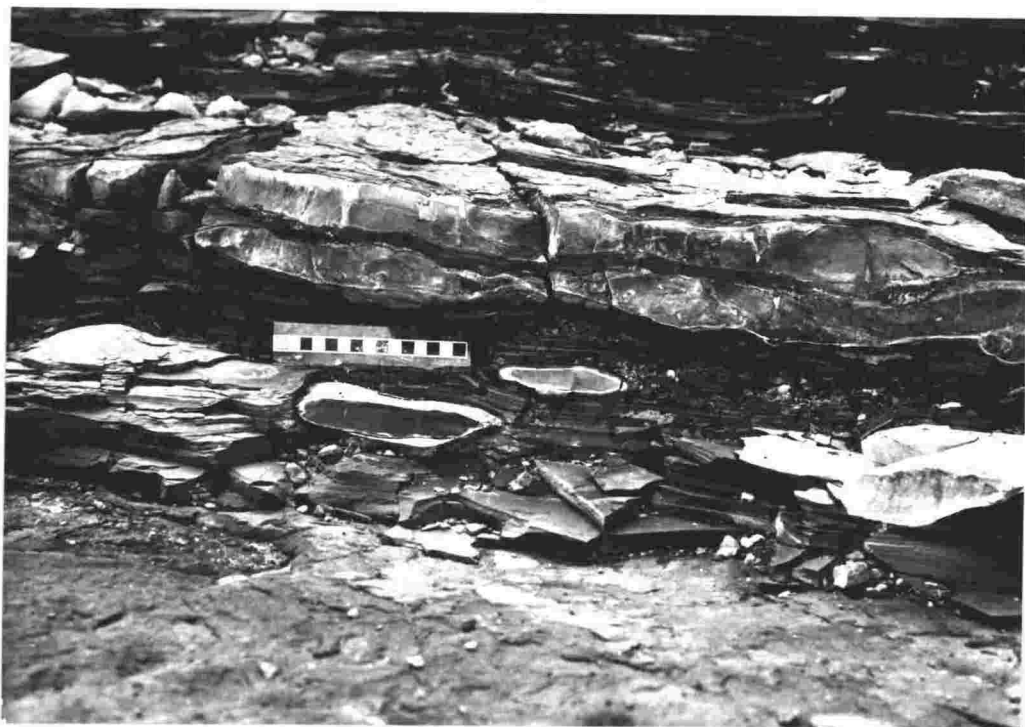
Fig. 4.39. Pisolitic limestones interbedded with laminated greenish
grey (5GY 6/1) siltstones, from L2, unit 3. Scale in cm.
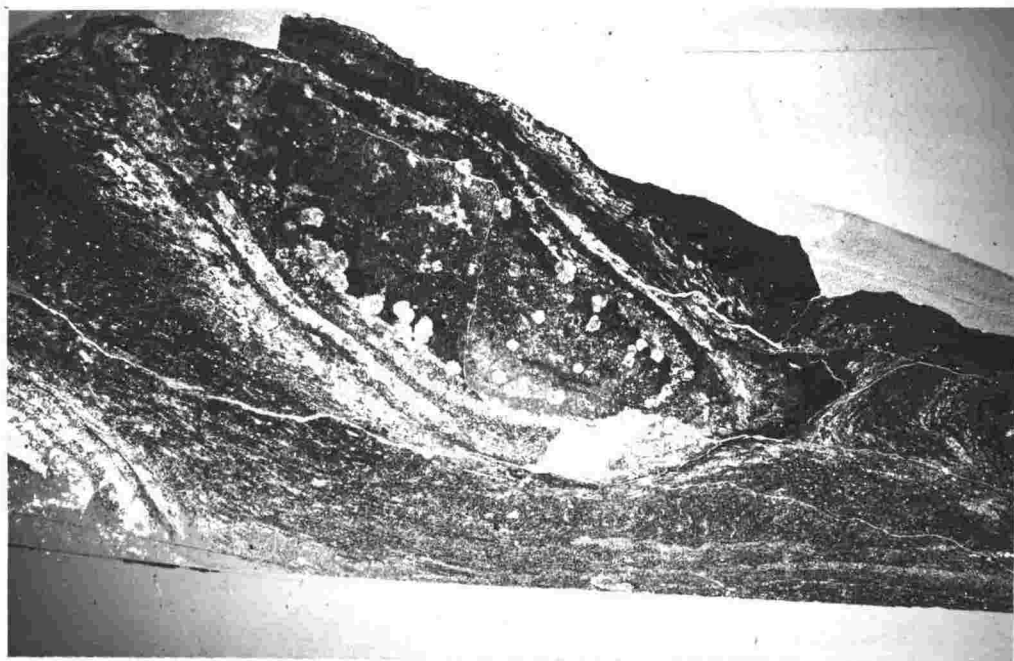
Fig. 4.40. Calcareous pisolite (in thin section) from P1, unit 14, showing
deformation of the bedding around the structure. The pisolite
is largely composed of cryptocrystalline calcite and is rimmed
by a zone of epidote (cf. calcareous nodules, Fig. 4.33).
Polarized light. Scale 5 cm = 10 mm.

epidote appears to be metamorphic, for the crystals are inter-
locking, well-formed and prismatic, and the same mineral
occurs in the host. It is thought to have formed as a product
of contact metamorphism from the neighbouring dolerite sills
and dykes (Fig. 2.1).

The well laminated claystone host lithology shows excellent
contemporaneous deformation bedding around the concretions,
especially the overlying sediment. This, plus the fact that
host sediment is not incorporated in the concretions, suggests
formation prior to inclusion in the host. They are therefore
considered to be calcareous pisolites, the lensoid or disk
shape resulting from postdepositional compaction. That they
were formed in a lake, is evidenced by the lacustrinal nature
of the host sediment; the fine grained and laminated claystone
lithology with thin, very fine to fine grained sandstone inter-
beds, the oscillation ripples, and the included conchostracans
(Chapter 7, Fine member dominated Sequences, Fig. 7.12;
Chapter 8, Conchostracans). It is suggested that calcium
carbonate-saturated lake waters provided the environment
for formation of the pisolites, (cf. oolites, Chapter 3)
produced as a result of direct precipitation of the dissolved
materials on nuclei in a "free rolling" environment, probably
in the higher energy, wave zone, of the lake edge. Calcium
carbonate was widespread in the alluvial plain sediments of
the Aztec Siltstone, especially in the form of kankar
('caliche') (Chapter 4, Nodules) in the fine member floodbasin
deposits, and the enrichment of it in lake waters would be
readily facilitated by rivers and streams draining from these
sediments, plus the seasonally arid or semi-arid climatic
conditions (see Conclusions) which would concentrate it by
evaporation. In some instances; the environment was possibly
too placid for pisolite development, and thus the simple beds
of pure limestone which are associated with the pisolites at
L2, unit 3 (Fig. 4.39), resulted.

The analcime (Chapter 5 p.154) found in the Portal
Mountain pisolites, is considered to be syngenetic like that
forming today in lakes of warm, arid or semi-arid regions

e.g. Lake Natron, Tanzania or China Lake, California (Hay, 1966). It is produced as a result of the chemical reaction of clay minerals in the Na-rich environment characteristic of the lakes in high evaporation areas. It would thus have co-precipitated with the calcite of the pisolite.

Organic Structures

ROOT STRUCTURES

Subvertical sinuous tubes at several localities in the Aztec Siltstone, have been interpreted as root casts (Barrett et al. 1971, p.609). They average 1 cm across, but vary in size from 1 mm up to 1.5 cm across, and form reticulate, furcating, and vertically tapering patterns typical of roots. The structures are recognizable from the host either by weathering, or a colour difference, e.g. greyish orange (10YR 7/4) tubes in a pale green (5G 7/2) host at A1, unit 20.

In many respects these root structures closely resemble the vein networks previously mentioned in this chapter. This is as expected, since roots closely follow cracks in the substratum. The term root structure, has only been applied where a case for roots seemed clear. A similarity may also exist between root structures and some burrows found in the formation (Chapter 4, Trace Fossils), but a distinction can be made on several grounds (Table 4.7).

Table 4.7. Features distinguishing burrows and root structures

Root Structures	Burrows
(1) Taper towards the base	(1) Parallel sided tubes
(2) Commonly bifurcating and veined	(2) Single tubes
(3) Variable sizes in one unit	(3) Same size throughout the unit
(4) Highly sinuous	(4) Straight or of low sinuosity

Primitive plant stems and spores have been collected
from units associated with these root structures, and from
the unit hosting structures at Mount Ritchie (A4, unit 42),
establishing the presence of plants in the area.

The best examples of root structures are at Mount Ritchie
(A4, unit 42, sample 23174, Fig. 2.1) (Figs. 4.41 and 4.42)
where black 'roots' are contained throughout 2 m of a fine,
massive, greenish grey, silty claystone. The surface of
some tubes showed well defined ridging along the length, a
feature common to many modern roots, and some of the roots
showed hair-like rootlets branching off horizontally from the
main vertical root (Fig. 4.43).
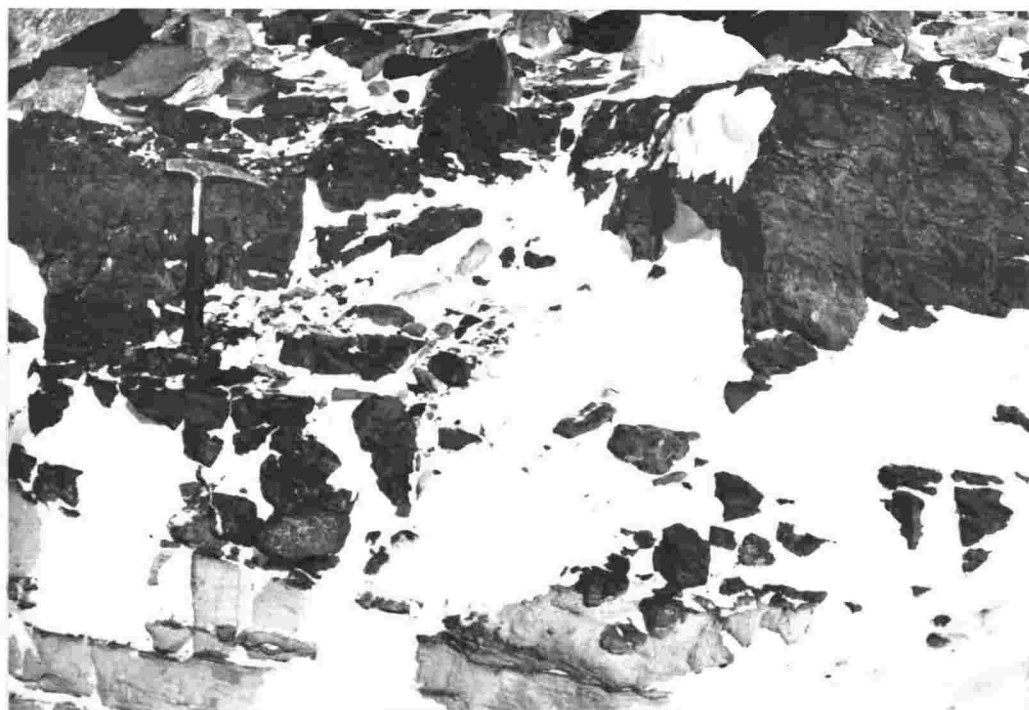
Fig. 4.41. Root horizon (at the level of the hammer) at A4, unit 42.
Plant fragments were collected from the same unit.

Fig. 4.42. A close-up of the root-cast structures in A4, unit 42,
showing their typical sinuous and bificating form. The
casts are approx. 2 cm in diameter.

Fig. 4.43. Hair-like rootlets branching off horizontally from the main
vertical root in a sample from A4, unit 42.

Longitudinal and transverse polished cross-sections of the roots clearly showed woody or cell-like structures (Fig. 4.44). In thin section, the 'roots' were seen to have a differing lithology to the host, being much richer in clays, and containing zones of roughly semi-circular shape, rich in clastic quartz grains and calcite (Fig. 4.45). Despite the black colour, however, no carbon was detected either in thin section or in a chemical analysis carried out by the Coal Research Association of the D.S.I.R., Lower Hutt. The black or dark grey colour was discovered to be due to a concentration of coarse-grained, opaque haematite, varying in size from 5 to 100 microns. It would thus appear that the carbonaceous parts have been replaced by haematite and other detrital products. This could occur if, after dying-off, the carbonaceous material was removed by oxidation and replaced by an oxidized infilling, namely haematite, detrital quartz grains and clays. Preferential oxidation of organic material and a thin zone of host material along root paths, is a common feature of modern soils.

Glennie and Evamy (1968), from an observation of modern root structures in an arid environment, noted that when a plant died, the root tissue oxidised fairly rapidly to carbon dioxide, thus making way for subsequent infilling of the former root with material from above.

Texturally, the surrounding fine greenish grey sandstone host of A4, unit 42, was highly inhomogeneous with localized patches rich in clastic quartz grains, and others rich in clays. Sediment mixing had obviously taken place. As presented in Chapter 5, p.99 (Fabric analysis), there is a remarkably close similarity of texture and quartz grain shape and size, between that of some known present day soils and that of sample 23174, lending support to the hypothesis that the unit and possibly many others with similar textural inversion (Folk, 1968, p.105), are palaeosol horizons.

In an attempt to determine the presence of further root-like structures, and to ascertain their effect on bedding features, samples were subjected to an X-ray radiograph examination. The experiment was unsuccessful, as the thickness
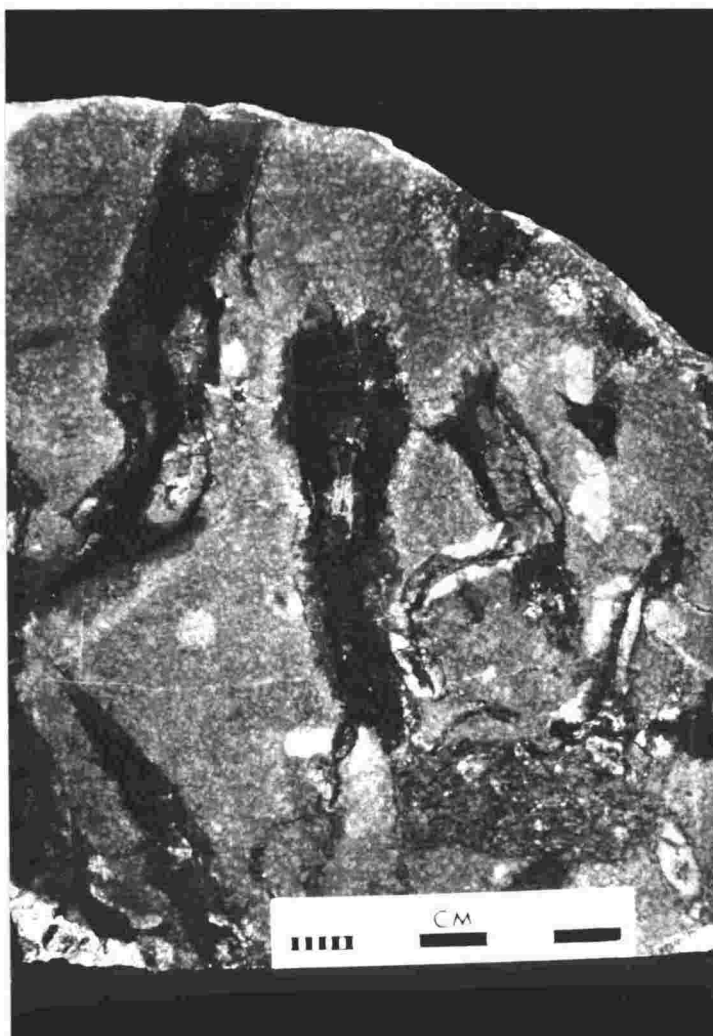
Fig. 4.44. A polished slab of the root-bearing unit 42 in section A4. The longitudinal cross-section shows the roots to have a woody or cell-like structure.
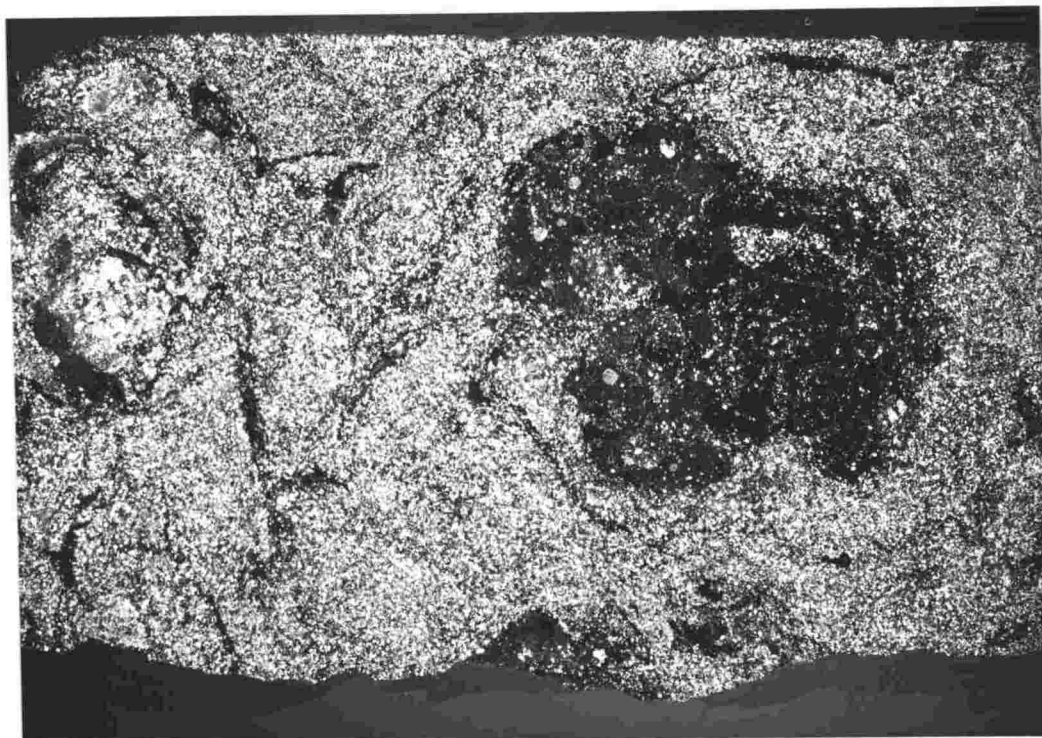
Fig. 4.45. A thin section cross-section of a root (dark patch) from A4, unit 42, showing it to be filled with clays, detrital quartz grains, calcite, and haematite. The host rock is a calcareous silty claystone (Table 5.9). Texturally the host is very inhomogeneous and displays sediment mixing, a common characteristic of soils in thin section. Polarized light. Scale 5 cm = 10 mm.

of rock slab required was too great to permit good resolution on the apparatus available.

Conclusion

The small size of the roots, and the fact that they were not seen to penetrate vertically for more than 50 cm depth, suggests that they originated from shallow rooting, and small plants, probably less than 3 m in height. This is supported by the small size (less than 5 cm width) of the plant fragments (stems) recovered from the formation. (Further discussion on Aztec flora in Chapter 8 p.228).

TRACE FOSSILS

A characteristic feature of many units throughout the Aztec Siltstone, is the presence of vertical or sub-vertical, straight, parallel-sided channels or tubes, thought to be the fossil paths of burrowing organisms. They occur as single (non-bifurcating) tubes, averaging 1 cm diameter, 5 to 10 cm in apparent length, and 3 to 5 cm apart, evenly distributed throughout the bed (Fig. 4.46). The host lithology is generally a fine-grained deposit i.e. siltstone or claystone, but is, in some cases, a fine or very fine sandstone.

The tubes are of two types. (1) those with tube infillings composed of material derived from the host; orthotubules (Brewer, 1964), (2) those with tube infillings composed of material derived from the overlying bed from which they originate; metatubules (Brewer, 1964). The infillings generally do not show any structural form in thin section i.e. are not organized into recognizable aggregates and show no directional arrangement with regard to the external form. They are therefore of the isotubule class (Brewer, 1964).

Tubules in greenish grey units are commonly infilled with a greyish red haematitic sediment, as a result of them passing into and in some cases through, greyish red lenses or beds contained within the host greenish grey unit (Fig. 4.46).

Fig. 4.46. An extensively burrowed horizon at A1, units 2 and 3. Scale in cm.
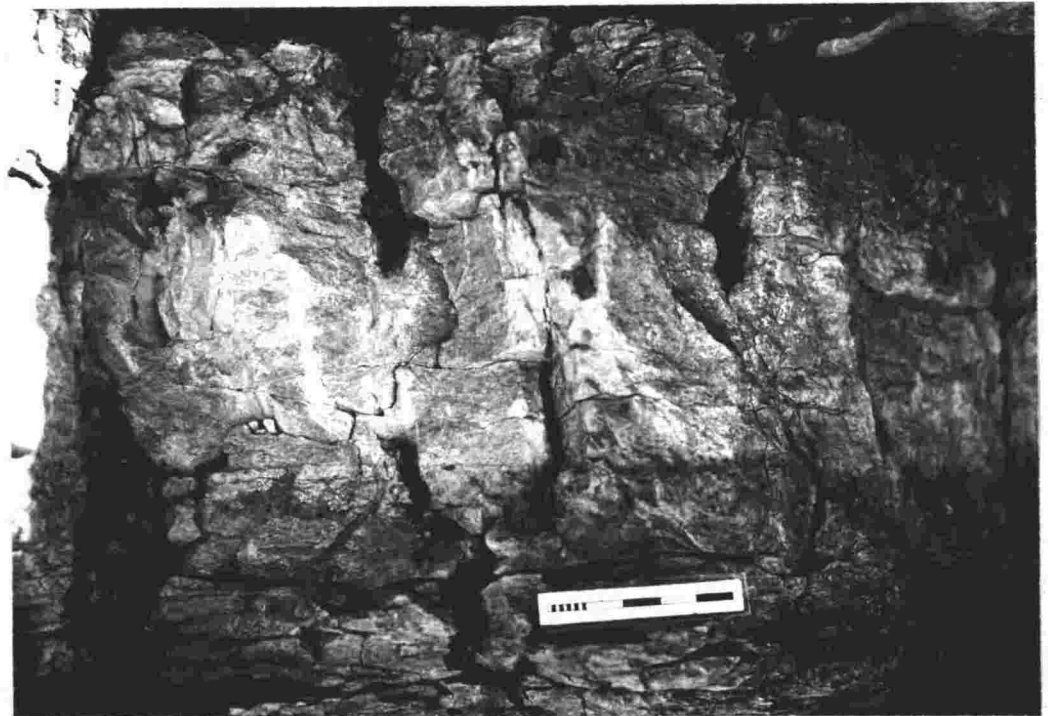
Fig. 4.47. Red burrows or tubules which pass through a thin sandstone interbed and have been partially reduced as a result. Location A1, unit 11. Scale in cm and mm.

Where red tubules pass into sandstone or coarse siltstone lenses contained within a finer grained host, they commonly convert to green tubules (Fig. 4.47) and 4.48) as a result of the reducing environment generally present in these more permeable coarse-grained beds.

The fact that the tubules are infilled with haematite-rich sediment but that the host does not contain haematite suggests that haematite, or its precursory mineral, was present in the sediment at the time of biogenic reworking.

The tubules are a penecontemporaneous feature, considered to have been produced by organisms which derived food from burrowing in the unconsolidated sediment. Early workers on the Problematica of the Beacon Supergroup called the tubules *Scolithus* (Vialov, 1962; Webby, 1968) and believed them to be the feeding and dwelling traces of invertebrates of a sea-worm, based upon previous evidence from similar burrows, by Seilacher (1967). However, a marine environment for the Aztec Siltstone now seems very unlikely (see Conclusions, p.254).

Davidson (1891), and Smith and Hein (1971), showed the extensive reworking capabilities of burrowing organisms of a similar type to those envisaged for the Aztec Siltstone. The latter reference specifically relates to the biogenic reworking of non-marine sediments, a subject neglected in past literature. Extensive reworking in the Aztec Siltstone lithologies has taken place (Fig. 4.49), and I would suggest that much of the textural inversion and immaturity (Folk, 1968, p.105) i.e. inhomogeneity, poor sorting, bimodality and mixed grain size-rounding, shown by many units of the Aztec Siltstone (Chapter 5), including the destruction of visible bedding characteristics, could be due to this reworking and mixing by burrowing organisms. Other red beds, for example the Brunswick Shale, the Chugwater Formation, the Fountain Formation, and the Sabaneta Formation, all have many units which have been "extensively worked by burrowing organisms" (Van Houten, 1964b, p.657).
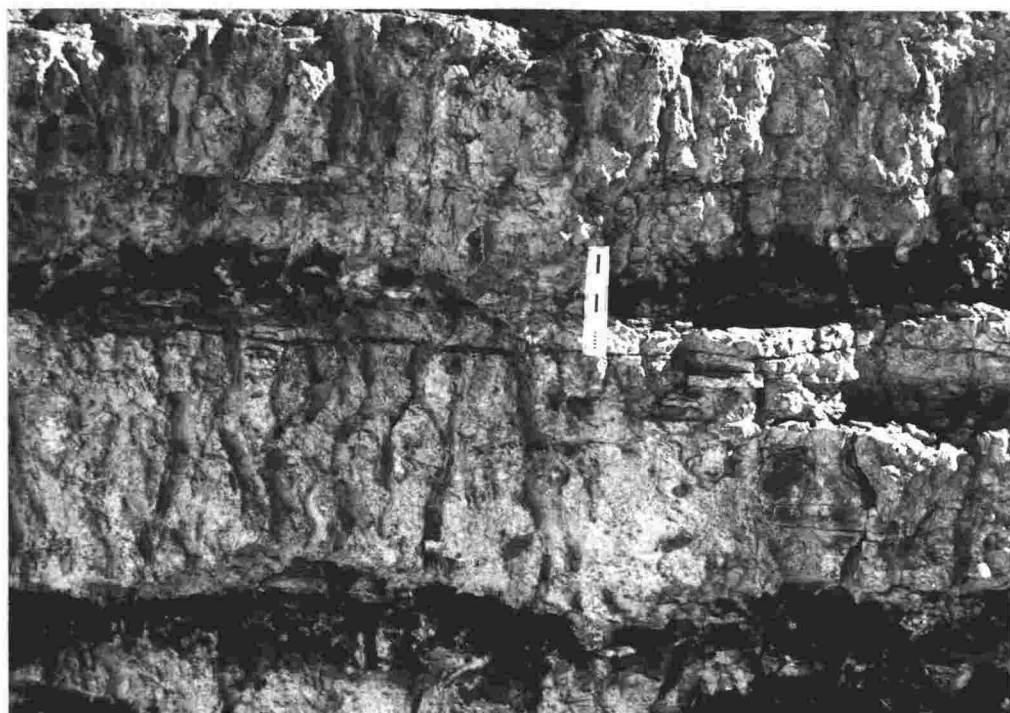
Fig. 4.48. Burrows or tubules which pass through a sandstone interbed and have been reduced. Location Al, unit 2. Scale in cm.

Fig. 4.49. Extensive bioturbation by burrowing organisms which has almost completely destroyed bedding features and has left only isolated patches of green sediment in the now massive red unit. Location Al, unit 1. Scale in cm.

Trace fossil markings other than burrows were observed from the formation, the most noticeable being a large specimen of *Beaconites antarcticus,* found at Beacon Heights (B2, unit 5). This enigmatic fossil was also thought to be of possible marine origin by Vialov (1962, p.729). Examples of other possible "animal tracks" were noted at Mount Metschel (M1, unit 1), and the Lashly Mountains (L2, units 5, 7, and 12) (Fig. 4.50), as bumps, pits, and lineated furrows, the latter being 1 to 2 mm across.
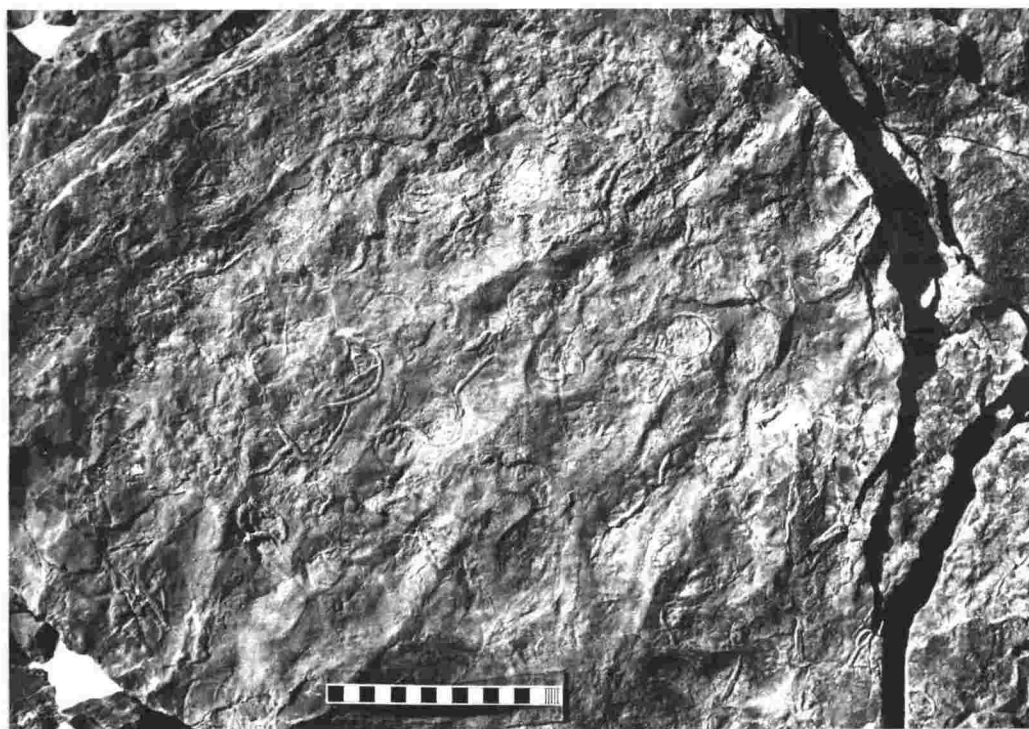
Fig. 4.50. Trace fossil trails similar to worm trails at L2, unit 12. Scale in cm.

CHAPTER 5

PETROLOGY

Approximately 100 thin sections from throughout the
Aztec Siltstone were examined in detail, and representative
sections were selected for grain size and modal analyses.
The fine-grained samples required a more diverse petrographic
study involving X-ray diffraction and X-ray fluorescence
spectroscopy in combination with the microscopic examination.

Textures

FABRIC

Sandstones

Most sandstones of the Aztec Siltstone are homogeneous,
although a few samples (e.g. 23184) show inhomogeneity on a
microscopic scale. This manifests itself as layers of well
sorted sand grains, each layer having a markedly different
mean grain size.

Most sandstones appear to show no preferred grain
orientation, because of the high sphericity of the detrital
grains, although lower sphericity grains in a few samples tend
to lie with long axes parallel to bedding (e.g. 23235 and 23438).

Siltstones and Claystones

The fine-grained sediments of the Aztec Siltstone are of
two types, either horizontally-stratified or unbedded (Fig. 4.1).
Both consist of detrital quartz grains embedded in an illitic
and chloritic clay matrix, and the stratified examples commonly
show, in thin section, a concentration of detrital grains
corresponding to bedding planes. The bedded lithologies
generally have a homogenous fabric with little or no optical
orientation or local concentration of the clay matrix. A few

samples have a fabric in which the clay as a whole exhibits preferred parallel orientation. Brewer (1964) considers this as the fabric normal to argillaceous sediments.

The unbedded samples, however, have a more complex fabric consisting, in thin section, of local concentrations of clays, detrital grains, haematite, or calcite, and channels, cracks and voids filled with haematite and clays. The clays in these samples have a distinctive optical orientation pattern.

The unbedded lithologies have a fabric very similar to modern soils, and so have been classified using the system for soil fabric analysis of Brewer (1964). This classification was found to apply well to the features found in the Aztec lithologies.

The unbedded lithologies of the Aztec Siltstone consist of varying concentrations of skeleton grains (i.e. grains which are relatively stable and not readily translocated, concentrated or reorganized by soil-forming processes) of sand and silt-sized quartz grains embedded in an s-matrix or plasma of illitic and chloritic clays and haematite. The skeleton grains very commonly show rims of optically orientated clay (free or embedded grain argillans, Fig. 5.1), or ferri-argillans where they incorporate haematite as in the case of the red samples. Many of the grain argillans show a strong continuous orientation of the clays.

The s-matrix of the unstratified Aztec samples typically has a sepic plasmic fabric, i.e. the plasma has anisotropic domains with various patterns of preferred orientation. Most common is the lattisepic fabric, where the plasma has a flecked orientation pattern, but there are two sets of very short, discontinuous plasma separations usually orientated approximately at right angles to each other (Fig. 5.2). In some cases the plasma exhibit a complex striated orientation pattern (omnisepic fabric, Fig. 5.3).

Therefore, incorporating the grain argillans (skelsepic fabric), the fabric of the Aztec samples is generally skel-lattisepic or skel-masepic.
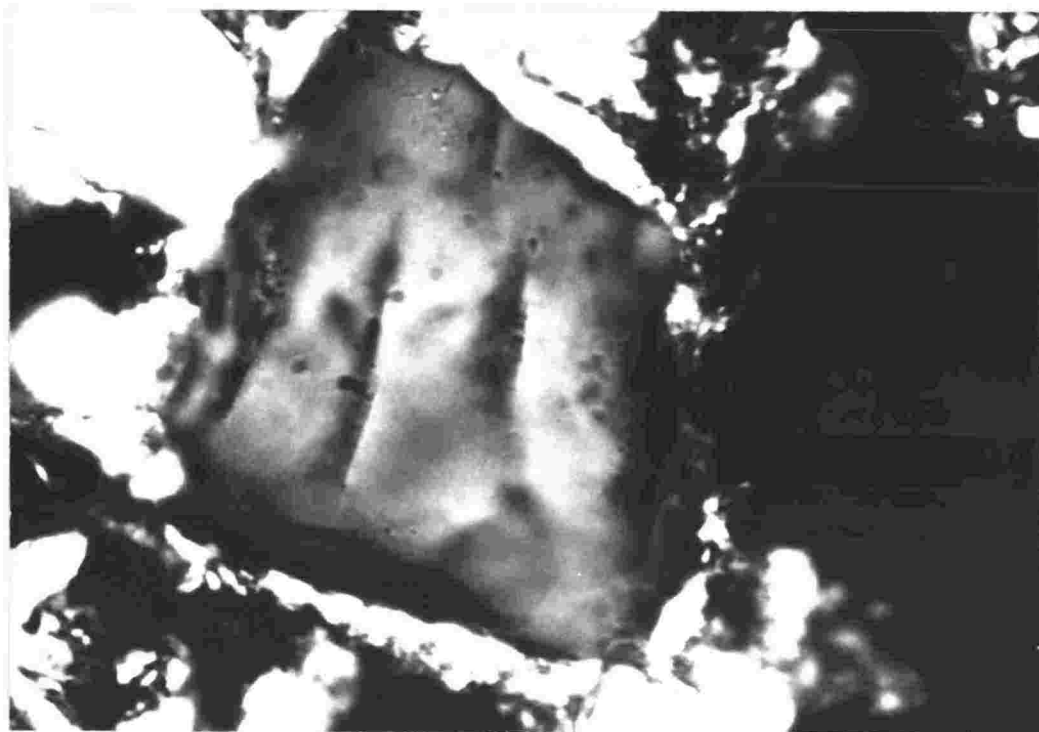
Fig. 5.1.   A detrital quartz grain rimmed by optically orientated
clay (free or embedded grain argillan).   Sample 23432, a
silty claystone from Ll, unit 17.   Polarized light.
Scale 5 cm = 0.07 mm.
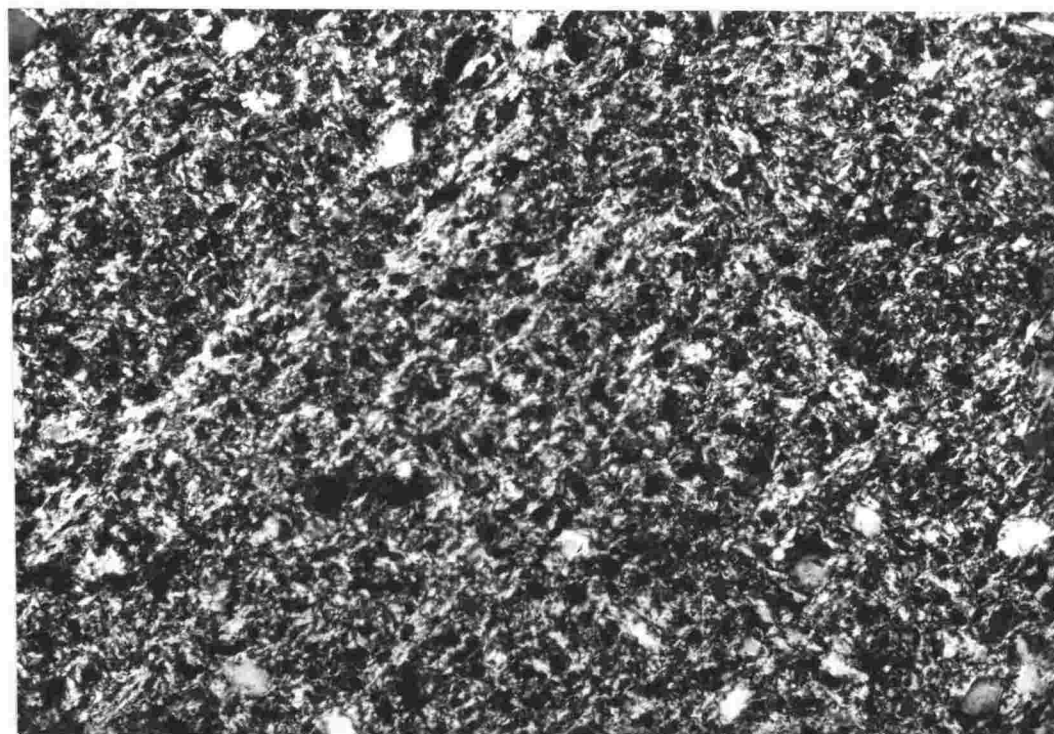
Fig. 5.2.   Optically orientated clay matrix in a claystone, sample 23233
from Al, unit 1.   Detrital grains are quartz.   The clay has a
flecked orientation pattern with two sets of very short,
discontinuous plasma separations usually at right angles
to each other (lattisepic fabric).   Polarized light.   Scale
5 cm = 0.34 mm.
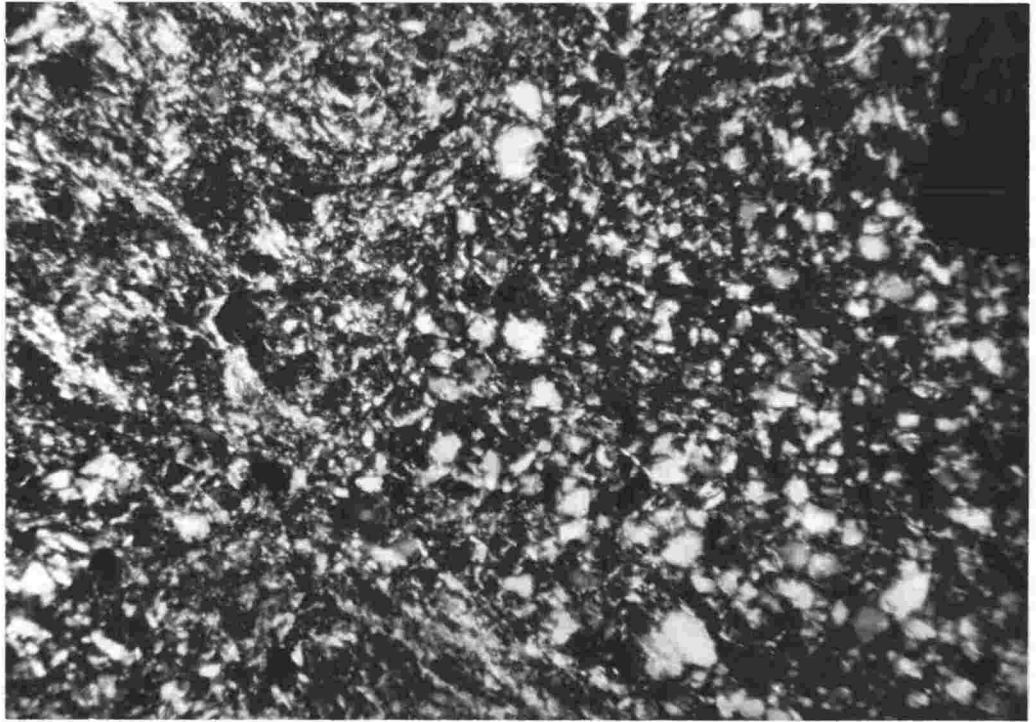
Fig. 5.3.   Optical orientation of the clay matrix of a silty claystone
sample 23249, from Al, unit 31.   Detrital grains are quartz.
The matrix shows a complex striated orientation pattern
(omnisepic fabric) which includes the lattisepic fabric of
Fig. 5.2.   Polarized light.   Scale 5 cm = 0.35 mm.
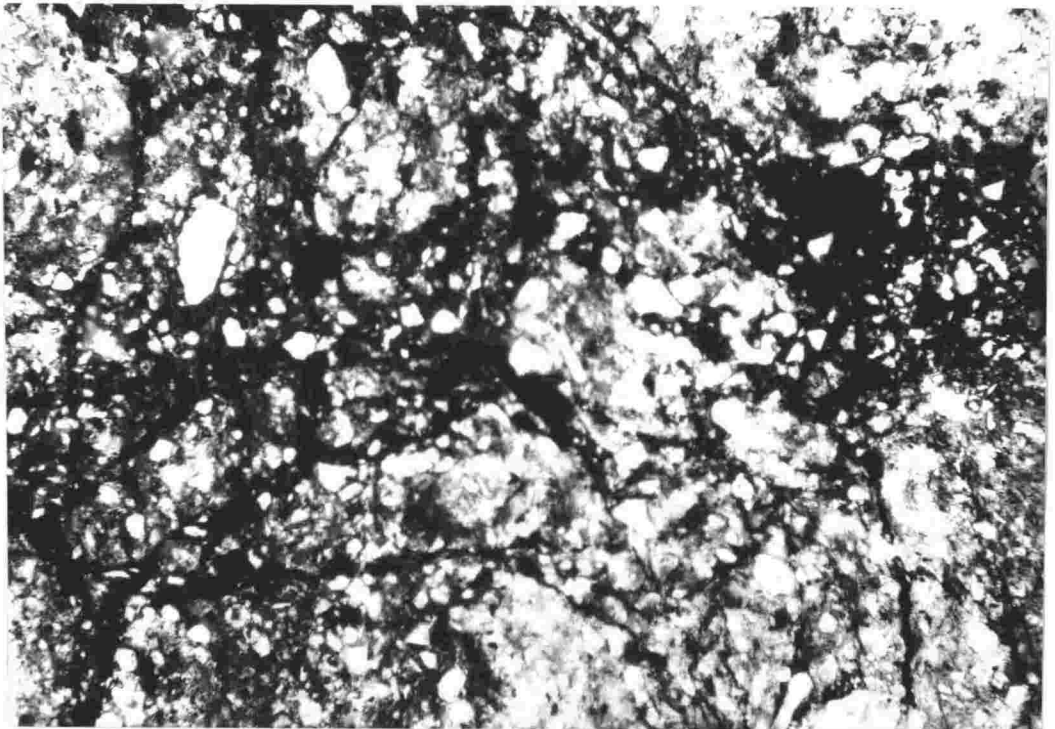
Fig. 5.4.   Channels and veins infilled with haematite (skew-plane
haematans), in sample 23243, Al, unit 22.   Plain light.
Scale 5 cm = 0.86 mm.

The unbedded lithologies have channels and veins filled with clays, calcite, and haematite in the case of the red samples, that are irregularly arranged throughout the matrix (Figs. 5.4, 5.5). These features are very similar in shape, distribution and composition, to the infilled skew-planes (formally planar voids that traverse the plasma in an irregular manner) in modern soils. As with modern soil skew-planes, the Aztec examples are commonly lined or infilled with optically orientated clay minerals (skew-plane argillans, Fig. 5.5).

Glaebules, specifically nodules of calcite (see Nodules, Chapter 4, p.73) and haematite (haematans) are common in the plasma (Fig. 5.6).

Genesis

Grain argillans may form by illuviation, diffusion or stress mechanisms (Brewer, 1964, p.231). However, the Aztec examples are most probably illuvial in origin because of their sharp boundary and strong optical orientation. Ferri-argillans especially, are unlikely to be formed by diffusion or stress mechanisms, including diagenesis (Brewer, 1964).

Preferred orientation of clay minerals to give a plasmic fabric of the type seen in the Aztec samples is common in soils. It is thought to be the result of pressure and tensions on clay mineral grains, produced by wetting and drying and consequent swelling and shrinkage (Brewer, 1964, p.336). Wetting and drying of the Aztec sediments was probably a frequent and widespread physical process, as suggested by the abundance of mudcracks and vein networks throughout the formation (Fig.2.1). Skelsepic fabric, i.e. optical orientation of plasma around skeleton grains, may also result from swelling pressures since skeleton grains present a solid surface against which pressures can be exerted.

Sepic fabrics, like those in the Aztec sediments, are considered to develop most readily in illitic and chloritic plasma because these clays have relatively large grains which will reorientate by pressure more readily than do the smaller grains, such as montmorillonite (Brewer, 1964, p.339).
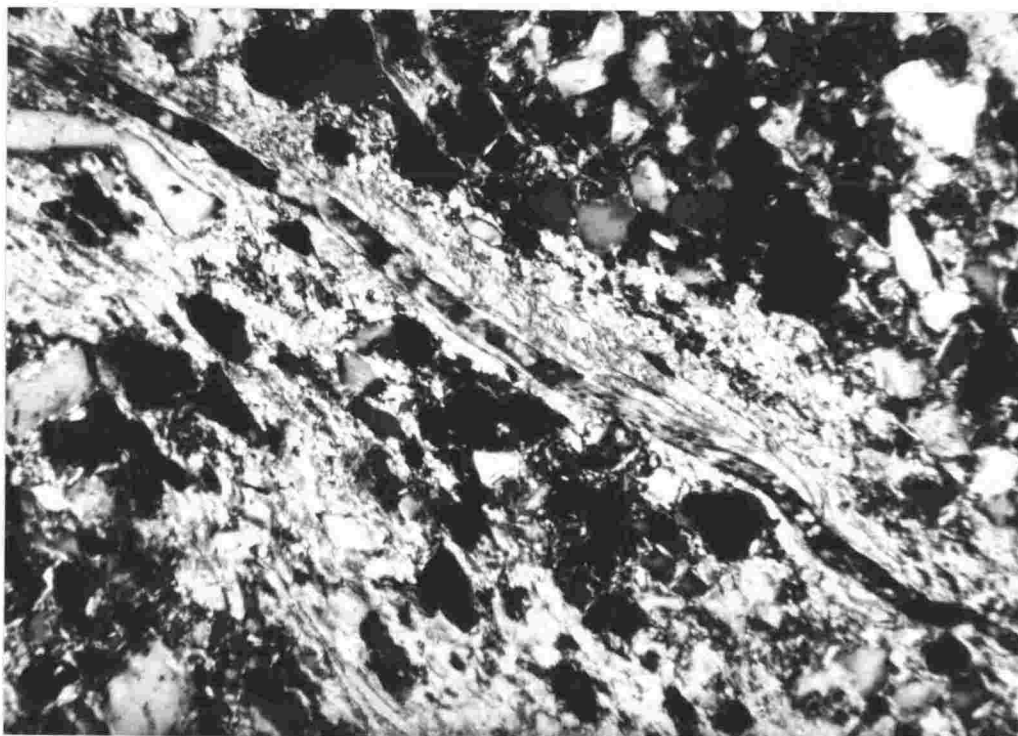
Fig. 5.5.   A channel lined and bordered by optically orientated clay
            minerals (skew-plane argillans). Polarized light.
            Scale 5 cm = 0.35 mm.
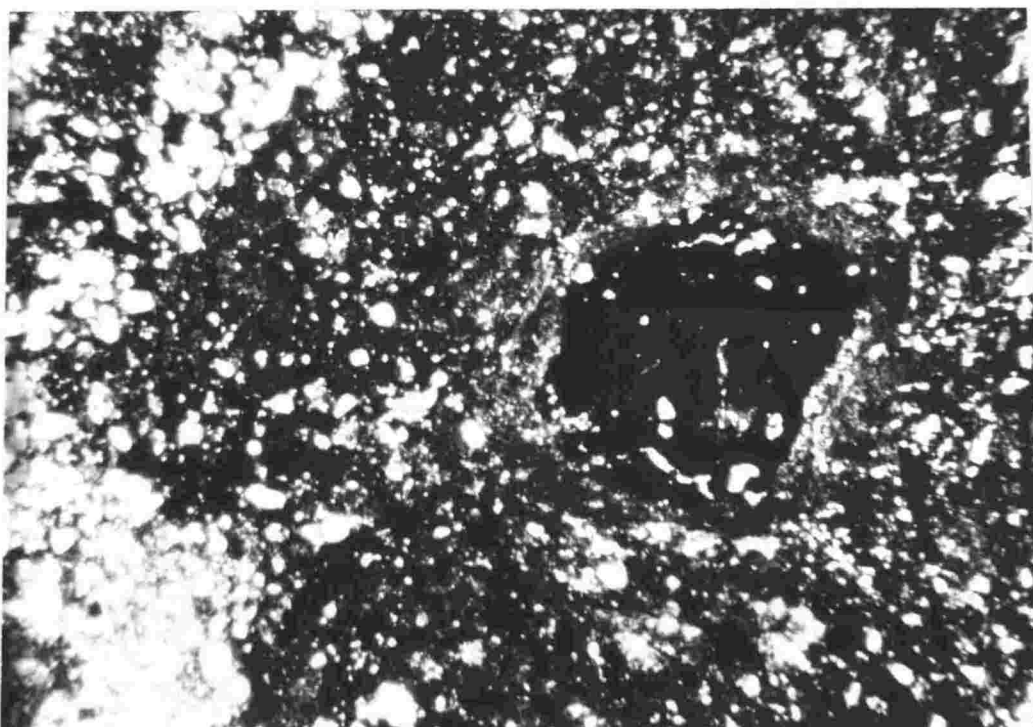
Fig. 5.6.   A nodule or glaebule of haematite (haematan) in sample 23243,
            A1, unit 22. The glaebule is surrounded by haematitic clays
            and patches and zones of detrital quartz grains. Plain light.
            Scale 5 cm = 1 mm.

Preferred orientation of clay mineral grains in sediments may occur as a result of deposition from suspension, or by recrystallization of unstable minerals to form more stable clay minerals and micas in the latter stages of compaction (Meade, 1960). However, this is not considered as the mechanism generally applicable to the Aztec fine-grained sediments as both processes produce an overall preferred orientation of the plasma (unistral fabric) and not the zoned or sepic pattern that is most common.

Skew-planes are another soil feature found in the Aztec lithologies and are also considered to originate primarily through shrinkage and swelling during wetting and drying. (Brewer, 1964).

The calcitic and haematitic glaebules in the Aztec fine-grained samples are also evidence for pedological processes, involving the mobilization and segregation of soil products. The calcite glaebules and their soil origin is discussed with nodules (Chapter 4, p. 73).

The unbedded fine-grained samples of the Aztec Siltstone typically have textural inhomogeneity on a microscopic scale, consisting of zones rich in detrital quartz grains and others rich in clays or possibly calcite (Fig. 5.6a). As expected, these sediments are extremely poorly sorted, and have a continuous particle size distribution, from clay size up to coarse sand size. This texture appears to bear no relationship to sedimentological processes, and is thought to be a pene-contemporaneous feature induced by pedogenic processes including the translocation and illuviation of soil plasma. (See Chapter 6, Soil Chemistry, p.188 for further evidence). This fabric is typical of normal soils, although some inhomogeneity was undoubtedly added to by biogenic reworking (see Trace Fossils, p.94).

It has been shown (above) that many of the micromorphological features characteristic of modern soils are found in the unbedded, fine-grained lithologies of the Aztec
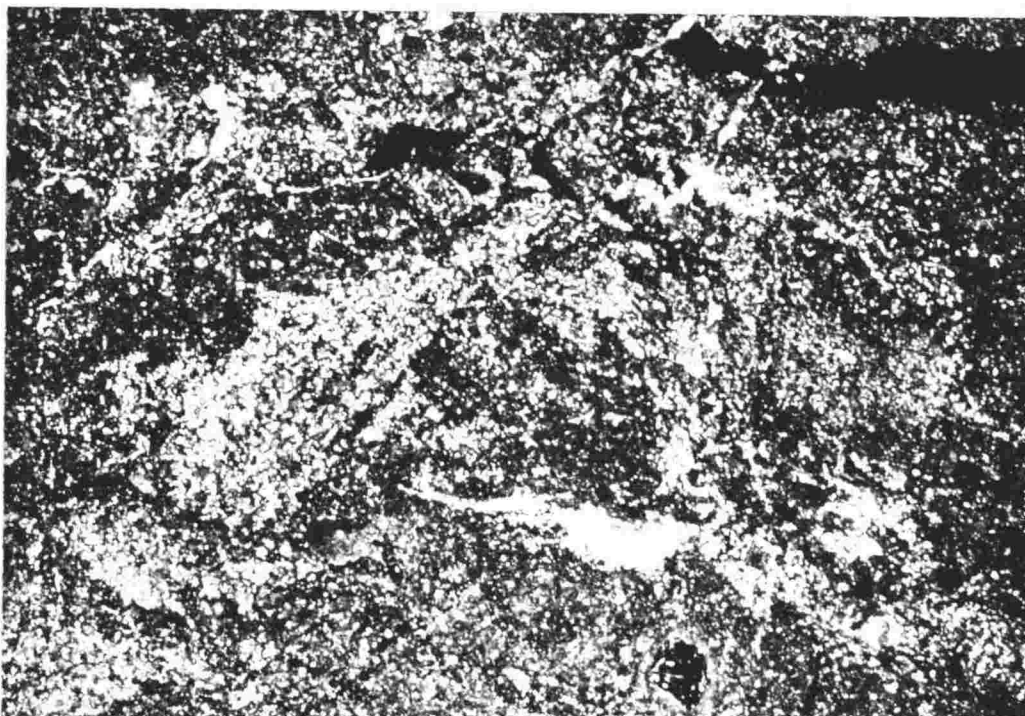
Fig. 5.6a. Textural inhomogeneity in sample 23243 showing zones rich in detrital quartz grains and others rich in clays, haematite pigment or calcite. Plain light. Scale 5 cm = 5 mm.

Siltstone. These features together with the vein networks and calcareous nodules, provide substantial evidence for pedogenesis on the Aztec alluvial plain.

GRAIN SIZE

Method: The grain size distribution of samples of the Aztec Siltstone was determined by direct measurement of grains in thin section, because the lithologies were too well cemented to be disaggregated and sieved. The measurement technique of Friedman (1958), and Adams (1974) was employed. The apparent long axes of 250 grains were measured using a graduated micrometer eyepiece. The grains were selected, by a Swift automatic point counter, from an area covering as much of the thin section as was possible. Thin sections in most cases had been cut normal to bedding. The horizontal and vertical point count interval was chosen to be larger than the largest grain, so that each grain was only measured once, thus avoiding a

reduction in reliability (Dennison and Shea, 1966). Class
boundaries were selected at approximately one half phi intervals.

Sandstone cement, such as calcite and quartz, was
eliminated from the determination because it is of post-
depositional origin and therefore does not relate to the
depositional condition of the sandstone. A clay matrix was
present in some sandstones analysed (Table 5.5) but was not
incorporated into the cumulative curve and the grain size
statistics because it was considered to have originated after
deposition of the sandstone, by sediment mixing and translocation
of clays. The fact that it is not present between sand grains
in close contact in many samples, supports this contention in
those examples. The interbedded sandstone-claystone
characteristics of the Aztec formation would readily facilitate
the migration of clay, probably in colloidal suspension, into
the well sorted and therefore highly permeable sandstone beds,
especially during the early post-depositional period. This
would have been aided by the bioturbation and soil forming
processes that were common in the sediments (Chapter 4).

The graphic mean grain size and the inclusive graphic
standard deviation of Folk and Ward (1957) were calculated
for the samples.

$$\text{Graphic Mean (Mz)} = \frac{\phi_{16} + \phi_{50} + \phi_{84}}{3}$$

$$\text{Inclusive Graphic Standard Deviation } (\sigma_I) = \frac{\phi_{84} - \phi_{16}}{4} + \frac{\phi_{95} - \phi_5}{6.6}$$

These values were then corrected to sieve size equivalents
using the conversion equations (values in phi units) of
Adams (1974).

$$\text{Sieve mean} = \text{thin section mean} + 0.40$$

$$\text{Sieve standard deviation} = 0.82 \text{ (thin section standard deviation)}$$

The value of the constant for the conversion of thin
section graphic mean size to an equivalent sieve value is
dependent upon the average axial ratio of the grains (Adams,
1974). This ratio was determined for a typical sandstone
from the Aztec Siltstone and found to be 0.70, based upon the
measurement of 20 grains. This value was then applied to all
other sandstones analysed for grain size distribution.

Skewness and kurtosis values were not determined because
it had been found, by Friedman (1962) and Adams (1974), that
results obtained from thin section analysis could not be
reliably related to sieve values.

Results: A plot of mean grain size versus standard deviation
shows a high degree of sorting and a fine grained character
for the sandstones analysed (Appendix Table 2; Figs 5.7,
5.8). The average grain size is 2.86 ϕ (fine-grained
sandstone). The average sorting value is 0.43 ϕ, which is
in the well-sorted class of Folk (1968).
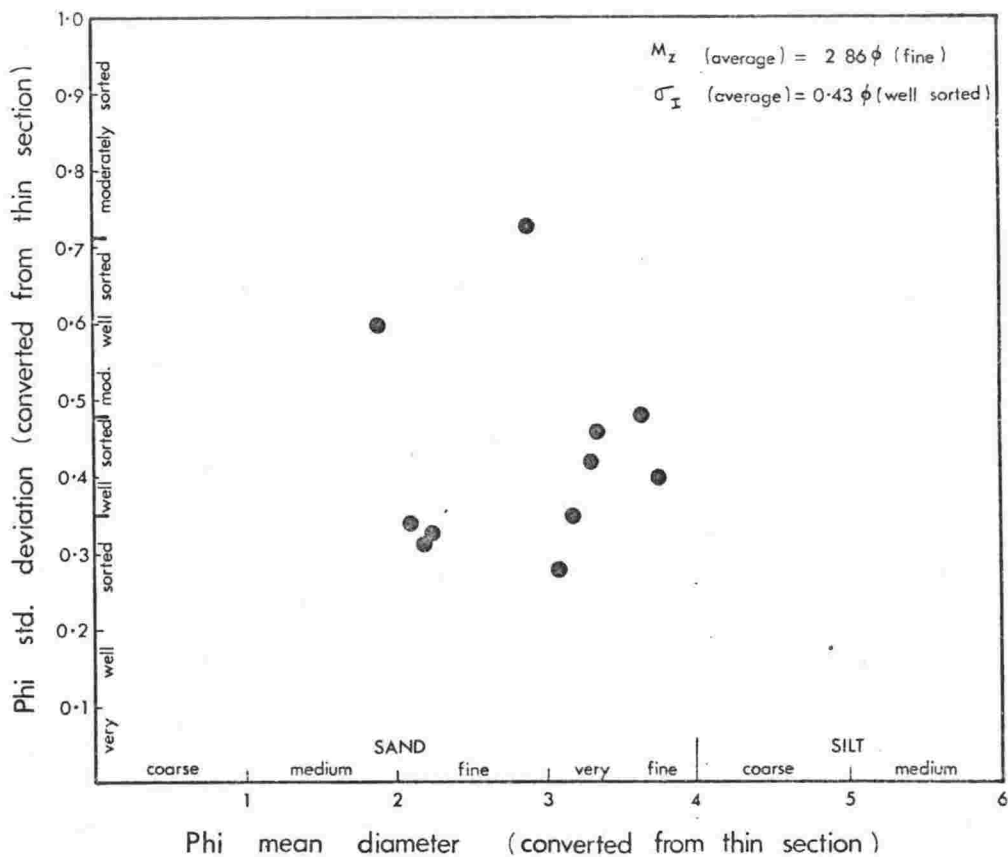
Fig. 5.7. Textural characteristics of sandstones from the Aztec Siltstone,
based on measurements of quartz grains in thin section. Data
presented in Appendix Table 2.
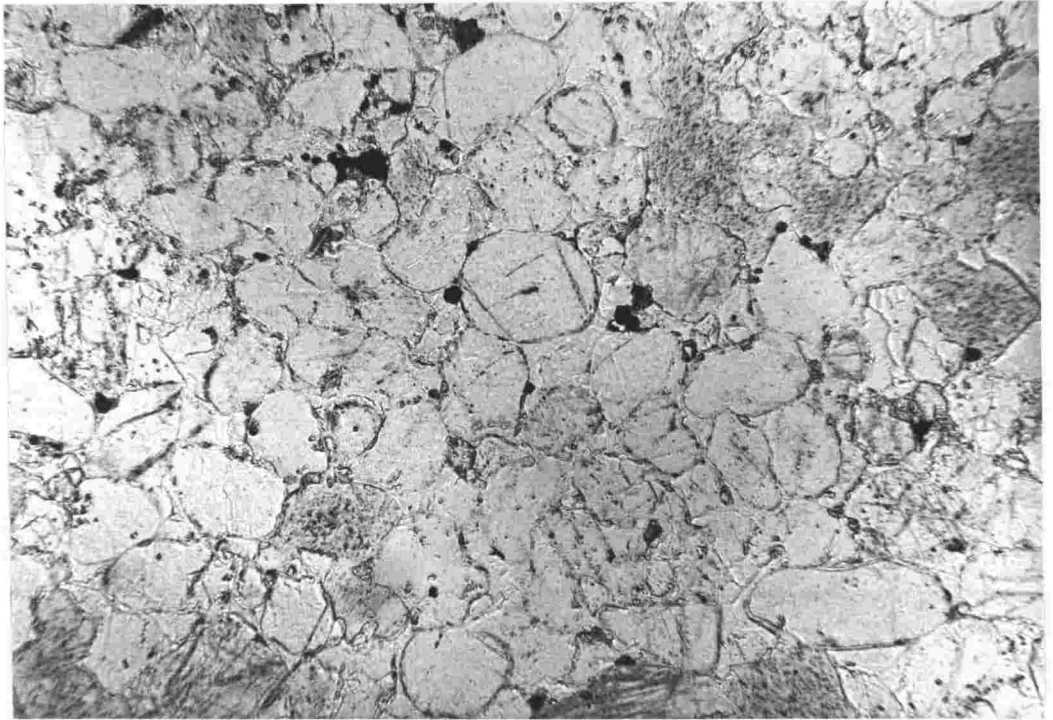
Fig. 5.8. Photomicrographs of a fine-grained (M_z = 2.10 ϕ) and very well sorted (σ_I = 0.34 ϕ) quartzarenite, sample 23315, P1, unit 23. Note the well-rounded grains ($\bar{X}_r$ = 0.84)
(a) Plain light. (b) Polarized light. Scale 5 cm = 1.10 mm.
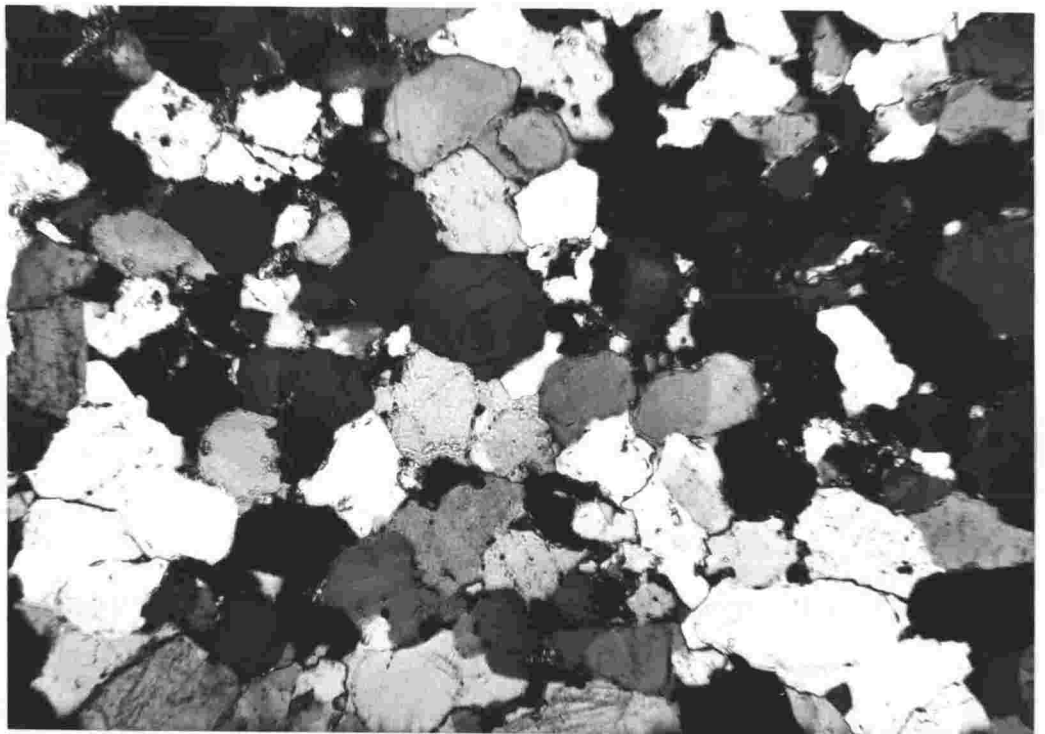
The sandstone deposits of the Aztec Siltstone are believed to be stream channel and point bar sediments (Chapter 7, p.205). In agreement with this, the grain size and sorting values of the Aztec sandstones are in the range determined for modern stream channel and point bar sands, for example, those of the Mississippi and Colorado Rivers (Allen, 1965a, p.141).

The fine-grained lithologies of the formation could not be classified by grain size, into the quarter or half phi classes as with the sandstones, because of the difficulty in optically measuring grains finer than 6 ϕ. However, 45 samples, representing a cross-section of the fine-grained units of the formation, were classified by the procedure previously outlined, using the three classes of sand (0-3 ϕ), silt (4-8 ϕ) and clay (greater than 8 ϕ). A minimum of 250 and up to 500 points was used for each thin section.

The grain size results for the fine-grained lithologies were plotted on the ternary diagram of Picard (1971, Fig. 3) for the textural classification of fine-grained sediments (Fig. 5.9). This shows that a high percentage of the samples plot in the claystone quarter of the diagram (Figs. 5.9, 5.10, 5.11 and 5.31) with silty claystone as the dominant class. It also demonstrates an absence of lithologies containing greater than 55 percent silt size fraction. Thus, true siltstones are not present in the formation, and those lithologies that have been described as siltstones in the outcrop descriptions (Askin *et al.* 1971; Barrett and Webb, 1973) are more clay-rich than was estimated from hand specimen, and are most likely clayey siltstones, mudstones, or silty claystones.

From a textural analysis of 751 recent fine-grained sediment samples, Picard (1971) showed that silty clay was the principle lithology. Although he also plotted 234 fine-grained clastic rocks and found that the siltstone group predominated, he stated that the relationship was biased by the small number of grain size studies done on the claystone and mudstone group of sediments. He concluded that ancient
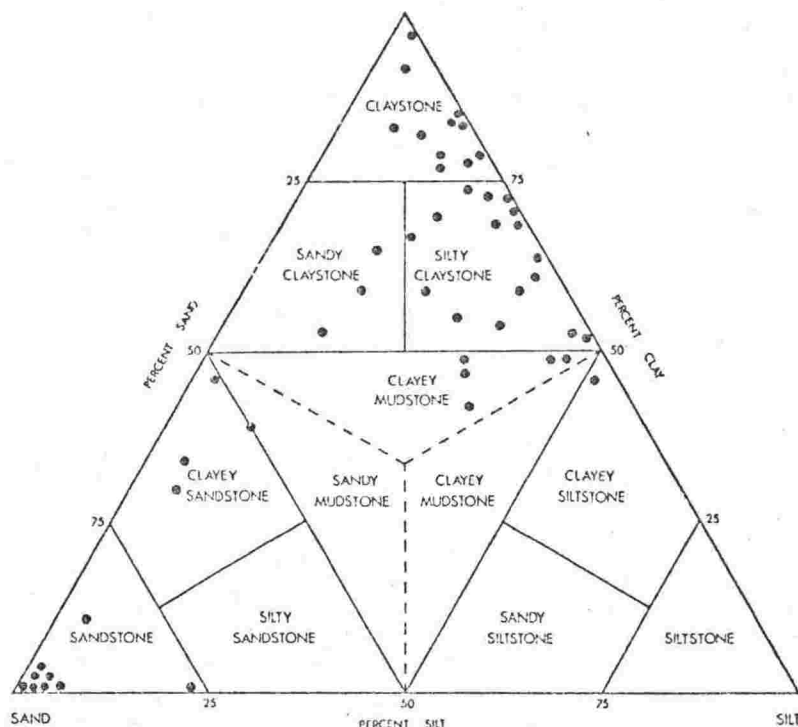
Fig. 5.9. Textural classification of Aztec Siltstone sediments using the classification of Picard (1971). Data in Table 5.9.

fine-grained rocks contain relatively more claystone and mudstone than is generally indicated.

Although overall poor sorting was a characteristic of the Aztec fine-grained lithologies, a number of samples analysed by thin section are polymodal with well defined modes in the sand and silt fraction (Figs. 5.12 and 5.19; Appendix Table 1). This has been demonstrated by plotting cumulative and frequency curves for three examples (Fig. 5.13). The polymodal character is considered to be due to sediment mixing by the same processes which gave rise to the immature sandstones that show textural inversion (Maturity, p. 125). These are simply the finer grained equivalents.

The fine-grained lithologies of the Aztec are considered to be the overbank or suspension deposits of a sinuous, meandering river system (Chapter 7). In agreement with this conclusion it is noted that the fine-grained lithologies of the Aztec are comparable, in grain size characteristics, with the topstratum or overbank deposits of modern meandering river systems, including the floodbasin deposits (Allen, 1965a)
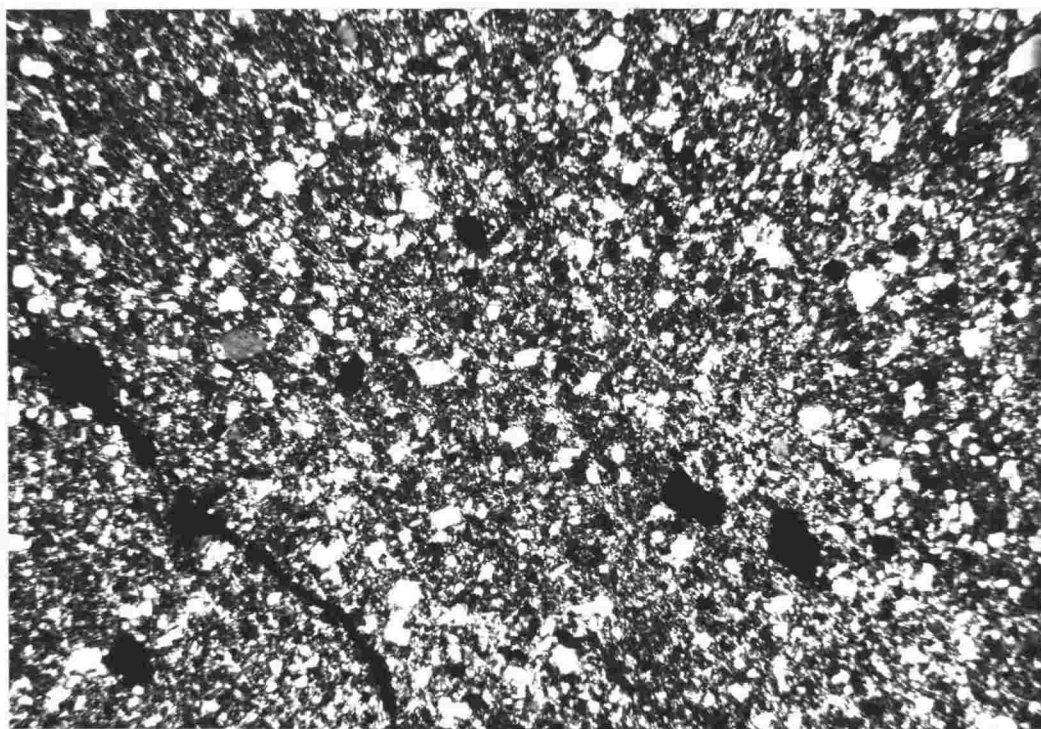
Fig. 5.10. A typical silty claystone with silt-size detrital quartz
grains set in an illitic and chloritic clay matrix.
Sample 23230, Al, unit 1. Polarized light. Scale
5 cm = 1.10 mm.
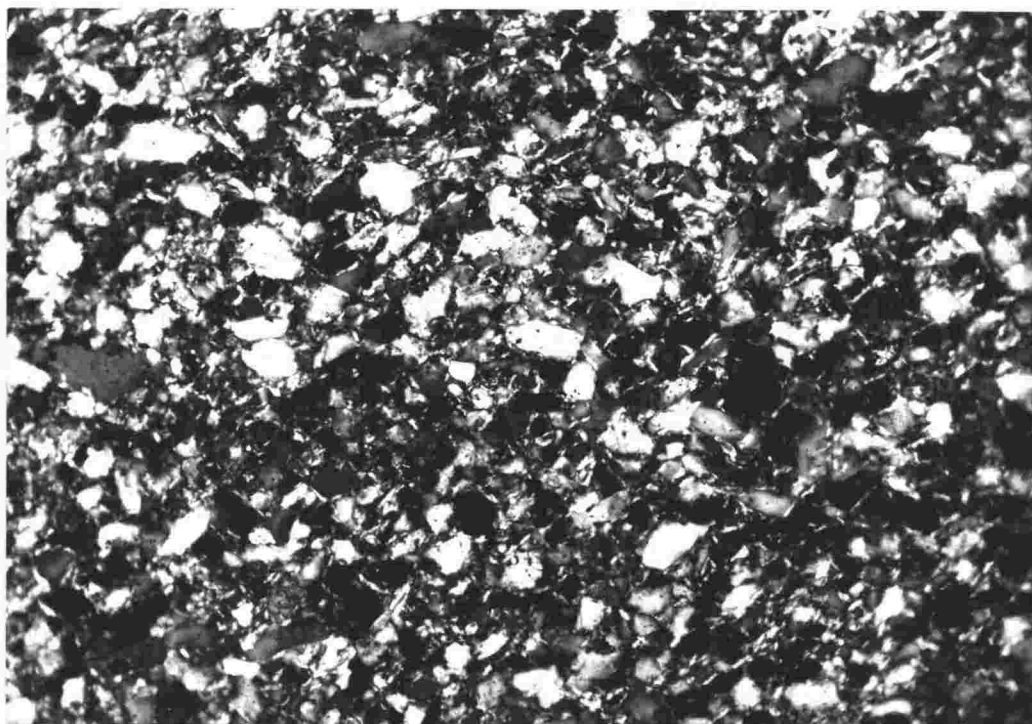
Fig. 5.11. A typical clayey siltstone with silt size detrital quartz
grains set in a matrix of illitic and chloritic clays.
Sample 23235, Al, unit 2. Polarized light. Scale 5 cm = 0.34 mm.
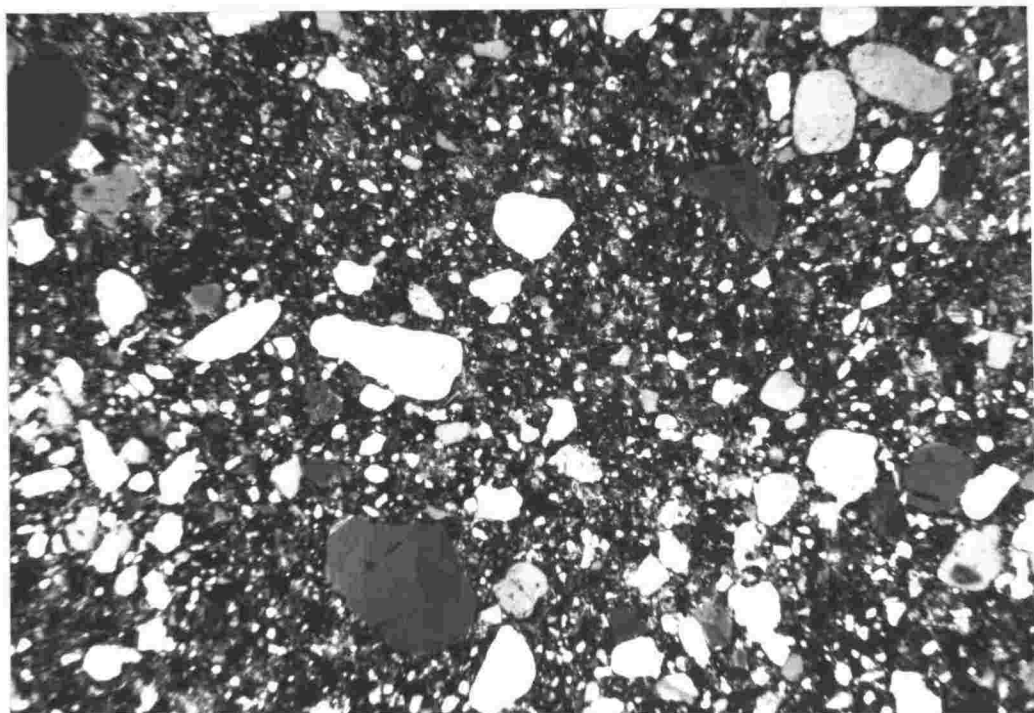
Fig. 5.12. A typical polymodal, silty claystone, sample 23304, Pl,
            unit 7, consisting of rounded, fine to medium sand-size
            quartz grains, in a finer grained matrix of very fine
            sand-size and silt-size quartz grains, and clays (see
            also Fig. 5.13). Polarized light. Scale 5 cm = 1.10 mm.

and, to a lesser extent, the finer-grained levee deposits
(cf. the Mississippi, Fisk, 1944, 1947; the Niger, Allen,
1964c, 1965d) and the swale-fill deposits (Allen, 1965a,
p.145).

GRAIN SHAPE

     Estimates of roundness and sphericity were made on the
clastic quartz grains of silt and sand size (Appendix Table 1).
A total of 49 samples from the Aztec Siltstone were selected
from each of the observed textural classes, and in those with
a polymodal size distribution, estimates of roundness and
sphericity were made for each mode. A further 12 samples
from the underlying Beacon Heights Orthoquartzite were
examined for comparison.

     Most samples were too indurated to be easily disaggregated
and all estimates were made on thin sections. For each thin
section the roundness and sphericity of 50 individual grains
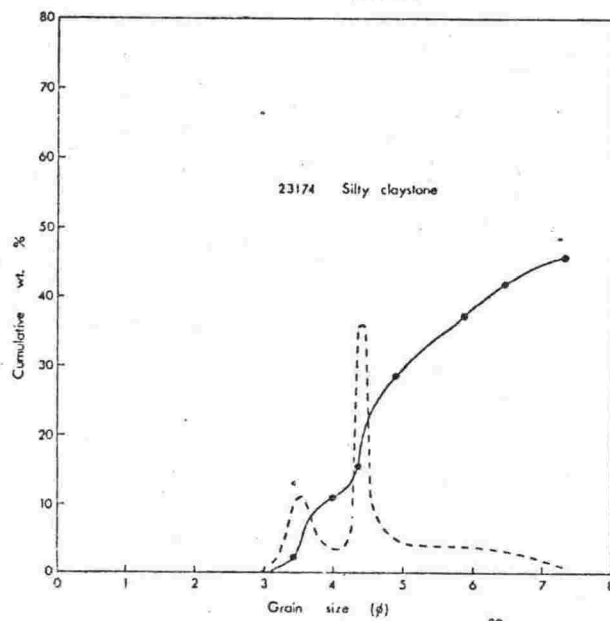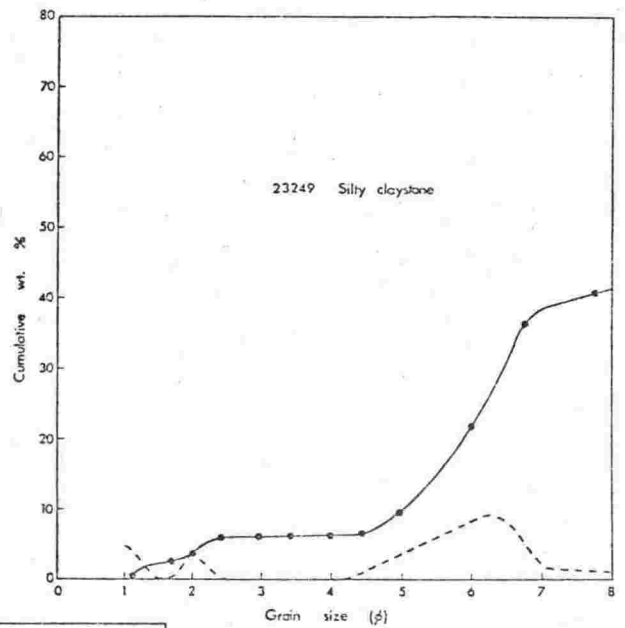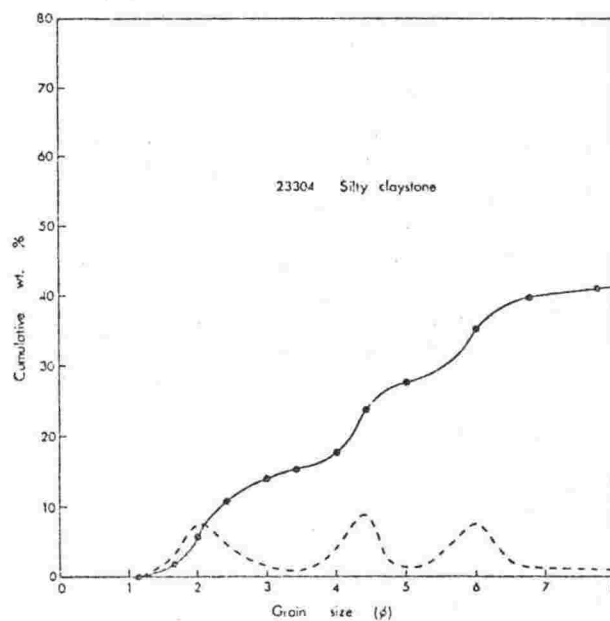
Fig. 5.13. Cumulative (solid line) and frequency (broken line) curves of three polymodal silty claystones from the fine-grained Aztec Siltstone sediments.
(a) 23174, A4, unit 42; (b) 23249, A1, unit 31;
(c) 23304, P1, unit 7.

115.

was determined by comparison with sets of grain silhouettes
from the standard roundness-sphericity chart (Fig. 5.14) of
Krumbein and Sloss (1963, p.111 Fig. 4-10). Although this
chart was initially intended specifically for sand size
grains, it nevertheless enabled comparative estimates of
the roundness and sphericity to be made for silt grains also.
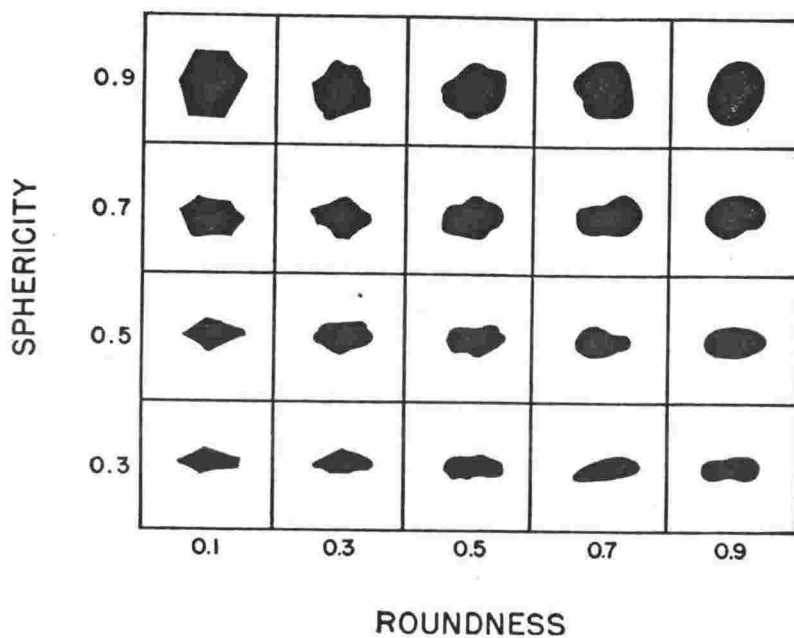
Fig. 5.14. Grain silhouettes used for visual estimation of roundness
and sphericity. (From Krumbein and Sloss, 1963).

Back checking was carried out from time to time to
ensure consistent estimation, and to check on operator error
(Table 5.1).

Table 5.1. Duplicate determinations of roundness and sphericity
for samples from the Aztec Siltstone, based on 50
sand size grains for each. $\bar{X}_r$ = mean roundness,
$\bar{X}_s$ = mean sphericity.

	23174		23256		23586	
	A	B	A	B	A	B
$\bar{X}_r$	0.31	0.33	0.38	0.36	0.78	0.79
$\bar{X}_s$	0.66	0.69	0.75	0.73	0.82	0.84

Gilbert, in Williams, Turner and Gilbert (1954, p.281),
concluded that thin sections lend themselves to a qualitative
evaluation of roundness and sphericity, but stated that round-
ness is more reliably represented than sphericity. He
reasoned that as the slice of a section represents only one
plane through each grain, and therefore two random diameters,
commonly it will not adequately represent sphericity, but may
allow a reasonable estimation of roundness.

The dependency of roundness upon size is shown by
Figure 5.15. The line is based upon the sandstones only, for
the roundness values from the siltstones may be anomalous,
as explained later in this section. There is a moderately
strong relationship between the two factors, in agreement
with Russell and Taylor (1937) and Pettijohn and Lundahl
(1943). The maximum value for rounding is reached for grains
of about 0.75 ϕ and, for a mean grain size of less than
approximately 3.8 ϕ , the graph indicates that the predicted
roundness is less than 0.3.

Because of the high sphericity typical of the clastic
grains of the Aztec Siltstone, orientation and packing effects
will be minimal, and thus by Griffith's scheme, a thin slice
revealing a random two dimensional view of the grain will more
closely approximate the true three dimensional shape of the
grains. This was checked by comparing grains in a thin section
with those in a grain mount from an easily disaggregated
sandstone (Table 5.2). By this method, the original shape
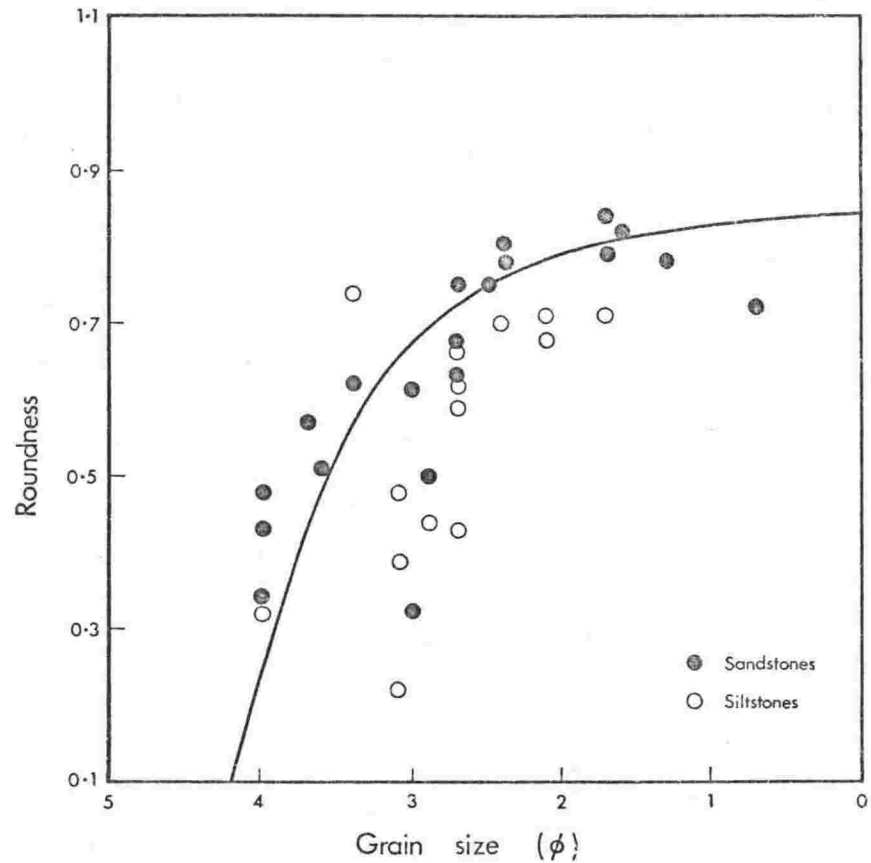
Fig. 5.15. Relationship between mean roundness and mean grain size for
samples of sand size quartz grains in the Aztec Siltstone.
Data from Appendix Table 1. Means could be used because of a
low standard deviation of grain size and roundness in individual
samples. The line, which was fitted by eye, is based on the
values for sandstones alone.

and size of individual grains could be clearly observed, as no
quartz overgrowths would be seen.

Table 5.2. Comparison of roundness and sphericity of 50 sand
size grains in thin section and in grain mount.
$\bar{X}_r$ = mean roundness, $\bar{X}_s$ = mean sphericity.

	Sample 23430	
	Thin section	Grain mount
$\bar{X}_s$	0.62	0.59
$\bar{X}_r$	0.72	0.75

Table 5.3. Mean and standard deviation of the roundness and sphericity values for samples of the Aztec Siltstone, based on 50 sand or silt size grains from each sample. Standard deviation is based on means of individual samples. $\bar{X}_r$ = mean roundness, $\bar{X}_s$ = mean sphericity. Data from Appendix Table 1.

Locality	Sandstones							
	A4	A1	M1	P1	P4	L1	L2	B2
$\bar{X}_r$	0.75	0.57	0.79	0.79	0.67	0.62	0.75	0.72
σ_r	–	0.13	–	0.06	–	–	–	0.14
$\bar{X}_s$	0.84	0.72	0.85	0.79	0.78	0.72	0.78	0.80
σ_s	–	0.03	–	0.08	–	–	–	0.06
N	1	2	1	3	1	1	1	4
	Siltstones and Claystones							
$\bar{X}_r$	0.27	0.43	0.37	0.60	–	0.57	0.58	0.59
σ_r	0.07	–	–	0.11	–	0.16	0.01	0.12
$\bar{X}_s$	0.70	0.65	0.74	0.76	–	0.74	0.78	0.78
σ_s	0.04	–	–	0.06	–	0.04	0.04	0.05
N	3	1	1	5	–	8	2	4

Table 5.4. Roundness and sphericity data from the Aztec Siltstone and Beacon Heights Orthoquartzite, showing a significant variation in roundness of sand size grains from sandstones and those in siltstones or claystones. $\bar{X}_r$ = mean roundness, $\bar{X}_s$ = mean sphericity. Data from Appendix Table 1.

| | Aztec Siltstone | | |
| | Sand Grains | | Silt Grains |
	Sandstone	Siltstone and Claystone	Siltstone and Claystone
$\bar{X}_r$	0.71	0.53	0.24
σ_r	0.11	0.15	0.09
$\bar{X}_s$	0.78	0.75	0.75
σ_s	0.06	0.05	0.09
N	14	17	28
	Beacon Heights Orthoquartzite		
$\bar{X}_r$	0.75	0.68	0.3
σ_r	0.08	-	-
$\bar{X}_s$	0.79	0.76	0.7
σ_s	0.06	-	-
N	10	1	1

The data show (Tables 5.3 and 5.4) that, for most samples, sand-size clastic quartz grains of the Aztec Siltstone, have a consistently high sphericity and are rounded, the characters of a supermature sediment (Folk, 1968, p.103).

The roundness and sphericity of the sand-size quartz grains in the sandstones of the Beacon Heights Orthoquartzite and the Aztec are very similar (Table 5.4). This suggests a similar high degree of reworking of the quartzose sediment of both formations, possibly with the two formations being derived from a similar parent. The compositional and textural characters of sandstones from the two formations are very similar, for example the lack of feldspar in both, the similar percentages of strained quartz grains and chert grains, and the similar inclusions of rutile needles, vacuoles, and dust in the quartz grains.

A few sand grains from the Aztec Siltstone comprise a well-rounded detrital quartz grain surrounded by a quartz overgrowth that is itself well-rounded (Fig. 5.16). This indicates that the Aztec source material included mature sediments, containing detrital grains of high roundness, like those of the more mature Taylor Group sediments.
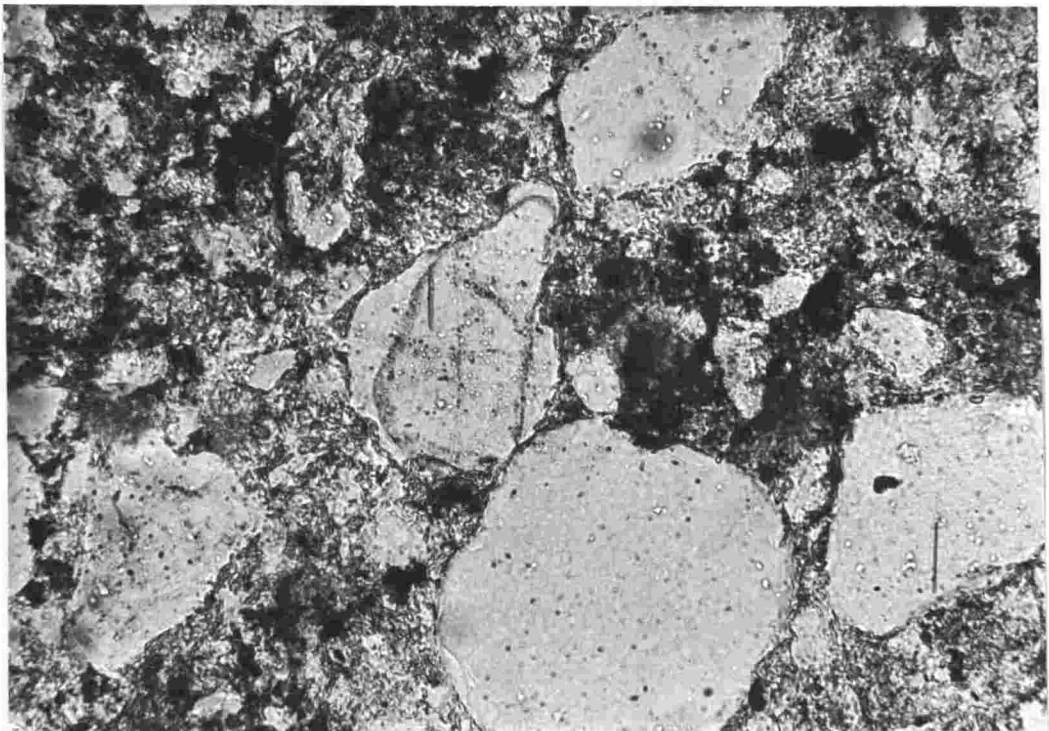
Fig. 5.16. A rounded sand size quartz grain which incorporates a rounded grain within it. Sample 23304, P1, unit 7. This suggests a sedimentary source rock for the Aztec Siltstone. Plain light. Scale 5 cm = 0.22 mm.

The factor most obvious from the analysis is the marked difference in the roundness of the sand-size quartz grains in sandstone, and those in the finer lithologies of the Aztec Siltstone (P less than 0.001; t = 3.9; d.f. = 29). The difference could be due to either a difference in source material, transportation and depositional processes, or post-depositional effects.

Two different types of source material is an unlikely explanation, as the composition, type and abundance of inclusions, and mode of extinction for the sand grains in both sandstone and siltstone are identical. It is most probable that the Aztec sand grains were all derived from a single source common with the Beacon Heights Orthoquartzite, and that the differences in roundness resulted from either depositional or post-depositional processes.

A process of selective sorting has probably contributed to the predominance of low roundness grains in the siltstone beds. Pettijohn and Lundahl (1943) noted that less rounded grains settle from a suspension more slowly than more rounded grains of the same diameter. Thus, they are carried further in suspension and are more likely to be deposited with finer grained sediments.

However, post-depositional solution is also an effective process for reducing roundness. Griffiths (1958 and 1960) and Kuenen and Perdok (1962) noted that quartz grains are more angular and irregular in contact with carbonate than in un-cemented areas of the same rock. The solution of quartz is facilitated by a high pH due to dissolved carbonate (Krauskopf 1956; Fig. 5.17).

Krauskopf (1967, p.66) showed that the pH of solutions in contact with calcite should theoretically have a value in the range of pH 8-10, with the lower value for solutions in contact with atmospheric CO_2 (near surface), and the higher value for solutions at depth out of contact with the atmosphere. The equilibria involved are:

$$H_2O + CO_2 \qquad CO_3^= + 2H^+$$

$$CaCO_3 + H_2CO_3 \rightleftharpoons Ca^{2+} + 2HCO_3^-$$
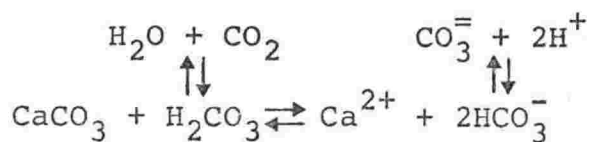
Thus if the pCO_2 is increased, (i.e. exposed to atmospheric CO_2) then the equilibrium is shifted to the right, and the pH will be lowered.
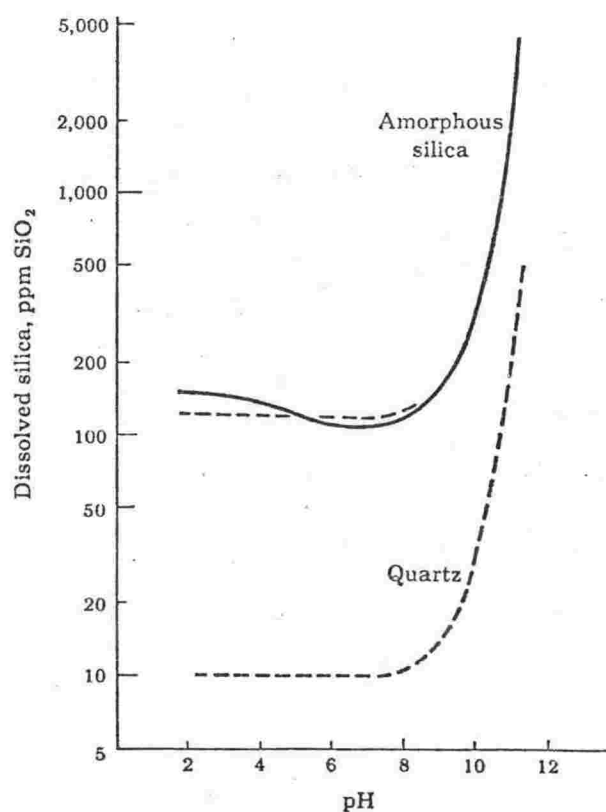
Fig. 5.17. Solubility of silica at 25°C (Krauskopf, 1967). The solid line shows the variation in solubility of amorphous silica with pH as determined experimentally. The upper dashed line is a calculated curve for amorphous silica, based on an assumed constant solubility of 120 ppm SiO_2 at pH's below 8 and on a value of -9.9 for log k_1 for H_4SiO_4. The lower dashed line is the calculated solubility of quartz, based on the approximately known solubility of 10 ppm SiO_2 in neutral and acid solutions.

The very high calcite content of the Aztec Siltstone as nodules and cement, in particular for the finer grained lithologies, makes it likely that some quartz solution has taken place (as for example in the calcite cemented sandstones, Fig. 5.18), and the irregular embayed character of many grain boundaries throughout the finer grained lithologies supports this (Fig. 5.19). The irregularity of the embayments clearly indicates that they are points of chemical solution, and not fractures.
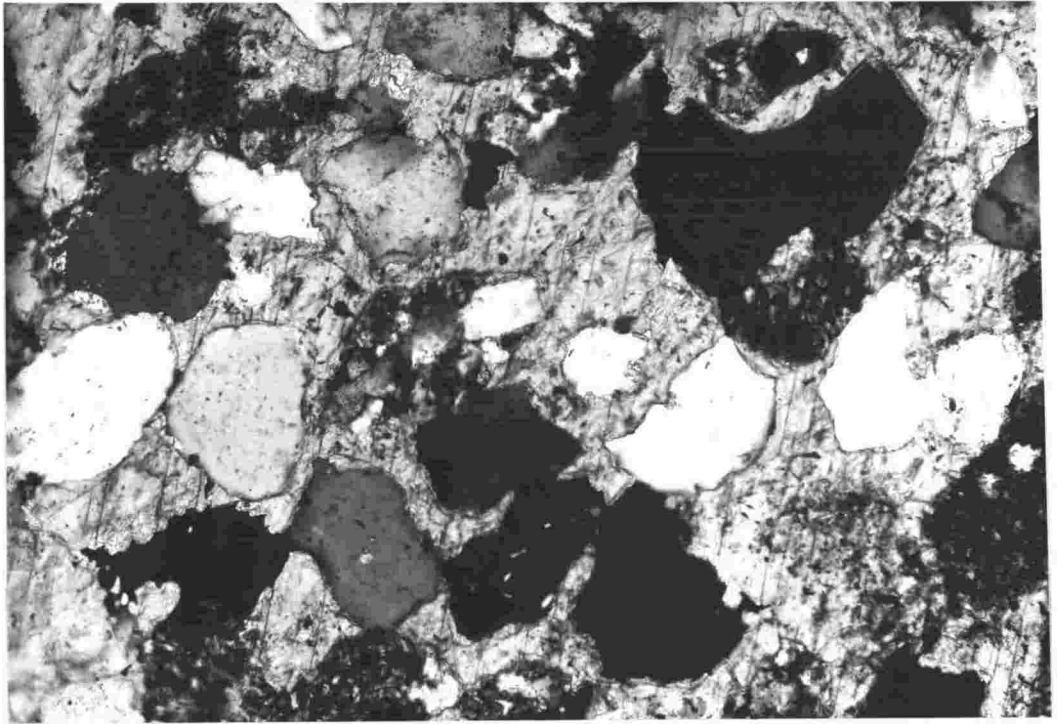
Fig. 5.18. Irregular embayments in detrital, sand size, quartz grains
that are cemented by optically continuous calcite. Sample
23246 from section A1. The embayments are the result of
solution of the quartz induced by the calcite. Polarized
light. Scale 5 cm = 0.34 mm.
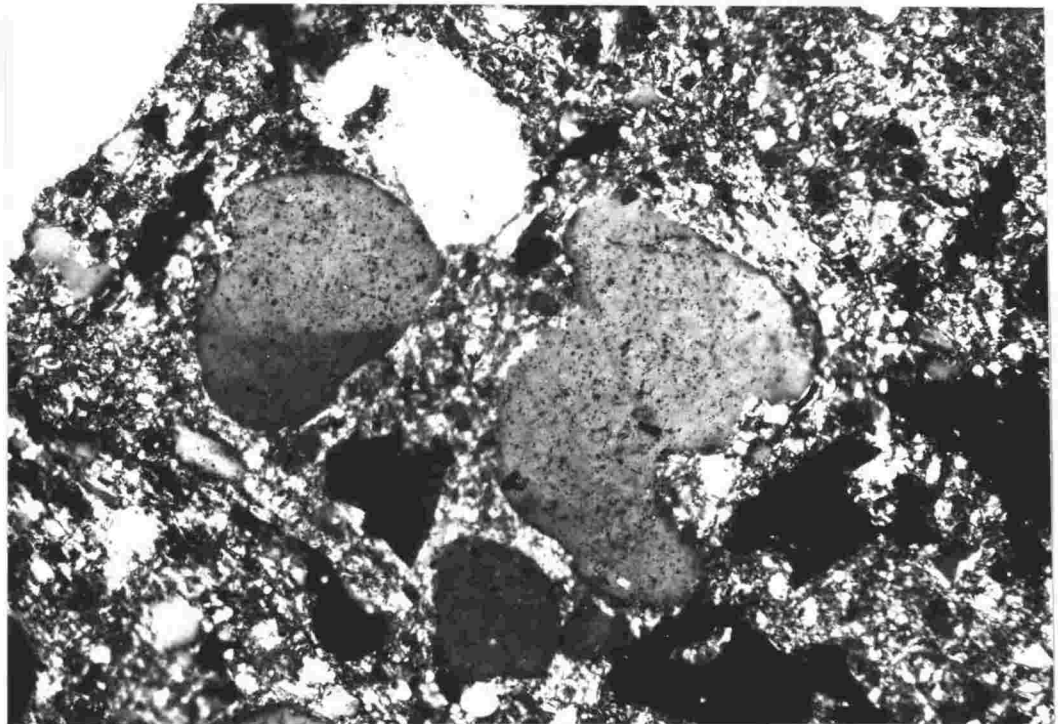
Fig. 5.19. Irregular embayments in detrital sand size quartz grains in
a polymodal silty claystone, sample 23304, P1, unit 7. The
embayments are possibly a result of post-depositional
solution of quartz induced by calcite. Polarized light.
Scale 5 cm = 0.34 mm.

Many of the finer grained units of the Aztec Siltstone have undergone pedogenesis (Chapters 4, 5, 6), and it is thought that the soil-forming processes, which include the chemical solution of quartz grains as well as comminution and biologic activity, have all contributed to a lowering of quartz grain roundness. As an example sample 23174 is from a soil horizon containing root cast structures, and has a relatively low roundness for the quartz sand grains (Appendix Table 1).

The sphericity values of the silt fraction are extremely consistent, mostly 0.7 with a few at 0.9 (Appendix Table 1). Roundness values range from 0.1 to 0.3. Figure 5.15 shows this as the approximate predicted value for the roundness of all silt-sized particles, but sample 23584 has a higher roundness than expected. It is from a burrowed bed, and the greater roundness is attributed to rounding in the digestive tracts of the burrowing organisms (Kindle, 1919).

The roundness-size relationship evident from Figure 5.15, may also be used to indicate a degree of reworking and maturity for the Aztec Siltstone. Pettijohn (1957, p.64) noted that only a mature sediment should attain such a relationship between rounding and grain size. The fact that there is such a relationship throughout, also strongly supports the concept of a single uniform source area for the sediment.

In summary, the roundness and sphericity of the sand-size quartz grains of the Aztec Siltstone is moderately high, but it is most probable that the source material also had a moderately high roundness and sphericity. Sand-size quartz grains in the sandstones of the Aztec have a high roundness, similar to those of the underlying Beacon Heights Ortho-quartzite, but those in the finer beds are less rounded. The chief cause is thought to be post-depositional chemical solution of grain surfaces, promoted by the widespread occurrence of calcite in the finer beds.

MATURITY

The sandstones of the Aztec Siltstone, in general, fall
into the two end member categories of the textural maturity
index of Folk (1968) (Appendix Table 1). Those without a clay
matrix or with a matrix of less than about 5 percent, generally
have a sorting value (σ_I) less than 0.5 ϕ and invariably have a
roundness (ρ of Folk) over 3.0. These then, are supermature
sandstones. The other group are immature sandstones and have
a clay matrix which forms from 5 to 50 percent of the sample.
This group, which includes clayey sandstones, is gradational
with the sandy claystone and mudstone groups (Fig. 5.9).
However, these poorly sorted sandstones are, in most examples,
a special case, because they contain clastic grains which are
themselves well rounded and well sorted (Figs. 5.20 and 5.21).
These sandstones thus display textural inversion (Folk, 1968,
p.105).

The supermature sandstones constitute approximately 75
percent of the sandstones analysed (Appendix Table 1). These
point bar and channel sands have a higher than normal maturity
index for river channel sediments. Normal river channel
deposits fall into the submature and mature classes (Folk,
1968, p.106), but as pointed out by Folk, a factor of time must
be taken into account. The supermature sandstones of the Aztec
Siltstone appear to have resulted from the reworking of older
sedimentary formations, possibly those of the Taylor Group.
Hence, much of the supermature character of the sandstones
was probably inherited, as the older Taylor Group sediments are
themselves well-rounded and well-sorted. The supermaturity
is also considered to be a product of a tectonically stable
environment of deposition, with a slow sediment influx (Folk,
1968), resulting in extensive reworking of the sediment. This
facilitated the increased rounding and sorting of the grains.

Sandstones with textural inversion constitute approximately
25 percent of the sandstone samples examined from the Aztec
formation. Numerous forms of textural inversion exist, but
one of the most common is of well rounded and sorted clastic
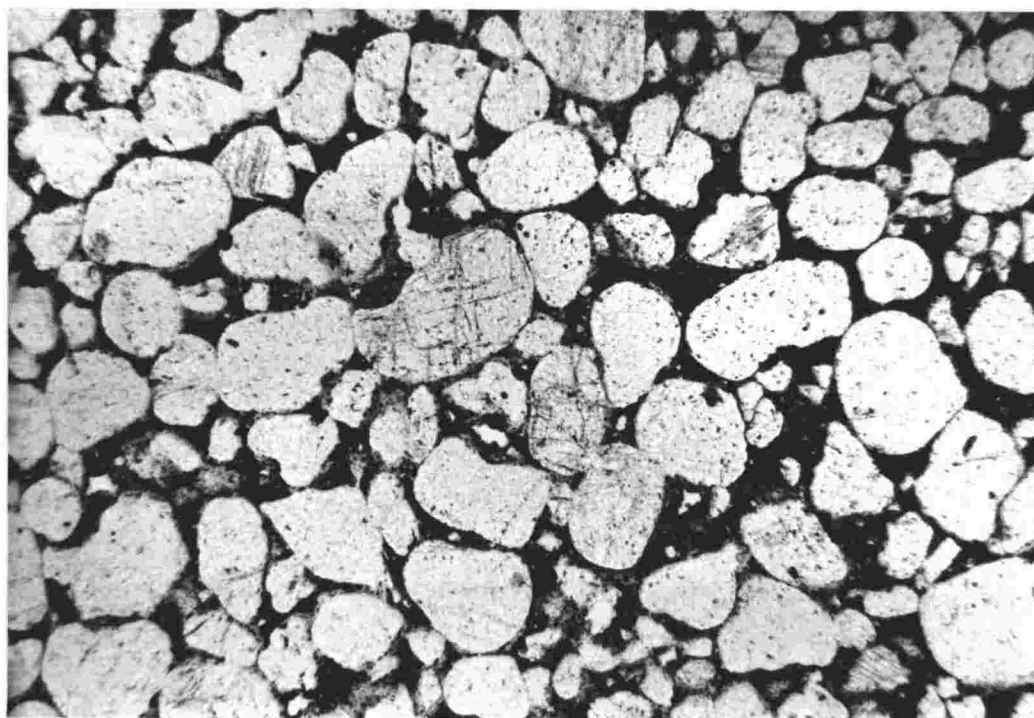
Fig. 5.20. Texturally inverted (immature) sandstone consisting of well
rounded and well sorted medium sand size quartz grains
hosting a green, clay matrix. Sample 23579, B2, unit 1.
Such sandstones are a result of post-depositional sediment
mixing. Plain light. Scale 5 cm = 1.10 mm.
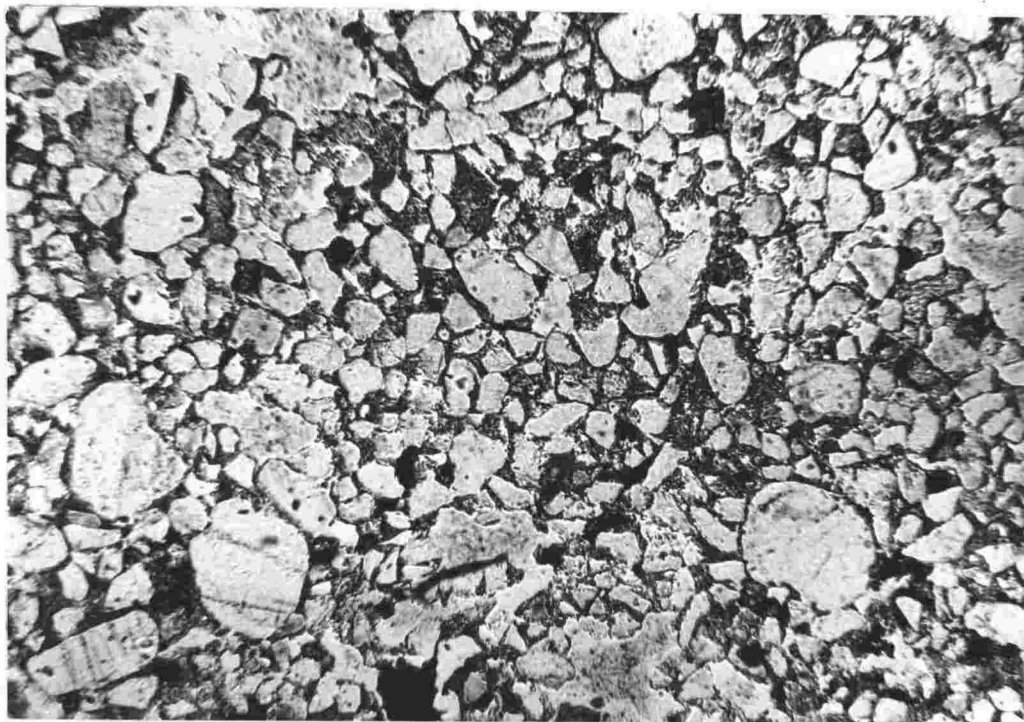
Fig. 5.21. Texturally inverted (immature) clayey sandstone, consisting
of well rounded and well sorted medium sand size quartz grains,
sub-angular and well sorted very fine sand size quartz grains,
and a clay matrix (see also Appendix Table 2). Sample 23438.
L1, unit 29. Plain light. Scale 5 cm = 1.10 mm.

quartz grains embedded in a clay matrix (Figs. 5.20 and 5.21).
In the main, these sandstones are not thought to be simply
poorly sorted fluvial sandstones, because they have a strongly
polymodal character with well sorted sand-sized (possibly silt-
sized) and clay-sized modes. These texturally inverted sand-
stones are considered to have resulted from sediment mixing
of one type or another.

The interbedded sandstone-claystone character of the Aztec
Siltstone would have readily facilitated textural inversion
through the migration of clays, probably in colloidal suspension,
into the well sorted and therefore highly permeable sandstones,
especially during the early post-depositional period. The
bioturbation of sediments is another cause of textural inversion,
and one that was common for the Aztec Siltstone. Examples of
sediment mixing by burrowing organisms are numerous in the
formation (Figs. 2.1 and 4.46; see also Chapter 4, Trace
Fossils) and where this has taken place within interbedded
sequences of well sorted sands and clean clays, the result has
[...] a homogeneous mass of clayey, immature sand. Textural
[invers]ion can also occur when high energy process destroy a
deposit, the kind of destruction that is likely to
[...]vial plain during high energy but short lived.
[...]ns.

been caused through post-depositional sediment mixing, or by

the reworking of older sediments in the source area.
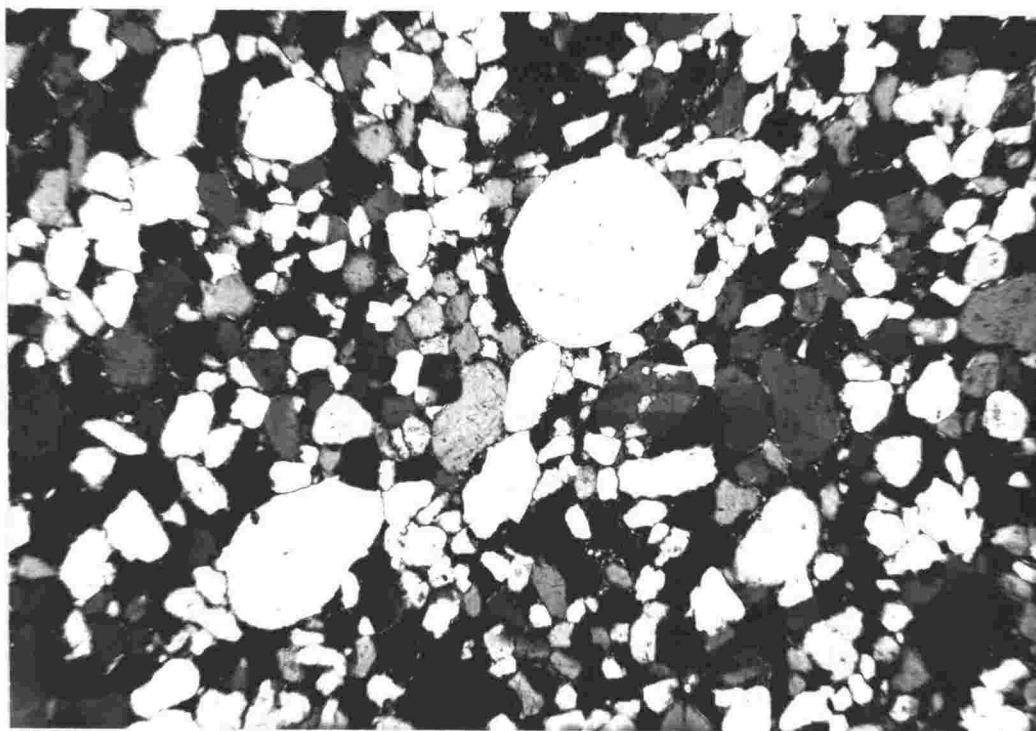
Fig. 5.22.   Texturally inverted (immature) sandstone, consisting of two
             well sorted sand size quartz modes. Thus the sandstone is
             only moderately sorted overall (σ_I = 0.73 ϕ) (see also
             Appendix Table 1) sample 23581, B2, unit 3. Note the
             difference in grain roundness of the two modes. Polarized
             light. Scale 5 cm = 1.10 mm.

The immature sandstones of the formation are difficult
to allocate to a specific environment of deposition because of
sediment mixing which produced the textural inversion. However,
the presence of these immature sands does indicate that the final
environment of deposition was one of low energy, or else the
sediment would have been reworked just prior to burial. Immature
sediments such as these are common to the floodbasin environment
(Folk, 1968).

Composition

SANDSTONES

Modal Analysis

Thin section modal analysis was carried out on 12 sand-
stone samples selected as representative of the formation. (A thin

section modal analysis of the fine-grained lithologies was not
practical because of the small grain size.) The determinations
were done by the Glagolev-Chayes method, using a Swift
automatic point counter with a horizontal point count interval
of 0.3 mm and a vertical interval of 1 or 2 mm. For each thin
section, between 500 and 600 points were counted, and the
samples classified according to the scheme of Folk (1968).

Most of the sandstone samples are quartzarenites (Table
5.5, Figs 5.8 and 5.23),although a single example of a
sublitharenite was found. Most are cemented by quartz over-
growths, but many include some post-depositional clay matrix
(Fig. 5.24). Calcite cement is present in approximately 15
percent of the samples (Fig. 5.25). The matrix has been
zeolitized in a few cases (e.g. to heulandite in 23319 ,
Table 5.7), zeolitization having taken place possibly due to
contact metamorphism by the sills and dykes of the Jurassic
Ferrar Dolerite. Chert grains are present in many sandstone
samples but generally constitute less than 1 percent of the total.
Heavy minerals are rare but include well-rounded grains of
tourmaline, zircon, and very rare garnet and rutile.

Lithic fragments are present in many sandstone beds,
though they average only one percent. They are of a silty
claystone composition in most cases, and intraformational
in origin. K-feldspar is very rare and in every case is
extensively altered to sericite. Plagioclase was not detected
in any of the samples examined.

The major constituent of all sandstones is quartz, generally
as well-rounded grains (see Grain Shape, p.113) showing straight
to slightly undulose extinction. The grains generally contain
a few inclusions in the form of scattered vacuoles often
arranged in lines through the grain. Microlites are rare,
but some grains contain hair-like rutile needles. Quartz of
the above described type is a common product of plutonic rocks
(Folk, 1968, p.71).

Two of the sandstone samples thin-sectioned (23241 and 23246)
contained some quartz grains which were coated with crypto-
crystalline haematite pigment (Fig. 5.26). Generally the grains

Table 5.5. Modal analyses (in percent) for sandstone samples of the Aztec Siltstone. (* less than 1 percent).

Location	Sample	Quartz		Feldspar		Lithic	Chert	Calcite	Zeolites	Heavies	Cement	Matrix	Rest
		Plut.Qtz	Meta.Qtz	K-spar.	Plag.						(Qtz)	(clay)	
A4	23175	82	1	*	0	0	0	0	0	0	17	0	0
"	23183	77	*	0	0	0	1	1	0	1	20	0	0
Al	23241	66	0	0	0	0	*	15	0	*	17	2	0
"	23250	81	1	*	0	2	1	0	0	*	13	2	0
Pl	23315	75	1	0	0	*	0	0	1	0	22	1	0
"	23319	59	0	*	0	1	0	0	3	*	37	*	0
L2	23458	76	2	0	0	1	*	0	*	*	20	*	1
B2	23581	80	0	0	0	0	0	0	0	0	17	3	0
"	23586	84	0	0	0	0	*	0	0	0	16	0	0
"	23588	76	1	*	0	0	0	0	0	0	23	*	0
H6	25138	78	1	*	0	0	0	0	0	0	21	*	0
"	25144	64	4	0	0	8	3	0	0	0	17	3	*
	Mean	74.8	0.9	0	0	1.0	0.4	1.3	0.3	0.1	20.0	0.9	0.1
	Std Dev.	7.8	1.2	0	0	2.3	0.9	4.3	0.9	0.3	6.1	1.2	0.3
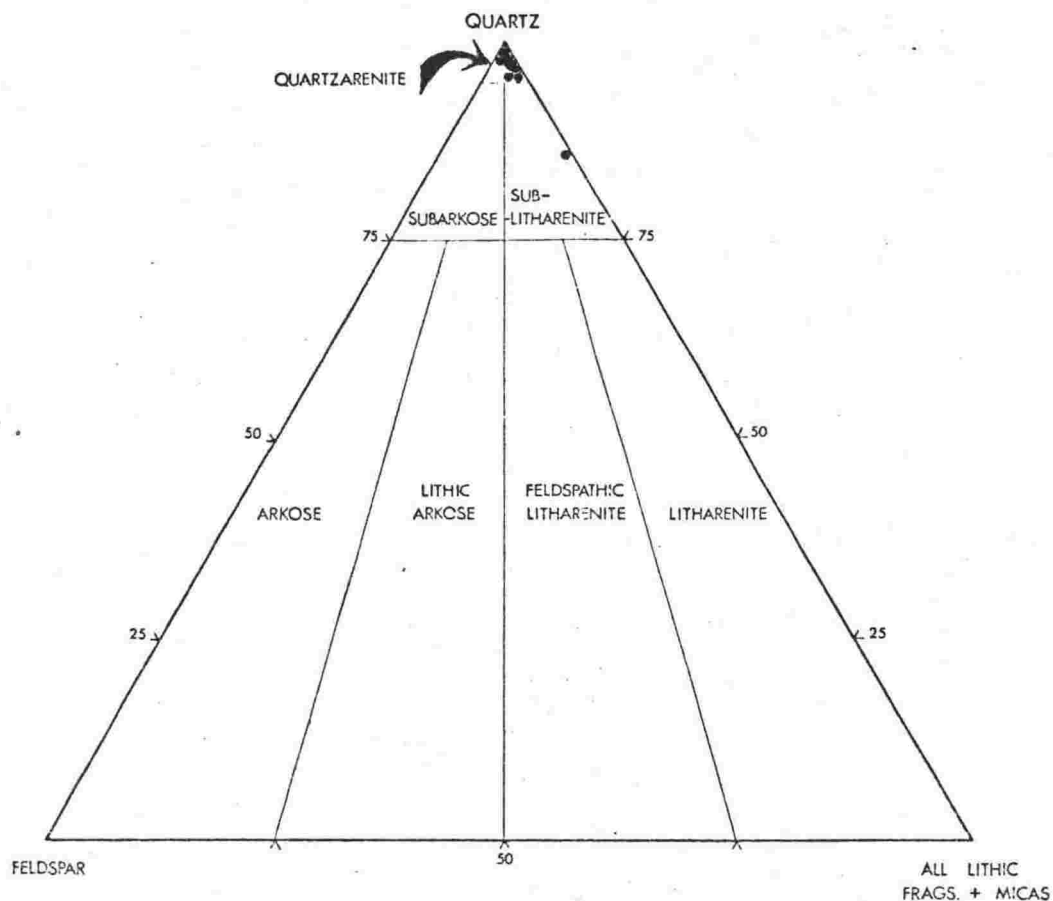
Fig. 5.23. Composition of 12 sandstone samples from the Aztec Siltstone. All but one are quartzarenites. Data from Table 5.5.
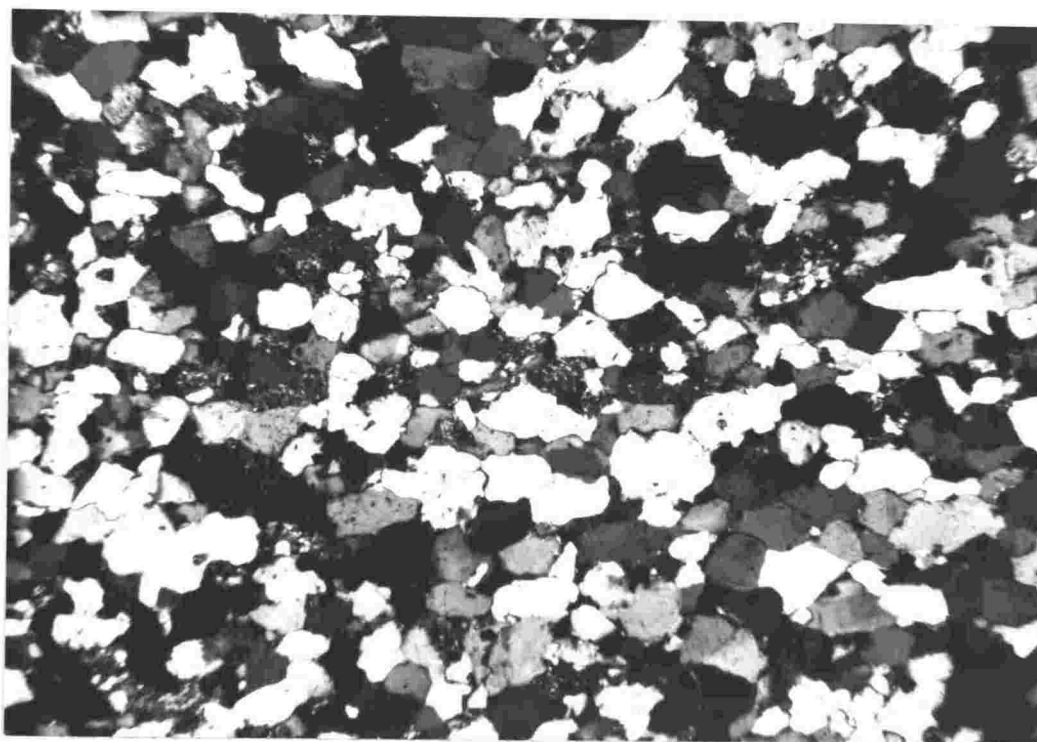
Fig. 5.24. A photomicrograph of a fine grained quartzarenite, sample 23250, A1, unit 32 (see also Table 5.5 for composition). Polarized light. Scale 5 cm = 1.10 mm.
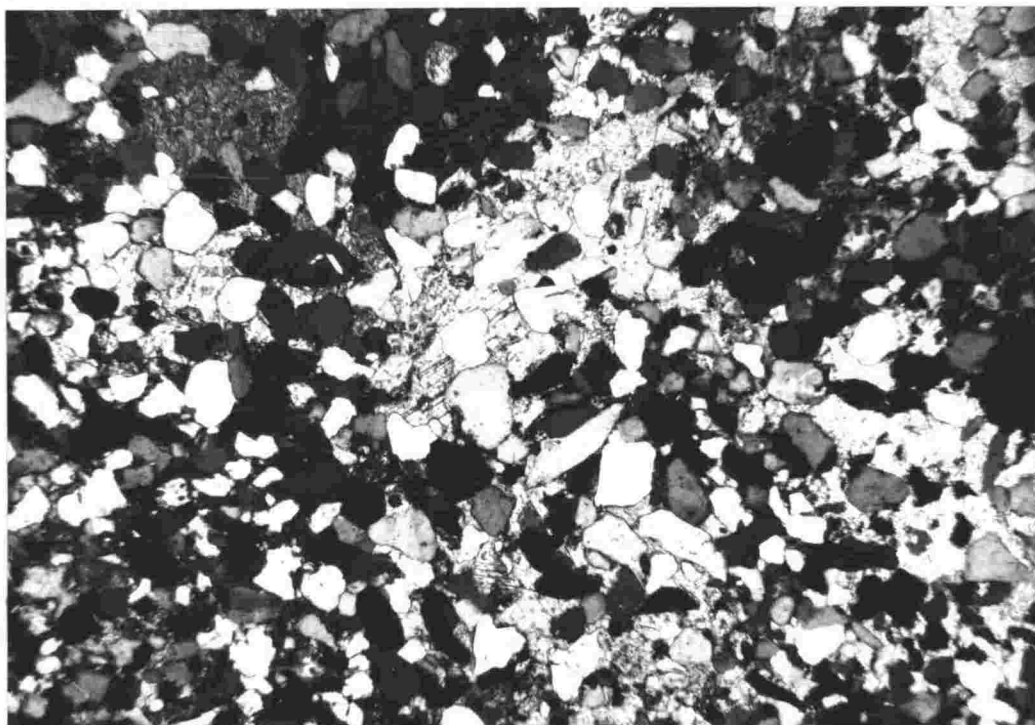
Fig. 5.25. A photomicrograph of a very fine grained quartzarenite that
            is cemented by calcite, commonly in large optically
            continuous grains. Sample 23241, A1, unit 14. (see also
            Table 5.5 for composition). Polarized light. Scale
            5 cm = 1.10 mm.
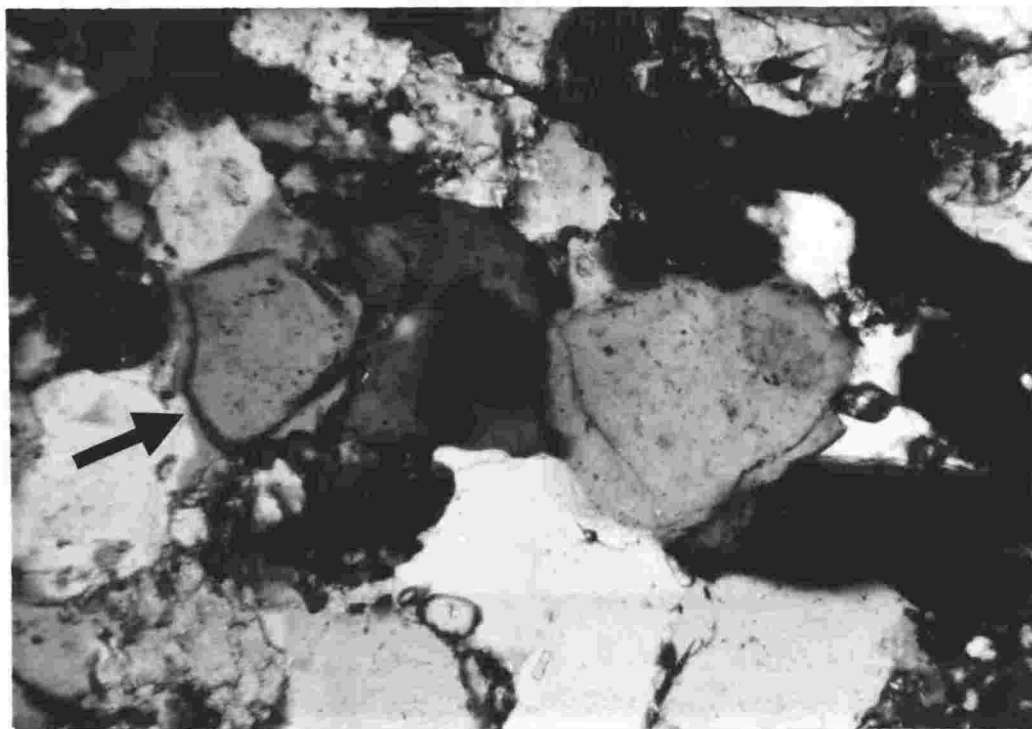
Fig. 5.26. Haematite completely rimming (on the detrital grain boundary)
            a quartz grain in a very fine-grained quartzarenite, sample
            23246, A1, unit 26. Only a few such grains were found in the
            sample. Polarized light. Scale 5 cm = 0.35 mm.

were completely rimmed (on the detrital grain boundary) with haematite which had since been overgrown by the quartz cement. These reddened grains must have acquired their haematite coatings prior to cementation of the sandstone, and were probably red when last deposited. They were probably derived from the local reworking of earlier reddened Aztec sediments.

Stretched metamorphic quartz (or sheared quartz) sand grains were present in most sandstones (mean = 0.9 percent). They were identified by their composite nature, a strong undulose extinction, and a tendency to be more elongate than the well-rounded, common quartz grains. Quartz grains with reworked overgrowths are present (Fig. 5.16), although rare, in some sandstones of the formation. They indicate an older quartzite source for the formation.

The extremely high quartz content of the Aztec Siltstone indicates intense weathering in the source region, or recycling; probably the latter in view of the trend in the Taylor Group sediments (arkosic and more angular at the base). The chert grains are suggestive of a sedimentary source, as is the lack of feldspars and mica, since the extended period of weathering and the extensive abrasion from reworking would have eliminated these relatively unstable constituents. The presence of only ultra-stable heavy minerals suggests repeated sediment reworking over a long period. Although little can be said about the original source lithology, the mixed types of quartz grains found in the Aztec formation are representative of both plutonic and metamorphic sources.

Some sandstones contain a clay matrix which is considered to have been post-depositionally introduced. It is probable that clays from the interbedded fine-grained units were carried into the sandstones by colloidal suspension.

SILTSTONES AND CLAYSTONES

Analytical Methods

X-ray Diffraction

X-ray diffraction analysis was used to determine bulk
mineral composition of fine-grained samples and of the matrix
of sandstones in the Aztec Siltstone. Sandstone matrix was
concentrated by partial crushing and sieving to reduce the
percentage of detrital quartz. Nodules, concretions and
unknown minerals from voids and lenses were also examined by
X.R.D. and thin section.

The samples were first crushed (~200 mesh) and than
precipitated onto glass slides from an acetone suspension.
Duplicate slides were prepared from many samples; one was
X-rayed before and after heating to 550°C for 4 hours. The
other was X-rayed for expandable clays after the rock powder
had been treated with warm (70°C) 10 percent HCl solution for
12 hours, and then sedimented onto a glass slide. This procedure
was carried out in order to test for the presence of kaolinite
after removing the neighbouring and masking chlorite peak.

The samples were analysed using a Phillips X-ray
Diffractometer, with Nickel filtered CuKα radiation generated
at 36 kv and 18 mA and directed by a 1° beam slit and a 0.2°
detection slit. The samples were scanned at 2° 2θ/min. from
4° to 45° 2θ and at 1/8° 2θ/min. from 24° to 25.5° 2θ, the
latter to check for kaolinite. The chart speed, time constant
and flow-counter count rate settings were adjusted to give
optimum results.

Interpretation of the diffractograms was carried out using
the A.S.T.M. Powder Data File. Accurate d-spacings were obtained
by reference to the detrital quartz present in each sample. In
the case of the clay minerals, special characteristics were
tested for (Table 5.6, Fig. 5.27). Kaolinite was not detected
in any sample X-rayed, even after the HCl treatment to remove
the overlapping chlorite peak (3.54 Å) and a slow scan (1/8° 2θ

Table 5.6. Characteristics used for the identification of clay minerals in the Aztec Siltstone samples.

Mineral	Effects of various pre-treatments on basal spacings				Notes
	Air-dry basal spacing	Glycolated	Heated 4 hrs at 550°C	Warm 10% HCl, 12 hrs	
Kaolinite	7.1 Å 3.58 Å	Unaffected "	Both peaks vanish	Unaffected "	7 Å peak stronger than 3.5 Å peak
Illite	10 Å 4.5 Å 3.3 Å 2.56 Å	Unaffected " " "	Peaks sharpened	Unaffected " " "	
Chlorite	14.2 Å 7.12 Å 4.75 Å 3.54 Å	Unaffected " " "	14.2 Å peak enhanced, remainder diminished	Diminished peaks	14 Å peak changed to 13.7 Å which is indicative of Fe-chlorites that show shrinkage parallel to c.
Montmorillonite	15 Å	Expands to 17.5 Å	Collapses to 10 Å	Unaffected	Swelling on glycolation.
Vermiculite	14 Å	Unaffected	Collapses to 10 Å	Unaffected	No swelling on glycolation.

min.) from 24.5° to 25.5° 2θ (3.58 Å peak) after the method
of Biscaye (1964).

Chlorite was present in most samples, characterized by
a non-expanding peak at 14.2 Å which was enhanced after heating
of the sample to 550°C for 4 hours (Fig. 5.27). The other
chlorite peaks were diminished or removed by the heat treatment.

Illite was present in most samples as shown by peaks at
10 Å, 4.5 Å, 3.3 Å and 2.56 Å. It is possible that some 3T
muscovite is also present in samples, as suggested by a strong
peak at 4.9 Å. However, this could not be confirmed because
of the complete overlap with illite peaks including the 4.9 Å
peak.

The samples examined showed no expansion of peaks
following treatment with ethylene glycol (12 hours in atmosphere
saturated with glycol at 60°C), establishing that expandable
clays e.g. montmorillonite, vermiculite or swelling chlorites,
were not present.

Peak heights above background were used as a measure of
peak intensities instead of peak areas. Moore (1968) showed
that peak height is an adequate representation of peak
intensity for orientated samples. Relative abundances were
then calculated from peak intensities (Table 5.7). A recalcu-
lation of peak intensities to percentages for each specimen was
not attempted for two main reasons. Firstly, the result would
be, at best, semi-quantitative because of the intensity
variations which arise solely through sample preparation. This
is especially true in the case of the clays. Secondly, there
is no known satisfactory method for determining the mineral
percentages in a sample containing six or more components,
particularly when three are clays.

Infrared Spectrophotometry

Six samples were analysed by infrared spectrophotometric
methods, using a Perkin Elmer Grating Infrared Spectrophoto-
meter (model 337) at the N.Z. Geological Survey, Lower Hutt.
The results (Table 5.8) are in agreement with the X-ray
diffraction and X-ray fluorescence data (Tables 5.7 and 5.10)
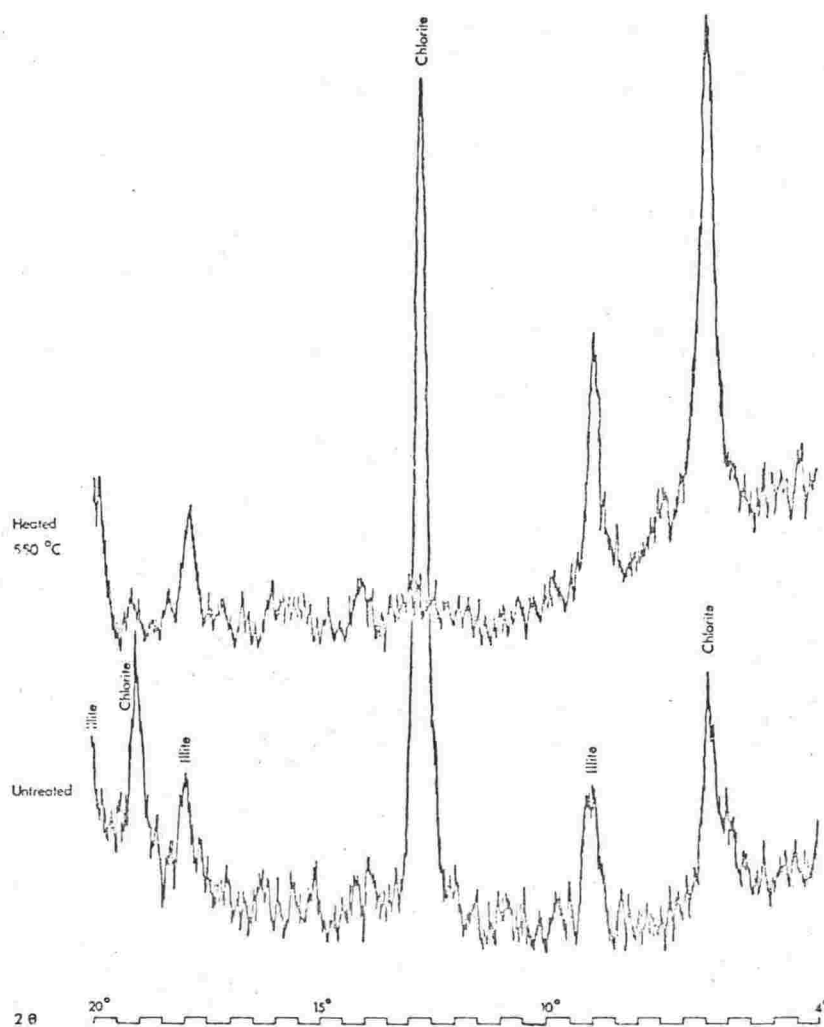
Fig. 5.27.   Variations in the X-ray diffraction pattern of bulk
             sample 23310, a fine-grained sample, after heat treatment
             at 550°C for 4 hours.   The 14.2 Å chlorite peak was
             enhanced but other chlorite peaks have been greatly
             diminished.   The illite peaks have been sharpened.

Table 5.7 Minerals identified by X-ray diffraction, in samples from the Aztec Siltstone. Peak intensities, obtained from peak heights, were used to obtain relative abundances. x-present, xx-common, xxx-abundant, xxxx-very abundant. Modal analyses, either partial or complete, are given for most samples in other sections of the thesis.

Location	Sample	Lithology	Colour	Quartz	Illite	Chlorite	K-feldspar	Na-feldspar	Haematite	Calcite	Prehnite	Epidote	Analcime	Laumontite	Heulandite	Others
A4	23174	SiClSt	10GY 5/2	xxx	x	x				xxx			x			
A1	23228	"	1OR 4/2	xxx	xxx	xx		xx	xx							
"	23229	"	"	xxx	xxx	xx		xx	xx				x			
"	23230	"	N5	xxx	xxx	xx		xx	x							
"	23230	Nodule	-	xxx	xx	xx		xx		x		xxx				
"	23233	ClSt	5G 6/1	xxx	xxx	xxx		x								
"	23233	Nodule	-	xxx	xx	xxx		xx		x		xxx				
"	23235A	SiClSt	1OR 4/2	xxx	xxx	xx		x	xx							
"	23237	Nodule	-	xx						xxxx						
"	23240	ClMSt	5G 6/1	xxx	xxx	xxx		x	x				xxx			
"	23243	ClSt	1OR 3/4	xxx	xx	xx		xx	xx	xx		xx	xx			
"	23243	Sphere	-	xxx	xxx	xx			x	x			xxx			
"	23244	ClSt	5P 4/2	xxx	xx	x		x	xx	xx						
"	23244	Nodule	-	xxx	xx	xx			x	xxx	x					
"	23245	"	-	xx						xxxx						
"	A1-15	SiClSt	1OR 4/2	xxx	xxx	xx		xx	xx							
"	A1-16	"	5G 6/1	xxx	xxx	xx		xx	x							
M1	23256	SiClSt	1OR 4/2	xxx	xxx	xx		x	xx							
"	23260	ClSt	"	xxx	xxx	xx		x	xx							
"	23260	Nodule	-	xx					x	xxx		x	xx			
"	23274	"	-	xx				x			x	xx	xx			x grossular x apatite
"	23281	ClSt	5GY 8/1	xxx		xx					xxx	xx				x
"	23281	Nodule	-		x	x				xxx	xx				xx	x grossular
P1	23300	Concretn.	-													xxxx pyrite
"	23304	SiClSt	5GY 6/1	xxx	xx	xxx	xx	x				x		x		
"	23306	Nodule	-	x						xxxx						
"	23307	"	-	x						xxxx						
"	23310	ClSt	5GY 6/1	xxx	xx	xxx		xxx				x				
"	23310	Concretn.	-							xx		xx	xxx			
"	23316	Nodule	-							xxxx						
"	23319	SSt	5GY 8/1	xxx	xx	xx		x		x					xx	
"	unit 14	Fish bone														xxxx apatite
L1	23424	Concretn.	-	xx												xxxx pyrite
"	23425	Lst	N3	x						xxxx						
"	23429	Lense	-	x						xxxx						xxxx gypsum
"	23436	Nodule	-	x						xxxx						
"	23440	Concretn.	-	amorphous iron oxides xx												
* "	23432R	SiClSt	5R 4/2	xxx	xxx	xx		x	xx							
* "	23432Gr	"	5GY 6/1	xxx	xxx	xx		x	x							x
"	23437	ClSt	"	xxx	xxx	xxx		x	x	x						
* "	L1-19R	SiClSt	1OR 4/2	xxx	xxx	xx			xx							
* "	L1-19Gr	"	5G 6/1	xxx	xxx	xx										
L2	L2-13	"	5GY 6/1	xxx	xxx	xxx		x								
"	L2-16	Pisolite								xxxx						
* AZ	AZ-06	SiClSt	1OR 4/2	xxx	xx	x		x	xx				x			
* "	AZ-07	"	5G 6/1	xxx	xx	x		x								
"	AZ-19	ClSt	1OR 4/2	xxx	xxx	xx		x	xx							
B2	23579R	"	1OR 4/2	xxx	xxx	xxx		x	xx							
"	23582	SClSt	N9	xxx	xxx	xx			x							x

* red-green or red-grey pairs.

Table 5.8.   Infrared spectrophotometric analyses of fine-grained samples of the Aztec Siltstone.
(Analyst, R. Soong).

Location	Sample	Lithology	Colour	Quartz (%)	Feldspar (%)	Illite (%)	Chlorite* (%)	Calcite (%)	Iron oxides/ hydroxides** (%)	Amorphous siliceous material (%)
A1	23228	SiClSt	10R 4/2	46±3	3±3	33±5	15	-	3	+
"	23240	ClMSt	5G 6/1	58±3	-	30±5	12	-	-	+
"	23243	ClSt	10R 3/4	28±3	4±3	34±5	15	16±3	3	+
P1	23304	SiClSt	5GY 6/1	56±3	5±3	17±5	22	-	-	+
"	23321	ClMSt	5GY 8/1	63±3	-	27±5	10	-	-	+
L1	23432	SiClSt	5R 4/2	57±3	-	36±5	4	-	3	+

+ denotes traces to small quantities.

- denotes either completely absent or not detected.

* approximate value, calculated by subtracting the total of other element percentages from 100%.

** determined by classical wet chemistry.

Feldspar includes plagioclase and/or K-feldspar.

and with the thin section analyses (Table 5.9). Difficulty was experienced with chlorite detection because the main chlorite peak is overlapped by an inseparable water peak. Values for chlorite percentages (approximate only) have been estimated by assuming that the low cumulative percentages of all other minerals is due to unaccounted for chlorite. This gives values that are consistent with the X-ray diffraction data.

The quartz percentage includes both detrital quartz and quartz cement. The iron oxide/hydroxide value is due to haematite, the percentage of which was determined by wet chemistry (Table 5.11).

Mineralogy

The fine-grained lithologies of the Aztec Siltstone consist chiefly of quartz (detrital and authigenic), illite (plus some 3T muscovite possibly), chlorite, and subordinate Na-feldspar, calcite, haematite, analcime, epidote and rare prehnite, laumontite, heulandite, gypsum and pyrite (Tables 5.7, 5.8 and 5.9).

Quartz

Quartz is present, in abundance, in all samples, largely as detrital grains of silt size (Figs. 5.10 and 5.31), but also as a cement introduced during diagenesis. The sand and silt fraction of most fine-grained rocks (Fig. 5.9) consists entirely of detrital quartz.

Illite

Illite is the most abundant clay mineral in the Aztec Siltstone (Tables 5.7 and 5.8). Its concentration was determined from the K_2O values obtained from XRF analyses (Tables 6.3 and 6.4, p.180). In the fine-grained sediments it constitutes an average of 37 percent (σ = 8 percent) of the bulk samples analysed (Table 5.10) Red fine-grained samples, as a group, have a slightly higher illite content than the green (Table 5.10). This is shown best in red-green paired samples. The

Table 5.9. Mineral compositions (in percent) of thin-sectioned samples of Aztec Siltstone, based upon:
(1) Point count data, including modal analysis for sandstones (Table 5.5), and grain size analysis of the fine-grained lithologies (p.141, Fig. 5.9).
(2) Infrared analysis (Table 5.8)
(3) X-ray fluorescence analysis (Tables 6.3 and 6.8).
(4) X-ray diffraction analysis (Table 5.7).
(5) Visual estimation in thin section.

Location	Sample	Lithology	Colour	Analytical Method	Quartz	K-spar	Plag.	Mica	Illite and chlorite	Lithic	Cement (Qtz)	Haematite	Heavies	Calcite	Zeolite	Epidote	Others
H6	23138	SSt	5GY 5/1	1	79	<1	-	-	<1	-	21	-	-	-	-	-	-
	23144	SSt	N9	1	68	-	-	-	3	8	17	-	-	-	-	-	3 chert
A4	23174	SiClSt	10GY 5/2	1,4	46	-	-	-	52	-	-	1	-	1	-	-	<1 prehnite
	23175	SSt	5YR 8/1	1	83	tr	-	-	-	-	17	-	-	-	-	-	-
	23182	SClSt	5GY 8/1	1	.41	-	-	<1	58	-	-	-	-	-	-	-	carbonaceous
	23183	SSt	5R 8/2	1	77	-	-	-	-	-	20	-	1	1	-	-	1 chert
	23184	ClMSt	5G 7/1	1	51	-	-	1	47	-	-	-	1	-	-	-	-
A1	23228	SiClSt	10R 4/2	1,2,3,4	31	-	3	-	48	-	15	3	-	-	-	-	-
	23228	Nodule	-	5	15	-	-	-	15	-	-	-	-	60	-	10	- *
	23230	SiClSt	N5	1,3,4	27	-	<1	-	72	-	-	1	<1a	<1	-	<1	-
	23233	ClSt	5G 6/1	1,3,4	16	-	<1	-	84	-	-	tr	-	-	-	-	-
	23233	Nodule	-	1,4	15	-	-	-	10	-	-	-	-	45	-	30	-
	23234	SSt	5R 8/2	5	70	-	-	-	3	-	22	tr	<1b	-	2	-	-
	23235	ClSiSt	5G 6/1	1,3	54	-	-	-	46	-	-	tr	tra	-	-	-	-
	23235A	SiClSt	10R 4/2	1,3,4	29	-	-	-	68	-	-	3	-	-	-	-	-
	23237	SiClSt	10R 4/2	1,3	31	-	-	-	66	-	-	3	-	-	-	<1	carbonaceous
	23237	Nodule	-	4	-	-	-	-	-	-	-	-	-	100	-	-	-
	23238	ClMSt	5B 7/1	1	58	-	-	-	41	-	-	1	<1a	-	-	-	-
	23240	ClMSt	5G 6/1	1,2,3,4	53	-	tr	-	40	-	10	<1	-	-	1	-	-
	23240A	Nodule	-	5	-	-	-	-	-	-	-	-	-	100	-	-	-
	23241	SSt	10R 8/2	1,3	66	-	-	-	2	-	17	tr	<1c	15	tr	tr	-
	23243	ClSt	10R 3/4	1,2,3,4	22	-	4	-	48	-	-	3	-	16	6	1	-
	23244	ClSt	5P 4/2	1,4	21	-	<1	-	42	-	-	2	-	35	-	-	-
	23245	Nodule	-	4	-	-	-	-	-	-	-	-	-	100	-	-	-
	23246	SSt	5R 8/2	5	70	<1	-	-	-	-	5	<1	<1d	17	<1	3	4 chert
	23249	SiClSt	5G 8/1	1,3	41	-	-	-	59	-	-	tr	-	-	-	<1	carbonaceous
	23250	SSt	N8	1,3	82	tr	-	-	2	2	13	-	tra	-	-	-	1 chert
M1	23254	SSt	N8	5	81	-	-	-	-	2	17	-	tr	-	-	-	-
	23256	SiClSt	10R 4/2	1,4	30	-	-	-	66	-	-	3	-	-	-	1	-
	23256	Nodule	-	5	-	-	-	-	-	-	-	-	-	95	-	4	1
	23260	ClSt	10R 4/2	1,4	23	-	-	-	73	-	-	3	-	-	-	1	-
	23281	ClSt	5GY 8/1	1,4	8	-	-	-	47	-	-	-	-	-	-	15	30 prehnite *
	23281	Nodule	-	4	-	-	-	-	2	-	-	-	-	70	13	-	15 prehnite *
P1	23301	SSt	5Y 8/1	5	80	-	4	-	4	-	12	-	<1	-	-	-	-
	23304	SiClSt	5GY 6/1	1,2,3,4	41	3	2	-	39	-	13	-	-	-	tr	tr	2 unknown
	23306	Oolite	-	4	-	-	-	-	-	-	-	<1	-	100	-	-	-
	23310	ClSt	5GY 6/1	1,4	3	-	-	-	87	-	-	-	-	-	-	10	-
	23310	Concretn.	-	4	-	-	-	-	-	-	-	-	-	35	50	15	-
	23315	SSt	N9	1	76	-	-	-	1	tr	22	-	-	-	1	-	-
	23316	SiClSt	5GY 6/1	1	33	-	-	-	66	-	-	<1	-	-	-	1	-
	23319	SSt	5GY 8/1	1,4	59	<1	-	-	tr	1	37	-	<1	-	3	-	-
	23321	ClMSt	5GY 8/1	1,2,3	51	-	tr	-	37	-	12	-	-	-	-	-	-
L1	23422	ClSt	N2	5	21	-	-	1	-	-	-	-	-	63	-	-	15 carbonaceous*
	23429	ClSt	N1	5	15	-	-	-	75	-	-	-	-	-	-	-	10 carbonaceous*
	23430	ClSSt	5Y 8/1	1	70	-	1	-	26	1	-	2	-	-	-	-	-
	23432	SiClSt	5R 4/2	1,2,3,4	39	-	tr	-	40	-	18	3	-	-	-	-	tr
	23433	ClMSt	5G 8/1	1	51	-	-	<1	47	-	-	-	1	-	-	-	1 magnetite
	23436	Nodule	-	4	6	-	-	-	-	-	-	-	-	94	-	-	-
	23437	ClSt	5GY 6/1	1,3,4	15	-	-	-	85	-	-	tr	-	-	-	-	-
	23438	ClSSt	5Y 8/1	1	54	-	-	<1	41	-	-	-	<1	-	-	-	<1
	23440	SiClSt	5GY 7/2	1	27	-	-	-	72	-	-	1	-	<1	-	-	-
	L1-19R	SiClSt	10R 4/2	1,3,4	45	-	-	-	52	-	-	3	-	-	-	-	-
L2	23453	SiClSt	5GY 6/1	1	26	-	-	-	74	-	-	tr	-	-	-	-	-
	23458	SSt	N8	1	78	-	-	-	tr	1	20	-	<1	-	<1	-	1
	23461	ClSSt	5Y 7/2	1	61	-	1	-	38	-	-	-	<1	-	-	-	-
	L2-13	SiClSt	5GY 6/1	1,4	48	-	-	-	52	-	-	tr	-	-	-	-	-
B2	23579	ClSt	10R 4/2	1,3,4	17	-	-	-	80	-	-	3	-	-	-	-	-
	23579	ClSSt	5GY 6/1	1,3	66	-	-	-	34	-	-	-	-	-	-	-	-
	23581	SSt	5GY 8/1	1	80	-	-	-	3	-	17	-	-	-	-	-	-
	23582	SClSt	N9	1,4	47	-	-	2	51	-	-	-	-	-	-	-	<1 carbonaceous
	23584	SClSt	10R 4/2	1,3	35	-	-	-	62	-	-	3	-	-	-	-	-
	23586	SSt	N9	1	84	-	-	-	-	-	16	-	-	-	-	-	<1 chert
	23588	SSt	N9	1	77	<1	-	-	tr	-	23	-	-	-	-	-	-
AZ	AZ-20	ClSt	10R 4/2	1,3,4	18	-	-	-	79	-	-	3	-	-	-	-	-

* Percentages approximate only.
a zircon
b garnet
c tourmaline and zircon
d zircon, tourmaline and garnet

Table 5.10. Illite content in fine-grained samples of the Aztec
Siltstone, based upon the K_2O content (determined by
X.R.F.) of each sample (Table 6.3, and p.   )

	Location	Sample	Lithology	Colour	Illite (%) (±5%)
	Al	23228	SiClSt	1OR 4/2	34
	"	23230	"	N5	38
	"	23233	ClSt	5G 6/1	48
	"	23235A	SiClSt	1OR 4/2	51
	"	23237	"	"	48
	"	23239	"	"	55
	"	23240	ClMSt	5G 6/1	35
	"	23240A	"	5GY 6/1	35
	"	23243	ClSt	1OR 3/4	32
	"	23249	SiClSt	5G 8/1	26
*	"	Al-05R	"	1OR 4/2	25
*	"	Al-05Gr	"	5G 6/1	19
*	"	Al-15	"	1OR 4/2	48
*	"	Al-16	"	5G 6/1	42
	P1	23304	"	5GY 6/1	17!
	"	23321	ClMSt	5GY 8/1	24
*	L1	23432R	SiClSt	5R 4/2	36
*	"	23432Gr	"	5GY 6/1	34
	"	23437	ClSt	"	41
*	"	L1-19R	SiClSt	1OR 4/2	36
*	"	L1-19Gr	"	5G 6/1	34
++	L1	L1-12a	SiClSt	1OR 4/2	35
++	"	-12b	"	"	35
++	"	-12c	"	"	39
++	"	-12d	"	"	42
+++	"	L1-13a	"	"	35
+++	"	-13b	"	"	34
+++	"	-13c	"	"	39
+++	"	-13d	"	"	40
	B2	23579R	ClSt	1OR 4/2	46
	"	23579Gr	ClSSt	5GY 6/1	29
*	"	23584R	SClSt	1OR 4/2	34
*	"	23584Gy	"	N5	29
*	AZ	AZ-06	SiClSt	1OR 4/2	36
*	"	AZ-07	"	5G 6/1	40
+	"	AZ-17	ClSt	5G 6/1	39
+	"	-18	"	1OR 4/2	35
+	"	-19	"	"	38
+	"	-20	"	"	40

Mean illite content = 37

Std deviation = 8

* red-green or red-grey pairs

+ ++ +++ taken from a single unit

! determined by infrared spectrophotometric methods, Table 5.8.

difference revealed only by K_2O determinations on the bulk
samples (Tables 6.3 and 6.4), as the X.R.D. analysis lacked
sufficient sensitivity. The mean K_2O for the 14 red samples
of 3.42 percent gives an illite concentration of 40.2 percent,
compared with 34.6 percent for the 14 green based on a K_2O
concentration of 2.94 percent. The paired samples showed
similar values.

It is thought that some illite was leached from the green
sediments during the reduction and removal of haematite in
solution. Further evidence for leaching of illite and other
products during reduction is presented in Chapter 6.

Illite occurs as cryptocrystalline flakes that compose
the greater part of the matrix of the fine-grained Aztec
lithologies. Optical orientation of illite (and chlorite)
suggestive of pedogenic processes, was observed in a number
of unbedded thin sectioned samples and has been discussed
earlier (p. 99 Fabric analysis).

The illite is thought to have a pale green colour, even
though it is normally masked by the green of chlorite in thin
section. When illite bearing samples were treated with HCl
to remove the chlorite, they still retained a pale green
colour, which is attributed to the illite. Keller (1953)
considered that the green colour of common sedimentary rocks
was due, in large part, to illite.

A large proportion of the illite in the fine-grained
lithologies of the Aztec is thought to be of detrital origin,
probably inherited, by reworking, from older sediments.
However, it is probable that some other clay species were
altered to illite by the depositional environment of the Aztec,
namely the soil processes. Further alteration of the clays may
have taken place as a product of prolonged diagenesis, where,
for example, kaolinite, montmorillonite, vermiculite or any
mixed-layer clay minerals may have been converted to illite
or chlorite (Millot, 1970 p.306-321, 327-329).

Chlorite

Chlorite is the subordinate clay mineral in the Aztec Siltstone, but nevertheless is a common constituent of most clay-rich sediments (Tables 5.7 and 5.8). Chlorite percentages do not appear, from X-ray diffraction analysis, to depend upon the colour of the sample (Table 5.7, see the red-drab pairs).

In thin section chlorite is generally present as a cryptocrystalline product but in some instances is visible as flakey crystals up to 10 microns in size, green in colour, with slight pleochroism. The green colour of the chlorite is responsible for the bulk of the green colour of the fine-grained lithologies of the Aztec Siltstone. This was confirmed by removing the chlorite, in solution, from a green silty-claystone (23304) by treatment with HCl. The process greatly reduced the intensity of the green colour. It was noted also, that the green colour underlies, but is masked by, the red haematite pigment in the Aztec red lithologies. This was demonstrated when the red pigment was removed, by sulphite reduction (Meyra and Jackson, 1960), and exposed a normal looking green illitic and chloritic clay sample.

The X-ray diffraction patterns for chlorite showed a non-expanding peak at 14.2 $\overset{o}{A}$ which was enhanced after the sample had been heated to 550°C for 4 hours. Other chlorite peaks were diminished or removed by the heat treatment (Fig. 5.27). This suggested the presence of Fe-chlorites (chamosite) in the samples (Schoen, 1964; Henson, 1973; Lajoie and Chagnon, 1973).

As with illite, chlorite is considered to be largely of detrital origin, i.e. it was inherited from the source material, but was possibly modified by pedogenic processes in the depositional environment. It is possible that small amounts of the chlorite may be a product of prolonged diagenetic alteration of some other clay mineral. Millot (1970 p.328) noted that chamosites are produced by the silication of iron sesquioxides from sedimentation, a process favoured by an alkaline environment as shown by the proximity of calcite. These ingredients and conditions would have been common in the fine-grained sediments of the Aztec Siltstone.

Genesis of the Clay Minerals

The illitic and chloritic clay mineral assemblage of the fine-grained beds of the Aztec Siltstone may not be of genetic significance. Illite is the most abundant clay mineral on earth (Millot, 1970 p.8) and has a widespread distribution. It is the common weathering product of feldspars, micas and other clays, under a wide range of conditions, and is also a product of the diagenetic or low grade metamorphic alteration of kaolinite, chlorite, montmorillonite, vermiculite or any mixed-layer clay (Millot, 1970). Hence illite, as well as chlorite, may be inherited directly from the weathering of igneous, metamorphic or sedimentary rocks, they may be the products of a specific pedogenic condition which altered the inherited clays, or they may be the neoformed products of prolonged diagenesis or low grade metamorphism.

Illite is the common clay mineral in a great variety of soil types. However, it is relatively most abundant in the zonal soils of poorly drained, low rainfall or seasonally low rainfall regions, because its formation and stability is, favoured by the alkaline and high K^+ ion concentrations which are common in soils of these regions. Some terra rossa, for example, show only illite and its weathered products (Millot, 1970, p.110). Hence, despite the doubt that an illitic and chloritic clay mineral assemblage in an ancient sediment is of any genetic significance (Van Houten, 1964b, 1973), it is of value to note that the climatic and pedogenic conditions during the formation of the unbedded fine-grained sediments (soils) of the Aztec Siltstone were favourable for the production and stability of these minerals. These conditions have already been specified by the kankar, abundant mudcracking, vein networks, gypsum lenses and analcime in the formation (Chapter 4).

The lack of kaolinite (kaolinite being a clay mineral dominant in well-drained acid soils of humid regions) in the soils of the Aztec Siltstone may be taken as further evidence to sustain the hypothesis of a dry or at least seasonally dry

climate during the Upper Devonian in southern Victoria Land,
although it must be stressed that kaolinite may be readily
illitized by prolonged diagenesis. Kaolinite does appear in
some other red beds (p.239) and the author considers that if
it were originally present in the soils of the Aztec, then
there should be some trace of it in the Aztec rocks. A
discussion concerning kaolinite in red beds is given in
Chapter 9, p.238.

It should not be concluded that illitic and chloritic
clays were the only clay minerals in the soils of the Aztec,
because the other clays most likely to have been present in
small amounts, namely montmorillonite (considering the
relatively high Ca^{2+} ion concentration in the fine-grained
lithologies),would have been modified by long term diagenesis
to illite or chlorite.

Haematite

Haematite is common in the fine-grained beds of the Aztec
Siltstone (Table 5.7) and is the agent responsible for the
red colour that characterizes 30 percent of these fine-grained
lithologies. The mean haematite concentration in the red
lithologies is 3.01 (σ = 0.63) percent (Table 5.11), but the
maximum is only 4.12 percent (L1-13d) despite an intense and
uniform red colouration (1OR 4/2) in the hand specimen and thin
section of all red samples. The powerful pigmenting ability
of the haematite is due firstly to its extremely fine grain
size (approximately 0.25 to 5 microns, as determined from
microscopic examination and by Scanning Electron Microscope
(Fig. 5.28), and secondly to its crystalline form, which is
as hexagonal plates flattened parallel to the basal pinacoid,
001, axis (Fig. 5.29). The S.E.M. photograph shows the
hexagonal haematite plates to be stacked in their growth
positions on the detrital quartz grain. This negates the
possibility that the haematite, in this sample, was of a
separate detrital origin.

Although the most common form of haematite is as crypto-
crystalline hexagonal plates, it also occurs as larger composite

Table 5.11   Haematite weight percentages in red, grey, and green
fine-grained lithologies of the Aztec Siltstone. The
haematite was extracted by the method of Mehra and
Jackson (1960) and its concentration was determined
by Atomic Absorption Spectroscopy. Reproducibility,
based upon duplicate extractions for eight samples
is ±0.04 percent. Variations in the time of
extraction (greater than 15 min.), the temperature
(between 70° and 80°C), and the stirring rate, did
not significantly alter the value of the percentage
of extractable Fe determined.

	Location	Sample	Lithology	Colour	Haematite (%)
	A1	23228	SiClSt	1OR 4/2	3.20
	"	23235A	"	"	3.18
	"	23237	"	"	2.50
	"	23239	"	"	3.90
	"	A1-05R	SiClSt	1OR 4/2	2.14
	"	A1-15	"	"	3.96
	L1	23432R	"	5R 4/2	2.69
+	"	L1-12a	"	1OR 4/2	1.86
+	"	-12b	"	"	2.69
+	"	-12c	"	"	3.26
+	"	-12d	"	"	1.99
++	"	L1-13a	"	"	2.60
++	"	-13b	"	"	2.50
++	"	-13c	"	"	2.83
++	"	-13d	"	"	4.12
	"	L1-19R	"	"	3.20
	B2	23579R	ClSt	"	3.90
	"	23584R	SClSt	"	3.30
	AZ	AZ-06	SiClSt	"	2.75
+++	"	AZ-18	ClSt	"	1.32
+++	"	-19	"	"	2.69
+++	"	-20	"	"	2.02

Mean red   = 3.01

Std. deviation   = 0.63

	Location	Sample	Lithology	Colour	Haematite (%)
	A1	23230	SiClSt	N5	0.89
	B2	23584Gy	SClSt	N5	0.72

Mean grey   = 0.80

Std. deviation   = 0.12

	Location	Sample	Lithology	Colour	Haematite (%)
	A1	23233	ClSt	5G 6/1	0.23
	L1	23432Gr	SiClSt	5GY 6/1	0.30

Mean green   = 0.26

Std. deviation   = 0.05

+,++,+++ taken from a single unit. Only the means of these
values were incorporated into the mean for all red
samples.

grains, approximately 20 to 200 microns in length. These are
made up of clusters of smaller (5 to 10 micron) grains of
haematite. In some cases the composite grain itself has a
euhedral crystal form (Fig. 5.30) suggesting *in situ* growth,
probably as an alteration product. The composite grains are
generally opaque except for the grain margins which, because
they are thinner, are translucent and have the blood red
colour typical of haematite. This so-called "black haematite"
is seen best in the green fine-grained lithologies where it is
not completely masked by the haematitic pigment as it is in the
red lithologies.
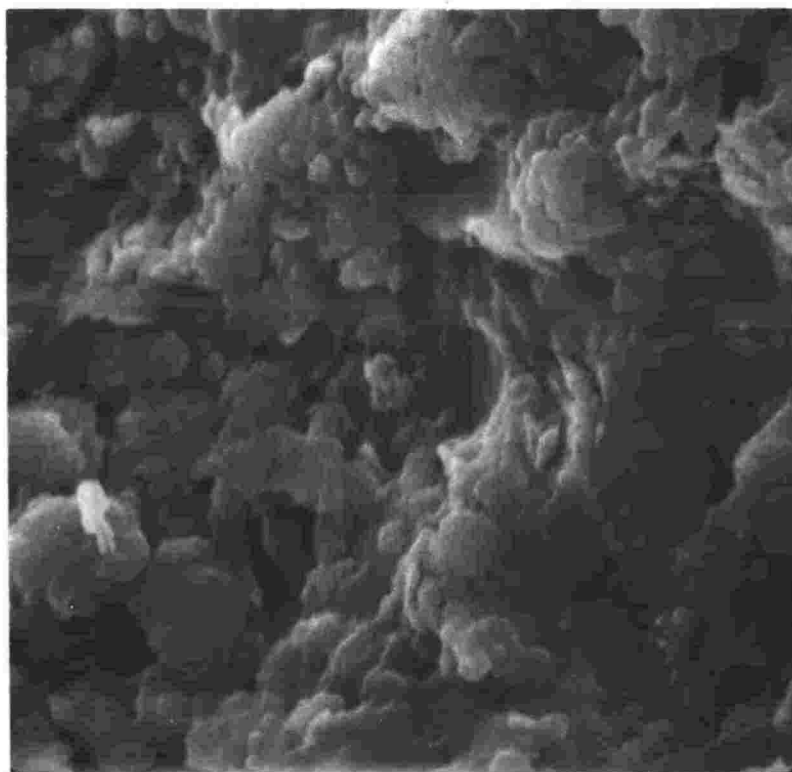
Fig. 5.28. A Scanning Electron Microscope photograph of the surface of
a detrital quartz grain coated with haematite pigment. The
detrital grain is from a red sandy claystone, sample 23584.
The pigment is composed of hexagonal plates which have a mean
grain size of approximately 0.5 micromillimetres and appear
to be stacked in their growth positions on the detrital
quartz grain. Scale 5 cm = 4 µm.
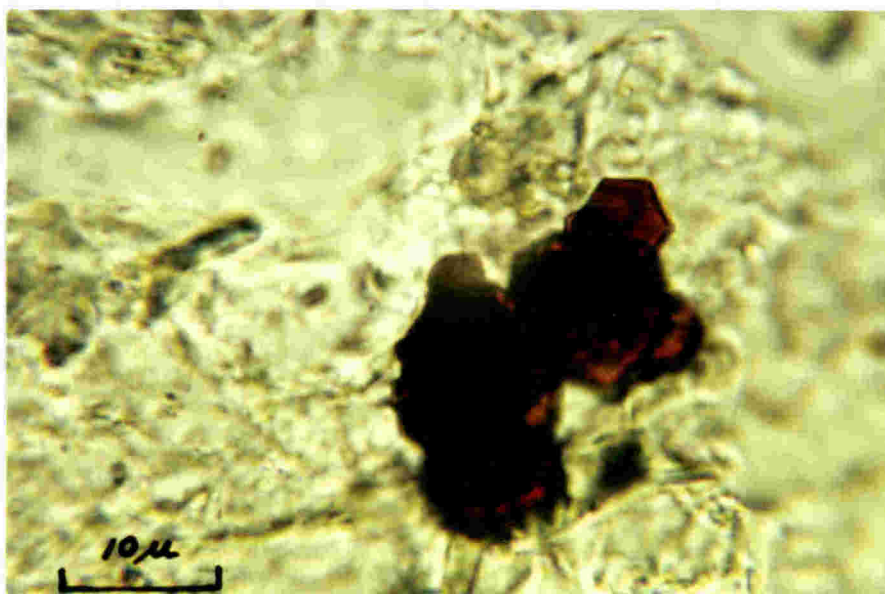
Fig. 5.29. Euhedral haematite grains characteristic of the red pigment
in the Aztec red beds. The grains are hosted by a green
illitic and chloritic clay matrix. Plain light.

Fig. 5.30. A euhedral, composite grain of haematite ('black haematite'),
probably a post-depositional alteration product of ilmenite
or magnetite. Sample 23230. Plain light. Scale 5 cm = 0.03 mm.

"Black haematite" has been widely reported from other red bed sequences (Creer, *et al.* 1954; Blackett, 1956; Irving, 1957; Van Houten, 1961a, 1968; Picard, 1965; Thompson, 1970; McBride, 1974). Runcorn (1959) and Van Houten (1961a) considered that the black grains of ilmenite and magnetite commonly reported in red beds were often incorrectly identified and are predominantly "black haematite", better known as specularite.

Van Houten (1961a, 1968, 1972) found that the black grains in red beds of Tertiary and Recent age were predominantly ilmenite and magnetite, whereas in the older red beds the black grains were mainly specularite and martite (two forms of "black haematite"). This suggested that the "black haematite" grains are post-depositional alteration products derived from inherited grains of ilmenite and magnetite. Such a deduction is supported by the growth form of the "black haematite" grains found in the Aztec samples. Ilmenite and magnetite were not detected in thin section or X-ray diffraction studies of Aztec samples.

Haematite pigment, in general, completely permeates the red lithogies of the Aztec and is concentrated in the clay matrix (Fig. 5.31). Commonly, it was observed to have concentrated in patches, veinlets and stringers (Fig. 5.4), suggesting that it had been mobilized in the unconsolidated sediment. Haematite was found to completely coat detrital quartz grains, even those in close contact (Fig. 5.32), establishing that it was not introduced as a diagenetic product after consolidation of the sediment.

Rare grains of haematite other than the "black haematite" were observed in a number of the green fine-grained lithologies of the Aztec that were examined in thin section (e.g. 23316, 23579). The haematite is coarser-grained (5 to 10 microns) than the normal red pigment, and is considered to be a remnant product left when the larger grains did not completely dissolve during the reduction phase which dissolved the haematite and exposed the green bed. Two green lithologies, for example (23233 and 23432Gr) have haematite percentages of 0.23 and 0.30 percent respectively (Table 5.11).
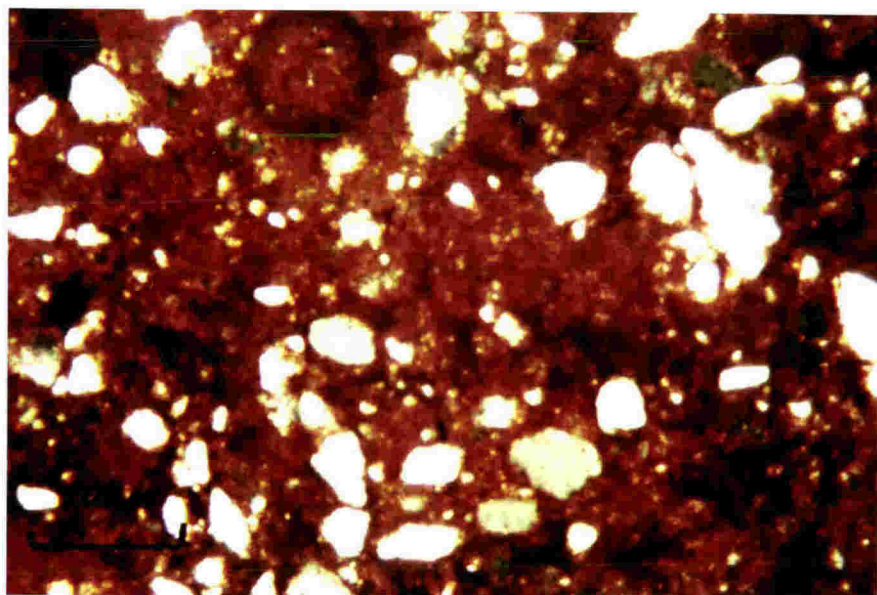
Fig. 5.31. Haematite pigment dispersed throughout the matrix of a typical
red silty claystone (sample 23243, Al, unit 22). The silt
grains are quartz. Plain light. Scale 5 cm = 0.25 mm.
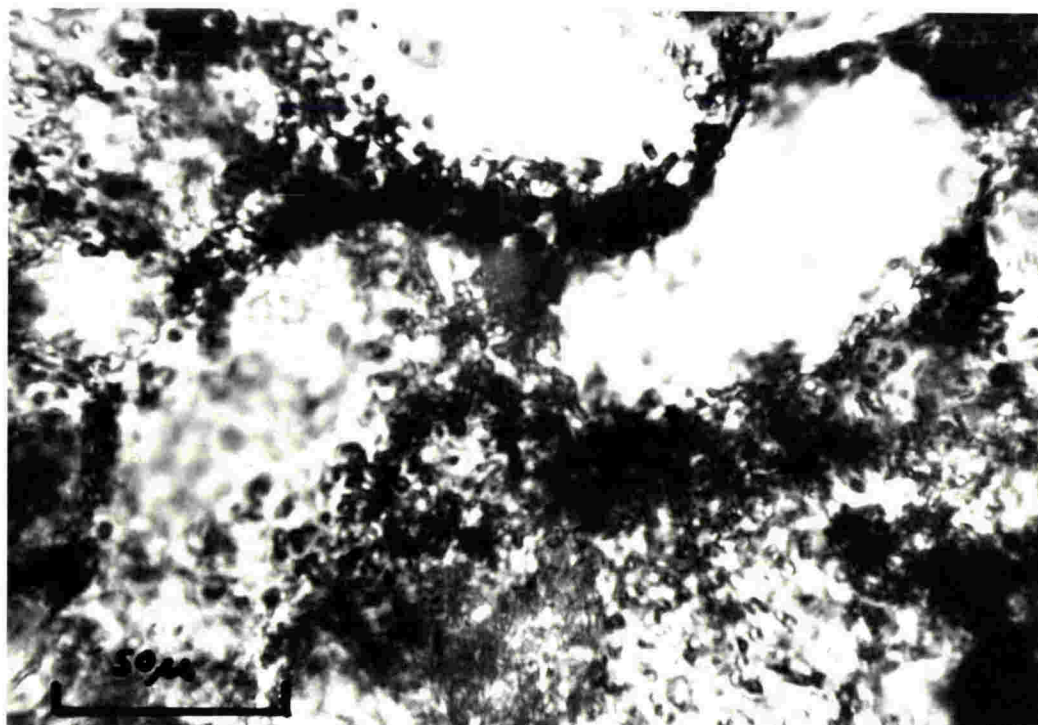
Fig. 5.32. Haematite pigment completely rimming detrital quartz grains in
close contact, thus establishing that it is not a diagenetically
introduced product. Plain light. Note the 50 µm bar for scale.

Grey fine-grained lithologies are common in the Aztec (Chapter 3 p.16) and generally occur at the junction between red and green rock. Thin section studies of these grey samples showed that the colour was generated by the presence of relatively coarse-grained, almost opaque haematite, 5 to 10 microns in size, in combination with the green colour of an underlying illitic and chloritic clay matrix. The mean haematite concentration was found to be 0.80 (σ = 0.12) percent (Table 5.11). A grey rather than a red colour is due to the lower concentration and the increased grain size of the haematite. It is thought that the grey lithologies originated, by reduction, which brought about the partial solution of haematite removing the cryptocrystalline red pigment, but leaving some of the larger grains.

The grey is a transitional zone lithology, and thus varies considerably in thickness. It is close to non-existent in very localized and well defined red-green transitions that occur within single units (Fig. 4.5), but may exist as a zone many centimetres wide, particularly in the case where reduction has been induced at the upper contact of a red fine-grained bed, by the influence of an overlying channel sandstone deposit.

Thin sections across the boundary between red-green pairs of fine-grained Aztec lithologies showed (Fig. 5.33) that in going from the red to the green, the only lithologic change was in the haematite concentration, which progressively decreased toward the green exposing the larger haematite grains and the underlying green illitic and chloritic clays.

The mean haematite concentration in the Aztec red lithologies of 3.01 percent (Table 5.11) contrasts with a value of 0.9 percent obtained for 14 fine-grained samples of other ancient red bed sequences (Walker and Honea, 1969, Table 3). The high value for the Aztec is probably due to the comparatively fine-grained nature of the red lithologies, with less detrital quartz and correspondingly more clays and haematite.
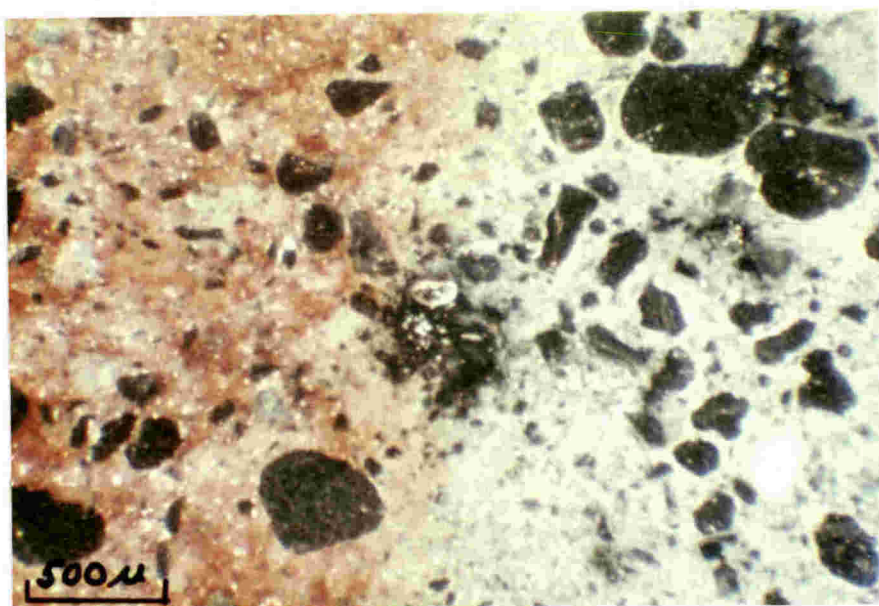
Fig. 5.33. A photomicrograph taken of a sharply defined red-green
boundary zone in sandy claystone, sample 23584, showing
that there is no textural difference between the red and
the green portions. As confirmed by bulk chemical analysis
(Chapter 6) the only lithologic difference is in the
haematite content of the red. Plain light.

Combined evidence for the time of emplacement of the
haematite in the red beds of the Aztec Siltstone is given in
Chapter 9.

Calcite

Calcite is common in the fine-grained deposits of the
formation. Mostly it is present as nodules (kankar) and these
have already been discussed (p. 73). A number of the fine-
grained samples examined by thin section showed calcite
(Tables 5.8 and 5.9) as a cryptocrystalline product disseminated
throughout the illitic and chloritic clay matrix. This calcite
is non-detrital, and is considered to have precipitated pene-
contemporaneously from interstitial waters which evaporated
during subaerial exposure of the fine-grained overbank sediments.

The formation of calcite is probably associated with
pedogenic processes, as suggested by the calcite found
concentrated in voids, veins, and cracks, that are considered
to be soil features. Sample 23174 for example has concentrations

of cryptocrystalline calcite filling former "root" channels
(Fig. 4.45). These delicate root structures could not have
survived burial to more than a few metres had they not been
filled with calcite at an early stage.

The carbonate found in modern loess soil profiles has
the same form as that found in the Aztec fine-grained beds.
For example, the loess of the Russian plain contains calcite
in a cryptocrystalline (1 to 4 microns) form encountered
both in a dispersed form and in accumulations confined to the
walls of pores, cracks and holes made by roots (Morozova, 1964).

Dolomite or ankerite was not found in the formation either
in hand specimen or by X-ray diffraction analysis.

Analcime

Analcime occurs sporadically in the fine-grained beds of
the Aztec Siltstone (Tables 5.7 and 5.9). It occurs as a micro-
crystalline product disseminated through the clayey matrix in
siltstone and claystone beds, and is also found associated with
the cryptocrystalline calcite of syngenetic pisolites, and
nodules (p. 138). Analcime was found in unbedded calcareous
nodule bearing silty claystone units considered to be soil
horizons e.g. L1, unit 26.

The analcime is not thought to be metamorphic as its
occurrence is not related to the proximity of the host sediment
to dolerite sills or dykes. Also, in the case of the pisolites
the host rock does not contain analcime, which suggests that
the pisolitic analcime is syngenetic.

All analcime in the Aztec Siltstone is thought to be
syngenetic and produced by chemical sedimentation in a saline,
alkaline environment, either in lake bottom muds or in a soil.
Both modern and ancient analogues serve as examples. Lake
Natron in Tanzania contains analcime in the lake bottom muds,
which has resulted from primary-chemical precipitation (Hay,
1966, p.87). The analcime is thought to have been derived by
reaction of the illite rich clays (similar to the Aztec
Siltstone) in the Na-rich lake waters. An ancient example
of this is found in the Triassic Lockatong Formation of Wyoming

where the analcime was produced either by direct crystallization,
or by early diagenetic reorganization of colloidal alumino-
silicates or clay minerals in deposits of a saline lake (Van
Houten, 1962, 1965). Analcimolites, considered to be of a
similar origin are found in the Mesozoic strata of the central
Sahara (Joulia *et al.* 1959) and the Congo Basin (Vanderstappen
and Verbeek, 1959; Lepsersonne, 1960), and in the Popo Agie
Member of the Chugwater Formation (Triassic) of Wyoming (Keller,
1952).

Analcime also forms readily in saline alkaline soils of
some semi-arid or arid regions (Hay, 1966 p.21). Examples are
found in the San Joaquin Valley of California where the analcime
concentrates near the surface of soils with a pH of 9.5 or
higher.

Analcime also forms readily from the alteration of
tuffaceous sediments, but this is discounted for the Aztec as
volcanic glass was not identified in any analcimic samples.

The analcime of the Aztec Siltstone is thought to have
been produced by direct precipitation or by the early diagenetic
alteration of clays or alumino-silicates in a saline, alkaline
environment, either in pluvial lake bottom muds or in soil
profiles. The pisolitic analcime was almost certainly formed
in a lacustrinal environment, but the analcime of the other fine-
grained deposits is more likely to be of a pedogenic origin.

Many of the fine-grained, overbank deposits of the Aztec
underwent soil-forming processes (Chapters 4, 6, 9 and Conclusions)
and it has already been shown, by the common appearance of kankar
in the profile (Fig.2.1), that some soils were alkaline. Direct
evidence for high evaporation which may have produced saline
conditions in soils and in lakes during the Upper Devonian in
southern Victoria Land, comes from the presence of gypsum
lenses in the formation (Fig. 2.1, p.17). No halite pseudo-
morphs were observed in the formation.

Na-feldspar

Albite was present in very minor amounts (less than 1
percent) in most fine-grained samples studied (Table 5.7).

It was present, as observed in thin section, as a microcrystalline product disseminated through the clay matrix. Only one sample examined contained albite as recognizable detrital grains (23304).

There is some uncertainty as to exactly when the authigenic albite formed and it is not possible to decipher the crystallization history of albite from thin sections. Albite may form in non-marine, clay-rich rocks by replacement of the clay (Levina, 1959; Hay, 1966; Folk, 1968). This process takes place most readily in the Na rich waters of saline, alkaline playa lakes, with Si and Al ions provided from the breakdown of clays. Authigenic albite may also be produced from the *in situ* alteration of analcime, and in the case of the Aztec Siltstone, this is considered the most probable origin.

$$NaAlSi_2O_6 \cdot H_2O + SiO_2 \rightleftharpoons NaAlSi_3O_8 + H_2O$$

analcime   quartz   low albite
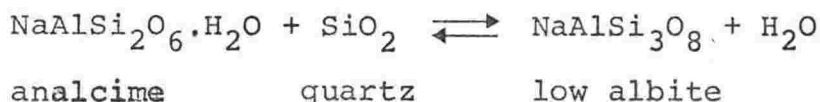
The equilibrium condition for this transition, at hydrostatic pressures (P_{H_2O}) of 3 kbars or less, is $190^{\circ}C$ (Thompson, 1971)(Fig. 5.34). The presence of metamorphic epidote (p.158, Table 5.7) in the Aztec lithologies indicates that the sequence was subjected, at least locally, to temperatures of this magnitude.

The authigenic albite of the non-marine Triassic Lockatong Formation of New Jersey and Pennsylvania is thought to have been produced by the alteration of analcime, probably aided by the low temperatures ($300^{\circ}C$) generated by neighbouring dolerite intrusion (Van Houten, 1965).

Albite may also be produced from analcime at near-surface temperatures. Campbell and Fyfe (1965) suggested that the analcime-albite-quartz equilibrium temperature can be lowered from $190^{\circ}C$ to $65^{\circ}C \pm 35^{\circ}C$ in a saturated solution of NaCl. An example of this is shown by the Green River Formation of Wyoming, where the salinity of interstitial waters favoured the dehydration of analcime to form albite at temperatures of between 50 and
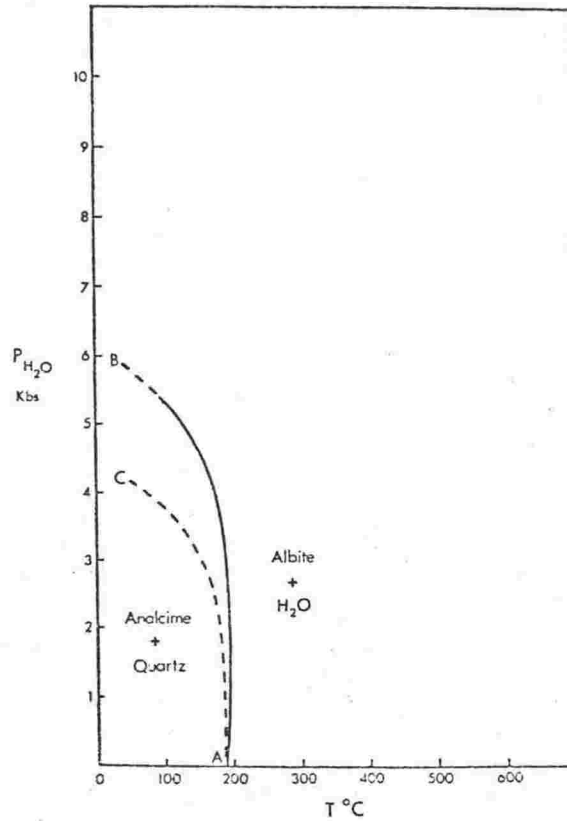
Fig. 5.34. Pressure-temperature diagram for univariant equilibria.
AB is the equilibrium curve for analcime + quartz   albite +
H_2O (Thompson, 1971). AC is the curve of Campbell and Fyfe
(1965) for the same reaction.
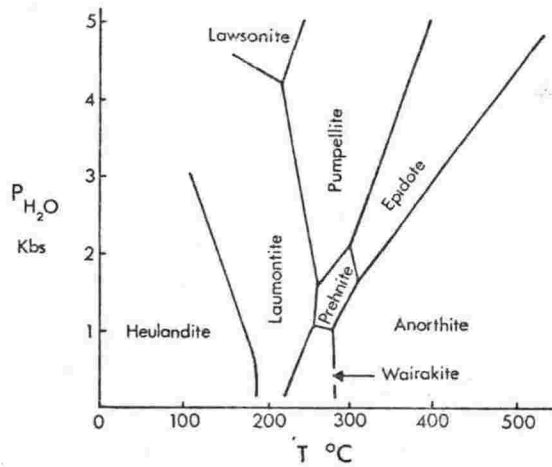
Fig. 5.35. Pressure-temperature diagram for some Ca-Al silicates.
(After Coombs, 1953, 1971).

75^OC (Hay, 1966 p.94). Unfortunately, there is no direct
evidence of saline conditions during Aztec deposition, although
it is not unlikely that the seasonal aridity, proposed for the
formation (see Conclusions), may have given rise to saline
ponds and pools.

Laumontite

Laumontite was detected by X-ray diffraction (Table 5.7) in subordinate amounts in two samples analysed. It was observed in thin section as a microcrystalline product in the matrix, in the case of the nodule (23281) associated with calcite and prehnite. Laumontite is considered to be formed by contact metamorphism with the Jurassic Ferrar Dolerite. Both samples containing the laumontite lie within close proximity to dolerite sills. The association of laumontite with other metamorphic calcic alumino-silicates in sample 23281, supports a metamorphic origin.

Epidote

Epidote is present in some fine-grained deposits of the Aztec, particularly those from sections M1 and P1. It occurs as microcrystalline, pale yellow-green, euhedral (prismatic) crystals (Fig. 4.33) commonly concentrated in or around voids and calcareous nodules but, in the samples from M1 it is found disseminated throughout the matrix, commonly overgrowing detrital quartz grains.

From its form, the epidote is obviously a post-depositional mineral. It is thought to have been formed by contact metamorphism, as a result of the Ferrar Dolerite intrusion. It probably originated from the metamorphic alteration of the precursory calcic alumino-silicates, laumontite or prehnite (Coombs, 1953, 1971; Seki, 1972; Fig. 5.35) with which it is associated in section M1.

$$\text{laumontite} + \text{haematite} \rightleftharpoons \text{epidote} + \text{quartz} + Al_2O_3 + H_2O$$

$$\text{prehnite} + \text{haematite} \rightleftharpoons \text{epidote} + H_2O$$
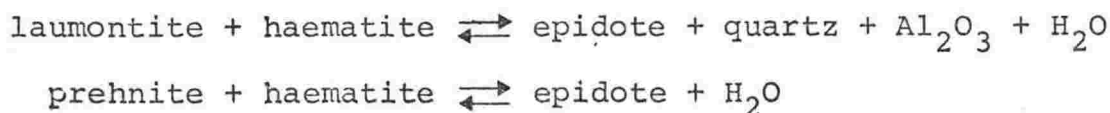
Section M1 has undergone more extensive metamorphic alteration because of a 200+ m thick dolerite sill which directly overlies the section. This is established by the metamorphic mineral assemblage in the sediments, including prehnite, laumontite, and grossular, as well as epidote

(Table 5.7). The stability conditions of this mineral assemblage (Fig. 5.35) suggests that these sediments were probably at a maximum temperature of between 350 and 400°C. The low temperature stability limit of epidote has been estimated at about 220$\pm$50°C for P_{total} of 1 to 6 kbars (Seki, 1972). The temperature, as computed from the equations of Jaeger (1957, 1959) for the temperature in the neighbourhood of a cooling igneous sheet, for the Aztec sediments at Ml is approximately 300 to 350°C. This is in excellent agreement with the metamorphic mineral assemblage temperature.

The purplish colour (5P 4/2 or 5RP 4/2) of some of the samples from section Ml has been produced by the combination of the yellow-green epidote and the red haematite of the matrix.

Prehnite

Prehnite was found only in samples from section Ml, the section where metamorphic alteration was greatest. Undoubtedly, the prehnite was generated by thermal metamorphism of the sediments, brought about by the overlying sill (200+ m thick) of Ferrar Dolerite.

Thermal Metamorphism

The intrusion of Ferrar Dolerite into the Aztec Siltstone during the Jurassic appears to have induced only local contact metamorphism. The dolerite has, in general, effected little change to the sediments of most of the Aztec sections described, with the exception of Ml, and portions of Pl, SB and SEA. These exceptions contain metamorphic mineral assemblages e.g. laumontite, prehnite, epidote, and grossular, which suggest temperatures of about 350°C. The presence of authigenic albite in most sections suggests that temperatures may have reached 200°C on a regional basis, but the presence of analcime suggests that temperatures cannot have greatly exceeded this value. The conditions for the formation of authigenic albite in the Aztec have not been fixed, and temperatures may have been considerably lower as suggested by the analcime.

CHAPTER 6

CHEMISTRY

Analytical Methods

The major element chemistry of 46 samples of the Aztec Siltstone was determined largely by X-ray Fluorescence Spectroscopy. Atomic Absorption Spectroscopy was used for the determination of Na values. Wet chemical methods of Shapiro and Brannock (1962) were employed to determine the Fe^{2+} and Fe^{3+} values, and a loss on ignition (at $1000^{\circ}C$ for 4 hours) was carried out to determine the volatile content.

Sample powders for analysis were prepared by grinding approximately 70 g of the rock (prepared as approximately 1 cm^3 fragments), in a tungsten carbide 'Tema' swing mill for 70 seconds. This reduced the sample to smaller than 5 ϕ, a size that gives a representative sample when analysing splits of 0.5 g (Kleeman, 1967). The only contamination resulting from the sample preparation was tungsten and cobalt from the 'Tema'.

The X-ray fluorescence technique of Norrish and Chappell (1967) and Norrish and Hutton (1969) was employed for the analysis of Aztec samples, using glass discs consisting of an homogeneous fusion of lithium tetraborate and lithium carbonate flux, lanthanum oxide as a heavy absorber, sodium nitrate and the sample. Mg, Al, Si, P, K, Ca, Ti, Mn, and Fe total were determined for each sample using a Siemens SRS-1 Spectrograph. The matrix corrections were carried out by iteration using either an I.B.M. 1130 or a Hewlett-Packard Model 9810A computer. U.S.G.S. standards and duplicate samples were analysed with each run to check on accuracy and precision (Table 6.1). The values show a high degree of precision and are in excellent agreement with the preferred chemical values reported in the literature.

Table 6.1. Measurement of accuracy and precision of X-ray fluorescence spectroscopic
methods, based upon duplicated and standard sample analyses.

Sample		Fe_2O_3	MnO	TiO_2	CaO	K_2O	P_2O_5	SiO_2	Al_2O_3	MgO	Na_2O	H_2O	CO_2	Total	L.O.I.
23228	1	5.44	0.05	0.74	1.23	2.87	0.12	71.97	12.10	1.96	0.52	3.21	0.03	100.24	3.48
23228	2	5.47	0.04	0.74	1.22	2.88	0.10	71.81	12.06	1.97	0.52	2.91	-	99.72	3.40
23579Gr	1	9.43	0.07	0.67	0.07	2.48	0.03	66.09	13.20	2.64	0.20	5.30	0.02	100.20	5.18
23579Gr	2	9.36	0.06	0.67	0.07	2.47	0.03	65.97	13.26	2.63	0.19	-	-	-	5.15
23579Gr	3	9.34	0.06	0.66	0.07	2.47	0.03	65.98	13.20	2.72	0.20	-	-	-	5.13
AZ-06	1	5.55	0.05	0.62	1.40	3.11	0.11	74.15	11.26	1.27	0.34	2.49	0.03	100.38	2.69
AZ-06	2	5.50	0.05	0.62	1.40	3.10	0.11	74.04	11.43	1.41	0.38	2.16	0.03	100.23	2.71
Ll-13b	1	4.67	0.03	0.63	0.37	2.92	0.06	75.18	10.90	1.58	0.19	3.64	0.04	100.21	4.05
Ll-13b	2	4.71	0.03	0.63	0.37	2.93	0.07	75.15	10.86	1.39	0.18	3.48	0.04	99.84	4.14
G2		2.75	0.03	0.48	1.94	4.53	0.14	69.74	15.28	0.84	4.12	-	-	-	0.51
G2,	*	2.77	0.04	0.53	1.99	4.51	0.14	69.19	15.34	0.78	4.16	0.66	0.08	100.19	0.57
AGV-1		6.88	0.10	1.05	4.97	2.95	0.53	59.56	17.28	1.81	4.28	-	-	-	1.30
AGV-1	*	6.80	0.10	1.08	4.98	2.90	0.49	59.00	17.01	1.49	4.33	1.84	0.05	100.07	1.34
GA		2.81	0.08	0.35	2.43	4.16	0.13	70.25	14.84	0.97	3.50	-	-	-	1.01
GA	†	2.83	0.09	0.38	2.45	4.03	0.12	69.90	14.50	0.95	3.55	0.96	0.11	-	1.08
GSP-1		4.37	0.04	0.65	1.98	5.51	0.29	67.27	15.16	0.98	2.82	-	-	-	0.83
GSP-1	*	4.33	0.04	0.70	2.03	5.49	0.28	67.28	15.12	0.96	2.88	0.70	0.15	99.96	0.80

* Flanagan (1969).   † Roubault et al. (1968).

Na was determined by A.A. Spectroscopy, using a modified Tectron 4 Spectroscope, and the fusion method for sample preparation described by Slavin (1968). Excellent reproducibility and agreement with the accepted U.S.G.S. standards were obtained for the samples (Table 6.1).

Ferrous iron values were determined by the volumetric method of Shapiro and Brannock (1962) but with the modification of a CO_2 atmosphere during the heat digestion stage. This was found to inhibit the oxidation of Fe^{2+} released from the sample during digestion (Table 6.2). Ferric iron values were obtained

Table 6.2   Ferrous iron determinations using the method of Shapiro and Brannock (1962) with and without a CO_2 atmosphere during the digestion stage.

Sample	Without CO_2	With CO_2	Accepted *
G2	1.24	1.43	1.45
AGV-1	1.75	1.97	2.05
Ferrous ammonium sulphate	16.71	18.48	18.32

* Flanagan, 1969, except the ferrous ammonium sulphate value which is theoretical.

as the difference between the total percentage iron, as determined by X-ray fluorescence, and the ferrous iron value expressed as Fe_2O_3.

Total water, including both absorbed (H_2O^-) and crystal lattice water (H_2O^+), was determined by ignition of the rock powder at approximately $900^{\circ}C$ in a Penfold Tube (Shapiro and Brannock, 1962). Carbon dioxide values were also determined using the method of Shapiro and Brannock (1962 p.49) which employs a glass tube with a sidearm for the evolution and measurement of CO_2 generated by acid dissolution of the sample.

Chemistry of Siltstones and Claystones

The major element analyses are presented in Tables 6.3 and 6.4. The field location and description of samples is in Askin *et al.* (1971); Barrett and Webb (1973); Fig. 2.1, and the Appendix of this thesis.

SILICON

The fine-grained lithologies of the formation have silica percentages from 51.16 to 82.55 with a mean of 72.02. This is high compared with the average shale composition of 58.10 percent (Mason, 1966) but is near to the average composition of the Mississippi Delta sediment (Clark, 1924, p.509) and the Lower Old Red Sandstone sample (Van Houten, 1961b).

The high silica content is largely related to the low percentage of non-silicate minerals, e.g. carbonates, sulphates or oxides. Notably therefore, the sample with the lowest silica content (23243) has a high calcite content. The high silica is also partially due to authigenic silica cement. For example, of the 46 percent silica in 23228 (Table 5.8) only about 31 percent is as detrital quartz (Table 5.9), the rest being authigenic silica cement. The alkaline environment of the Aztec, as shown by the abundance of calcite, would have facilitated a higher than normal silica solution (Fig. 5.17). Silica-rich intrastratal solutions would have precipitated silica cement in the fine-grained overbank deposits of the formation when these beds were subaerially exposed.

The variation in silica content between paired red and green Aztec lithologies and the means of all red and all green lithologies is minimal and due to the differences in non-silicate mineral percentages in the samples. The lower value in the red is due to haematite and in some cases a higher calcite percentage in these samples. In the paired samples, where it is known that the red and green fractions are of identical textural character, the silica difference is due entirely to the haematite concentration in the red sample.

Table 6.3. Major element analyses of fine-grained samples of Aztec Siltstone. Values in weight percent. Fe, as Fe_2O_3, was incorporated in the total where FeO and Fe_2O_3 had not been determined. Exact sample locations given in stratigraphic section descriptions (Fig. 2.1) (Askin et al. 1971; Barrett and Webb, 1973) and in Appendix Table 4. Samples marked with symbols e.g. an asterisk, are sample pairs selected from closely adjacent positions on either side of the colour border.

	23228	23230	23233	23235A	23237	23239	23240	23240A	23243	23249	23304	23321	23432Gr*	23432R*	23437
SiO_2	71.81	71.70	67.49	67.57	64.48	61.52	73.37	64.66	51.16	81.39	79.49	82.55	76.01	74.26	67.74
Al_2O_3	12.06	12.85	15.24	14.34	16.01	17.33	12.43	16.10	13.20	8.94	9.49	8.30	11.06	11.31	14.09
Fe_2O_3	4.25	2.53	2.10	4.77	3.54	5.17	1.57	2.19	4.96	0.75	0.58	0.64	1.81	3.86	1.89
FeO	1.10	1.01	1.44	1.33	2.09	1.71	1.45	1.79	0.60	1.46	2.32	1.80	0.88	0.96	2.06
MgO	1.97	2.05	2.65	1.99	3.08	2.90	2.22	3.36	2.44	1.01	1.20	0.95	1.71	1.73	2.26
CaO	1.22	1.29	1.10	0.49	1.16	0.60	0.73	2.62	11.31	0.22	0.70	0.36	0.43	0.32	1.84
Na_2O	0.52	0.44	0.21	0.13	0.28	0.20	0.40	1.12	1.60	0.17	0.31	0.10	0.18	0.18	0.18
K_2O	2.88	3.20	4.12	4.34	4.08	4.73	3.03	2.96	2.69	2.18	3.26	1.98	2.94	3.06	3.51
TiO_2	0.74	0.77	0.80	1.02	0.78	0.68	0.76	0.76	0.61	0.79	0.63	0.67	0.62	0.63	0.73
P_2O_5	0.10	0.12	0.19	0.10	0.12	0.09	0.14	0.11	0.17	0.03	0.03	0.02	0.06	0.06	0.18
MnO	0.04	0.05	0.08	0.10	0.07	0.07	0.05	0.09	0.13	0.03	0.03	0.03	0.03	0.03	0.06
H_2O	3.06	2.94	3.73	3.22	3.59	4.06	3.14	3.92	4.13	2.53	1.89	1.87	3.33	3.26	4.18
CO_2	0.03	0.03	0.03	0.02	0.02	0.02	0.02	0.03	7.57	0.02	0.01	0.02	0.03	0.03	1.53
Total	99.78	98.98	99.18	99.42	99.30	99.08	99.31	99.71	100.57	99.52	99.94	99.29	99.09	99.69	100.25
L.O.I.	3.40	3.51	4.58	3.54	4.25	4.62	3.68	4.71	11.89	3.02	2.02	2.38	4.30	3.70	5.80
Fe as Fe_2O_3	5.47	3.65	3.70	6.25	5.86	7.07	3.18	4.18	5.63	2.37	3.16	2.64	2.79	4.93	4.18
Fe_2O_3/FeO	3.86	2.50	1.46	3.59	1.69	3.02	1.08	1.22	8.27	0.51	0.25	0.36	2.06	4.02	0.92
Colour	Red	Grey	Green	Red	Red	Red	Green	Green	Red	Green	Green	Green	Green	Red	Green
Location	Al	Al	Al	Al	Al	Al	Al	Al	Al	Al	Pl	Pl	Ll	Ll	Ll

164.

Table 6.3 cont.

	23579Gr	23579R	23584Gy	23584R	Al-05Gr	Al-05R	Al-15	Al-16	Ll-19Gr	Ll-19R	AZ-06	AZ-07	Ll-12	Ll-13	AZ-17	AZ-18-20
	+	+	++	++	x	x	xx	xx	xxx	xxx	**	**				
SiO_2	66.01	66.11	78.62	74.15	75.16	72.93	66.20	72.97	74.67	71.82	74.04	75.40	71.80	72.09	75.25	69.37
Al_2O_3	13.22	14.55	10.22	11.50	10.91	12.04	15.40	13.58	11.09	11.31	11.43	11.80	12.16	11.90	11.36	12.53
Fe_2O_3	2.68	5.94	1.97	4.34	1.78	3.18	5.53	1.95	2.07	4.98	4.20	1.79	4.42	4.61	-	5.38
FeO	6.03	2.38	0.76	0.80	0.89	0.93	0.97	0.75	0.87	0.89	1.17	1.21	0.32	0.66	-	0.59
MgO	2.66	1.48	0.92	0.94	2.04	2.03	2.32	2.21	1.83	1.67	1.41	1.50	1.42	1.64	1.27	1.66
CaO	0.07	0.06	0.12	0.15	1.85	0.85	0.59	0.63	1.47	1.19	1.40	1.16	0.74	0.72	0.86	2.47
Na_2O	0.20	0.18	0.17	0.20	1.45	2.04	0.15	0.12	0.11	0.10	0.38	0.14	0.15	0.17	0.23	0.39
K_2O	2.47	3.87	2.51	2.92	1.59	2.14	4.12	3.59	2.91	3.07	3.10	3.36	3.18	3.16	3.32	3.21
TiO_2	0.67	0.73	0.67	0.73	0.63	0.68	0.73	0.71	0.62	0.63	0.62	0.65	0.72	0.69	0.65	0.69
P_2O_5	0.03	0.04	0.03	0.04	0.07	0.08	0.08	0.07	0.08	0.07	0.11	0.10	0.06	0.06	0.10	0.13
MnO	0.06	0.02	0.06	0.07	0.08	0.06	0.05	0.04	0.06	0.05	0.05	0.05	0.04	0.04	0.03	0.05
H_2O	5.30	4.51	3.15	3.47	3.00	3.50	3.42	3.33	3.11	3.73	2.49	2.83	3.90	3.97	4.08	3.36
CO_2	0.02	0.03	0.02	0.02	0.03	0.28	0.02	0.03	0.78	0.58	0.03	0.03	0.33	0.28	0.03	0.12
Total	99.42	99.90	99.22	99.33	99.48	100.74	99.58	99.98	99.67	100.09	100.43	100.02	99.24	99.99	100.06	99.97
L.O.I.	5.15	4.89	3.50	3.92	3.49	3.59	3.92	3.53	4.22	4.51	2.71	3.24	5.08	4.72	4.50	3.99
Fe as Fe_2O_3	9.38	8.58	2.81	5.23	2.77	4.21	6.61	2.78	3.04	5.97	5.50	3.13	4.78	5.34	2.88	6.03
Fe_2O_3/FeO	0.44	2.50	2.59	5.42	2.00	3.42	5.70	2.60	2.38	5.60	3.59	1.48	13.81	6.98	-	9.12
Colour	Green	Red	Grey	Red	Green	Red	Red	Green	Green	Red	Red	Green	Red	Red	Green	Red
Location	B2	B2	B2	B2	Al	Al	Al	Al	Ll	Ll	AZ	AZ	Ll	Ll	AZ	AZ

Table 6.4.   Mean proportions of major elements (in weight percent) of samples of fine-grained Aztec Siltstone lithologies, taken from Table 6.3.

	1	2	3	4	5	6	7	8
SiO_2	72.02	73.73	69.87	73.37	70.89	70.87	58.10	69.96
Al_2O_3	12.49	11.97	13.14	11.94	12.67	11.66	15.40	10.52
Fe_2O_3	3.12	1.68	4.58	2.01	4.62	2.38	4.02	-
FeO	1.40	1.77	1.14	1.77	1.22	1.81	2.45	-
MgO	1.87	1.92	1.87	1.99	1.77	3.03	2.44	1.41
CaO	0.92	1.00	0.85	0.94	0.74	1.79	3.11	2.17
Na_2O	0.36	0.35	0.36	0.37	0.50	1.77	1.30	1.51
K_2O	3.16	2.94	3.42	2.81	3.23	2.29	3.24	2.30
TiO_2	0.70	0.69	0.72	0.65	0.67	0.54	0.65	0.59
P_2O_5	0.09	0.09	0.08	0.07	0.07	0.11	0.17	0.18
MnO	0.05	0.05	0.05	0.05	0.04	0.21	-	0.06
H_2O	3.39	3.30	3.54	3.48	3.48	2.76	5.00	5.74
CO_2	0.15	0.19	0.13	0.15	0.16	1.09	2.63	1.40
Total	99.72	99.68	99.75	99.60	100.06	100.31	98.51	99.31
L.O.I.	3.95	3.90	4.06	3.99	3.89	-	-	-
Fe as Fe_2O_3	4.68	3.65	5.86	3.98	5.98	4.39	6.74	3.47
Fe_2O_3/FeO	2.23	0.95	4.03	1.14	3.79	1.31	1.64	-

(1)   The mean of 31 typical red, grey and green Aztec samples.

(2)   "   "   " 14   "   green Aztec samples (13 for iron values).

(3)   "   "   " 14   "   red   "   "

(4)   "   "   " 6 green paired Aztec samples.

(5)   "   "   " 6 red   "   "   "

For comparisons:

(6)   Red sample of Lower Old Red Sandstone (Van Houten, 1961b).

(7)   Average shale (Mason, 1966).

(8)   Average Mississippi Delta sediment.   (Clarke, 1924 p.509).

ALUMINIUM

Al$_2$O$_3$ percentages vary from 8.30 to 17.33 with a mean of 12.49. The variation reflects changes in the quantity of clay in each sample. The variability of Al$_2$O$_3$ is unlikely to be greatly influenced by the clay mineral species present as there is very little difference in the Al$_2$O$_3$ content of illites and chlorites, the only clay minerals detected in the formation. That the variation in Al$_2$O$_3$ reflects the quantity of clay in each sample is demonstrated by the positive correlation of Al$_2$O$_3$ with K$_2$O plus MgO (Fig. 6.1). K$_2$O is present in illite only, whilst MgO resides in the chlorite minerals. There are exceptions to the trend brought about by significant percentages of minerals such as chamosite, which is an iron-aluminosilicate, and analcime, a sodium-aluminosilicate. Both minerals were detected in thin section or X-ray diffraction analyses or both; each adds aluminium to the sample but does not affect the K$_2$O or MgO percentage. The chamosite-bearing samples are 23579 and 23584, whilst those with analcime are samples 23240A, 23243 and Al-05. Sample 23304 is known from thin section, X.R.D. and infrared analyses (Table 5.9), to contain approximately 3 percent detrital K-feldspar. The effect of this has been to increase the K$_2$O content relative to aluminium (Fig. 6.1).

The mean Al$_2$O$_3$ content for the fine-grained Aztec samples is low compared with the average shale, reflecting a lower content of clays.

The variation of Al$_2$O$_3$ with red and green lithologies is minimal but there is a tendency, both in paired and unpaired average samples, for the red to have a higher Al$_2$O$_3$ content. This is thought to be due to a slightly higher clay content in the red samples compared with the green, a contention supported by a slightly higher K$_2$O and Na$_2$O and hence a higher illite percentage in red samples (Tables 5.10 and 6.3). It is thought that, in most instances, the green Aztec lithologies have been generated from red by *in situ* reduction and consequent solution and removal of ferric oxides (p.170). It is most

probable, therefore, that small amounts of clay were mobilized
and subsequently leached from the red sediments during this
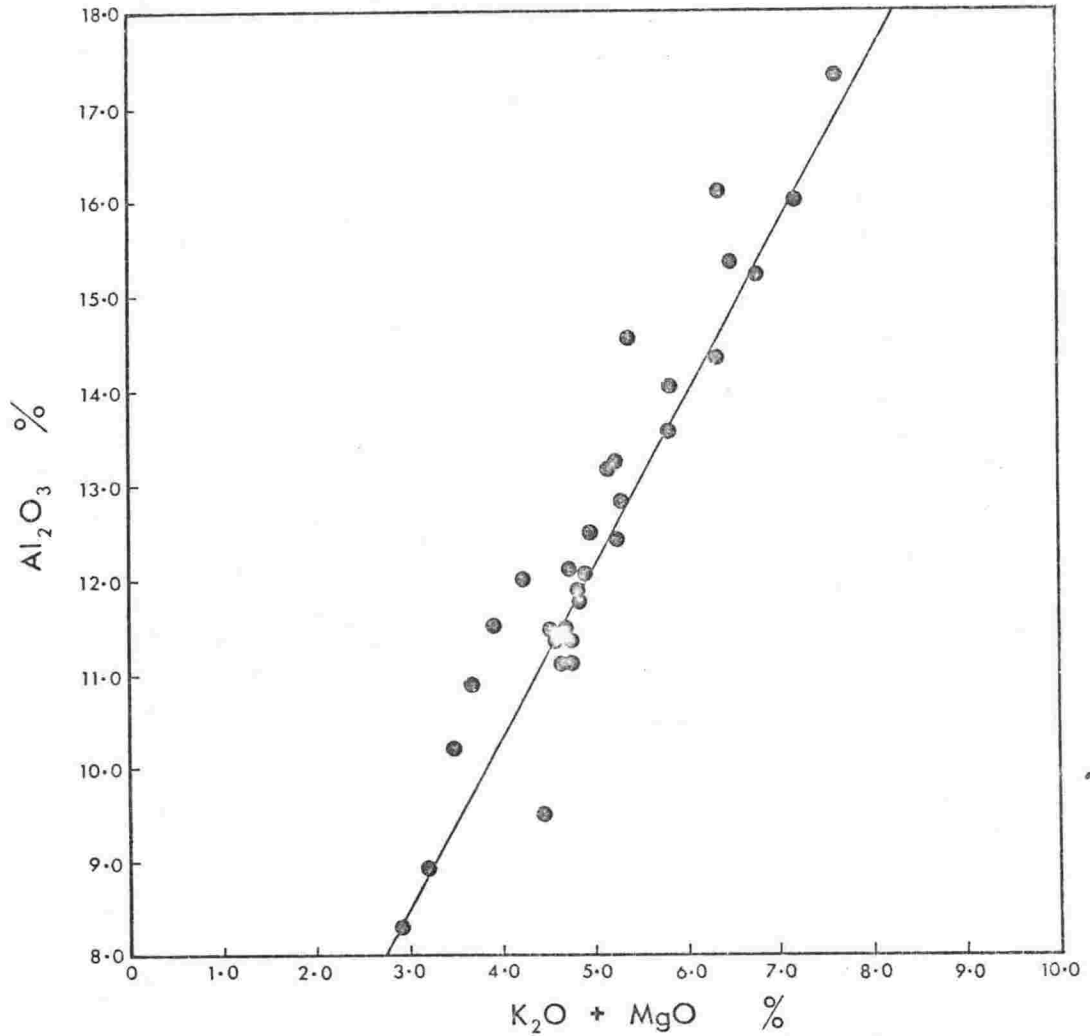
Fig. 6.1. Plot of Al_2O_3 versus K_2O + MgO for fine-grained Aztec
Siltstone lithologies. Data from Table 6.3.

reduction process.   A similar conclusion, based upon analogous
chemical data, was suggested by McBride (1974), for the red
beds of the Difunta Group of Mexico.

TOTAL IRON (as Fe_2O_3)

The iron of the fine-grained Aztec Siltstone lithologies is present in both ferrous and ferric forms and is contained in a number of different minerals (see below for details).

Total iron, expressed as Fe_2O_3, is significantly different in red and green samples (Tables 6.3, 6.4, 6.6, Fig. 6.2).
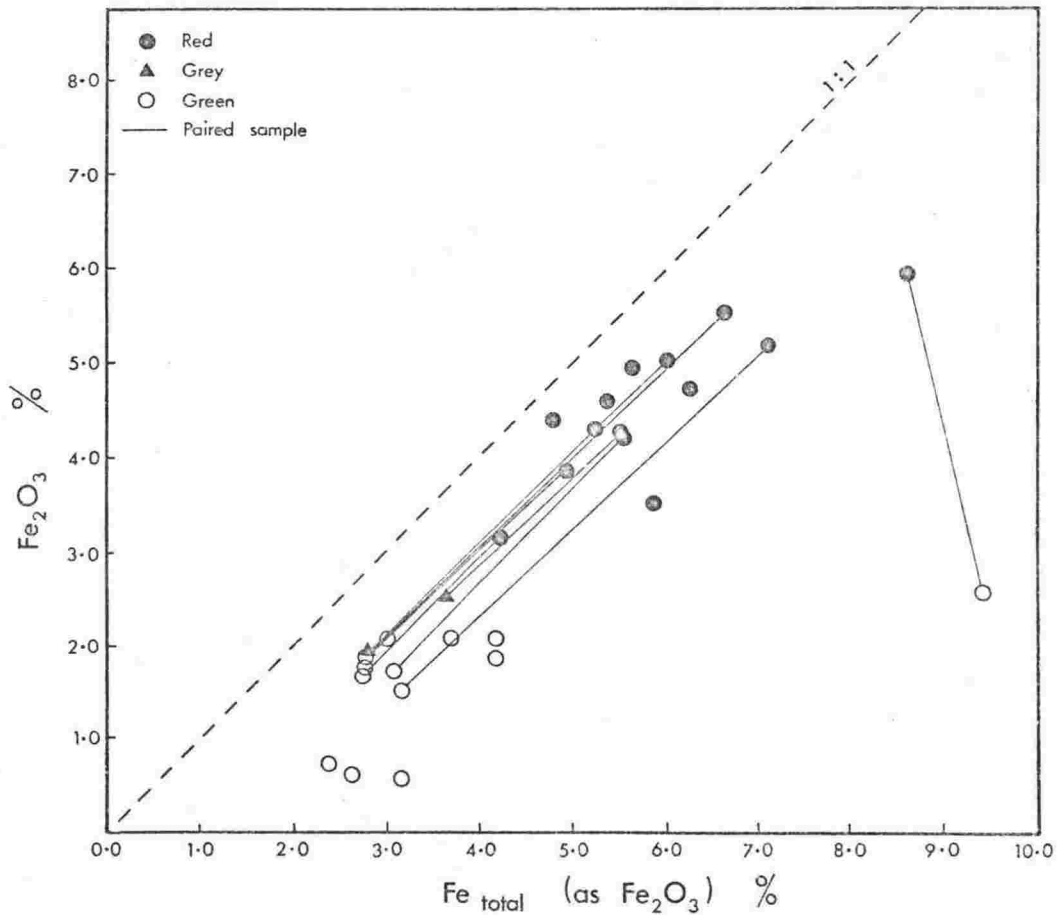
Fig. 6.2. Plot of Fe_2O_3 versus Fe total for fine-grained Aztec Siltstone lithologies. Data from Table 6.3.

The mean total iron content of the green samples is similar to that of the average Mississippi Delta sediment but the mean of the red samples is significantly higher. Both red and green mean total iron values are lower than that for the average shale, but this is not surprising despite the common misconception that "red beds" have high iron contents. The only requirement

for "red beds" is that they contain haematite in a concentration
sufficient to impart the red colour. Walker and Honea (1969)
noted that a concentration of haematite of less than 1 percent
was sufficient to colour many "red beds".

Walker and Honea (1969) determined the average total
iron content of 14 fine-grained ancient red lithologies to be
3.70 percent Fe_2O_3, which is much lower than the mean of the
Aztec red and is about the same as the mean of the Aztec
green samples. The high total iron in the Aztec "red beds",
compared with other "red beds", is attributed to the relatively
fine-grained nature of the Aztec sediments i.e. a high
proportion of clay-sized material including haematite, the
major Fe^{3+} bearing mineral (see below).

FERRIC IRON

There is a significant difference in the ferric iron
content of red, grey and green fine-grained Aztec Siltstone
samples (Tables 6.3, 6.4, 6.6, Fig. 6.3). The red samples have
the highest ferric iron content and a mean value of 4.58 percent.
This value is similar to that of the average shale but signi-
ficantly higher than for the Old Red Sandstone sample. The
ferric iron of the red samples is largely contained in the form
of haematite the concentration of which (Table 5.11), was
determined by the dithionite-citrate extraction method of
Mehra and Jackson (1960). The extractable iron (haematite)
was quantified by Atomic Absorption Spectroscopy. The red
fine-grained lithologies of the Aztec Siltstone average 3.01
percent haematite (Table 5.11) which means that on the average
1.57 percent (4.58-3.01) ferric iron (As Fe_2O_3) in red samples
(Table 6.7) is in a combined form, as ferric silicates,
probably in the chloritic clays. Minor amounts exist in illite
and secondary epidote. The individual sample values for
combined or non-haematitic ferric iron are given in Table 6.5.

The green fine-grained samples have a mean ferric iron
value of 1.68 percent. A small percentage of this is contained
as relic 'black haematite' grains (p.148), and as remnant

Table 6.5.   Ferric iron (combined, and probably as ferric silicates)
             other than as haematite, in samples of the fine-grained
             Aztec Siltstone lithologies. These values (in weight
             percent) have been determined by subtracting the haematite
             percentages (Table 5.11) from the total ferric iron values
             determined by X.R.F. (Table 6.3).

Location	Sample	Colour	Ferric iron as Fe_2O_3
Al	23228	10R 4/2	1.05
"	23235A	"	1.59
"	23237	"	1.04
"	23239	"	1.27
"	Al-05R	"	1.04
"	Al-15	"	1.57
Ll	23432R	5R 4/2	1.17
"	Ll-19R	10R 4/2	1.78
"	Ll-12a	"	1.82 ⎤
"	-12b	"	1.92 ⎬ 1.96
"	-12c	"	1.95 ⎨
"	-12d	"	2.17 ⎦
"	Ll-13a	"	1.69 ⎤
"	-13b	"	1.49 ⎬ 1.60
"	-13c	"	1.50 ⎨
"	-13d	"	1.72 ⎦
B2	23579R	"	2.04
"	23584R	"	1.04
AZ	AZ-06	"	1.45
"	AZ-18	"	3.26 ⎤
"	AZ-19	"	3.53 ⎬ 3.37
"	AZ-20	"	3.32 ⎦
		Mean red	1.57 σ = 0.62
Al	23230	N5	1.64
B2	23584GY	"	1.25
		Mean grey	1.45 σ = 0.28
Al	23233	5G 6/1	1.87
Ll	23432	5GY 6/1	1.51
		Mean green	1.69 σ = 0.25

patches of haematite pigment suggesting that the samples were
formerly red. Two typical samples (23233 and 23432Gr) gave
haematite concentrations of 0.23 and 0.30 percent (Table 5.11).
Therefore, the green samples contain most of their ferric iron
(approx. 1.4 percent Fe_2O_3) in a combined form, the concentration
of which is very close to that found in the red (1.57 percent).
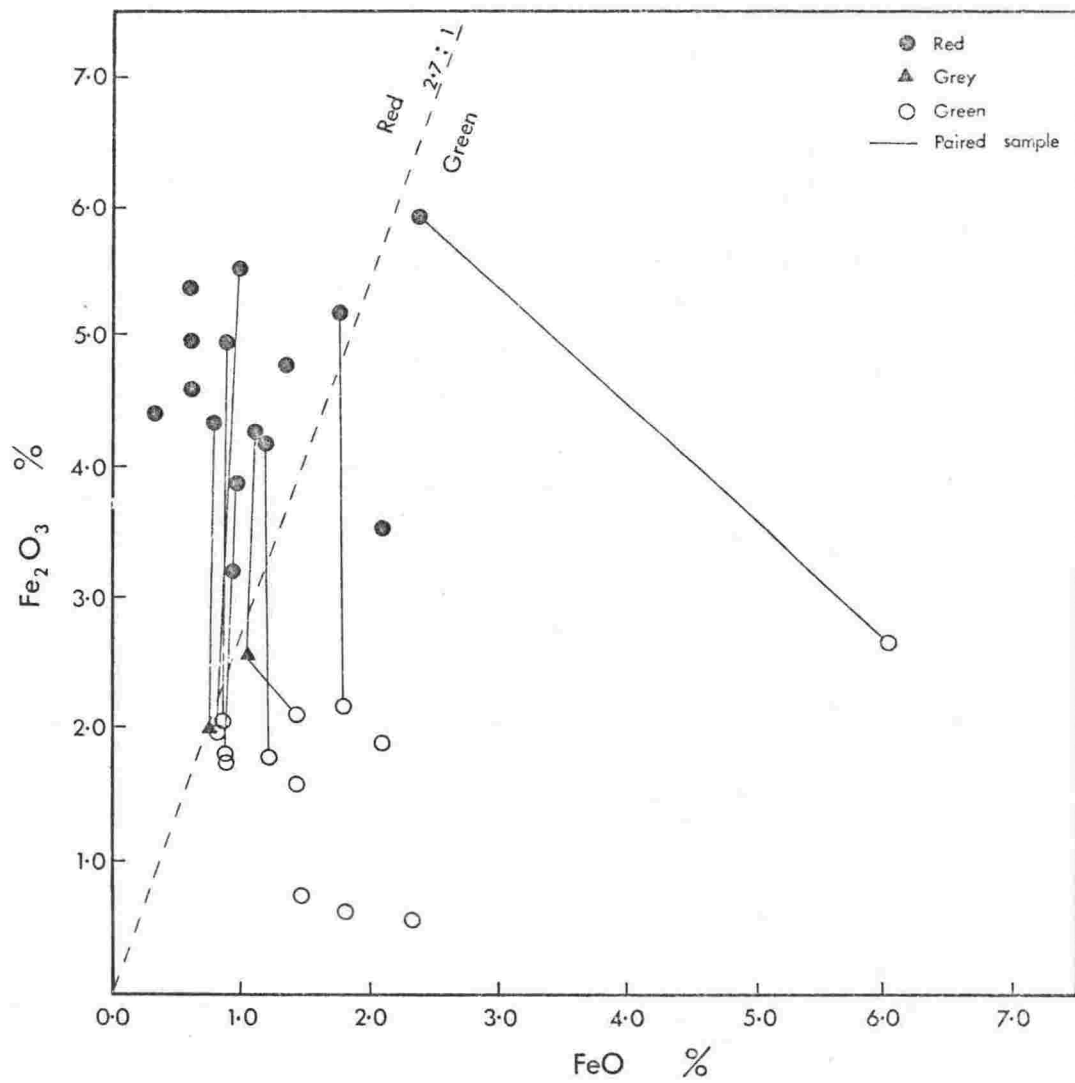
Fig. 6.3. Plot of Fe$_2$O$_3$ versus FeO for fine-grained Azted Siltstone
lithologies. Data from Table 6.3.

The grey samples are lithologies transitional between the red and the green and as expected have intermediate percentages of haematite (0.80 percent). Like the red and green lithologies, however, they have a mean combined ferric iron concentration of 1.45 percent.

As the means for combined ferric iron in red, grey and green samples are about the same (approximately 1.5 percent), then the mean chlorite mineral percentage, the main combined ferric iron-bearing mineral, should also be similar for each group. This is well demonstrated in individual paired samples (e.g. 23432) by both the major element chemistry, X.R.D. (Table 5.7) and thin section analyses. It is also further substantiated by the similar MgO percentages for red and green samples.

In summary, the differences in the total ferric iron concentrations between the red, the grey and the green groups of Aztec samples are due, almost entirely, to haematite. Also, the red, grey and green groups of samples contain similar combined ferric iron concentrations, largely as ferric silicates in chlorite.

FERROUS IRON

The ferrous iron percentage in the composite sample of the Aztec Siltstone fine-grained lithologies (1.40 percent) is similar to that in the Lower Old Red Sandstone sample (1.81 percent), but low compared with the average shale (2.45 percent).

FeO in the Aztec samples is contained largely in the chlorite clay minerals, possibly with minor amounts in illite, rare sulphides and secondary epidote. The mean value for all green samples of 1.77 percent is not significantly different (at the 0.05 level of significance) to that for the red (1.14 percent) (Table 6.6). The ferrous iron content of the red and green fractions of most paired samples is almost identical (within the experimental error) (Table 6.3, Fig. 6.3). The difference as seen in both the means for paired and unpaired samples, is a bias introduced by sample 23579, a red-green

Table 6.6.   Student t test on the significance of the Fe total,
Fe_2O_3, and FeO variations with colour. Values from
Tables 5.11, 6.4 and 6.5.

	Red	Green
Mean total Fe (as Fe_2O_3)	5.86	3.65
Std. dev. (σ)	1.09	1.81
No. samples	14	13
$P = 0.001$, $t = 3.68$, d.f. $= 25$ Therefore a significant variation		
Mean Fe_2O_3	4.58	1.68
Std. dev. (σ)	0.78	0.64
No. samples	14	13
$P \ll 0.001$, $t = 10.05$, d.f. $= 25$ Therefore a significant variation		
Mean FeO	1.14	1.77
Std. dev. (σ)	0.57	1.37
No. samples	14	13
$P = 0.15$, $t = 1.50$, d.f. $= 25$ Therefore no significant variation		

pair, in which the ferrous iron content of the green fraction
is very high, and very much higher than for the red (Figs.
6.2 and 6.3). From the field evidence (Askin et al.1971, p.70)
it was concluded that the unit from which the anomalous sample
was taken is a massive red bed that has undergone patchy
reduction resulting in irregular patches of greenish grey
sediment. It would appear that this reduction locally
dissolved the haematite (3.9 percent, Table 5.11) to expose
the green sediment but the ferrous iron so produced was retained
by the reduced sediment in the form of chlorite thus maintaining
the same total iron content in the red and green fractions
(Table 6.7).

Table 6.7. Oxidation states of iron in the red and the green
portions of sample 23579. Values in weight percentages.

	23579R		23579Gr
	Oxidized	Reduced (theoretical)	
Haematite	3.9	0	0
Fe_2O_3 combined	2.04	2.04	2.68
FeO	2.38	5.89	6.03

Sample 23579 is an exception, however, as can be seen from
Figures 6.2 and 6.3. In most cases the colour differences
have been produced by an absolute loss or gain of haematite by
the sediment, leaving the ferrous iron and the combined ferric
iron unchanged. Several lines of field evidence indicate a
colour change from red to grey or green by reduction.

(1)   Green patches in a massive red host, e.g. sample 23432,
       Fig. 3.4. Localized reduction has been induced probably
       by the incorporation of organic matter in the sediment as
       suggested by Friend (1966).
       The example of the green spheres at Al, units 21 and 22
       (Fig. 3.4) is strong evidence for localized post-depositional
       reduction. Reduction spheres similar to these have been
       reported from other red bed sequences, e.g. the Vernon
       shales (Miller, 1910), the red beds of the western U.S.A.
       (Tomlinson, 1916), the Catskill Formation (Friend, 1966)
       and the upper Flowerpot Shale (Wu, 1971). There is general
       agreement that the reduction was caused by organic material
       incorporated in the sediment, and in many examples the
       organic matter remains preserved in the core of the spheres.
       The Aztec examples did not contain organic matter, but, as
       pointed out by Tomlinson (1916), the quantity of organic
       matter necessary to accomplish the reduction of a patch of
       less than 5 cm diameter, like the Aztec examples, would be
       so small that it could easily be effaced or removed.

(2)   A green boundary layer at the contact of a massive red
      bed with an overlying sandstone e.g. samples 23233 and
      AZ-17, Fig. 4.26. In these examples reduction was
      induced by reducing solutions emanating from the overlying
      sandstone (see p.216 for details).

(3)   Green vein networks (Fig. 3.5, samples AZ-06 and AZ-07
      and Ll-19). Reducing solutions are believed to have
      followed cracks or former cracks in massive red units
      (see Vein Networks, p.67 for details).

(4)   Thin green beds within a massive red unit. These have
      formed probably by reducing solutions migrating along
      more permeable beds in a massive red unit (see p. 23
      for details). The example is sample 23584.

Two pairs of samples (Al-05R,   Al-05Gr and Al-16, Al-17)
were selected because they were considered to be examples of
haematite having been introduced into a green sediment and not
removed from a red sediment as is the usual case. The example
of Al-16 and 17 has already been discussed in part (p.
Fig. 4.5), and it was shown that the haematite pigment had
intricately followed bedding planes and vertical weaknesses
in the sediment. It would appear that the haematite was
introduced in the form of an iron-rich solution, probably as
a ferrous iron derived from the reduction of a neighbouring
red sediment. As the solution penetrated the sediment it
oxidized and precipitated hydrated ferric oxide which, at
some stage, converted to haematite.

As might be expected, there is no difference in the iron
chemistry (Figs. 6.2 and 6.3) between the above mentioned
pairs of samples, i.e. samples which had haematite added to
former green sediments, and the more common samples i.e. those
which had haematite removed by reduction.

It is thought that most of the green and grey lithologies
of the formation were derived from former red lithologies by
reduction and removal, in solution, of their haematite pigment
as has been demonstrated for the red-grey or red-green pairs
of samples. In agreement with this we find that the unpaired

red and green samples all plot in ferric-ferrous and total
iron fields similar to the paired samples (Figs. 6.2 and 6.3).
The mean Fe_2O_3/FeO ratios for the 13 green samples of 0.95
is markedly different from that for the 14 red, of 4.03
(Table 6.4). A ratio of 2.7 separates the green samples from
the red, with few exceptions. The two grey samples have a mean
Fe_2O_3/FeO ratio of 2.55, intermediate between the red and green.

MAGNESIUM

The composite sample of the fine-grained Aztec lithologies
contains 1.87 percent MgO which is low relative to the average
shale or the Old Red Sandstone sample, but higher than the
average Mississippi Delta sediment.

Magnesium is considered to be contained largely in the
chloritic clay minerals, as these generally contain between
3 and 35 percent MgO. Some magnesium is also contained in
illite, commonly between 1 and 4 percent MgO. Minor amounts
of dolomite may be present also, as there is a positive
correlation between MgO and CO_2. However, dolomite was not
detected in X.R.D. analyses. The mean magnesium value for
red samples is within the experimental error of that for the
green (Table 6.1). This is also true for the red-green pairs
of samples and the apparent difference (1.99 for green and
1.77 for red) was, in large part, introduced by the anomalous
sample 23579.

CALCITE

The mean CaO content of all Aztec fine-grained samples
is 0.92 percent, which is low with respect to the average
shale, the Old Red Sandstone sample and the average Mississippi
Delta sediment. CaO in the Aztec Siltstone is contained in a
number of minerals, including calcite, chlorite, illite and
epidote, with lesser amounts from gypsum, secondary zeolites,
prehnite and grossular, where present. Correlation between
CaO (after the calcite-contributing CaO has been subtracted)

and K_2O + MgO (representative of the clays) is positive
though weak (Fig. 6.4). The fact that it is weak suggests
that calcium is present in minerals other than clays.
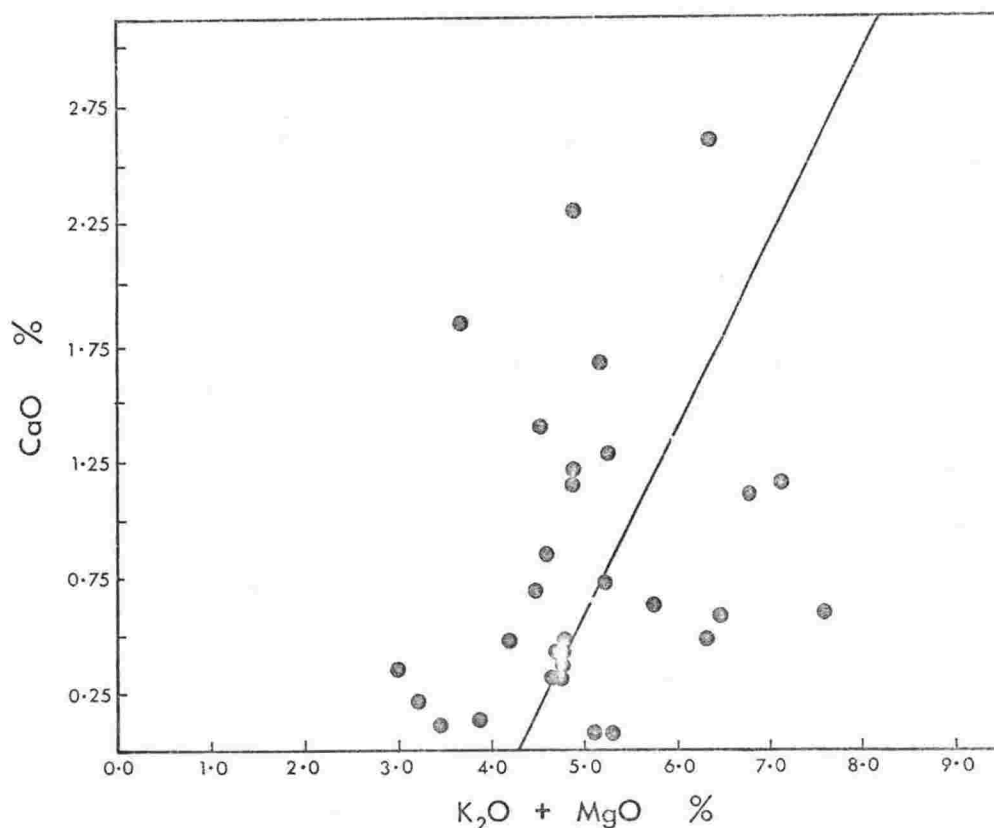
Fig. 6.4. Plot of CaO versus K_2O + MgO for fine-grained Aztec
Siltstone lithologies. The CaO due to calcite (calculated
from the CO_2 value) has been subtracted. Data from Table
6.3.

The low concentration of CaO in the fine-grained Aztec
lithologies compared with the other lithologies quoted in
Table 6.4, is due to the relatively small amount of matrix
calcite as determined by the lower CO_2 percentage. The Aztec
fine-grained lithologies contain only 0.34 percent matrix
calcite. Calcite is common in the fine-grained Aztec lithologies
but is largely contained in nodular form (see Nodules, p.73).
A small number of the fine-grained beds sampled did contain
a high matrix calcite content, e.g. sample 23243, but because
they constitute only a very small fraction of the total

lithologies of the formation they have not been included in
the means of the chemical analyses.

The CaO value is slightly higher for green samples than
for the red, both in the average paired and unpaired samples.
The difference is thought to be partially due to higher calcite
contents in the green samples as shown by the higher CO_2 mean
for all green as compared with all red samples, and partially
due to the slightly higher chlorite contents in the green samples.

SODIUM

Sodium is contained in a number of minerals in the Aztec
lithologies, principally analcime, authigenic Na-feldspar, and
illite. Assuming that the illite in the Aztec Siltstone contains
a normal Na_2O concentration of approximately 0.43 percent (Deer,
Howie and Zussman, 1966 p.251), then the amount of Na_2O in
these samples resulting from illite should be approximately
0.16 percent (0.15 percent in the green and 0.17 percent in
the red). Thus, approximately half of the sodium in the Aztec
fine-grained lithologies is derived from analcime or albite.
In the non-analcime bearing samples with an average Na_2O content
of 0.36 percent, albite may constitute up to approximately 2
percent of the sample by weight (assuming the albite to contain
approx. 10 percent Na_2O). However, as albite and analcime are
probably in equilibrium (see Chapter 5), it is most likely that
albite constitutes less than 2 percent by weight of the average
sample and more like 1 percent.

The mean Na_2O value for the Aztec fine-grained lithologies
of 0.36 percent is low with respect to the Old Red Sandstone
sample, the average Mississippi Delta sediment, and the average
shale. The very low mean value reflects the relatively low
albite content (approx. 1 percent) (p. 155), and a higher degree
of weathering, in the source region and possibly *in situ*, of
the Aztec Siltstone sediments.

The mean Na_2O values for unpaired red and unpaired green
samples are practically identical. However, in the paired
samples the red appear to contain slightly more Na_2O than their

associated green samples. A study of the individual red-green
pairs shows that, in general, the Na_2O values are similar. The
means have been biased by 2 sample pairs (A1-05Gr, A1-05R and
AZ-06, AZ-07) with high Na_2O contents. These samples contain
analcime (Table 5.7). The lower mean Na_2O value in the green
of the paired samples may be due to a partial solution of their
analcime during reduction.

POTASSIUM

K_2O is the third most abundant constituent (excepting H_2O)
of the fine-grained Aztec Siltstone lithologies. It is wholly
contained in the illitic clay minerals, with possibly some minor
amounts from sericite and mica. K-feldspar was recorded in
only one fine-grained sample (23304, Table 5.9). As illite is
the only K_2O bearing mineral (as determined by thin section,
X.R.D. and infrared analyses), its percentage in each sample
could be determined by dividing the K_2O percentage by 8.5, the
mean K_2O percentage in illite (Harder, 1970 p.163). The values
obtained (Table 5.10) showed excellent agreement with those
obtained from Infrared Spectrophotometric analysis (Table 5.8).

The mean K_2O content of the Aztec Siltstone samples of
3.16 percent is approximately the same as that for the average
shale (3.24 percent) but more than for the average Mississippi
Delta sediment or the Old Red Sandstone sample. However, the
other sediments probably contain K_2O-bearing minerals other than
illite, namely K-feldspar.

The mean K_2O values for both paired and unpaired green
and red samples show the same differences. Red paired samples
consistantly have slightly higher K_2O percentages than their
green associates (Table 6.3). The red sediments are therefore
believed to have a slightly higher illite content, brought about
probably by the leaching of illite from the green sediments
during reduction.

TITANIUM

TiO_2 is present in the fine-grained lithologies of the
Aztec Siltstone in a concentration approximating that of the
average shale but more than for the average Mississippi Delta
sediment or the Old Red Sandstone sample. Because of a similar
ionic radius, Ti^{3+} and Ti^{4+} can substitute for Fe^{3+} and Fe^{2+}
respectively in many minerals. However, plots of TiO_2 versus
Fe total, Fe_2O_3 combined, Fe_2O_3 total, FeO, and Fe + K_2O + MgO
combined, did not show a significant correlation. A plot of
TiO_2 versus the clays (represented by K_2O + MgO) is positive
although weak (Fig. 6.5). TiO_2 is a common minor constituent
of clays, in illite in a concentration of 0.81 percent and in
chlorites in percentages varying from 0.09 to 0.88 percent
(Deer, Howie and Zussman, 1966). The fact that the plot of
TiO_2 versus the clays is weak suggests that titanium is also
present in some other mineral form, possibly in the heavy
minerals rutile, brookite and anatase.
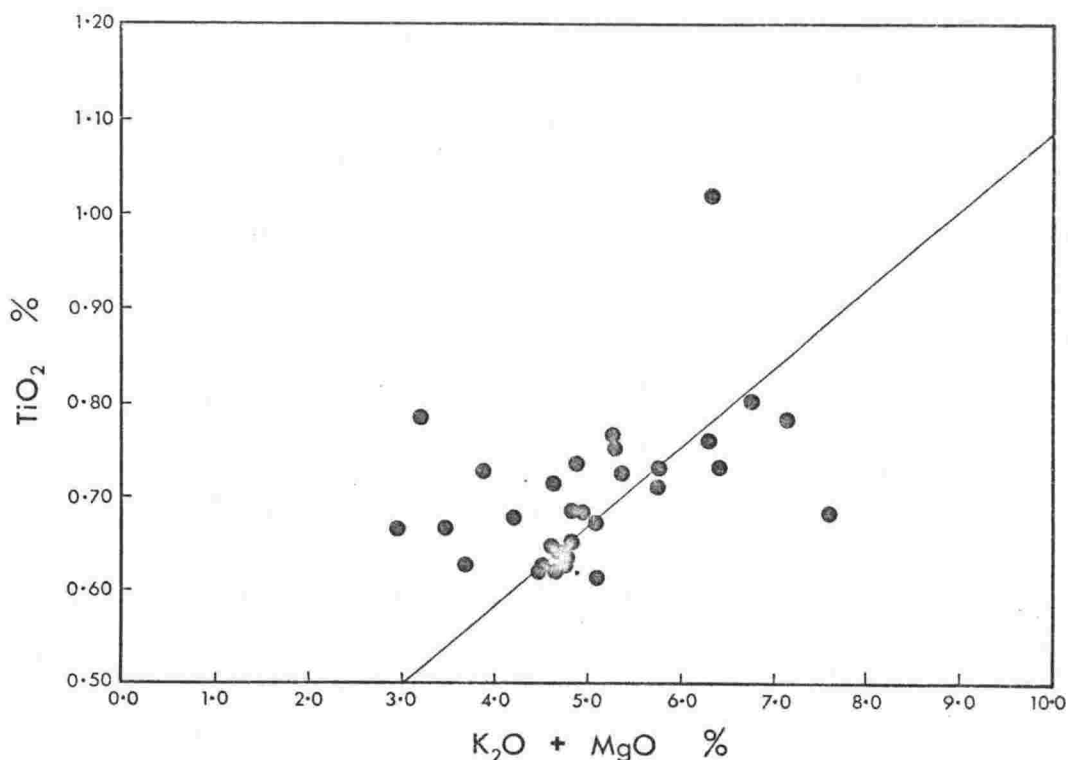
Fig. 6.5. Plot of TiO_2 versus K_2O + MgO for fine-grained Aztec
Siltstone lithologies. Data from Table 6.3.

The TiO_2 content of red and green lithologies is very
similar but with slightly higher values for the red. This
may reflect the slightly higher clay content of the red samples.

PHOSPHORUS

The mean P_2O_5 content of the fine-grained lithologies of
the Aztec is low with respect to the average shale, the average
Mississippi Delta sediment and the Old Red Sandstone sample.
Values vary from a minimum of 0.02 to a maximum of 0.19 percent.
Many of the fine-grained beds do however, contain appreciable
amounts of phosphorus in the form of phosphatic fish scales or
bones (Table 5.7). These fish remains generally occur as
scattered fragments but in some examples they are so abundant
as to form lenses of almost pure phosphatic material, e.g. A4,
unit 62.

The non-fish derived phosphorus may be present in a host
of minerals in the Aztec lithologies including the clays,
but is most probably present as apatite, either detrital or
chemically precipitated. Some nodules at M1 contained
appreciable amounts of apatite (Table 5.7, 23274). These
nodules may have nucleated about fish material, which is common
at M1.

There does not appear to be any significant correlation
between the phosphorus content of the fine-grained lithologies,
and their colour. Both red and green paired samples contain
similar amounts of P_2O_5 (Table 6.1).

MANGANESE

The mean MnO content of the Aztec Siltstone fine-grained
lithologies is low with respect to the Old Red Sandstone
sample but comparable to that for the average Mississippi
Delta sediment. The MnO percentages vary from a minimum of
0.02 to a maximum of 0.13 percent. Manganese is contained
in these samples in the chlorites. This is indicated by

the positive correlation of MnO and MgO (Fig. 6.6); the MgO is considered to originate solely from chlorite. Samples 23235A, 23243 and 23584, have unusually high MnO percentages; the additional MnO is possibly contained in epidote or pyrolusite (MnO_2), or both.
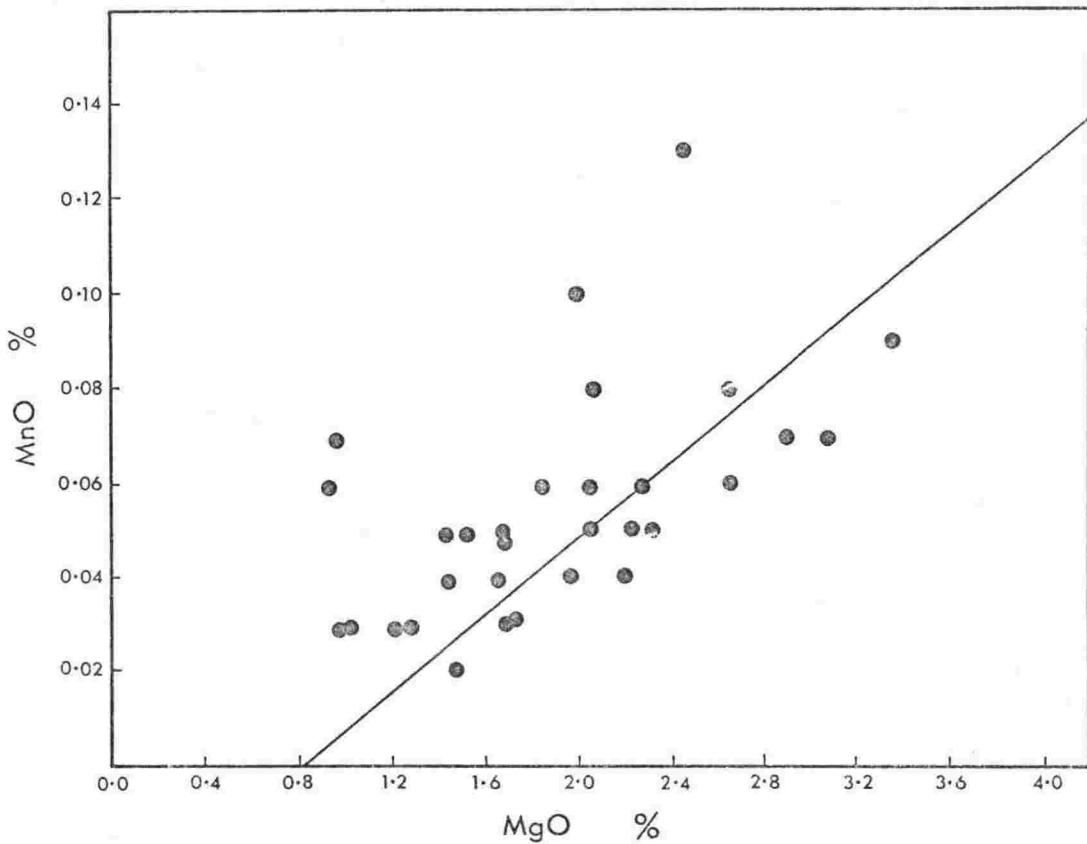
Fig. 6.6. Plot of MnO versus MgO for fine-grained Aztec Siltstone lithologies. Data from Table 6.3.

The MnO values for the red and green paired samples are similar. This is consistent with the suggestion above that the manganese resides in chlorite, because the chlorite content of red and green samples is also similar.

The Fe_2O_3/MnO ratio of sediments has been used as an indicator of their depositional environment. Strakhov (1957, II, p.483) gives a ratio of 64 for continental environments and 14 for marine waters, whilst Keith and Degens (1959) give 68 for continental shales and 11 for marine shales. These values reflect the ease with which iron is precipitated relative to manganese in the more oxidizing continental environment (Krauskopf, 1967 p.268). The fine-grained lithologies of the Aztec Siltstone have a mean Fe_2O_3/MnO ratio of 62.5 which is, as expected, close to that for continental sediments. However, while the mean of the red samples has a ratio of 92 that is obviously indicative of oxidising conditions and continental sediment, the mean of the green samples has a value of 33.5, which is closer to the marine value. The green samples have largely been produced from post-depositional reduction of the red by the solution and subsequent leaching of haematite (Fe_2O_3). Therefore, the lower Fe_2O_3/MnO ratio in the green samples does not necessarily indicate marine sediment but is merely a product of the reducing environment.

WATER

The water values include both absorbed (H_2O^-) and crystal lattice water (H_2O^+). The mean value for the Aztec samples is low with respect to the average shale and average Mississippi Delta sediment, but slightly higher than for the Old Red Sandstone sample. Most water is associated with the clays, with some minor amounts from calcite, epidote and the zeolites.

As expected, the red and green paired samples show no significant variation in H_2O content.

CARBON DIOXIDE (carbonate)

The mean acid-evolved CO_2 content of the fine-grained
lithologies of the Aztec Siltstone is very low with respect to
the Old Red Sandstone sample, the average shale and the average
Mississippi Delta sediment. The only carbonate detected in the
Aztec Siltstone was calcite (Tables 5.7 and 5.9) although very
minor amounts of dolomite may be present. The carbonate content
of the fine-grained Aztec samples is difficult to assess
because much of it is in nodular form. These nodules appear
to have depleted the fine-grained lithologies of matrix calcite.
A few calcareous fine-grained samples were noted and one, 23243,
was analysed but was not incorporated in the means of the chemical
analyses (Table 6.4) because it is representative of only a very
small proportion of the total lithologies of the formation.

The mean CO_2 value for all green samples is slightly
higher than the mean for all red samples, suggesting a slightly
higher calcite content in the green samples.

TRACE ELEMENTS

The totals for the analyses of the Aztec samples are
consistently low and this is thought to be due to undetermined
trace elements such as S, Cl, Zr, Rb and Sr. Sulphur, as
sulphates (gypsum) and sulphides (pyrite) is present in the
formation (Tables 5.7 and 5.9) and chlorine may have been
successively enriched in the Aztec Siltstone red beds by
repeated dry season evaporation. Free carbon was observed
in a few samples (Table 5.9)..

Many of the reduction spheres and veins noted at Al, units
21 and 22 (Fig. 3.4), contained malachite green centres. These
are concentrations of secondary copper minerals which were
extracted from intrastratal solutions when they came in contact
with the organic matter responsible for creating the green
sphere by post-depositional reduction and solution of the
haematite. It is thought that the copper is retained by the

formation of a stable organo-metallic complex. Copper forms
more stable compounds with humic substances than does any other
metal (Vinogradov, 1959 p.147) and is retained in soil profiles
by this method. Other elements such as vanadium, zinc, cadmium,
nickel, cobalt and molybdenum are affected in a similar way.
Wu (1971) found that cobalt, nickel and vanadium were
concentrated in red bed reduction spheres similar to the
Aztec examples.

Sandstone Chemistry

Two sandstone samples from the Aztec Siltstone, selected
as representative of the sandstones, were analysed for major
elements (Table 6.8). The Aztec sandstones are quartzarenites
(Fig. 5.23) and divide into two main types (Chapter 5 p.128,
see also Tables 5.5 and 5.9).
(a) Quartz cemented quartzarenites, represented by   .
      sample 23250 (Fig. 5.24).
(b) Calcite cemented quartzarenites, represented by
      sample 23241 (Fig. 5.25).

Both types commonly contain some clay matrix, as for example
the two samples analysed. Sample 23241 also contains a small
percentage of haematite pigment which gives it a pink colouration.
      Silicon in both samples is largely contained in the form of
detrital quartz, in percentages which are normal for a
quartzarenite (23250) or a calcareous quartzarenite (23241).
Both samples analysed contain clays which are largely
responsible for the percentages of Al_2O_3, MgO, FeO, K_2O,
Na_2O and TiO_2. A small percentage of zeolites in 23241
(Table 5.9) probably further adds to the Al_2O_3 and Na_2O
percentages.
      The total iron content of sample 23241 is higher than
sample 23250 because it contains haematite pigment as a
coating on detrital quartz grains. This is demonstrated by

Table 6.8. Major element analyses of sandstones from the Aztec
            Siltstone. Two samples have been included for comparison.
            Values in weight percent.

	23241	23250	1	2
SiO_2	77.23	94.81	85.3	95.4
Al_2O_3	4.39	2.15	7.2	1.1
Fe_2O_3	0.26	0.04	-	0.4
FeO	0.36	0.32	-	0.2
MgO	0.39	0.26	0.3	0.1
CaO	8.09	0.10	0.1	1.6
Na_2O	0.25	0.11	0.5	0.1
K_2O	0.42	0.59	3.2	0.2
TiO_2	0.15	0.10	0.2	0.2
P_2O_5	0.04	0.02	-	-
MnO	0.19	0.01	-	-
H_2O	2.48	0.40	1.1	0.3
CO_2	5.64	0.02	0.1	1.1
Total	99.89	98.93	99.6	100.7
L.O.I.	7.68	1.40	-	-
Fe as Fe_2O_3	0.66	0.40	1.6	0.62
Fe_2O_3/FeO	0.72	0.12	-	2.00
Colour	Pink	Grey	-	-

1. Average red bed sandstone (Cosgrove, 1973).

2. Mean quartzarenite composition (Pettijohn, 1963 p.15).

the higher Fe_2O_3 content of sample 23241 and as most of the
Fe_2O_3 will be as haematite, it shows that only 0.26 percent
haematite is sufficient to give a pink colouration to the
sample. The much higher total iron content of the average red
bed sandstone is undoubtedly due to a much higher haematite
content in these samples. Unlike most other red beds, the
Aztec Siltstone does not have red, haematitic, sandstones.
Even pink sandstones are extremely rare in the Aztec formation.

The Fe_2O_3/FeO ratios are both low compared with those of
the fine-grained sediments (Tables 6.3 and 6.4), however, the
pink sandstone clearly has a ratio higher than the grey, as
expected.

CaO is contained in clays in sample 23250, and in calcite
cement (13 percent, based on the CO_2 value of 5.64 percent)
in sample 23241. The phosphorus in both samples is possibly
present as detrital apatite or as an impurity in either the
clays or calcite.

Soil Chemistry

Almost half of the Aztec Siltstone consists of intervals
largely of fine-grained lithologies with a few thin sandstone
interbeds (fine-member units, Chapter 7, p.205). Many of
these finer than sand units and in particular those which are
unbedded, are thought to have undergone extended weathering
and soil development when they were subaerially exposed on the
floodplain. Two possible soil horizons were sampled for major
element variations with depth in the profile. These profiles
were chosen because they appear to be most complete and
contained a number of soil characterising features, e.g.
calcareous nodules, vein networks, etc (see Chapter 4).
The first soil profile, at L1, unit 17 (Askin et al, 1971)
was sampled at 0.7 m intervals from top to bottom (samples
L1-12). This sampling was repeated 2 m further along the
profile (L1-13) to give a measure of the variability within
a single profile. The second soil horizon, at Aztec

Mountain (AZ, Fig. 2.1) (Fig. 4.26), was sampled at 0.4 m
vertical intervals beginning with AZ-17 in the green reduction
layer.

It is assumed that there was no significant variation with
depth in the chemical and physical composition of the parent
sediments. The assumption is in part supported by the lack
of any observable progressive textural variation in either
profile in the field. Also, many of the down-profile element
variations are duplicated in the adjacent L1 profiles.
Duplication of these variation trends, many of which deal
with small percentage changes, would be unlikely to arise
from depositional processes.

The major element analyses are presented in Table 6.9 and
Figure 6.7.

SILICON

The trend is for SiO_2 to decrease with depth in the profile,
partially brought about by an increase with depth of the non-
silicate minerals, namely haematite and calcite, and partially
by an increase with depth, of clays relative to detrital
quartz.

ALUMINIUM

Identical trends are shown for Al_2O_3 by the three profiles,
with an initial slight decrease in Al_2O_3 followed by a
progressive increase with depth in the profile. As Al_2O_3
is largely contained in the illitic and chloritic clays
(see Chemistry of Siltstones and Claystones, p.163), the
trend suggests illuviation of clay. Increases in K_2O, MgO
and TiO_2 support this.

Table 6.9. Major element variations (down profile) within three soil profiles developed in fine-grained fine member units of the Aztec Siltstone.

	L1-12a	L1-12b	L1-12c	L1-12d	L1-13a	L1-13b	L1-13c	L1-13d	AZ-17*	AZ-18	AZ-19	AZ-20
SiO_2	75.32	73.40	68.26	70.20	74.89	75.15	69.82	68.50	75.25	73.44	68.75	65.93
Al_2O_3	11.04	11.08	12.39	14.11	11.05	10.86	12.29	13.40	11.36	11.21	12.65	13.73
Fe_2O_3	3.68	4.61	5.21	4.16	4.29	3.99	4.33	5.84	–	4.58	6.22	5.34
FeO	0.31	0.20	0.37	0.39	0.41	0.65	0.89	0.71	–	0.45	0.28	1.03
MgO	1.08	1.45	1.74	1.43	1.76	1.39	1.83	1.57	1.27	1.63	1.54	1.87
CaO	0.38	0.43	1.81	0.34	0.34	0.37	1.53	0.64	0.86	1.46	2.15	3.79
Na_2O	0.11	0.11	0.14	0.23	0.14	0.18	0.14	0.22	0.23	0.37	0.46	0.34
K_2O	2.95	2.94	3.30	3.53	2.99	2.93	3.29	3.43	3.32	2.95	3.27	3.41
TiO_2	0.70	0.64	0.72	0.80	0.68	0.63	0.68	0.78	0.65	0.64	0.70	0.74
P_2O_5	0.03	0.07	0.07	0.06	0.03	0.07	0.09	0.06	0.10	0.07	0.13	0.19
MnO	0.03	0.03	0.06	0.03	0.03	0.03	0.06	0.03	0.03	0.04	0.05	0.07
H_2O	4.06	3.70	3.38	4.46	3.63	3.64	4.20	4.40	4.08	3.04	3.76	3.28
CO_2	0.03	0.03	1.24	0.03	0.03	0.04	0.99	0.07	0.03	0.07	0.06	0.24
Total	99.72	98.69	98.69	99.77	100.27	99.93	100.14	99.65	100.06	99.95	100.02	99.96
L.O.I.	4.28	4.90	6.23	4.90	4.37	4.14	5.36	5.01	4.50	3.92	4.02	4.04
Fe as Fe_2O_3	4.02	4.83	5.62	4.59	4.75	4.71	5.32	6.63	2.88	5.08	6.53	6.48
Fe_2O_3/FeO	11.87	23.05	14.08	10.67	10.46	6.14	4.87	8.23	–	10.18	22.21	5.18
Colour	Red	Red	Red	Red	Red	Red	Red	Red	Green	Red	Red	Red

* FeO and thus Fe_2O_3 not determined because of complexing of diphenylamine sulphonate (Eh-indicator) with the sample.
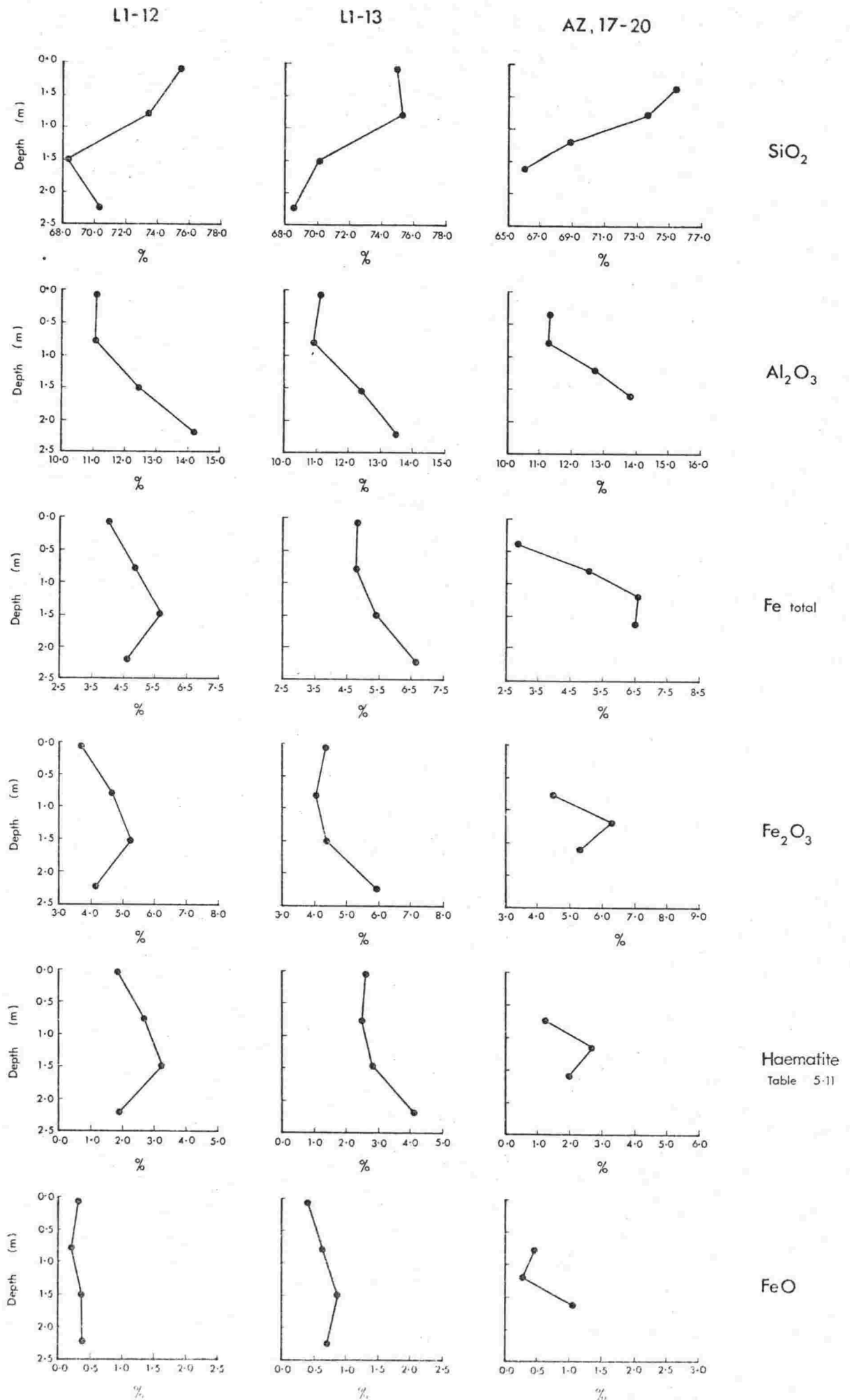
Fig. 6.7. Plots of the down profile major element variations from
Table 6.9.
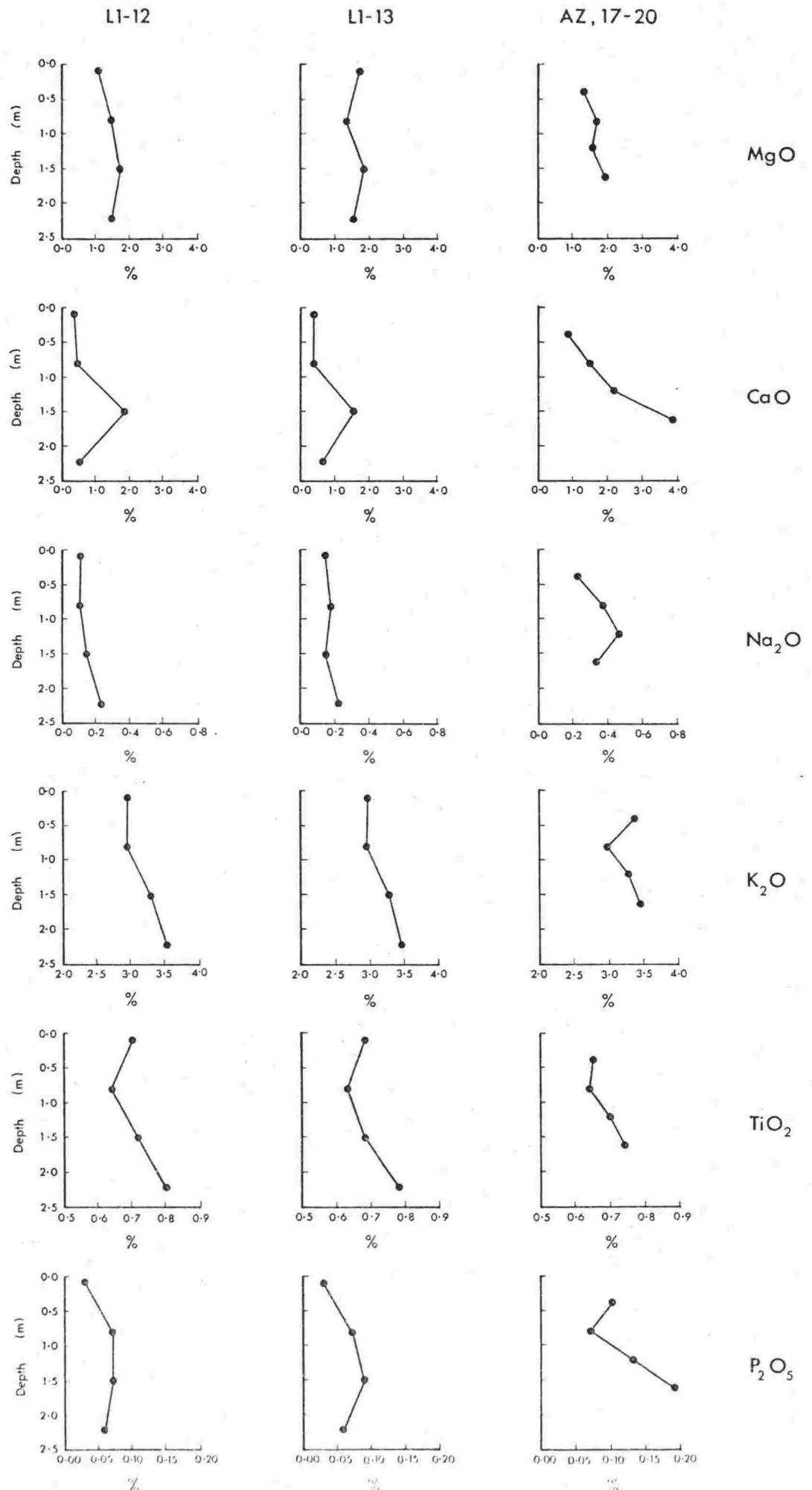
Fig. 6.7 cont.
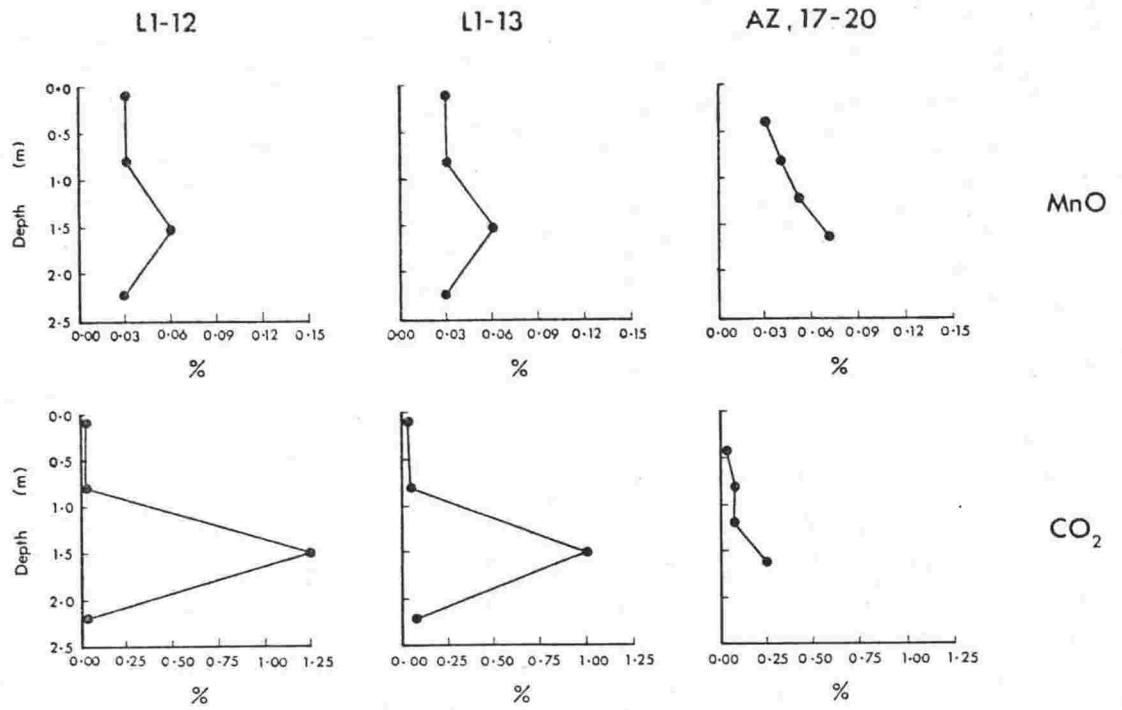
Fig. 6.7 cont.

IRON

Total iron displays variable trends within adjacent
profiles at L1, unit 17. However, all three profiles show an
increase in Fe with increasing depth in the profile, reaching
a maximum at 1.5 m in profile L1-12 and 1.2 m in profile AZ.
These variations are largely controlled by the changes in
ferric iron, specifically haematite.

The ferric iron in the Aztec Siltstone is largely as
haematite, with minor amounts as ferric silicates in the
illitic and chloritic clay minerals (see Chemistry of
Siltstones and Claystones, p.163). Thus the profile variations
in ferric iron are paralleled by those of haematite. Ferric
iron shows an overall increase in concentration from top to
bottom in the profile, and peaks at 1.5 m and 1.2 m in
profiles L1-12 and AZ respectively. This suggests that
haematite has been mobilized and has segregated at depth
in the profile, but the lack of a similar pattern of element
variation between profiles suggests that localized oxidation
and reduction may have affected the result.

The profile variations of FeO are small. There is no
agreement between profiles other than an overall increase in
FeO from top to bottom. This is probably due to downward
increases in the ferrous silicate containing illitic and
chloritic clay minerals.

MAGNESIUM

The profiles show little significant down-profile element
variation. Profiles L1-12 and AZ show slight downward increases
in MgO, and as MgO is contained in chloritic clay minerals
(Chemistry of Siltstones and Claystones, p. 163), the
increase may suggest a slight increase in chlorite concentration
with depth.

CALCIUM

CaO is largely contained as $CaCO_3$ in profiles Ll-12 and Ll-13, as shown by the correlation of the CaO and CO_2 variation diagrams (Fig. 6.7). Although there is excellent agreement between profiles Ll-12 and Ll-13, they both differ from profile AZ which contains calcium in other than a carbonate form (Table 5.7). The Ll profiles show no variation except for a CaO enrichment at 1.5 m, while the AZ profile displays a progressive increase in CaO with depth, possibly related to the illuviation of clays.

The element variations in the Ll profiles indicate that Ca has been mobilized and concentrated in a zone of enrichment at 1.5 m depth. This translocation of Ca to the lower portions of the profile has given rise to 'kankar' in the Ll profiles (see section descriptions, Askin *et al.* 1971, p.48, unit 17).

SODIUM

Na_2O increases slightly with depth in all profiles, and peaks at 1.2 m in profile Az. Sodium is contained in the form of analcime, albite and small amounts in the clays. The profile variations suggest a downward movement of sodium which might be expected in view of its relatively high mobility (Smyth, 1913; Tiller, 1958).

POTASSIUM

The K_2O profile variations are comparable with each other and with those of Al_2O_3. The initial decrease of K_2O is followed by successive increases with increased depth in the profile.

K_2O is entirely contained in illite in the fine-grained lithologies of the Aztec Siltstone, and therefore the comparability of the K_2O and Al_2O_3 profile variations is as expected. Illuviation of illite is suggested by both.

TITANIUM

The three profiles have variations in TiO_2 which are very similar, and are parallel to the Al_2O_3 and K_2O variations. This is as expected since titanium is largely contained in the clays (see Chemistry of Siltstones and Claystones, p.163). The downward increase in TiO_2 enhances the suggestion of clay illuviation, for if the increased clay of the lower horizons had been generated *in situ* then the TiO_2 value in this horizon would be expected to be lower than in the overlying horizons, because of the dilution effect of additional clay (c.f. the development of red-brown earth, Oertel, 1974).

PHOSPHORUS

The P_2O_5 variations of profiles L1-12 and L1-13 are similar but different from those of profile AZ. All profiles do, however, show a general trend toward increasing P_2O_5 with sample depth, although the increase is slight in the L1 samples and they peak at 1.5 m. The P_2O_5 variations do not compare well with any other element variations but bear some resemblance to the trends shown by K_2O. It maybe, therefore, that the P_2O_5 is taken up in the clays.

Phosphorus fixation in soils by ferric oxides, namely haematite, goethite and possibly maghaemite is widely established, and although there is not a linear correlation between haematite and P_2O_5, the high P_2O_5 samples tend to have high haematite contents. The converse is not true, as was found in other soil samples, by Taylor and Schwertmann (1974).

MANGANESE

The variation of MnO with sample depth is similar for all profiles. The variation trends are identical to those for CaO and CO_2, and show an enrichment at 1.5 m depth in the L1

profiles and a progressive increase with depth in the AZ profile.

Manganese exists in soils in two forms (Vinogradov, 1959 p.119), a mobile one in the form of Mn^{2+} compounds and an immobile form as Mn^{3+} or Mn^{4+}. At pH = 8 (the typical value for soils containing calcite, see Chapter 5, Grain Shape p.113) the mobile form hydrates.

$$Mn^{2+} + 2H_2O \rightleftharpoons Mn(OH)_2 + 2H^+$$
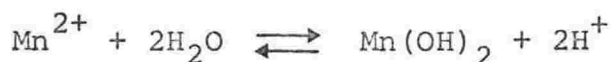
This hydrate is easily oxidised to manganic (Mn^{3+}) hydrate. Further oxidation leads to the formation of $MnO_2.nH_2O$ and finally to crystalline pyrolusite - MnO_2. Neither the Mn^{3+} compounds nor MnO_2 are soluble in soil solutions.

Hence, manganese precipitated in the alkaline, calcium carbonate rich horizons of the Aztec soil profiles. In the AZ profile, progressive precipitation took place with increasing $CaCO_3$ concentration.

These changes in MnO clearly indicate that diagenesis has not greatly altered the original Aztec soil chemistry.

CARBON DIOXIDE (carbonate)

The variations shown by CO_2 are parallel to those of CaO, and are due to variations in calcium carbonate content (see CaO p.177).

Summary

The chemistry of these unbedded Aztec fine-grained, fine-member profiles is consistent with and supports the supposition that they are ancient soils. Firstly, their element concentrations are similar to those found in the modern 'red or brown clay', 'red-brown earth', 'calcareous red earth' and 'red earth' soils of Australia (Table 6.10) (Stace *et al.* 1968)

which is consistent with a soils hypothesis. Secondly, the
Aztec profiles show very similar down-profile element variations
to those shown by many of the above mentioned Australian soils
(Table 6.10), which is supportive of a soils hypothesis.

Table 6.10. Major element analyses of the less than 2 mm
fraction of, (1) a typical Australian 'calcareous
red earth' soil, (2) a typical Australian 'brown
clay' soil. Both analyses are from Stace *et al.*
1968, Profile 24B p.255 and Profile 10I p.103
respectively.

| | 1 | | 2 | |
	a	b	a	b
SiO_2	80.79	69.69	82.73	69.06
Al_2O_3	9.75	15.69	8.69	18.37
Fe_2O_3	3.77	5.52	2.90	6.55
MgO	0.71	2.37	0.44	1.16
CaO	0.27	0.63	0.26	0.40
Na_2O	0.49	1.13	0.74	0.79
K_2O	1.44	2.17	1.65	2.16
TiO_2	0.58	0.65	0.81	0.92
P_2O_5	0.10	0.11	0.09	0.06
MnO	0.05	0.08	0.08	0.08

1a. Red clay loam, 20 cm from top of profile.
1b. Red clay, 50 cm from top of profile.
2a. Very dark grey-brown clay, 3 cm from top of profile.
2b. Very dark grey-brown clay, 20 cm from top of profile.

In the case of the modern Australian soils, and as postulated
for the Aztec profiles, these variations have resulted largely
from a reorganization of the soil plasma, especially clay
illuviation, translocation and deposition of carbonates, and
the mobilization and segregation of iron and manganese oxides
(Stace *et al.* 1968). A large proportion of the Australian soils
listed above probably developed under savanna climates (i.e.
warm and seasonally wet and dry), even though, in some cases

e.g. many of the 'calcareous red earth' and 'red earth' profiles, the present day climate is hot and semi-arid or arid. A savanna climate is suggested for the "soils" of the Aztec Siltstone.

None of the soil profiles examined in the Aztec Siltstone appear to have a complete A horizon. In most cases the upper surface of the profile has been eroded prior to deposition of the overlying coarse-member, channel sandstone, unit.

Isotope Analysis

CARBON AND OXYGEN ISOTOPE COMPOSITIONS

Introduction

Carbon and oxygen isotopic abundances in carbonate sedimentary rocks commonly enable a distinction to be made between those of a marine, and those of a continental non-marine depositional environment. Numerous analyses have shown (Clayton and Degens, 1959; Keith et al. 1964; Keith and Weber, 1964; Schmidt and Friedman, 1974; Dodd and Stanton, 1975) that in general, the δC^{13} and δO^{18} values for carbonates of a non-marine origin, are lower than contemporaneous marine counterparts. The carbon isotopic analyses are given as δC^{13}, in parts per thousand difference from standard where

$$\delta C^{13} = 1000 \left(\frac{C^{13}/C^{12} \text{ Sample} - C^{13}/C^{12} \text{ Std.}}{C^{13}/C^{12} \text{ Std.}} \right)$$

δO^{18} is expressed similarly in terms of O^{18}/O^{16} ratios. The Chicago PDB standard was used for the δC^{13} and the Standard Mean Ocean Water (SMOW) for δO^{18}.

A plot of carbon and oxygen isotopic compositions of carbonates from marine and fresh-water environments by Keith and Weber (1964) gave a separation better than 80 percent (Fig. 6.8).

Factors controlling carbon and oxygen isotopic compositions in carbonates (Keith and Weber, 1964) are as follows:

(1)   Isotopic composition of water, dissolved material and food web of the local environment of deposition,

(2)   Isotopic fractionation by carbonate-forming organisms during the precipitation of carbonate sediments,

(3)   Diagenetic and subsequent isotopic exchange.

Marine δC^{13} values are relatively consistent through geologic time and range from -3 to +3% (Keith and Weber, 1964). Non-marine δC^{13} values are more variable because the terrestrial environment is not as well buffered as the marine system, and subject to more local changes in the sources of carbon, chiefly atmospheric carbon, and C^{13}-deficient carbon from land plants and humus (Keith and Weber, 1964). Light carbon is added to ground waters and streams by way of dissolved carbon dioxide and bicarbonate produced by plant respiration and the oxidation of humus in soil.

Oxygen isotopic compositions of marine carbonates are highly variable, and show an irregular trend toward higher oxygen 18 content in progressively younger deposits (Keith and Weber, 1964;   Dontsova et al. 1972). The reasons given are post-depositional recrystallization and oxygen isotopic exchange with terrestrial waters (Clayton and Degens, 1959), or a change in δO^{18} of the oceans through geologic time (Keith and Weber, 1964). The latter case is favoured by recent evidence (Dontsova et al. 1972; Perry and Tan, 1972;   Schmidt and Friedman, 1975). Fresh-water carbonates of from Devonian to Tertiary age show an oscillatory variation in δO^{18} and have an overlap with marine δO^{18} values of Devonian age (Keith and Weber, 1964).

This study was undertaken to investigate, from carbon and oxygen isotope data, the depositional environment of the Aztec Siltstone and see how the conclusions compared with the wealth of previous evidence supporting a non-marine origin. The samples analysed included not only primary chemical precipitates (oolites and pisolites), but also kankar ('caliche') calcite

in the form of nodules, matrix calcite from fine-grained
sediments and calcite cement in sandstones (Table 6.11).

Table 6.11. Isotopic analyses of carbonates (calcite) from
the Aztec Siltstone. (Analyst I. M. Smolnicki,
N.Z. Institute of Nuclear Sciences, Gracefield).

Sample No.	Locality	Lithology	δC^{13}_{PDB}	δO^{18}_{SMOW}
23240A	Al	Nodule	-4.8	+11.5
23241	"	SdSt cement	-4.2	+10.2
23243	"	ClSt matrix	-3.8	+10.8
23245	"	Nodule	-5.2	+11.3
23246	"	SdSt cement	-6.1	+9.3
23279	Ml	SdSt cement	-6.4	+5.9
23306	Pl	Oolite	-8.6	+2.8
23307	"	Nodule	-6.1	+2.9
23310	"	Pisolite	-5.5	+2.8
23316	"	ClSt matrix	-6.4	+2.9
23422	Ll	ClSt matrix	+0.5	+9.9
23436	"	Nodule	-6.1	+12.7

Reference analyses: Te Kuiti Limestone and
Kaikoura Limestone.

SdSt = sandstone

ClSt = claystone

Analytical Procedures and Results

Samples were analysed by the procedures first described
by McCrea (1950), using 100 percent H_3PO_4 to liberate CO_2
from the carbonates. A kinetic fractionation factor of
1.01025 was used and Te Kuiti Limestone (Craig, 1957) served
as primary standard.

The total analytical error is within ±0.2 per ml for
both δC^{13} and δO^{18}.

All samples analysed give carbon and oxygen isotopic compositions well within the accepted field for non-marine carbonates (Fig. 6.8, Table 6.11). The mean δC^{13} value is -5.2‰ compared to -4.9‰ obtained for fresh-water limestones by Keith and Weber (1964), and all samples are within two standard deviations from their mean. The four forms of carbonate from the formation have δC^{13} values which are similar to each other. The nodules have a mean δC^{13} value of -5.6‰, comparing favourably with the δC^{13} values of present day Texan caliches, which range from -3.1 to -5.7‰ (Rightmire, in Valastro *et al.* 1968), with δC^{13} values for Lake Torrens (South Australia) paleosols and calcretes (pedogenic, illuvial carbonates) which range from -1 to -5‰ (Williams and Polach, 1971), and with δC^{13} values of caliche deposits discussed by Degens and Epstein (1964, p.37).
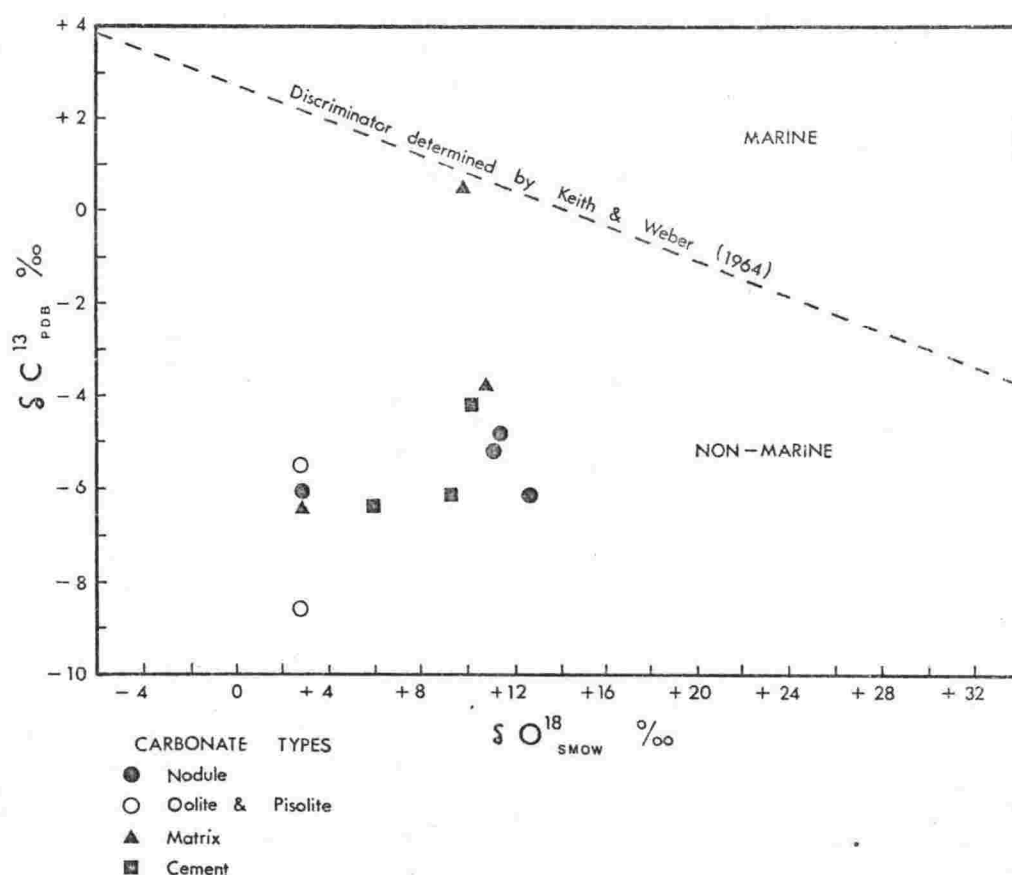
Fig. 6.8. Carbon and oxygen isotope compositions of carbonates (calcite) from the Aztec Siltstone.

The relatively low δC^{13} of the oolite sample is consistent
with its lacustrinal origin, in that light carbon is derived
directly from organic constituents during decomposition (Keith
and Weber, 1964) and the lacustrinal sediments of the Aztec
formation are the only ones to contain appreciable free carbon.
The pisolite, although considered to be of lacustrinal origin,
has a near 'normal' fresh-water δC^{13} value.

One of the samples analysed (one of three matrix carbonate
samples) had a much higher δC^{13} value than the rest, though
it still fell in the non-marine field of Figure 6.8. No
explanation can be given, though it may be significant that it
is the only one of the analysed samples to contain free carbon.

The mean δO^{18} value is +7.8‰ compared with +20.6‰
obtained for fresh-water (Devonian) limestone, and +22.3‰ for
marine (Devonian) limestone (Keith and Weber, 1964). Only one
of the twelve samples lies within two standard deviations of
the fresh-water mean given by Keith and Weber, with the other
11 samples giving values lighter than +12.3‰ . Although the
Devonian fresh-water limestone δO^{18} value of Keith and Weber
(1964) is based upon only four samples, the values are
reasonably consistent both internally, and with the oscillatory
trend shown by younger fresh-water limestone δO^{18} values, and
are therefore considered as reasonably reliable. The possible
reasons for the relatively low O^{18}/O^{16} ratios of the Aztec
samples are many.

(1) Enrichment of surface waters (with which the carbonates
are assumed to be in oxygen isotope equilibrium) in O^{16}. This
may have occurred through a number of processes. O^{18} depleted
precipitation, which results in O^{18} depleted surface water, is
characteristic of high latitude and cold climate regions, as a
product of successive O^{18}/O^{16} fractionations and relatively
low evaporation. However, the Aztec δO^{18} values are so low
as to be comparable with only polar snow, ice and meltwater
(Rankama, 1963 p.276). Contemporaneous polar influences are
considered highly improbable, especially in view of the many
sedimentary features of the Aztec Siltstone suggesting warm

temperatures and high evaporation e.g. kankar ('caliche'),
mudcracks, vein networks, red beds containing syngenetic analcime
and some gypsum lenses (Chapters 4 and 5).

(2)   Post-depositional contamination by carbonate from neigh-
bouring Jurassic dolerite sills and dykes was a possibility.
The vein calcite from these dolerites has a similar low δO^{18}
value to the Aztec samples analysed (a calcite vein in a dolerite
sill at Mount Metschel has a δO^{18} value of +7.2‰) and could
therefore have been responsible for the ratios if it were the
dominant contributor. However, the carbonates of at least
two Aztec samples (the oolite and the pisolite) clearly
precipitated at the time of deposition (Devonian). It is
concluded that contamination by carbonate from the dolerites
does not explain the low ratio.

(3)   The effect of raised temperature is a mechanism for
releasing the heavy isotope from carbonates (Tan and Hudson,
1971; Dontsova, 1972). However, Tan and Hudson showed that
oxygen isotope exchange in limestone due to intrusive heating
took place only in samples which had been excessively heated
due to their very close proximity to the intrusive body. They
showed that only samples within 1 m of a 3 m thick dyke were
effected, which is equivalent to those samples which had been
raised to temperatures greater than approximately $400^{\circ}C$ (using
the equations of Jaeger, 1957 and 1959, for the temperature in
the neighbourhood of a cooling igneous sheet). Although some
metamorphism of the Aztec Siltstone has resulted from Jurassic
intrusion, the temperature of the sediments on a regional basis,
was probably not significantly greater than approximately $200^{\circ}C$
according to the metamorphic mineral assemblage (Chapter 5).
However, it is noteworthy that the samples lying at closest
proximity to dolerite sills and·dykes do have the lowest δO^{18}
values, i.e. the samples from P1 and M1 (Table 6.11).

(4)   Tan and Hudson (1971) noted that exchange of calcareous
limestone with groundwater of convective systems heated by
distant intrusive centres, lowered the δO^{18} value of calcite by
4 to 7‰. Such an oxygen isotopic exchange may have been at
least partially responsible for the low δO^{18} values of the
Aztec Siltstone samples.

(5) It is possible that contamination of the Aztec carbonates by O^{16} enriched glacial meltwater bought about the low δO^{18} values. Continental glaciation followed the Aztec deposition in Carboniferous (?) times, as shown by the Metschel Tillite which disconformably overlies the Aztec Siltstone. Isotopically light meltwater from the retreating glaciers may have diffused through the underlying Aztec Siltstone and isotopically exchanged with the Aztec carbonate. However, almost complete isotopic exchange would be required to explain the very low δO^{18} values of the Aztec carbonates, which is at least the case of the primary precipitates (the oolite and the pisolite), is very improbable.

Conclusions

The carbon and oxygen isotopic compositions for the carbonates of the Aztec Siltstone strongly indicate a non-marine environment of deposition for the sequence, in agreement with the many other palaeoenvironmental indicators. The δC^{13} values also compare with the range found for modern pedogenic illuvial carbonates, but there is no clear evidence that soil processes changed the isotopic composition of the carbonate.

The δO^{18} values are much lower than expected for non-marine carbonates, but may have been influenced by thermal metamorphism induced by the Jurassic dolerite and by mixing with heated convective groundwaters generated by the dolerite intrusion. The highly variable nature of δO^{18} especially between similar carbonates of varying ages (Keith and Weber, 1964), and its greater susceptibility to isotopic exchange, makes it, on its own, an unreliable isotopic indicator of palaeoenvironmental conditions. Particular caution must be taken in using δO^{18} as a palaeosalinity indicator for carbonates of Devonian age, because not only do the isotopic values of marine and non-marine samples show some overlap (Keith and Weber, 1964), but so few non-marine carbonates have been analysed.

STRONTIUM ISOTOPE COMPOSITIONS

The isotopic compositions of strontium in carbonates from a nodule, a limestone lense and a fish plate from the Aztec Siltstone were analysed by Faure and Barrett (1973). The Sr^{87}/Sr^{86} ratio of the carbonates was found to be significantly higher than in marine deposits of the same age. The difference was attributed, by Faure and Barrett, to the non-marine origin of the Aztec samples. Other supposedly non-marine rocks from the Beacon Supergroup also showed similar high Sr^{87}/Sr^{86} ratios relative to their marine equivalents.

Sr^{87}/Sr^{86} ratios in carbonates may also be related to the present day age of a provenance, as shown by Faure and Barrett (1973).

$$t \simeq A + \frac{X - X_o}{(Rb/Sr)k\lambda}$$

where

t = age of the provenance relative to the Present

A = age of the fresh-water carbonate

X = Sr^{87}/Sr^{86} ratio of the provenance

X_o = assumed initial Sr^{87}/Sr^{86} ratio of the provenance

Rb/Sr = ratio of concentrations of these elements in the rocks of the provenance

k = defined by the relationship $Rb^{87}/Sr^{86} = (Rb/Sr)k$

λ = decay constant of Rb^{87} ($= 1.39 \times 10^{-11}$ y^{-1})

By applying the average Sr^{87}/Sr^{86} ratio for the Aztec carbonates, and the most probable range of Rb/Sr ratios for the Aztec provenance, an age for the source material of the Aztec Siltstone was calculated to be from 2.7 to 3.45×10^9 years. Ages in this range are common for the igneous and metamorphic basement rocks exposed along the coast of East Antarctica. It is probable, therefore, that the provenance of the Aztec Siltstone was the East Antarctic Shield.

CHAPTER 7

SEDIMENTARY FACIES AND PROVENANCE

Fining-upwards Sequences

The Markovian chain analysis of the Aztec Siltstone
strongly demonstrated the presence of a cyclic 'fining-upwards'
sequence within the formation as a whole (Chapter 3, p.33).
The concept of 'fining-upwards' cycles was first proposed by
Dixon (1921), and has since been studied and described in
great detail for the Devonian Old Red Sandstone facies of
Europe and Great Britain (Allen, 1962a, 1962b, 1963b, 1964a,
1965b, 1965c, 1970, 1974b; Friend, 1965; Moody-Stuart, 1966;
Leeder, 1973b), and for the Devonian Catskill facies of North
America (Allen and Friend, 1968). The studies have shown that
a fluviatile model of sedimentation, and more especially a
meandering stream model, best explains the observed cycles.
Studies of modern analogues support the hypothesis (Allen,
1965a; Visher, 1965a, 1965b; Moody-Stuart, 1966; Leeder,
1973a).

DESCRIPTION

The Aztec Siltstone 'fining-upwards' cycles as shown by
the Markov analysis for the entire formation (Fig. 3.14,
Table 3.3), are best demonstrated in the Lashly Mountain
section L2, units 10 to 21 (Figs 2.1 and 7.1),where there are
four cycles averaging 9 m total thickness and consisting of 60%
of sandstone to 40% of siltstone and claystone. A cycle
typically begins with a scoured surface cut into an underlying
siltstone forming the upper member of the underlying cycle
(Fig. 7.2). The scoured surface is commonly covered by a layer
of intraformational conglomerate, an accumulation of siltstone
clasts eroded from the underlying unit (Fig. 3.9).

INTERPRETATION

DESCRIPTION

	CYCLE 4		CYCLE 3		CYCLE 2		CYCLE 1	
	FINE MEMBER	COARSE MEMBER	FINE MEMBER	COARSE MEMBER	FINE MEMB	FINE MEMBER	COARSE MEMBER	COARSE MEMBER

INTERPRETATION

Base of next cycle.

Vertical accretion of suspended load from overbank floods. Floodbasin deposit with fluctuating watertable and prolonged exposure of upper deposit.

Channel deposit, probably a result of lateral accretion on a point bar. Decreasing bed shear stress. Siltstone clasts form lag concentrate in channel deeps and in the lower scour surface.

Erosion by migrating channel.

Vertical accretion of suspended load from overbank floods. Floodbasin deposit with little exposure.

Channel deposit probably a result of lateral accretion on a point bar. Possible levee deposits included. Strong variable currents. Siltstone clasts form lag concentrate in channel deeps.

Vertical accretion of suspended load from overbank floods. Probably a floodbasin deposit produced at less than ripple powers. Calcareous nodules suggest exposure and soil development.

Vertical accretion deposit from overbank floods. Probably a levee deposit. Exposure led to soil development and establishment of vegetation.

Channel deposit largely by lateral accretion on a point bar. Strong variation in current flow rate.

Erosion by migrating channel.

Vertical accretion of suspended load during overbank floods on the floodbasin, and including intercalation of levee material. Subaerial exposure with subsequent drying and deep cracking.

Vertical accretion of suspended load during overbank floods. Probably a levee deposit.

Channel deposit, probably a result of lateral accretion on a point bar. Strong variation in current flow rate. Siltstone clasts form a lag concentrate.

Erosion by migrating channel.

Top of previous cycle.

DESCRIPTION

Claystone, greyish red (10R 4/2). Some mottling. Vein networks throughout.

Claystone, grey to olive grey (5Y 5/2). Finely laminated and unbedded, papery to shaly.

Sandstone, fine to medium, laminated to very thin bedded, massive. Intraformational conglomerate throughout. Mainly trough cross-bedded, but finer and ripple-laminated in upper metre.

Siltstone, greenish grey (5GY 6/1). Some claystones. Ripple-laminated at intervals. Burrows.

Sandstone, fine, laminated, blocky to massive. Trough cross-bedding, parallel and ripple laminae. Intraformational conglomerates at 3.0 and 4.3 m. Trace fossil tracks at many levels. Several siltstone bands.

Siltstone, greenish grey (5GY 6/1), unbedded, massive.

Siltstone, greyish red (10R 4/2) with nodules and some grey mottles.

Sandstone, very fine, and siltstone, with burrows and roots.

Sandstone, fine, laminated, blocky to massive. Trough cross-bedding, parallel and ripple laminae.

Siltstone, greenish grey (5GY 6/1) and some very fine sandstone. Thin and thick bedded. Burrows, mudcracks and vein networks.

Sandstone, very fine, and ripple laminated.

Sandstone, fine, laminated, blocky to massive. Trough cross-bedding, parallel and ripple laminae. Siltstone laminae and lenses in lower 2 m. Intraformational conglomerates at 6.8 m.

LEGEND

Trough cross-stratified fine to medium sandstone

Ripple laminated fine to medium sandstone

Ripple laminated very fine to fine sandstone

Siltstone or claystone

Parallel laminated fine to medium sandstone

Scoured surface

Intraformational conglomerate

Red siltstone

B — Burrows
C — Conchostracans
F — Fish
M — Mudcracks
N — Calcareous nodules (kankar)
R — Roots
T — Trace fossils
V — Vein networks

Metres
6
5
4
3
2
1
0

Fig. 7.1. Description, diagrammatic representation, and interpretation, of the sedimentary sequence at L2, units 10 to 21.

Fig. 7.2. The contact between a massive, red (partially reduced), fine-grained, fine member unit (L2, unit 9) and a coarse member channel sandstone of the overlying cycle. A scoured surface separates the two. (see also Fig. 7.1).

Fig. 7.3. Trough cross-bedding passing upwards into ripple laminated bedding, in a fine grained channel sandstone, L2, unit 10. This is the coarse member unit of cycle 1, Fig. 7.1. Scale in cm.

A basal sandstone then follows, and is commonly fine to
medium grained, fining upwards to a fine or very fine sandstone
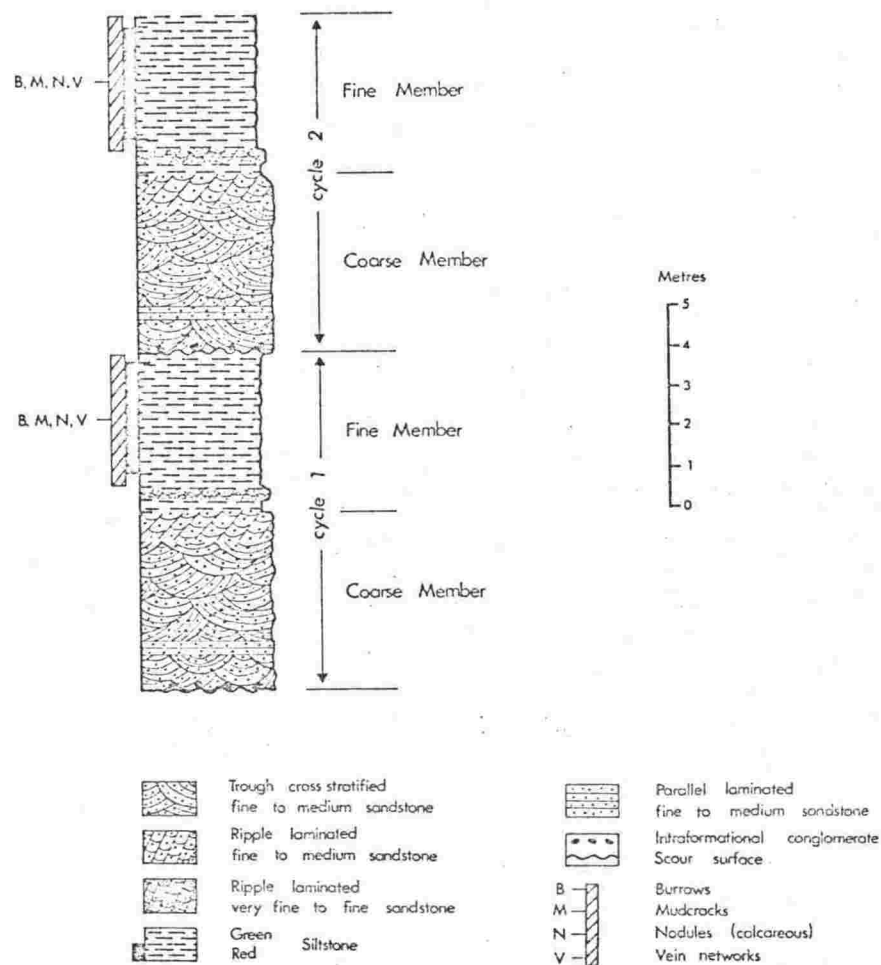
Fig. 7.4. The 'ideal' fining-upwards cycle for the Aztec Siltstone, based upon Markovian analysis, occurrence of sedimentary structures, and palaeochannel characteristics.

1965a). Siltstone clasts, as eroded products commonly lie across this erosion surface or are reworked into the swales and troughs (Chapter 3, Conglomerates). In some cases the clasts are present throughout the coarse member, attesting to continuous corrasion of the local banks of underlying fine member. Imbrication of clasts was also observed. They are interpreted as a lag deposit, similar to that seen in the scour pools of modern stream channels (Arnborg, 1957; Lattman, 1960).
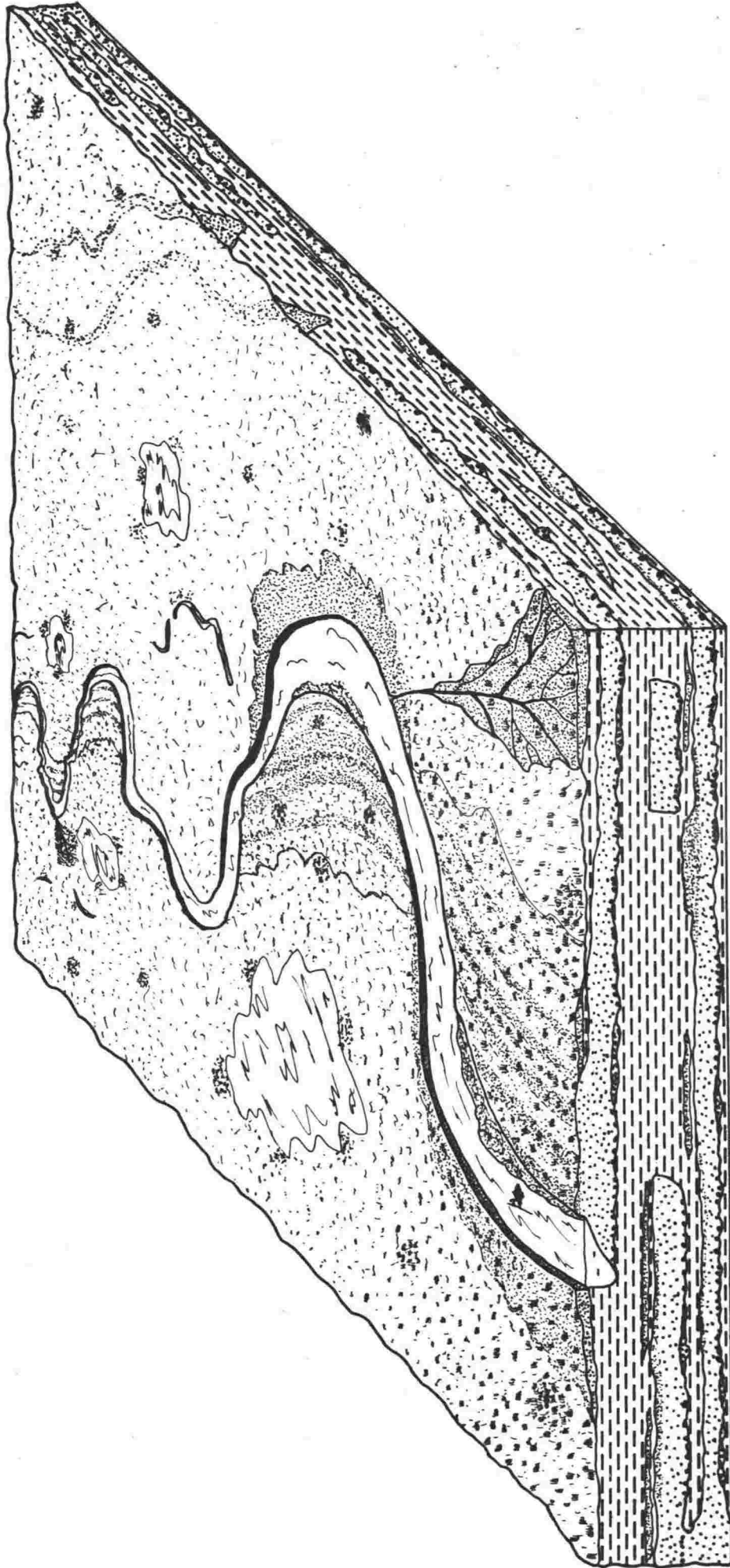
Fig. 7.5. A block diagram illustrating the genetic relationship of the various lithologies of the Aztec floodplain. The fining-upwards cycles have been generated by the meandering river migrating backwards and forwards across the slowly subsiding floodplain, depositing point-bar channel sands overlain by overbank fines in its wake.

The coarse member typifies a channel deposit resulting most probably from the lateral accretion of bed load material on a point bar of a high sinuosity channel (Fisk, 1944; Sundborg, 1956; Allen, 1970). The bedform types and the grain size show a systematic upward change in response to a declining bed shear stress from point bar toe to point bar top (Allen, 1970). The lateral meander of the stream channel causes the point bar deposit to successively overlie the former positions of the channel talweg, now recorded by the scoured surface.

The erosive power of the stream suggests high flow intensities, and this is confirmed by the presence of flat-bedded sandstone, in some cases showing parting lineations on the upper surfaces (Allen, 1964a, 1964b). The large-scale trough cross-bedding denotes a high intensity, lower flow regime state (Allen, 1964a; Harms and Fahnestock, 1965), also suggestive of flood-stage conditions on the floodplain.

Siltstone and claystone laminae and lenses are occasionally present in the coarse member, and suggest a local settling out of fines from suspension in ponded or slow moving waters.

Ripple-laminated very fine or fine sandstones occur in the upper-most portion of some coarse members. They characterise low intensity flow conditions in the lower flow regime (Allen, 1964a; Harms and Fahnestock, 1965).

Although a large proportion of the coarse members of the 'fining-upwards' cycles of the Aztec Siltstone are considered to have accumulated largely by lateral accretion on point bars, only one case was observed of direct evidence for lateral deposition. This came from a single example of large scale cross-bedding, in the Alligator Peak section (A1) unit 2, (Fig. 7.6). The cross-bedded set averaged 1.7 m thickness, and was exposed laterally for 23 m. The inclined strata had a maximum 'forset' dip of approximately 6 to 8 degrees. The upper and lower surfaces of the cross-stratal set were scoured and planar, and both contained reworked siltstone clasts and disarticulated fish plates in a medium grained sandstone lithology (Fig. 7.7). The individual strata show a fining-upwards from a fine sandstone to a fine siltstone or claystone.

Fig. 7.6. Large scale epsilon-cross-stratification (Allen, 1963a,
           1965b) in section A1, unit 2. This is an example of lateral
           accretion by point bar growth. Note the man for scale.
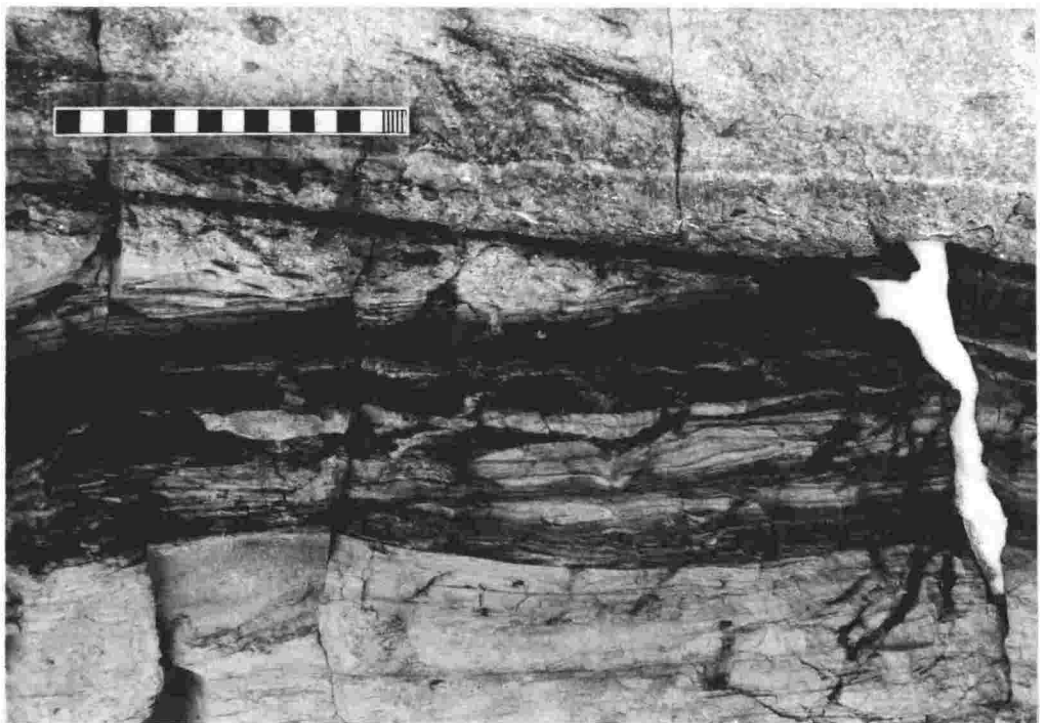
Fig. 7.7. The erosion or scoured surface forms the upper boundary of the
           large scale, epsilon-cross-bedded sets at A1, unit 2. Intra-
           formational conglomerate overlying the erosion surface includes
           disarticulated fish fossil remains. Scale in cm.

These large scale cross sets are examples of the epsilon-cross-stratification of Allen (1963a, 1965b), although the true sigmoidal shape of the individual cross-strata was not seen. This type of stratification is considered to be the most obvious indicator of lateral deposition from high sinuosity streams (Moody-Stuart, 1966; Allen, 1965b, 1970). Deposition took place on successive point bars as the stream channel laterally migrated; the grain size variation of the stratum reflecting the changing flow regime of the stream. The epsilon cross-strata should thus have a cross-stratal strike parallel to the current flow. For the Alligator Peak example, the strike is to the northeast, which is the mean direction of paleocurrent flow (Barrett and Kohn, 1975; see also p.225).

The reason for the general scarcity of observed epsilon-cross-stratification in the Aztec Siltstone, is considered to be a product of:

(1) The scarcity of outcrops striking at a high angle to component beds.

(2) The difficulty of recognition because of the low angle cross-stratal dip of the constituent beds (Allen, 1965b, p.172, 1966, 1970).

The siltstones and claystones of the fine member units of the 'fining-upwards' cycles, have a grain size and bed-form which suggests deposition by vertical accretion from a suspension, on the floodbasin, backswamp, or interchannel areas of the floodplain, during floods. They compare well with modern analogues described by Fisk (1944, 1947), Lorens and Thronson (1955), Allen (1965a), Coleman (1969), and Alexander and Prior (1971). Intercalations of thin, fine grained, horizontally stratified sandstone beds (Figs 7.1, 7.4, 7.5, 7.8) occur infrequently within the fine member units, and probably resulted from levee or crevasse-splay deposition (Fisk, 1944, 1947; Lorens and Thronson, 1955; Allen, 1964, 1965a, 1965b) during flood stage. They are most common in the first deposited overbank fines, close by the stream channel. They are recorded in the 'ideal cycle', determined for the Aztec Siltstone from

the Markov analysis (Chapter 3, p. 33 , Fig. 3.14, Table 3.3;
Fig. 7.4), as very fine to fine sandstone interbeds.
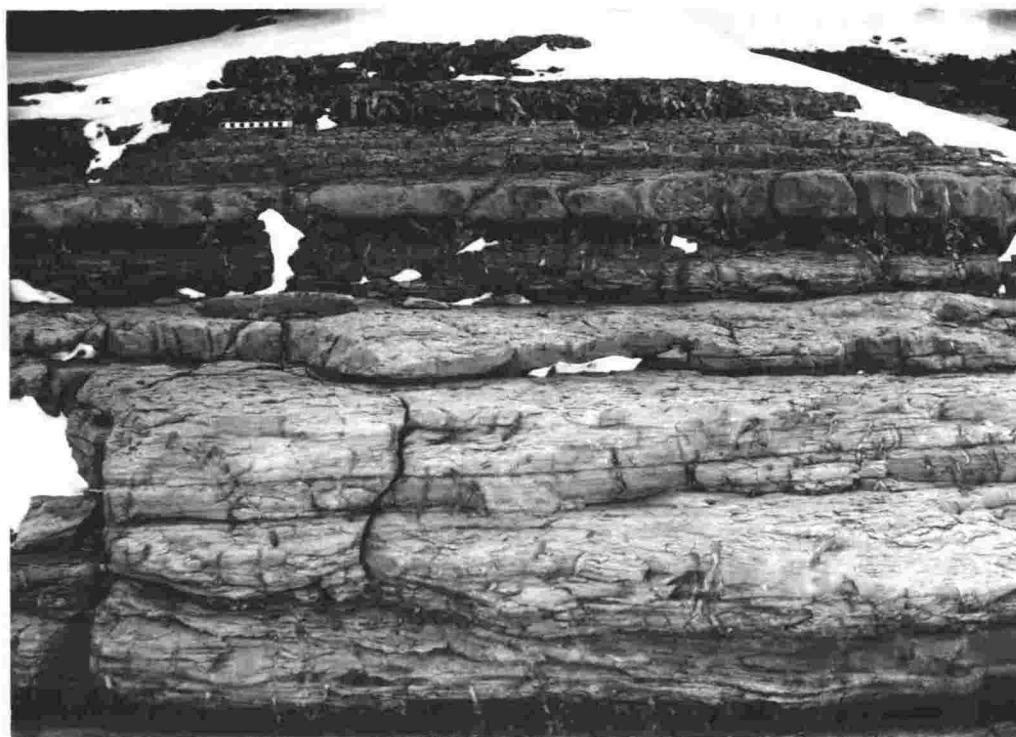
Fig. 7.8. Siltstone and very fine sandstone interbeds, interpreted
as levee and crevasse-splay deposits, at the top of the
coarse member and the base of the fine member of cycle
1, Fig. 7.1 (L2, units 11 and 12). The units have been
extensively bioturbated. Scale in cm.

At times other than during floods, the floodbasin deposits
would have been subaerially exposed. This is evidenced by the
presence in these deposits, of mudcracks, vein networks, burrows,
pedogenic calcareous nodules (kankar), roots, and in places plant
fragments (see Chapter 4 for detailed description). Where the
sediment had an appreciable relief (on alluvial ridges and
terraces etc), where the drainage was good (probably aided by
underlying permeable coarse member sandstones), and where the
ground-water table was low, the deposits were oxidized (as
exemplified by the red beds, Chapter 9) and soil development
took place (Chapters 4, 5, 6 and Conclusions). The kankar

('caliche') suggest that the period of subaerial exposure and
soil development which followed the deposition of the fine-
member of the fining-upwards alluvial cycles was extensive,
probably from 5,000 to 50,000 years (Chapter 4 p.81). Some
aeolian sedimentation (cf. loess) probably contributed to the
fine-grained, fine member deposits during the extended hiatus,
however, there is no direct evidence to substantiate the
suggestion.

It has been suggested that the regularity and prolonged
nature of these non-depositional periods in alluvial cycles is
indicative of ephemeral and thus allocyclic sedimentation, rather
than autocyclic sedimentation generated by the to-and-fro
migration of a channel-system across its floodplain (Steel,
1974b). However, the reduced nature of the channel sandstones
of the Aztec, suggests that they remained at or below the water
table (Chapter 9, p.251) and therefore could not have been
ephemeral. Allen (1974c) demonstrated, there are numerous
factors, including both allocyclic and autocyclic factors, that
can generate pedogenic carbonate bearing fining-upwards alluvial
sequences.

Some of the floodbasin sediments would not have had
sufficient relief to have been subaerially exposed for any
great period. Those sediments in the low lying areas of the
floodbasin e.g. the backswamp region, would for the most part
have been at or below the ground-water table, and with their
impaired drainage would have favoured the preservation of
included organic debris, thus generating a reducing environment.

Fluctuations in the ground-water table, possibly of a
seasonal climatic influence, are reflected in the mottled and
gleyed pattern of oxidation and reduction that is common in
the fine-member overbank sediments e.g. Fig. 7.1, and section
Al, unit 20, Fig. 7.9.

The 'ideal cycle' for the Aztec Siltstone (Chapter 3,
Fig. 3.14; Fig. 7.4) has a significant fine member colour
scheme. The very fine to fine sandstone levee or crevasse
splay interbeds are overlain by a green siltstone which in turn
is overlain by a red siltstone then a return to a green siltstone
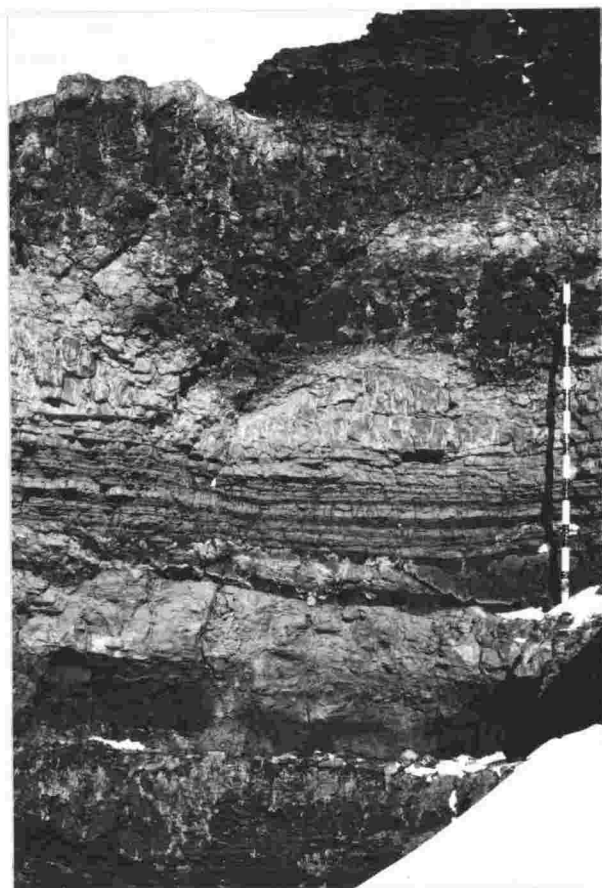
Fig. 7.9. Mottled and gleyed pattern of oxidation and reduction induced by a fluctuating ground-water table and reduction solutions migrating along more permeable horizons. Section A1, units 15-22. Staff is in dm.

at the top of the cycle. The initial deposited overbank sediment remained in a reduced state probably because of its low relief and therefore close proximity to the water-table and the reducing influence of the channel region itself. Plants probably grew in greatest abundance in the immediate vicinity of the channel area, and thereby enriched the channel sediments in carbonaceous debris which in turn effected a reducing environment to these sediments. As the water-table dropped, and drainage of the overbank sediments improved (the latter aided by more permeable underlying coarse member units), the oxidation necessary for the development and preservation of red beds was able to take place. However, when the meandering channel again crossed the oxidized overbank deposit, it reduced an upper layer of red siltstone as the reducing solutions percolated downward from the channel sands. Red siltstones overlain by sandstones, almost without exception, exemplify this with an upper thin (generally less than 0.4 m), green,

reduction layer in contact with the sandstone (Fig. 4.26).

Some of the thick (greater than 4 m) vertically accreted deposits of the Aztec Siltstone may have been produced in a situation where the main stream channel remained at a distance from the backswamp area for a long period, probably becoming entrenched below its former floodplain, and where gradual subsidence kept up with the steady overbank deposition. Thick units of fine member lithologies would also originate in a situation where a backswamp was being fed with sediment from more than one stream, i.e. at the site of interchannel flood-basins.

The repetitive fining-upwards sequence is thought to have been generated by the to-and-fro lateral migration of the stream across the alluvial plain. Sudden stream displacement or avulsion by the crevassing of levees during exceptionally high floods commonly occurred, thus producing a vertical profile that often deviates from the 'ideal' fining-upwards cycle. Avulsion also produced the discrete or isolated sandstone units that are found throughout the formation.

PALAEOCHANNEL CHARACTERISTICS

A large proportion of the Aztec Siltstone can be attributed to deposition from high sinuosity meandering streams as exemplified by the fining-upwards sequences, even although these sequences are not always obvious at the outcrop or from the section descriptions. They are best recognized by Markovian Chain analysis (Chapter 3, p. 33). An analysis of the formation shows 18 complete fining-upwards sequences in the sections of A1, A2, A4, M1, P1, L1, L2, and S9 (Appendix Table 3). Only those sequences defined by a lower scour surface were used. Many others are present, but were not used in the analysis as the scoured surface was not recorded, either because it was covered by snow or scree, or the section was not described in sufficient detail.

The mean thickness of the 18 sequences is 8.2 m, with a mean coarse member thickness of 4.3 m, and a mean fine member thickness of 3.9 m. The thickness variations of the members are displayed in Figure 7.10.
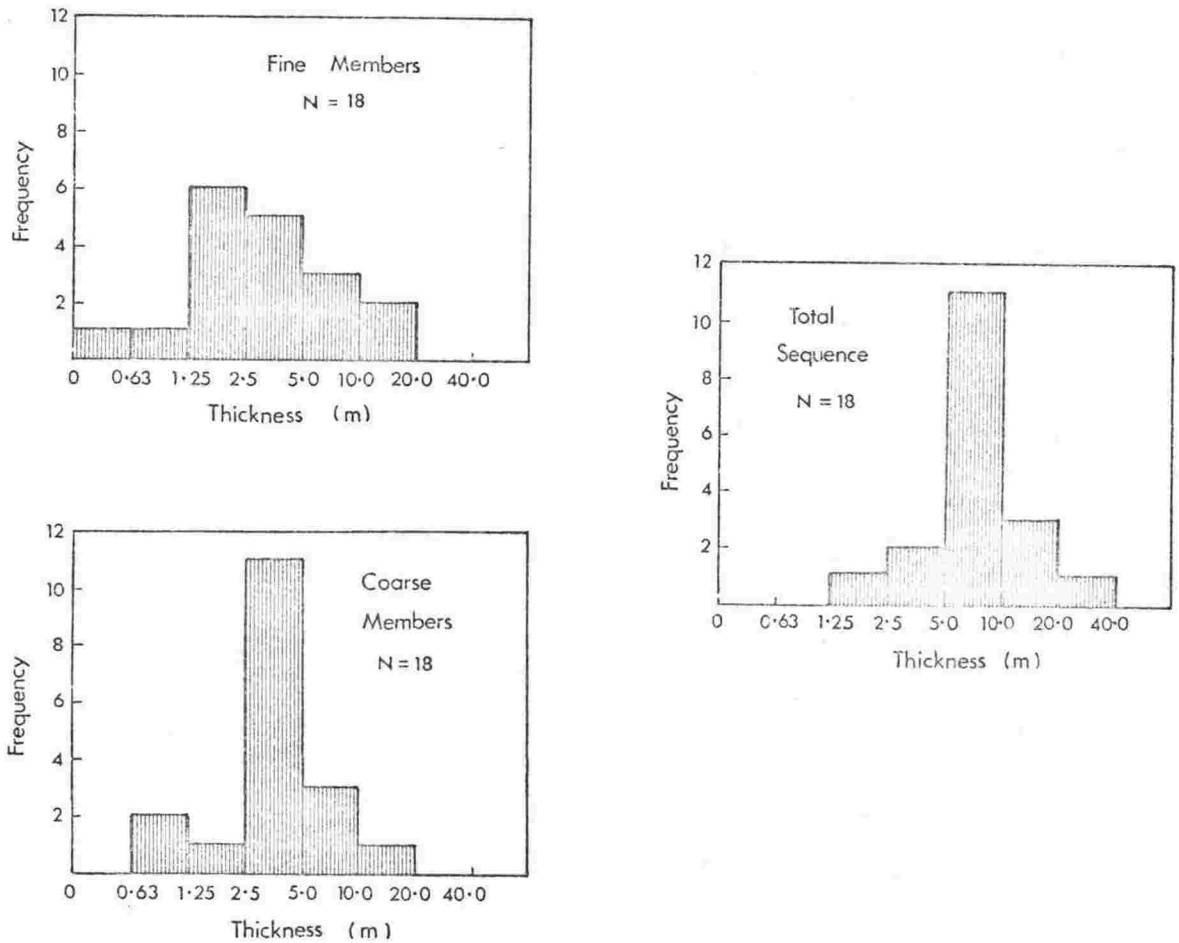
Fig. 7.10. Thickness variations of the members of fining-upwards sequences in the Aztec Siltstone, from sections A4, A1, A2, M1, P1, L1, L2, S9. Data in Appendix Table 3.

By comparison with modern point bars, it has been shown by Leeder (1973a), that there is a reliable correlation between bankfull width (w) and bankfull depth (h) for modern meandering rivers.

$$\log w = 1.54 \log h + 0.83$$

or $\quad w = 6.8 \; h^{1.54}$

where $\quad w$ = bankfull width

h = bankfull depth

$r = 0.91$

$\sigma = 0.35$ log units

The equation can be applied to palaeochannels that deposited alluvial 'fining-upwards' sequences for the Aztec Siltstone. The maximum channel depth (h) is taken as being equal to the coarse member thickness, assuming deposition from a single channel. Thus:

Maximum channel depth (h) $\quad = \quad$ 4.3 m

Then, the average channel

width $\quad w \quad = \quad 6.8 \; (4.3)^{1.54}$m

$= 64.3$ m.

Using the 95% confidence limits for the regression line (Leeder, 1973a) it can be said that, on the average, the sandstone members of the Aztec Siltstone were formed in sinuous channels not more than 320 m wide and not less than 13 m wide. These values are based on a maximum channel depth for bankfull width (Leeder, 1973a) because the epsilon-cross-stratification which establishes deposition from a single channel is lacking. In some cases it enables the direct measurement of bankfull width to be made. A more realistic estimate can be made for the sandstone member in the Alligator Peak section (Al unit 2, described earlier in this chapter) which displays epsilon-cross-stratification.

Maximum channel depth (h) $=$ 1.7 m

Thus, channel width $\quad w \quad = \quad 6.8 \; (1.7)^{1.54}$ m

$= 15.4$ m

Applying the 95% confidence limits shows that the sandstone was deposited from a sinuous stream channel not more than 77 m wide, and not less than 3 m wide.

When the width and the depth of the palaeochannel is determined, they can then be used in conjunction with Schumm's (1972 p. 1092) equation, to estimate the sinuosity of the depositing river.

$$\text{Sinuosity } P = \frac{3.5w}{h}^{-0.27}$$

Therefore

Sinuosity, $(P_{max.})$ = 3.0
and $\qquad P_{min.}$ = 1.3
the mean sinuosity = 1.95

This represents streams ranging from 'tortuous' to 'transitional' (Schumm, 1963), with a mean as 'tortuous'.

Leopold and Wolman (1960, p.771-774) give an equation relating bankfull width to free meander wavelength (Lm).

$$Lm - 10.9 \, w^{1.01} \qquad \sigma = 0.3 \text{ log units, determined by Leeder (1973a).}$$

For the Aztec Siltstone, using the mean bankfull width. (w) as determined from the epsilon-cross-stratification (A1, unit 2) then,

$$Lm_{(mean)} = 172 \text{ m.}$$

Non-'Fining-upwards' Sequences

COARSE MEMBER DOMINATED SEQUENCES

Many of the thick (greater than 5 m) sandstone units of the Aztec Siltstone are composed of a vertical succession of coarse member units completely lacking in fine member units. Such a sequence of laterally accreted point bar deposits, would suggest a repeated sequence of channel abandonment followed by subsidence without deposition, then a return of

the stream meander belt.   Any fines deposited on top of the
point bar appear to have been removed on the return of the
stream, by the erosive or scour phase which characterizes the
base of the channel sandstone.   Remnants of fine-member units
are commonly preserved within these multistorey sandstone
bodies as intraformational conglomerate (Fig. 7.11).   It is
most likely that the stream channel never migrated far from
the present site of the section, i.e. it kept reoccupying
former channel positions.   Such sandstones may represent a
whole channel belt rather than the passage of an individual
channel (Allen and Friend, 1968 p.54).

Fig. 7.11.   Intraformational conglomerate, consisting of siltstone and
claystone clasts from locally eroded fine member units,
mark the former channel base in a repeating or multistorey,
channel sandstone body. Location, AZ-18, 30 m from base
of Aztec Siltstone. Scale in cm.

In the basal portions of sections at Mount Ritchie (A4, units 7 to 33), and Beacon Heights (B2, units 3 to 5) are thick (up to 52 m), multistorey sandstone bodies. They do not show the typical characteristics of 'fining-upwards' sequences, but have many of the features characteristic of low sinuosity, braided channel complexes (Schumm, 1960, 1963, 1968; Doeglas, 1962; Allen, 1965a; Moody-Stuart, 1966; Williams and Rust, 1969; Smith, 1970, 1971). Some of these features are:

(1) Multistorey sandstone bodies frequently divided by scoured surfaces with intraformational conglomerates.

(2) Absence of epsilon-cross-stratification.

(3) Absence or a very low proportion of the finer deposits, i.e. siltstones or claystones.

(4) A low variability in palaeocurrent direction. (A standard deviation on 6 sets in the basal section of A4 of 25° compared with the 73° variation for the whole formation).

Both of the thick multistorey sandstones occupy the basal parts of the sections, and show a strong bedform resemblance to the conformable underlying Beacon Heights Orthoquartzite. As the Beacon Heights Orthoquartzite is considered to have been deposited from low sinuosity, braided streams (Barrett and Kohn, 1975), it is suggested that in the sections of Mount Ritchie (A4), and Beacon Heights (B2), the high sinuosity meandering streams characteristic of the Aztec Siltstone, were slower in developing.

FINE MEMBER DOMINATED SEQUENCES

A number of thick (usually greater than 10 m), siltstone and claystone units of the Aztec Siltstone do not conform to the ideal model of 'fining-upwards' sequences. Figure 7.12 describes a typical example from the Portal Mountain section (P1, units 4 to 22). The basal sandstone in cycle 1 is a typical channel deposit, containing the characteristic channel

INTERPRETATION

DESCRIPTION

	CYCLE 4		CYCLE 3		CYCLE 2	MIXED LACUSTRINAL & FLUVIATILE	CYCLE 1	
FINE	COARSE MEMBER	FINE	F	C	FINE	F	C	COARSE MEMB		FINE MEMBER	COARSE MEMBER

Interpretation column (top to bottom):

Base of next cycle.

Vertical accretion deposit from suspension of fines onto the floodbasin by overbank floods. Pluvial lakes probably developed.

Laterally accreted channel deposit plus some channel-fill deposit. Siltstone clasts forming the lag concentrate in the channel deeps.

Erosion by migrating channel.

Vertical accretion from overbank floods onto floodbasin areas, at less than ripple velocities. No exposure indicated.

Channel deposition by lateral accretion on a point bar.

Vertical accretion from overbank floods onto floodbasin areas.

Channel deposit probably a result of lateral accretion. Siltstone clasts on scoured lower surface.

Erosion by migrating channel.

Vertical accretion deposit from lacustrinal sedimentation, with some overbank deposition. Floodbasin deposit with groundwater fluctuations and periodic exposure. Probably pluvial backswamp lakes developed. Some crevasse-splay and levee interbeds.

Vertical accretion deposit from overbank floods, at less than ripple powers, and by suspension fallout. Floodbasin deposit with groundwater fluctuations, and periodic exposure indicated by nodules.

Probably channel-fill and lateral accretion deposit. Deposition of bed load in channels. Decrease in current flow. Siltstone clasts and disarticulated fish plates as intraformational deposit in scoured surface.

Erosion by migrating channel.

Top of previous cycle.

Description column (top to bottom):

Siltstone, greenish grey (5GY 6/1), ripple laminated, shaly. Burrows and fish plates.

Sandstone, fine, indistinctly laminated, massive.

Siltstone and bone breccia.

Sandstone, medium, indistinctly laminated, massive, interbedded with siltstone laminae and stringers. Intraformational conglomerates throughout.

Siltstone, greenish grey (5GY 6/1) unbedded, massive.

Sandstone, fine, trough cross-laminated, massive. Upper part ripple laminated.

Siltstone, greenish grey (5GY 6/1), parallel laminated, shaly.

Sandstone, fine, laminated, massive. Mainly parallel laminated but some ripple and low angle trough cross-lamination. Intraformational conglomerate at base.

Siltstone, greenish grey (5GY 6/1), laminated, shaly. Some fine sandstone interbeds at the base. Fish plates, conchostracans, plant stems, mudcracks, nodules and concretions.

Siltstone, greenish grey (5GY 6/1), unbedded, flaky. Nodules and vein networks.

Siltstone, pale greenish yellow (10Y 8/2) and moderate yellowish brown (10YR 5/4) laminated to thin bedded, massive. Oolites and nodules.

Siltstone, greenish grey (5GY 6/1). Unbedded in upper part and ripple laminated in lower part. Burrows, nodules and vein networks.

Siltstone, greenish grey (5GY 6/1), largely unbedded but some laminated and very thin bedded units. Massive. Nodules widespread.

Sandstone, medium in lower part grading up to fine in upper part. Laminated to very thin-bedded, massive. Intraformational conglomerate in base. Siltstone lenses throughout. Fish plates in base.

Metres 15 — 10 — 5 — 0

Fig. 7.12. Description, diagrammatic representation and interpretation of the sedimentary sequence at P1, units 4 to 22. For the legend see Fig. 7.1.

lag sediment of siltstone clasts eroded from the underlying top-stratum deposit. Siltstone laminae and lenses in the sandstone suggest a temporary waning of the stream. The 'fining-upwards' in grain size from a medium to a fine sandstone, indicates a decreasing 'bed shear stress' and therefore a lowering of current velocities in the point bar environment (Allen, 1964a, 1965a, 1970).

The basal channel sandstone is overlain by a thick (36 m) siltstone and claystone sequence. The bed form structures (well laminated), and the grain size (high clay percentage) suggests a vertical accretion deposit produced by the accumulation of fines from overbank floods and from lacustrinal deposition, on the backswamp areas of the floodplain. Vein networks, calcareous nodules, and extensive burrowing, suggests temporary subaerial exposure of some of the deposit, however, the lack of this evidence coupled with the presence of oolites in part of the sequence, strongly supports lacustrinal deposition. A backswamp area with lakes and ponds probably initiated as ox-bow lakes, is the most likely environment for deposition. The great accumulated thickness of sediment suggests that the environment was maintained for a considerable period of time. Modern floodbasin deposits lying at a distance from the main stream channels, contain similar sediments (Fisk, 1944; Allen, 1965a; Coleman, 1969).

Only minor crevasse-splay and levee interbeds were recorded.

The mixed lacustrinal and overbank fluviatile deposit is truncated by the scoured surface of cycle 2, which is of the classic 'fining-upwards' type described earlier. It may however incorporate the sandstone of cycle 3 as a crevasse-splay or levee interbed. Cycle 4 is another normal 'fining-upwards' sequence. These cycles obviously signify the return of the normal meandering stream channel.

This mixed lacustrinal, and overbank fluviatile sedimentation pattern is considered as a probable origin for the thick siltstone and claystone sequences in the sections at Alligator Peak (S.E.A., 37.8 m to 60.6 m and 83.8 m to 108.0 m), the south Warren Range (A6, units 30 and 31),

Portal Mountain (Pl, unit 34), the Lashly Mountains (Ll, units 8, 10, and 27; L2, units 3 and 5), Kennar Valley (KV, 28.4 m to 46.5 m), and Mount Fleming (FL, 32.5 m to 40.4 m).

In summary the Aztec Siltstone conforms to a sedimentation model of high sinuosity meandering streams criss-crossing a broad plain. Inter-fluve areas included ephemeral features such as low-lying backswamps, small lakes and ponds, marshes, and possibly playas.

Sediment Transport Direction

The Aztec Siltstone lithologies contain numerous indicators of sediment transport directions or paleocurrent flow vectors. These include channel-fills, small and large scale cross-bedding, symmetrical and asymmetrical ripples, and parting lineations. Barrett and Kohn (1975) have measured and analysed directional sedimentary structures in the Aztec Siltstone (Fig. 7.13) as part of a paleocurrent analysis of the Beacon Supergroup of south Victoria Land. The paleocurrent pattern for the Aztec Siltstone is unimodal with a northeast direction, but there is a high variability in cross-bed orientation. They concluded that the Aztec Siltstone was deposited from highly sinuous, meandering streams, which is consistant with the model of alluvial plain sedimentation proposed in this chapter.

The underlying alluvial plain sediments, the Beacon Heights Orthoquartzite, also has a paleocurrent trend to the northeast, though the variability in cross-bed orientations is much lower than for the Aztec Siltstone (Barrett and Kohn, 1975). Because of the low variability and lack of fines in the Beacon Heights Orthoquartzite, Barrett and Kohn concluded that it was deposited from low sinuosity, braided streams. They proposed that the development of a plant-covered land surface and the formation of the first humic soils increased production of fines and decreased run-off and level of flood
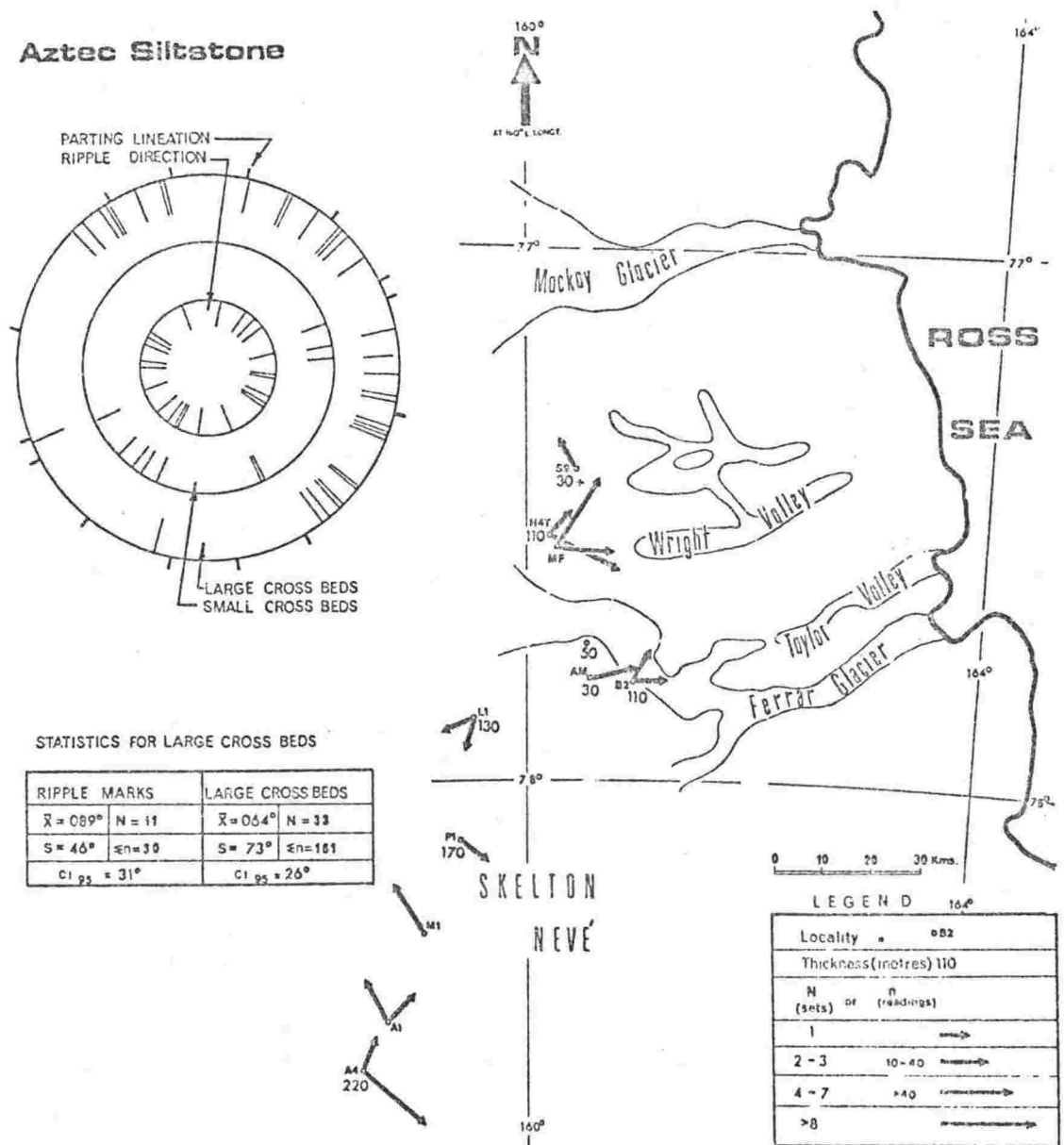
Fig. 7.13. Palaeocurrent map of the Aztec Siltstone (from Barrett and
Kohn, 1975).

discharge sufficiently to have effected the change in the
stream pattern from a braided one for the Beacon Heights
Orthoquartzite to the meandering one of the Aztec Siltstone.

The paleocurrent analysis shows that the sediment of the
Aztec Siltstone came from the southwest, that is, from the

East Antarctic craton west of the Ross Ice Shelf.   This is
also true for the two underlying formations, the Arena Sandstone
and the Beacon Heights Orthoquartzite (Barrett and Kohn, 1975,
Fig. 3.6).

CHAPTER 8

PALAEONTOLOGY

The Aztec Siltstone is the oldest formation in the Beacon Supergroup, in south Victoria Land, containing datable fossil assemblages. Fossil fish are abundant throughout the Aztec, and fossil macro and micro-flora, and conchostracans are present at a number of localities.

Fish

Fossil fish from the Aztec Siltstone were first discovered during Scott's *Terra Nova* Expedition of 1911-13 (Debenham, 1921, Woodward, 1921). Further samples were collected for study in 1957-58 (Gunn and Warren, 1962; White, 1968), 1968-69 (Ritchie, 1969; McKelvey *et al.* 1970a, 1970b; McKelvey *et al.* 1972), and 1970-71 (Barrett *et al.*1971; Ritchie, 1971, 1974, 1975).

The fossil fish remains are found at all levels of the Aztec Siltstone and at most outcrop localities. The fossil material is best preserved in the fine-grained, overbank sediments, where it appears that fish were concentrated by, and died as a result of, streams and ponds evaporating. Fossil fish remains are also found in sandstones as a channel lag deposit (Fig. 4.14). This material is generally disarticulated and fragmented. Extensive pavements covered with the disarticulated fragments of fish fossil material are common in the Aztec and some bone beds consisting entirely of fossil fish remains were noted - e.g. A4, unit 62.

Fossil material includes jaws, teeth, skulls, dermal plates and fin spines (Figs 8.3, 8.5 and 8.6). The fish specimens identified include the antiarch *Bothriolepis* (Figs 8.2 and 8.3), the arthrodires *Groelandaspis* (sp. *antarcticus*) (Fig. 8.1) and *Phyllolepis*, crossopterygians (Figs 8.4, 8.5 and 8.6), *Ctenodus* (dipnoans or lungfish), the acanthodian *Gyracanthides*, palaeoniscids, and the elasmobranch *Ctenacanthus* (Woodward, 1921; White, 1968; McKelvey, 1972; Ritchie, 1971, 1974, 1975, and pers. comm. 1975).

Fig. 8.1. A reconstruction of the arthrodire *Groenlandaspis*. (Drawn by A. Ritchie)
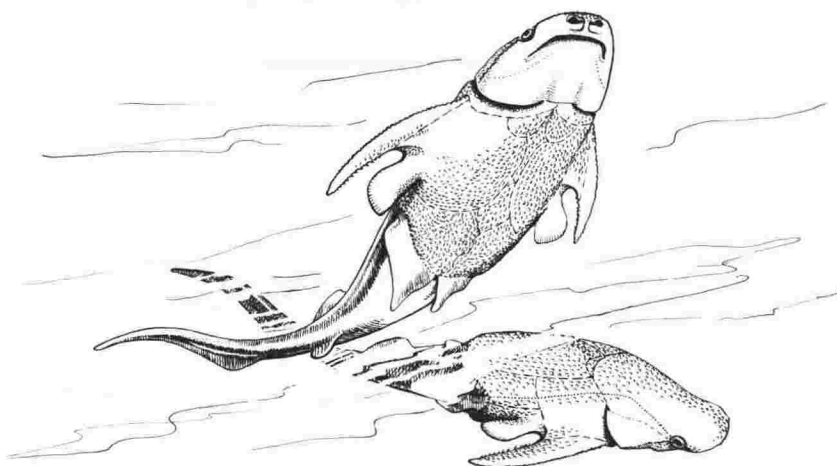
Fig. 8.2. A reconstruction of the antiarch *Bothriolepis*.
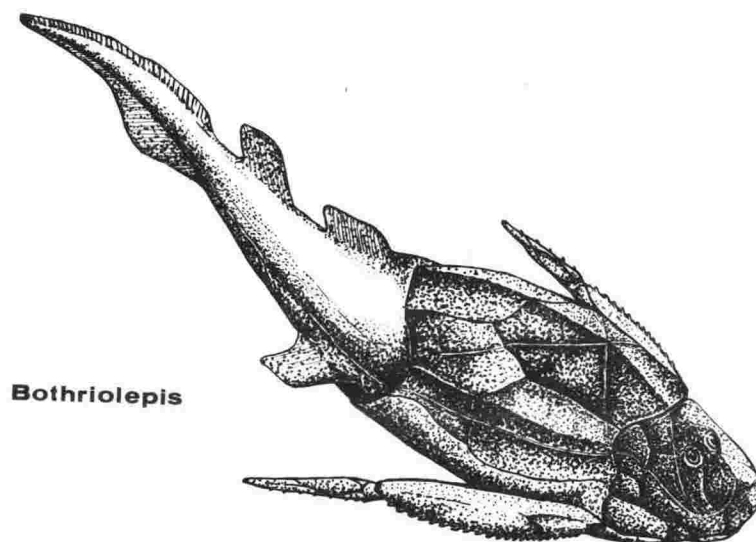
Bothriolepis

Fig. 8.3. A pavement littered with the armour-plate remains of *Bothriolepis*. The head-shield of *Bothriolepis* in the centre of the photograph clearly shows the dorsal cavity which contained the eyes.

5 cm = 12 cm
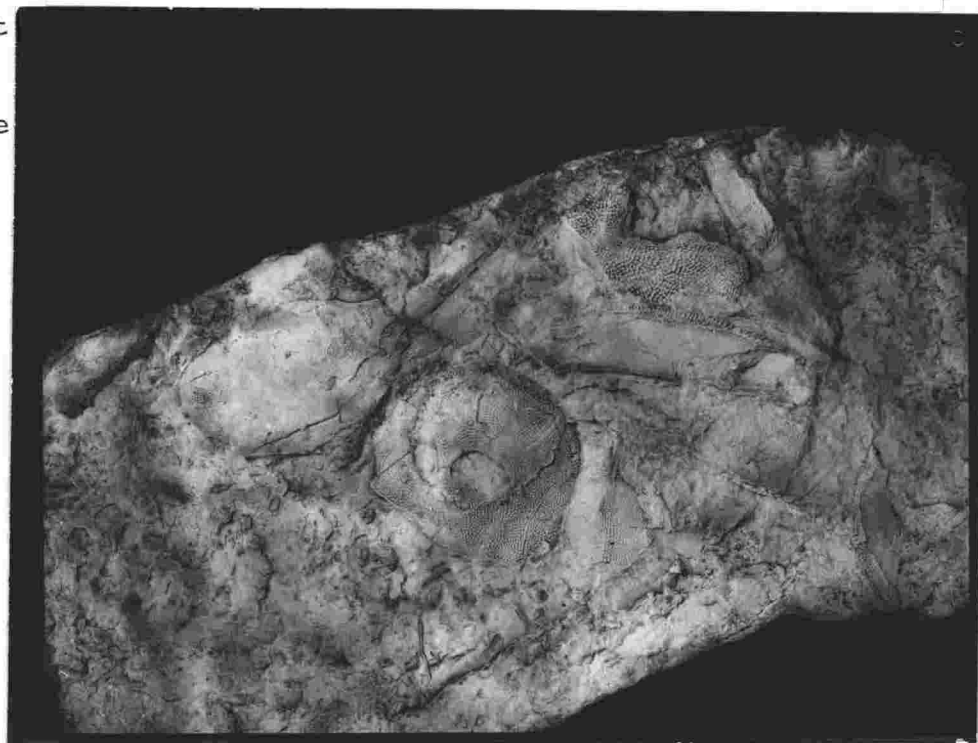
Fig. 8.4. A reconstruction of *Gyroptychius*, a Middle Devonian crossopterygian very similar to the Aztec specimens. (After Jarvik).
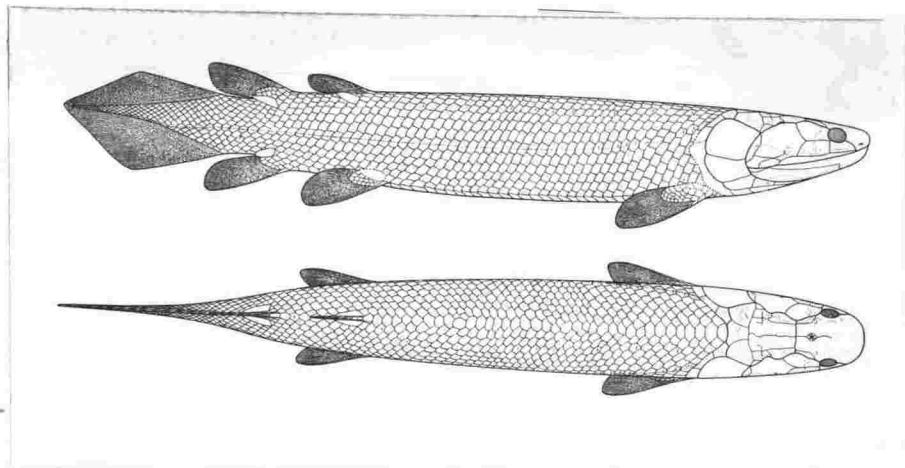
Fig. 8.5. The lower jaw of a crossopterygian specimen from the Lashly Mountains (L2). The photograph shows the internal surface of the left side of the jaw, with well-developed carnivorous teeth.

Fig. 8.6. A dorsal view of the skull of a crossopterygian specimen from the Lashly Mountains (L2).
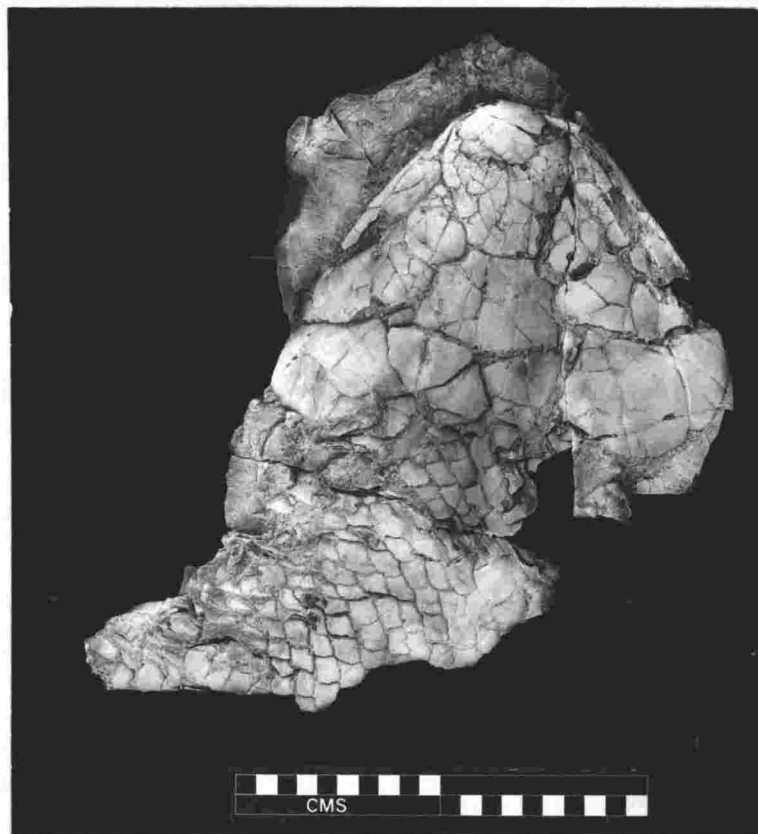
The age of the fossil fish fauna is Middle to Late
Devonian. Woodward (1921) suggested an Upper Devonian age,
White (1968) an upper Middle Devonian age, McElroy (1969)
a Middle or preferably Upper Devonian age, and Ritchie (1969,
1974, 1975) an Upper Devonian age. Ritchie (pers. comm. 1975)
suggested a Famennian and possibly Strunian age. An Upper
Devonian age is in agreement with the micro-floral assemblage
(Helby and McElroy, 1969).

The Aztec fish fauna are strongly endemic in character
(White, 1968). In particular, *Bothriolepis* and
Groenlandaspis are found in the Upper Devonian sediments
of the Catskill-Old Red Facies of N. America, Great Britain,
Europe and Greenland, and in the Upper Devonian of China,
Russia and Australia (White, 1968; Ritchie, 1969, 1971, 1974,
1975; Young, 1974, pers. comm. 1974). This cosmopolitan fish
fauna is invariably found in non-marine sediments, although
the recent discovery of *Bothriolepis* in marine reef deposits
in the Kimberleys of Western Australia (Ritchie, 1971) indicates
that some of the bothriolepids lived in marine conditions, a
factor which would have aided the worldwide dispersal. The
fish may have had both a fresh-water and a saltwater tolerance,
similar to modern salmon.

Conchostracans

Conchostracans were found in three Aztec sections, P1,
L1 and L2. They consisted of small (less than 15 mm) white
calcareous shells or black molds, with, in some examples,
concentric growth rings.

Conchostracans, like most branchiopods, are non-marine
invertebrates and are confined mainly to fresh-water, and
rarely to brackish-water, ponds, pools and lakes (Woods,
1926; Moore et al. 1952; Barnes, 1963). Barnes (1963),
stated that modern branchiopods, including conchostracans,
are confined to temporary pools, springs, and small ponds.

Flora

The Aztec Siltstone only rarely contains any trace of carbonaceous or former carbonaceous material (Fig. 2.1), which is consistent with a highly oxidising depositional environment. Consequently plant fossils are rare. Nevertheless a microfloral assemblage has been extracted from the Aztec Siltstone at Aztec Mountain by Helby and McElroy (1969), who found it to contain a variety of spore types, suggesting a diversity in floral types living in the local environment. The assemblage is dominated by *Geminospora lemurata* (Balme, 1962) and similar to an assemblage of Frasnian age from Western Australia. Spores have recently been extracted, but not yet identified, from a number of other localities (R. Kyle, pers. comm., 1975).

Plant macrofossils are extremely rare in the Aztec Siltstone. At A4, unit 42, a simple dichotomous branching, leafless, *Rhynia*-type of plant was found (Fig. 8.7). It did not contain any terminal sporangia. The unit containing this plant also had a number of poorly preserved stems, and abundant sinuous roots (Chapter 4, p.89). An overlying unit (44, fig. 8.8) yielded several well-preserved stems.

Lycopods were not found in the formation but it is known that they had evolved in the area by the time of Aztec deposition because they are contained in the underlying Beacon Heights Orthoquartzite (Plumbstead, 1962; Barrett *et al.* 1971).

The concentration of living plants on the Aztec alluvial plain cannot be accurately gauged, but, the widespread evidence of oxidation (as demonstrated by the red beds) and soil desiccation (mudcracks and vein networks) indicates a scarcity of plant life at the time.
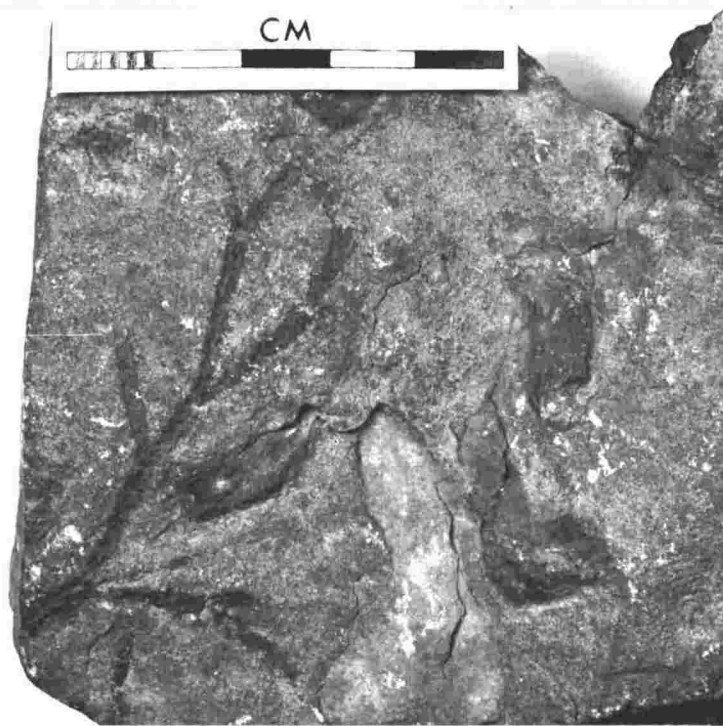
Fig. 8.7.   A simple dichotomous branching leafless, *Rhynia*-type plant
            from A4, unit 42.
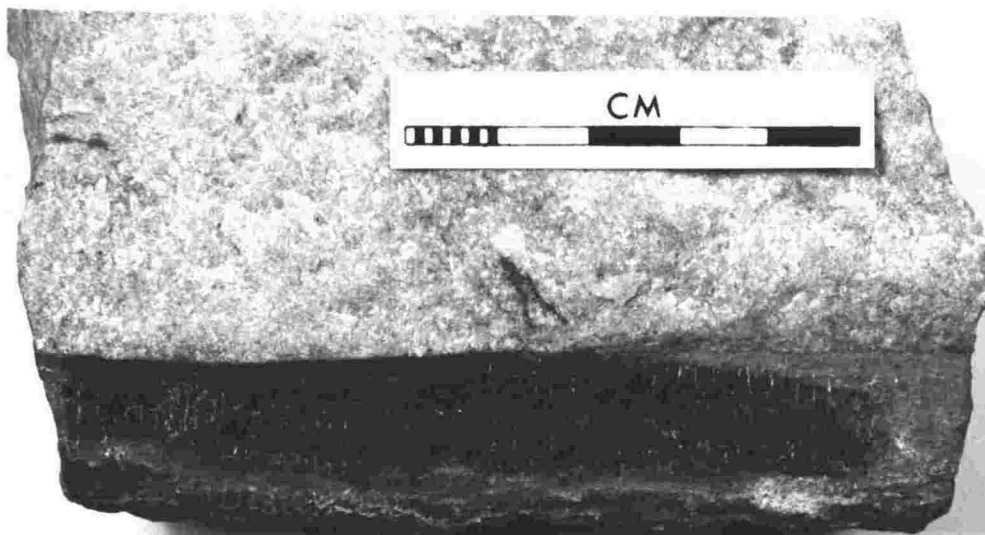
Fig. 8.8.   A carbonized plant stem from A4, unit 42.

CHAPTER 9

RED BEDS

A red bed is generally understood to be "a sandstone, siltstone, or mudstone made of detrital grains set in reddish-brown mud matrix or cemented by precipitated reddish-brown ferric oxide", (Van Houten, 1964a p.647). It is evident from the voluminous literature on the subject that there is a multiplicity of processes that may be involved in the formation and preservation of red beds.

The Controversy

The controversy began in the mid 19th century and gathered momentum in the early 20th century (Walther, 1908, 1909; Barrell, 1908; Tomlinson, 1916; Bailey, 1926; Raymond, 1927). There were two schools of thinking, one appealing to aridity and hence desert conditions, the other favouring high humidity and temperature and thus a tropical environment for formation.

There was early agreement by authors that the red pigment was haematite, commonly in a very finely crystalline form (Barrell, 1908; Tomlinson, 1916; Dorsey, 1926). Friend (1966 p.281) observed from electron photomicrographs that the haematite in red beds consists of well-developed platy hexagonal crystals averaging 0.25 microns across. The crystals form a pigment coating larger detrital grains or are dispersed throughout the matrix of a sediment, giving the macroscopic appearance of a red stain.

Most 'red-bed' sequences are not entirely red, but contain a percentage of drab lithologies. In the case of the "variegated" red-bed sequences, the percentage of drab lithologies can be very high. Drab beds owe their colour to the presence of green clays, illite, chlorite, and possibly montmorillonite (Grim, 1951; Robb, 1949; Keller, 1953; Picard, 1965; Thompson, 1970; McBride, 1974). Keller (1929, 1953) showed that removal of haematite pigment by reduction exposes the green matrix,

with a possible but not necessary formation of green chlorite
(Thompson, 1970 p.613-614).

Chemical analyses of red and associated non-red beds
of a similar size and texture reveal the following (Van Houten,
1961 p.104-106):

(1) Greater total iron and ferric iron content in red rocks
     than non-red rocks, although colour is not simply due to
     this factor.

(2) For red-drab pairs, Fe_2O_3 is higher in red than drab beds.

(3) Red rocks have a Fe_2O_3:FeO ratio greater than 2:1, but
     most drab rocks have a ratio less than 2:1.

Thus green or grey beds in red-bed sequences are not derived
from red-coloured beds solely by reduction of Fe_2O_3, which
would result in a corresponding increase in FeO for green or
grey beds, but also by the removal in solution of Fe^{2+} (Keller,
1929; Eichhoff and Reineck, 1953; Jones, 1965; Picard, 1965;
Friend, 1966; Wu, 1971). Keller (1953) showed that because
of the presence of green Fe^{3+} silicates, some beds may have a
high Fe^{3+}, and still be green or grey. Thus the conditions for
formation of red-beds must be those which provide a stable
environment for the Fe^{3+} ion and compound it as an oxide
rather than a silicate.

Regardless of the climatic conditions invoked for the
formation of red beds, presence of the red pigment is widely
accepted as indicative of oxygenating, continental or terrestrial
processes (including some in paralic environments). An oxidising
environment is required for the formation of haematite, and must
persist throughout diagenesis if the haematite is to remain
unchanged. The marine environment is most commonly reducing,
brought about partially by the incorporation of organic
matter, both marine and terrestrial, and partially by the action
of the decay of marine organisms. Red detritus carried into
marine environments is most commonly reduced immediately
following deposition. Red detritus carried by certain rivers
in Nova Scotia is deposited in Pictou Harbour as reduced dark
grey sediment (Dawson, 1848, vol. V. p.29), and the red
sediments of the Catskill facies that were carried beyond the

delta and into the Devonian sea were almost entirely reduced
(Dunbar and Rodgers, 1957).

HUMIDITY AS A FACTOR

The idea that humid conditions are necessary for the
formation of red beds largely arose from an application of the
principle of uniformitarianism. Geologists observed that red
tropical soils, namely laterites, represent the greatest
accumulation of recently formed haematite. Thus, writers
like Knowlton (1919), Dorsey (1926), and Raymond (1927)
concluded that fossil red beds were derived from red soils
developed in tropical uplands. Support for a humid as opposed
to an arid climate for haematite production in part also came
from common observation of the fact that recent deserts are
"practically never red", (Dorsey, 1926 p.141), but are yellows,
browns, and whites (Russell, 1889; Walther, 1908; Raymond,
1927; Dunbar and Rodgers, 1957 p.210). Examples of present
day red desert soils and sands have been reported (Jessup,
1961; Kubiena, 1963; Melton, 1965; Stace et al. 1968)   .
but there has been general agreement that they formed during
earlier, moister episodes in deserts, probably during the
pluvial periods which characterised glacial periods during
the Pleistocene Epoch.

Krynine (1949), recognized five classes of red beds, and
concluded that "most primary, detrital, red beds are formed
under warm and moist climatic conditions, possibly in tropical
savanna type climates". He specifically noted a mean annual
temperature of greater than 16°C and an annual rainfall of
over 100 cm for the red weathering of silicates.

Van Houten (1948) studied the Cenozoic red beds of the
Rocky Mountains, and reached a similar conclusion. He suggested
that the red material was developed in a warm, humid upland
and eroded and redeposited in a humid lowland environment,
principally a piedmont and valley-flat situation. The hypothesis
was later modified (Van Houten, 1961b) to account for those red
beds which were obviously deposited in an arid or semi-arid

environment, for example those red beds which contained abundant evaporite deposits or aeolian sandstone. He contended that these deposits were reworked from upland regions of higher humidity, where the colour was authigenic, into arid or semi-arid lowland basins of deposition. Van Houten (1961b, p.121) noted that "a climate somewhat drier than that of the source area will support less abundant vegetation and a lower water table, thus favouring preservation of red pigment".

Those who hold to the hypothesis of moist humid conditions for haematite formation, explain the few recent red desert sediments as,

(1)   eroded from neighbouring, more humid regions.

(2)   formed during a more humid period of the Pleistocene,

(3)   eroded from ancient red beds, i.e. they are second cycle, or secondary red beds, e.g. "the Northern Sahara red sands are reworked fluvial Oligocene red sands" (Krynine, 1949 p.67).

If the colour pigment of red beds is detrital, then, as Krynine noted (1949 p.66), the background to red beds so formed will be red. Any drab zones are attributed to *in situ* reduction induced by the presence of organic matter incorporated in the sediment. The decay of organic matter by biologic (e.g. anaerobic bacteria) and chemical activity invariably produces a local reducing condition. This results in the instability of any haematite present. Krynine (1949 p.62) simplified the equation thus,

$$Fe_2O_3 + C + O_2 = Fe_2O_3 + CO_2 \quad \text{(oxidising condition, haematite stable)}$$

$$2Fe_2O_3 + 2C = 4FeO + C + CO_2 \quad \text{(reducing condition, haematite removed)}$$
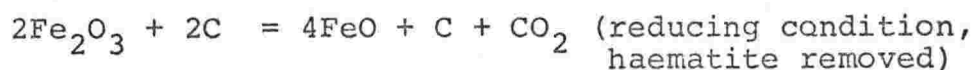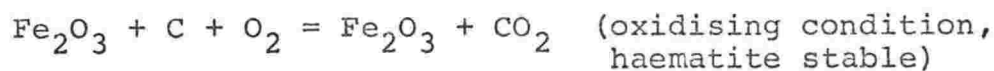
However, what of the many 'red bed' sequences in which more than half of the strata are non-red (e.g. Jones, 1965 p.239-240)? Do the drab beds all result from reduction and removal of haematite, or are they possibly due to a lack of haematite formation?

The preservation of red beds, with the implied lack of organic material, is in itself a rough palaeoclimatic indicator. The soils of arid or semi-arid climates will support little vegetation, and hence the sediments derived from there will in turn, contain a low carbonaceous content. However, other climates, and especially temperate climates, will sustain abundant vegetation which in due course is incorporated into the sediment and thereby gives rise to reducing conditions during diagenesis. The presence of organic matter in sediment is considered to be the major reason for the lack of red beds formed or deposited in temperate regions of the earth. This is at least true for post-Devonian sediments, but prior to the establishment of terrestrial vegetation during the Devonian, the accumulation and preservation of red bed material was possible over much wider areas of the globe and in many climates (Chukhrov, 1973). This is possibly a contributing reason for the abundance of Devonian and older red beds. Chukhrov suggests that the development of vegetation restricted red beds to predominantly desert territories, where the organic matter did not create a reduction environment in diagenesis.

Problems of the "humidity" hypothesis

A detailed study of the mineralogy of red beds poses a number of problems for the hypothesis that depends upon lateritic conditions for haematite formation. The first concerns the clay mineralogy. The most common clay is illite, accompanied by subordinate chlorite and mixed-layer clays (Grim, 1951; Nordmeyer, 1959 p.7-8, 12-13; Salger, 1959; Schmitz, 1959 p.65, 84; Folk, 1960 p.10, 34 and 1962 p.567; Echle, 1961 p.35; Van Houten, 1961b, Table VI; Krumm, 1962 p.481; McBride, 1974). Kaolinite, montmorillonite, corrensite, and sepiolite are less common in red beds. However, if red beds are a result of reworking of lateritic soils, then the kaolinite content should be higher, especially as kaolinite is one of the dominant clay minerals in fluviatile deposits (Weaver, 1958 p.258; Millot, 1970 p.139). The paucity of

kaolinite in red beds has been attributed to diagenetic
alteration to illite (Grim, 1951 p.228; Swineford, 1955
p.161-163; Schmitz, 1959 p.84; Van Houten, 1961b p.116-119,
1964 p.651; Walker, 1973, 1974a). The illitization of
kaolinite has been well demonstrated, in thin section, by
Millot (1970 p.239-243). Van Houten (1961b p.119) cites the
illite-rich Miocene red beds from the Ebro Basin, Spain, as
an example of kaolinitic alluvium which has diagenetically
altered to illite.

However, kaolinite is recorded, in some cases in abundance,
from some ancient red beds, e.g. the Devonian Catskill facies
(Friend, 1966), the Lower Old Red Sandstone (Wilson, 1971),
and the New Red Sandstone (Henson, 1973). Thus it is
questionable whether diagenetic alteration of kaolinite to
illite has taken place in those red beds devoid of kaolinite.
Possibly the high calcium environment which is so common in
red beds has promoted the formation of clays other than the
potassium-rich kaolinite, e.g. montmorillonite. The author
suggests that the simplification of the clay mineral assemblage
of sediments older than Carboniferous (Weaver, 1959) especially
in respect to the paucity of kaolinite, has a relationship to
the evolution of terrestrial flora, and in particular to the
establishment of heavily forested areas. Prior to the Early
Carboniferous, forested vegetation of the type that now
characterizes the sub-equatorial climatic zones of the world
and is an integral part of the lateritic profile developed in
these zones, did not exist. This means that laterization
resulting in the widespread formation of kaolinite, probably
was not possible. The lateritic profile develops today under
moist conditions, generally tropical or sub-tropical, where
extensive weathering and leaching leads to the removal of
silica, lime, magnesia and the alkaline elements, and a
consequent concentration of iron and aluminium hydroxides.
A relatively thick vegetative or forest cover is essential
for the full development of a latosol, not only because it
provides the organic acids used in chemical weathering and
shields the soil from erosion in these high rainfall regions,

but also because without it the soil profile would rapidly desiccate, thus inhibiting laterization and hence the formation of kaolinite.

Another stumbling block to the primary detrital origin of red beds from lateritic soils is that "no one has yet documented an occurrence of red beds which can be demonstrated to have formed in this manner" (Walker, 1967a p.354). Although red soils are extensively developed in the tropics, the alluvium of such areas is not red, but has a distinct tan or brown hue. Krynine (1950) claimed that there were red sediments on the coastal piedmont of Tabasco in southern Mexico, which he attributed to reworking of upland red soils, but Walker (1967b p.917) observed that the alluvium is greyish brown, "because the red detritus is masked by more abundant non-red material".

ARIDITY AS A FACTOR

Some of the earliest analysts of red beds concluded that they were developed under desert conditions (Goodchild, 1897; Frass, 1899; Lomas, 1907, 1909; Bosworth, 1907, 1912; Walther, 1908, 1909; Thomas, 1909; and others). This concept received wide acceptance until the 1940's when the "humidity" or "detrital" theory gained favour. The suggestion that ancient red beds are indicative of an arid environment largely arose from the association of some red beds with extensive evaporite deposits (e.g. the Keuper red beds) and aeolian sandstone (e.g. the Late Triassic Chugwater red beds of Wyoming). Other features such as ventifacts, abundant mudcracking and the paucity of organic matter in the sediments were consistent with such an hypothesis. This association of red beds with aeolian deposits, desiccation marks, and evaporites indicates for Van Houten (1961b p.122) "at least temporary dry conditions during deposition, and in some cases local desert environments", but he added that "they do not imply accumulation in vast deserts like the great high pressure or trade wind deserts today".

Formation of the red pigment and its accumulation as red
beds in an arid or semi-arid environment must result largely
from *in situ* processes, in contrast to the "humidity" hypothesis
where transportation away from the area of formation is required
for preservation of the red colour. For the "aridity"
hypothesis mineralogical changes must take place within the
body of the sediment to produce the haematite pigment. Miller
and Folk (1955) observed that haematite in many red beds was
not present at the points of contact of sand grains,
demonstrating that the haematite in these cases was post-
depositional. By so doing, they established that the climate
of the source area did not necessarily govern haematite
production, but that conditions within the sediment after
deposition were of major significance.

OXIDES OF IRON

Any hypothesis to explain the origin of red beds must give
a satisfactory derivation of haematite. The "humidity"
hypothesis as previously described, derives the red pigment
from laterites developed under warm humid conditions in the
source area. Tomlinson (1916), in assuming an origin of red
beds from the reworking of ferruginous residual soils,
attributed the haematite to a transition by dehydration in the
soil, from goethite ($Fe_2O_3.H_2O$) and limonite ($2Fe_2O_3.3H_2O$),
both common constituents in the lower horizons of lateritic
soils.

$$Fe_2O_3.H_2O = Fe_2O_3 + H_2O \qquad \text{(dehydration)}$$
$$\text{(goethite)} \quad \text{(haematite)}$$

$$2Fe_2O_3.3H_2O = 2Fe_2O_3 + 3H_2O \quad \text{(dehydrated)}$$
$$\text{(limonite)} \quad \text{(haematite)}$$
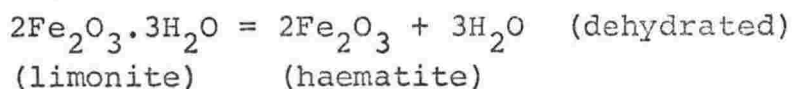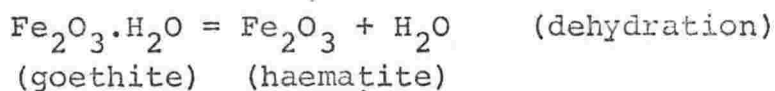
Raymond (1927) and Krynine (1949) maintained that warm
humid conditions favoured the dehydration of hydrous ferric
oxides. From thermodynamic considerations, Smith and Kidd

(1949) stated that goethite is stable with respect to haematite at temperatures below 130°C and so will not spontaneously dehydrate to produce *in situ* red beds. Van Houten (1961 p.111) noted these conclusions as corroborating a primary detrital origin of red pigment. However, Berner (1969 and 1971 p.197), from similar thermodynamic considerations to those of Smith and Kidd (1949), contradicts their conclusions and states that "thermodynamically the transformation of limonitic goethite to haematite during diagenesis is feasible", and shows this to be in agreement with similar results of Langmuir (1970). Later work by Langmuir (1971) demonstrated that goethite has no thermodynamic stability relative to well-crystallized haematite under normal geologic conditions. He showed that dehydration of goethite to form haematite may take place at depth as well as on the land surface, and so consequently may be completely unrelated to palaeoclimatic conditions. Recently, Fischer and Schwertmann (1975) demonstrated by laboratory simulation, that haematite is formed by 'internal dehydration' of an aggregated amorphous ferric hydroxide, and showed that the process is favoured by increasing temperature.

Walker (1967a) reported the progressive *in situ* formation of red beds under a hot arid environment in the Sonoran Desert, Mexico. Reddening was observed to increase with age from the light grey of recent alluvium, to the red Pliocene alluvial deposits. He concluded that time, in the order of millions of years, was the critical factor in reddening, and listed the three forms of iron oxide pigment (p.360).

(1) yellowish to reddish-yellow amorphous ferric hydrate in Pleistocene soils.

(2) red ferric hydrate, amorphous to X-rays, in older Pleistocene soils.

(3) red, well-crystallized haematite, in Pliocene deposits.

Thus it was established that haematite may develop *in situ*, as a result of the slow progressive dehydration of hydrous ferric oxides under a hot arid environment. Later, Walker (1974b) showed that "red beds can also form diagenetically in moist

tropical climates by processes of intrastratal alteration that are analogous to those forming red-beds diagenetically in deserts". The diagenetic formation of haematite could well explain many of the ancient red-beds and in particular explain why there are only rare examples of Recent red sediments on the Earth's surface.

In 1961 Van Houten proposed that the reason for the apparent inconsistency of the non-red alluvium (usually grey, brown and yellow according to Jones, 1965; Van Houten, 1968; Walker, 1967b) of present day tropical rivers draining from lateritic areas, was because brown hydrohaematite is an intermediary in the dehydration of hydrous ferric oxide. MacKenzie (1957) and Scheffer et al. (1957) had previously suggested that hydro-haematite is the principle ferric oxide in brown soils of cooler climates, and in warmer climates laterization ages hydrohaematite to haematite and concentrates it. Chukhrov (1973) studied a very common hydrated form of haematite called ferrihydrite ($2.5Fe_2O_3.4.5H_2O$), and noted that it converts to haematite with time and diagenesis. He concluded that ferri-hydrite is produced by weathering in upland areas, and carried in suspension and deposited with the other detrital substances, where, with a continued oxidising environment, it later dehydrates to haematite and consequently produces red beds. Walker (1967a, 1967b, 1974b) favours an in situ origin for the hydrated ferric oxide which will, with time and a continued oxidising environment, dehydrate to form haematite. He suggests that the hydrated ferric oxide is produced by intrastratal alteration of iron-bearing grains in the sediment, most commonly hornblende and biotite, when the intrastratal environment has an Eh-pH in the stability field of that compound (see Garrels and Christ, 1965, for the diagrams of the Eh-pH stability fields of iron minerals). However, Van Houten (1972) suggests that the hydrated ferric oxide is largely a detrital product and notes that "there is enough free brown hydrated ferric oxide in tropical savanna alluvium to produce haematite pigment in a red bed simply by post-depositional dehydration and crystallization in an oxidizing environment of burial".

Walker and Honea (1969) showed that in ancient red beds, on an average, only 0.7% iron is extractable (present as haematite) thus demonstrating that, "essentially all sediments, regardless of type of parent material or type of source-area weathering conditions (moist or arid), contain enough iron to produce bright red sedimentary rocks if the interstitial environment, either during or subsequent to the time of deposition, favours the formation and preservation of iron oxide".

In summary, the possible mechanisms for red-bed formation are

(1)   Ferric oxide brought in, as haematite, from the source in colloidal suspension and deposited with the other detrital products (Raymond, 1927;   Krynine, 1949, 1950). The source sediment may be red soils (latosols) as suggested by the above authors, or possibly an older red bed sequence which is being reworked.

(2)   *In situ* aging and dehydration of yellow or brown hydrous ferric oxides (limonite, goethite, ferrihydrite, and possibly maghaemite) to haematite, in an oxidizing environment (Van Houten, 1964b, 1968, 1972).   The hydrous ferric oxides may be detrital or developed *in situ*.

(3)   Diagenetic haematite formed by the *in situ* alteration of iron-bearing, detrital, silicate minerals (Walker, 1967a, 1967b, 1974b).   The alteration probably involves hydrated ferric oxides as intermediary minerals.

(4)   A combination of the above processes.

Most red beds have probably undergone some redistribution of iron in solution, with subsequent precipitation as haematite, or more likely hydrous ferric oxides.   This applies most particularly to "variegated" red-bed sequences.   Thus, red-beds themselves are not satisfactory palaeoclimatic indicators, though some contain features that in themselves indicate palaeoclimate.. The only factor common to all red beds is an oxidizing environment for the formation and preservation of red pigment.   Unless reworked and rapidly deposited red beds can therefore be regarded as reasonably reliable indicators of

non-marine (possibly including paralic) deposition for
sediments younger than Devonian.

Aztec Siltstone Red-Beds

The Aztec Siltstone is a typical "variegated" red-bed
sequence, in that it contains interbedded red and drab
lithologies. Red (1OR 4/2) lithologies, either siltstone,
claystone, or mudstone, constitute 15 percent of the entire
formation, and 30 percent of the fine-grained lithologies.
The sandstone is either greenish grey, grey, white, or pink,
but never red.   The red lithologies of the formation are fine-
grained, vertically accreted, overbank sediments (Chapters 3
and 7).

TIME OF REDDENING

The time of reddening of the Aztec Siltstone is difficult
to fix exactly. The haematite, or possibly some precursory·
mineral, was either detrital or formed as a penecontemporaneous
product because the Aztec Siltstone contains red intraclasts
incorporated into non-red sandstone units (Chapter 3, p. 27,
Fig. 3.8). Further evidence for a detrital or penecontempo-
raneous origin of the red pigment arises from the inclusion of
the haematitic pigment in the kankar ('caliche') and the oolite
sample (23306). Both of these products crystallized on or
near the surface of the Aztec alluvial plain (Chapters 3 and 6).
Consistent with a detrital or penecontemporaneous origin for
the pigment is the fact that many of the red-drab colour
boundaries conform to bedding and other sedimentary structures
e.g. burrows (trace fossils), roots, and vein networks
(Chapter 4). In some of the soil horizons in the formation,
e.g. Al, unit 22, sample 23243, the haematite pigment is
concentrated into channels (skew-plane haematans, Fig. 5.4)
and concretions (haematans, Fig. 5.6). These structures are
characteristic soil features and attest to the detrital or
penecontemporaneous origin of the pigment.

In addition to the above evidence for an early origin of
the pigment, a small number of sandstone beds contain some
detrital quartz grains which are completely rimmed by haematite
pigment. In a few examples e.g. 23241 the haematite imparts
a pink colour to the sample. The haematite is not contained
in the matrix, and could therefore not have arisen from post-
depositional processes. These samples are considered to be the
products of local reworking of earlier reddened Aztec sediments
and further substantiate the case for early reddening.

The common occurrence of reduced, drab, upper and lower
portions of the fine-member red beds, as exemplified by the
'ideal' fining-upwards cycle (Chapter 7, Fig. 7.4), also
suggests that the red or red-inducing product must have been
present at or soon after deposition.

The bulk chemistry (Chapter 6) rules out the possibility
that the pigment derives from the *in situ* alteration of iron-
bearing minerals as suggested for some red beds by Walker
(1967a, 1967b, 1974b). If this had been the case, then it
would be expected that the total Fe content of the red and
associated drab lithologies would be the same. However, this
is not the case (Chapter 6, Fig. 6.2). The only iron-bearing
minerals in the Aztec are the illitic and chloritic clays.
If the iron for the haematite had derived from these clays it
would be expected that the clay content of the red and green
paired samples would be proportionately different. This was
not found (Chapter 6). If other iron-bearing minerals had
existed in the Aztec prior to reddening e.g. hornblende or
biotite, then the sandstones should also contain these minerals,
but they do not (Chapter 5).

If the red pigment or its precursory mineral had been
introduced after consolidation of the formation, then it would
be expected that the more permeable lithologies e.g. sandstones,
would be most affected. However, the sandstones never contain
a red pigmented matrix.

The basal units of the disconformably overlying formation,
the Metschel Tillite, contain red lithologies, considered to
be the reworked products of the uppermost units of the Aztec

Siltstone. This means that the Aztec Siltstone had attained its red-inducing product at least prior to the Carboniferous (?)-Early Permian glaciation.

There is no evidence to establish that the haematite of the Aztec Siltstone was a detrital product. The scan electron microscope photographs of haematite pigment coating a detrital quartz grain (extracted from a red sandy claystone, 23584) (Fig. 5.28) shows the individual platy haematite grains stacked in what is obviously their growth position, thus supporting an *in situ* as opposed to a detrital origin for the pigment. A few examples of *in situ* haematite growth were noted in thin section e.g. Fig. 5.30, where coarse-grained haematite had formed as an alteration product (Chapter 5 p.148). Although this establishes that the conditions were right for *in situ* haematite growth, the bulk of the haematite is not considered to have been formed in this manner because the haematite so formed is coarse grained and unlike the pigment.

The haematite pigment of the Aztec Siltstone is generally of a perfect euhedral form, as clay-sized hexagonal plates (Fig. 5.29). This feature requires an *in situ* as opposed to, a detrital origin according to Wilson (1971, p.1006), who believed that the perfect euhedral form could not be inherited. However, the author suggests that although it is consistent with the *in situ* formation of haematite, it is not proof because it is possible that the very fine grain crystal size of the pigment may have allowed it to survive the rigors of fluvial transportation.

The absence of red sandstone, even although a high percentage of the Aztec sandstone contains some clay matrix, is further evidence consistent with the view that the haematite was not detrital.

Therefore, it would appear that the red pigment was produced *in situ*, probably at some time before deposition of the overlying unit. The red lithologies of the Aztec were all fine-member, overbank deposits which in general were subaerially exposed for periods of between 5,000 and 50,000 years, based upon the kankar ('caliche') evidence (Chapter 4). Most of these units probably developed as soils (Chapter 4, Nodules,

Vein Networks; Chapter 6, Soil Chemistry). It is concluded
that the haematite pigment developed in these sediments at
some stage during subaerial exposure. The pigment is not
thought to have resulted from intrastratal alteration of iron-
bearing minerals as has been previously discussed, but is
considered to have been produced from the progressive, *in situ*
dehydration of detrital, brown or yellow, amorphous and poorly
crystalline hydrated ferric oxide. This is consistent with
the modern view that red beds do not derive the bulk of their
red pigment directly as a detrital product by, for example
the reworking of haematite rich soils or sediments in the
source region, and that most were deposited as non-red
alluvium (Van Houten, 1968, 1972; Walker, 1974b). Van Houten
(1972) noted that hydrated ferric oxides are a common
constituent of savanna alluvium, and it is a savanna climate
which is indicated for the Aztec Siltstone by the kankar
('caliche'), the vein networks, and the other sedimentary
structures (Chapter 4), and by the analcime (Chapter 5).
The hydrated ferric oxide was probably derived from the
reworking of yellow or brown ferric oxide-bearing soils in ·
the source region (Van Houten, 1972).

The progressive dehydration of the free ferric oxide in
the Aztec Siltstone would have been favoured by the hot, wet
and dry savanna climate. Langmuir (1971) noted that haematite
forms separately or with goethite in soils which are alternately
wet and dry. He further stated that "in soils subject to
periodic desiccation by sunlight,hematite formation from fine-
grained goethite at the soil-air interface is accelerated by
the presence of low water vapour pressures and soil temperatures
which occasionally reach 70° to $80^{\circ}C$." Adler (1970, p.337)
also notes a hot climate as favouring the formation of
haematite, and Fischer and Schwertmann (1975) observed that
increasing temperature favours the dehydration of ferric
hydroxide to form haematite. Another condition favouring the
formation of haematite relative to goethite is an increased
absorbed Ca and Mg in the clay fraction (Taylor and Graley,
1967), a condition which is indicated for the Aztec fine-
grained lithologies by the kankar ('caliche').

The various pedogenic processes which affected the fine-grained units may also have contributed to the production and distribution of the haematite pigment. Millot (1970, p.111) notes a number of mechanisms prevailing in the reddening of soil profiles under warm hot and dry climates.

(1) The humid season guarantees hydrolysis and the release of iron.

(2) The dry season mineralizes the organic matter and fixes the iron.

(3) The result depends on the alternative action of these two seasons.

(4) The intensity of vegetation, of hydrolysis and of the release of iron will depend on the duration and temperature of the humid season.

(5) The destruction of organic matter and reddening will depend on the vigour of the dry season.

DRAB LITHOLOGIES

If the hydrated ferric oxide was deposited as an integral part of the fine-grained lithologies of the Aztec Siltstone, then the drab lithologies must have been produced from the red or potentially red, by *in situ* reduction and removal of the haematite pigment or hydrated ferric oxide. This is evidenced by the common observation, in thin section and in the field, of drab beds containing remnant haematite as isolated grains or patches of red pigment (Chapters 3 and 5). *In situ* reduction can be demonstrated to have taken place at the top and bottom of most red fine-member units (Chapters 3 and 7), and reduction spheres and zones within massive red deposits are a common feature. Further examples of post-depositional reduction occur where red intraclasts show green reduction rims (Fig. 3.8), and in vein networks where the veins have acted as channels for the downward percolation of reducing solutions which derived from overlying channel sandstones (Chapter 4 p. 67).

The bulk sediment chemistry shows that the only difference between the red and associated non-red lithologies is in the haematite content of the red (Chapter 6). This suggests that the haematite or precursory mineral was almost completely removed from the drab layers on reduction.

The feasibility of producing drab sediment from red was demonstrated by artificially reducing a red sample in the laboratory. The resultant solution of the haematite pigment exposed a typical green sediment (Chapter 5 p.144).

Some fine-grained units of the Aztec Siltstone consist of alternating, thin (less than 10 cm), red and green beds (Chapter 3 p. 23). It was observed that the colour change invariably corresponded to small grain size variations in the unit; the green beds were the coarser grained lithologies. Also, on close inspection of massive red beds containing drab layers and lenses, it was discovered that invariably the drab layer was cored by relatively coarse grained lithology. These observations suggest that reducing solutions migrated along more permeable horizons and locally removed the red haematite pigment by reduction.

The widespread post-depositional reduction of the Aztec obviously lead to considerable redistribution of iron in the fine-grained sediments. How much of the iron that was removed from the drab sediments was completely removed from the basin of deposition in groundwater systems, and how much was locally introduced into the red sediments is unknown. A number of examples of the latter i.e. localized *in situ* reddening resulting from the post-depositional introduction of iron in solution, were observed from the formation e.g. Al, unit 16, Chapter 4 p. 48, Fig. 4.5. In these samples it is thought that ferrous iron-bearing solutions, derived from the reduction of neighbouring layers, migrated into green sediments and upon oxidation precipitated ferric iron, probably as hydrated oxide which layer dehydrated to haematite pigment.

The same processes of solution and precipitation of iron through localized oxidation and reduction are responsible for the mottled red-drab patterns commonly seen in the fine-

grained lithologies of the Aztec Siltstone (Fig. 7.9). These
processes probably take place at the air/groundwater interface
and are caused through fluctuations of the water table, probably
seasonal-climate induced. They are considered to be analogous
to gleying processes in soil profiles. Included organic matter
and permeating reducing solutions have probably further
complicated the oxidation-reduction process in the Aztec
examples.

Much of the reduction of the overbank sediments probably
took place in the backswamp region of the floodbasin. Here,
the water table was high, which, on a savanna floodplain,
would have encouraged plant life and other organic activity
that in turn would have effected a reducing medium. Pluvial
ponds and ox-bow lakes were common in the backswamp region and
invariably the sediments deposited from them are reduced
(Chapter 7).

The sandstones of the Aztec Siltstone are never red, but
are either greenish grey, grey, or white. If the hydrated
ferric oxide, which penecontemporaneously gave rise to the
red pigment, was detrital then those sandstone beds containing
clay matrix might be expected to be red. However, the clay
matrix is always drab. From a study of the 'ideal' fining-
upwards cycle (Chapter 7) it has been shown that the coarse
member, channel sandstones invariably had a reducing influence
as shown by the reduced overlying and underlying fine-member
lithologies, and the included red intraclasts which commonly
have a green, reduced rim. It is suggested that whereas the
fine-grained, overbank sediments were, in most instances,
subaerially exposed above the water table for considerable
periods (between 5,000 and 50,000 years based on the kankar
('caliche') evidence, Chapter 4), so that most of the included
organic matter was oxidized, the coarse-member, channel
sandstones remained close to or below the water table (Dunbar
and Rodgers, 1957, p.215; Friend, 1966). Any organic matter
incorporated into these sandstones probably survived for a
time, thereby effecting reducing conditions. In a markedly
seasonal climate of the type suggested for the Aztec Siltstone

with an arid or semi-arid period, it is probable that plant life and therefore organic debris was concentrated in the active channel region.

It is suggested that the reduction of the iron in the sandstones took place soon after deposition, because this would be the time of greatest organic concentration and therefore greatest reducing capacity, and also because iron was still in the hydrated form. As an amorphous and poorly crystalline product it would be easily altered and dissolved.

It is concluded that the fine-grained sediments of the Aztec Siltstone included as a detrital product, an amorphous and poorly crystalline, yellow or brown hydrated ferric oxide (Fig. 9.1). Those fine-grained overbank sediments that were exposed above the water table for considerable periods (5,000 to 50,000 years) were reddened by the progressive *in situ* dehydration of their included hydrated ferric oxide to form crystalline haematite pigment. However, those sediments, including both fine member and coarse member types, that remained waterlogged, below the ground-water table, and in association with organic matter, were invariably reduced and lost their free ferric oxide in solution. The latter particularly affected the sediments of the backswamp region of the floodbasin, including the sediments of pluvial ponds and ox-bow lakes. Some later post-depositional reduction also occurred, including the reduction spheres, reduction channels, reduced burrows, reduced vein networks, and the reduced layers immediately underlying the scour surface at the base of the coarse-member, channel sandstones. *In situ* reddening by the localized introduction of iron oxide transferred from drab layers, is undoubtedly part of the process that resulted in the variegated and mottled horizons of the Aztec Siltstone.

ALLUVIUM   LITHIFIED SEDIMENT

BROWN OR YELLOW

Hydrated ferric oxide	Oxidation	Haematite
(Brown or yellow)	——————————————————→	(Red)
Illitic and Chloritic	Subaerial exposure	Illitic and Chloritic
Clays	warm temperature	Clays
(Green)	low rainfall	(Green)
	(seasonal)	
Quartz	high pH	Quartz
	high Eh	
	time, 5,000-50,000	
	years	
	no organics	

RED

reduction
water logged
high rainfall
low pH
low Eh
organics

GREY
INTERMEDIATE

LITHIFIED SEDIMENT

GREEN

| Illitic and Chloritic |
| Clays |
| Quartz |

Fig. 9.1.   Factors leading to the formation of the Aztec Siltstone
            red-beds.

CONCLUSIONS

The Aztec Siltstone is a "red-bed" sequence deposited on a broad low lying alluvial plain during Late Devonian times in southern Victoria Land, Antarctica. The following conclusions have been drawn from this study.

(1) The formation has a maximum thickness of 217 m but has been eroded at the top by the Carboniferous (?)-Early Permian continental glaciation. The erosion bevelled the formation by planing increasingly greater amounts off the more northerly sections, and locally cut a deep valley into the formation.

(2) The formation consists of an interbedded sequence of sandstone (50 percent of the formation), siltstone, and claystone. Locally it contains minor beds of carbonaceous siltstone and claystone, limestone, and intraformational conglomerate. The sandstone is quartzarenite with detrital grains consisting mainly of plutonic quartz with minor chert, feldspar, metamorphic quartz, and a trace of heavy minerals. Sandstone textures average fine-grained and well sorted, although sandstone with textural inversion is common. The latter resulted largely from sediment-mixing including bioturbation, pedogenesis, post-depositional translocation of clays from interbedded fine-grained units, and possibly minor aeolian effects. Some of the textural inversion also arose from the reworking of quartzarenite from the source area.

(3) The Aztec Siltstone is considered to be of non-marine origin for several reasons.

(a) Fining-upwards sedimentary cycles are characteristic of fluvial deposition.

(b) The carbon and oxygen isotope compositions are strongly non-marine in character.

(c) Conchostracans, which are found in the formation, are non-marine invertebrates.

(d) The fish species that are found in the formation are fresh-water types, although they may have had a marine tolerance.

(e) The strontium isotope evidence is consistent with a non-marine origin.

(f) Red beds of Devonian and younger age are most commonly of non-marine origin.

(g) The soil features including the kankar ('caliche'), mudcracks, rain impressions, and the red beds, denote a terrestrial environment with extended subaerial exposure.

(h) The association of roots, plant matter and spores in the formation suggests a terrestrial environment.

(4) The Aztec Siltstone was deposited from highly sinuous (tortuous), meandering streams that criss-crossed the broad low lying alluvial plain. These streams probably had an average depth of 1 to 2 m and a width in the range 3 to 77 m. The streams characteristically gave rise to fining-upwards cycles of sedimentation consisting of laterally accreted channel sandstones deposited by point bar migration, and vertically accreted overbank sediments which were carried as suspended load into the floodbasins during floods. Some overbank deposition of bed load material formed levees, and stream avulsion and crevassing during flood stage produced crevasse-splay deposits.

The 'ideal' fining-upwards cycle, determined by Markovian analysis, consists of a basal laterally accreted fine to medium channel sandstone overlain by a unit of green fine-grained vertically accreted overbank sediment which contains a thin interbed of very fine to fine sandstone of levee or crevasse-splay origin. The green siltstone or claystone is followed by red siltstone or claystone that is invariably capped by green siltstone or claystone produced by post-depositional reduction of the red.

(5) Some of the streams on the Aztec alluvial plain at times became entrenched, and with gradual subsidence, maintained a steady deposition of sandstone, thus building up thick sequences of sandstone (multistorey sandstone bodies). Some of the thick fine-grained deposits also resulted from stream entrenchment.

The erosive ability of streams on the Aztec alluvial plain is attested by a scour surface at the base of most channel sandstone beds and cutting into the fine-grained lithologies of the underlying cycle. Siltstone clasts as eroded products (intraformational conglomerate or channel lag) lie in the swales and troughs of the erosional surface.

(6) Stream diversion or avulsion gave rise to a vertical profile that deviates from the 'ideal' fining-upwards cycle, and generated the discrete or isolated channel sandstone units of the formation. Avulsion occurred during exceptionally high flood conditions, and is largely an autocyclic phenomenon, although some allocyclic factors probably had some influence.

The overall bimodal sandstone-siltstone distribution with time through the Aztec suggests that allocyclic mechanisms, possibly of tectonic or base-level control, did affect the deposition. Climate changes sufficient to have influenced discharge and thus sedimentation to the degree observed, appears unlikely because there is no observable change with time in the proportion of red beds in the formation, as would be expected from such marked climatic variations.

(7) The interchannel, floodbasin areas were the sites of deposition of the fine-grained deposits consisting mainly of clay-rich overbank sediments. Other floodbasin sediments include some lacustrinal deposits from pluvial ponds and ox-bow lakes, and palustrinal deposits from the backswamps.

(8)   Subaerial exposure was a feature of the floodbasin
sediments, with the exception of those in the low-lying
areas, at or below the ground-water table e.g. the
backswamp, lake or pond areas. Those floodbasin
sediments which had a relatively high relief, on
alluvial ridges and terraces, a good drainage (probably
aided by underlying permeable sandstone lithologies)
and thus a low ground-water table, were oxidized, and
where these conditions were maintained for considerable
periods, these sediments underwent soil development.
Other overbank sediments which remained near or below
the ground-water table, developed reducing conditions,
fostered by the incorporation of organic debris.

(9)   The kankar ('caliche') suggests that there was a period
of prolonged subaerial exposure and soil development
which followed the deposition of the fine member of the
fining-upwards alluvial cycles. This period probably
extended from 5,000 to 50,000 years.

(10) Soil development in many of the fine member, overbank
sediments is indicated by a number of factors.

    (a) Calcareous nodules are analogous to the kankar
        ('caliche') of modern Pedocal soils

    (b) The chemistry of some fine member sequences is
        analogous to that in many of the 'red-earth',
        'red-brown earth', 'calcareous red earth', or
        'red or brown clay' soils of Australia. The
        chemistry includes (i) the bulk sediment major
        element chemistry, and (ii) the down-profile major
        element variations. The latter shows the
        illuviation of clays, the translocation and
        deposition of carbonates, and the mobilization
        and segregation of iron and manganese oxides.

        The carbon isotope values of the carbonate nodules
        are consistent with their being pedogenic carbonates.

    (c) The micromorphological fabric of many of the fine-
        grained overbank sediments is similar to that in
        modern soils and includes free or embedded grain

argillans, ferri-argillans, sepic plasmic fabric
(commonly lattisepic), skew-planes and haematans.

(d) Wavey or pseudo-bedding in some fine member units
     is analogous to the gilgai soil phenomenon.

(e) Roots and associated plant fragments and spores in
     some fine member units indicate soil formation.

(f) Vein networks are comparable with soil features.

(g) The analcime is possibly a soil product.

(h) Quartz grain solution embayments in the fine-grained
     lithologies are possibly related to soil conditions.

(11) The change in sedimentation from the Beacon Heights
      Orthoquartzite that conformably underlies the Aztec
      Siltstone, to the Aztec itself, corresponds to a change
      from braided to meandering stream deposition. This
      change was undoubtedly influenced by the establishment
      of evolving vegetation on the alluvial plain that
      stabilized the sediments and aided soil processes.
      However, major floods would have caused periodic
      flushing of sediment from the system, thereby aiding
      the creation of the sedimentary cycles.

(12) The climate of the Late Devonian in southern Victoria
      Land, Antarctica, is thought to have been hot, and
      seasonally wet and dry (savanna climate). This is
      indicated by numerous factors.

(a) The kankar ('caliche') is a valuable palaeoclimatic
     indicator that suggests a hot and markedly seasonal
     climate, with an arid or semi-arid period and an
     annual rainfall of less than 65 cm.

(b) The Aztec soils have an analogous chemistry to that
     for Australian Pedocal soils that formed under
     savanna climates.

(c) Vein networks are the product of deep vertical
     cracks in the soils of regions having a hot and
     strongly seasonal climate with an arid or semi-arid
     period.

(d) Mudcracks, including syneresis cracks, are consistent
     with the savanna climate model.

(e)   Rain impressions are most commonly found in the
       sediments of pluvial ponds and ephemeral streams
       of seasonally arid or semi-arid regions.

       Temporary aridity is suggested for the Aztec climate
by the isolated occurrence of syneresis cracks that were
formed in saline lakes, analcime in pisolites and soil
matrix, and primary gypsum lenses. Temporary, possibly
seasonal aridity is also indicated by the occurrence of
concentrations of unreworked fossil fish material.
These deposits probably resulted from the concentrating
of living fish as streams and ponds dried up.

(13)   The red lithologies of the formation are invariably fine-
       grained overbank sediments; the sandstones are either
       grey or white but never red. The compositional variation
       between red and associated drab samples is simply a
       product of the haematite content of the red; both
       contain very similar proportions of the other minerals,
       namely clays and quartz grains. The colour of the
       green lithologies is caused by the green illitic and
       chloritic clay matrix, but this green is suppressed by
       the haematitic pigment in the red sediments. The grey
       lithologies of the formation are transitional lithologies
       in that they contain a low concentration of haematite
       pigment.

(14)   Reddening of the Aztec Siltstone was a penecontemporaneous
       process that took place in the floodbasin sediments
       during their prolonged subaerial exposure. The haematite
       pigment was derived largely from the *in situ* and
       progressive dehydration of detrital amorphous and poorly
       crystalline brown hydrated ferric oxide, in those sedi-
       ments which maintained an oxidizing environment.
       Sediments which remained in a water-logged state, below
       the ground-water table, and in association with organic
       matter, were invariably reduced and lost their free
       ferric oxide in solution. Later post-depositional
       reduction of some red beds produced reduction spheres
       and channels, reduced burrows and vein networks, and the

reduced layers immediately underlying the scoured surface at the base of the coarse member channel sandstones. Some chemical redistribution of iron contributed to the variegated and mottled horizons of the formation.

(15) Rounded quartz overgrowths, textural inversion, chert grains, diverse types of quartz, a high degree of grain rounding and the presence of only ultra-stable heavy minerals, are features of the quartzarenites of the Aztec Siltstone which together suggest a sedimentary source rock for the formation. The palaeocurrent directions indicate that the source region was to the southwest of the present outcrop area, and in the direction of the East Antarctic Craton which now lies beneath the Polar Plateau.

The strontium isotope data suggest an age for the source material of the formation of from 2.7 to 3.45×10^9 years. Ages in this range have been found for the igneous and metamorphic basement rocks exposed along the coast of East Antarctica. As the mixed types of quartz grains in the formation also indicate a mixed igneous and metamorphic terrain as the original source material, it is probable that the original provenance of the Aztec Siltstone was the East Antarctic Shield.

Appendix Table 1.   Textures of the thin sectioned
                     lithologies of the Aztec Siltstone.

The grain size of all samples thin sectioned was
determined approximately, by measuring 20 grains chosen to
be representative of the mean. The values were then corrected
to sieve equivalents (Adams, 1974). The sandstone mean grain
size, obtained by averaging all 'approximate' values, is the
same as that obtained from the detailed grain size analysis
of 11 sandstones (p.264). This establishes that the
approximating method is reasonably accurate.

The sorting for sandstones has been expressed by the
Folk (1968) classification, and for the finer-grained
lithologies the classification of Picard (1971) has been
employed. Picard's classification assigns good sorting to
those rocks that contain more than 90 percent silt or clay
sized material, fair to those that contain 75 to 90 percent
silt or clay, and poor to those containing less than 75 percent
silt or clay.

Maturity indices apply to sandstones only.

Abbreviations

ClSt = claystone   SiClSt= silty claystone
SClSt = sandy claystone   ClMSt = clayey mudstone

etc.

$\bar{X}_s$ = mean sphericity $\bar{X}_r$ = mean roundness

x = clay present as a mode, in a percentage greater than
     5 percent.

p = poor   F = fair   G = good   Ws = well sorted
MWs = moderately well sorted   Sm = supermature
Text.in. = textural inversion.

Sample	Lithology	Colour	Sand Grains $\bar{X}_s$	$\bar{X}_r$	Silt Grains $\bar{X}_s$	$\bar{X}_r$	Modes (φ units) sand	silt	clay	Sorting	Maturity
					Section A4						
23174	SiClSt	10GY 5/2	0.68	0.32	0.9	0.2	4.0	5.0	x	P	–
23175	SSt	5YR 8/1	0.84	0.75	–	–	2.5	–	–	Ws	Sm
23182	SClSt	5GY 8/1	0.73	0.22	0.9	0.2	3.1	5.8	x	P	–
*23183	SSt	5R 8/2	0.66	0.34	–	–	4.0	–	–	Ws	Sm
23184	ClMSt	5G 7/1	–	–	0.7	0.3	–	5.0	x	P	–
			0.73	0.41	0.8	0.2					
	Sandstones		0.84	0.75			23182 size/rounding inversion				
	Fine-grained liths.		0.70	0.27			(*not incl.) 23183 orientated parallel to bedding				
					Section A1						
23228	SiClSt	1OR 4/2	–	–	0.7	0.3	–	4.6	x	P	–
23230	"	N5	–	–	0.7	0.3	–	5.3	x	P	–
23233	ClSt	5G 6/1	–	–	0.7	0.3	–	6.0	x	F	–
23234	SSt	5R 8/2	0.70	0.43	–	–	4.0	–	–	Ws	Sm
23235	ClSiSt	5G 6/1	–	–	0.7	0.1	–	4.6	x	P	–
23235A	SiClSt	1OR 4/2	–	–	0.7	0.2	–	6.0	x	P	–
23237	SiClSt	"	–	–	0.6	0.1	–	6.0	x	P	–
23238	ClMSt	5B 7/1	–	–	0.7	0.1	3.6	4.7	x	P	–
23240	ClMSt	5G 6/1	–	–	0.7	0.1	3.0	6.0	x	P	–
23241	SSt	1OR 8/2	0.72	0.51	–	–	3.6	–	–	Ws	Sm
23243	ClSt	1OR 3/4	–	–	0.9	0.3	–	4.4	x	P	–
23244	ClSt	5P 4/2	–	–	0.7	0.3	–	5.0	x	F	–
23246	SSt	5R 8/2	0.66	0.32	–	–	3.0	–	–	Ws	Sm
23249	SiClSt	5G 8/1	0.65	0.43	0.7	0.3	2.7	5.8	x	P	–
23250	SSt	N8	0.72	0.63	–	–	2.7	–	–	Ws	Sm
			0.69	0.46	0.7	0.2					
	Sandstones		0.72	0.57							
	Fine-grained liths.		0.65	0.43							
					Section M1						
23254	SSt	N8	0.85	0.79	–	–	1.7	–	–	Ws	Sm
23256	SiClSt	1OR 4/2	0.74	0.37	0.7	0.1	3.4	6.0	x	P	–
23260	ClSt	1OR 4/2	–	–	–	–	x	x	x	F	–
23281	ClSt	5GY 8/1	–	–	–	–	–	–	x	G	–
			0.80	0.58	0.7	0.1					
	Sandstones		0.85	0.79							
	Fine-grained liths.		0.74	0.37							
					Section P1						
*23299	SSt	5Y 8/1	0.79	0.74	–	–	0.7	–	–	Ws	Sm
23301	SSt	"	0.70	0.72	–	–	0.7	–	–	Ws	Text.in.
"			0.84	0.82			1.6				
23304	SiClSt	5GY 6/1	0.79	0.70	0.9	0.3	2.4	5.4	x	P	–
23310	ClSt	5GY 6/1	–	–	0.9	0.3	–	5.2	x	G	–
23315	SSt	N9	0.83	0.84	–	–	1.7	–	–	Ws	Sm
23316	SiClSt	5GY 6/1	0.76	0.66	0.7	0.1	2.7	5.0	x	P	–
23319	SSt	5GY 8/1	0.81	0.61	–	–	3.0	–	–	Ws	Sm
23321	ClMSt	"	0.68	0.44	0.9	0.2	2.9	5.7	x	P	–
			0.78	0.69	0.8	0.2					
	Sandstones		0.79	0.79			*Beacon Heights Orthoquartzite				
	Fine-grained liths.		0.76	0.60			23301 Two quartz sand size modes				
					Section P4						
*23412	SSt	N9	0.83	0.75	–	–	0.7	–	–	Ws	Sm
"			"	"			1.7				
*23413	SSt	"	0.82	0.78	–	–	1.7	–	–	Ws	Sm
			0.82	0.76							
23414	SSt	"	0.78	0.67	–	–	2.7	–	–	Ws	Sm
			0.78	0.67							
	Sandstones		0.78	0.67			* Beacon Heights Orthoquartzite				
	Fine-grained liths.		–	–							

263.

Sample	Lithology	Colour	Sand Grains $\bar{X}_s$	$\bar{X}_r$	Silt Grains $\bar{X}_s$	$\bar{X}_r$	Modes (φ units) Sand	Silt	Clay	Sorting	Maturity
						Section L1					
*23421	SSt	5Y 8/1	0.64	0.54	-	-	3.4	-	x	P	Text.in.
			0.64	0.54							
23422	ClSt	N2	-	-	0.7	0.3	-	4.6	x	F	-
23429	"	N1	-	-	0.8	0.3	-	6.0	x	F	-
23430	ClSSt	5Y 8/1	0.72	0.62	-	-	3.4	-	x	P	Text.in.
23432	SiClSt	5R 4/2	0.74	0.62	0.7	0.3	2.7	5.0	x	P	-
23433	ClMSt	5G 8/1	-	-	0.7	0.2	x	x	x	P	-
23437	ClSt	5GY 6/1	-	-	0.7	0.2	-	4.9	x	F	-
23438	ClSSt	5Y 8/1	0.77	0.71	-	-	1.7	-	x	P	Text.in.
"			0.70	0.39			3.1				
23440	SiClSt	5GY 7/2	-	-	0.9	0.3	-	5.7	x	P	-
			0.73	0.58	0.8	0.3					
Sandstones			0.72	0.62			* Beacon Heights Orthoquartzite				
Fine-grained liths.			0.74	0.57			23438 Two quartz sand size modes				
						Section L2					
*23450	SSt	N9	0.79	0.72	-	-	2.1	-	-	Ws	Sm
*23452	SSt	"	0.80	0.74	-	-	2.4	-	-	Ws	Sm
			0.80	0.73							
23453	SiClSt	5GY 6/1	0.80	0.59	0.7	0.3	2.7	5.4	x	P	-
23458	SSt	N8	0.78	0.75	-	-	2.7	-	-	Ws	Sm
23461	ClSSt	5Y 7/2	0.75	0.57	-	-	3.7	5.0	x	P	Text.in.
			0.78	0.64	0.7	0.3					
Sandstones			0.78	0.75			* Beacon Heights Orthoquartzite				
Fine-grained liths.			0.78	0.58							
						Section B2					
*23570	SSt	N9	0.82	0.81	-	-	2.7	-	-	Ws	Sm
*23573	"	"	0.83	0.81	-	-	1.6	-	-	Ws	Sm
*23575	"	"	0.81	0.84	-	-	2.4	-	x	P	Text.in.
*23576	ClSt	5GY 8/1	0.76	0.68	0.7	0.3	2.1	5.0	x	F	-
*23578	SSt	N9	0.80	0.81	-	-	2.7	-	-	Ws	Sm
			0.80	0.79	0.7	0.3					
23579	ClSt	1OR 4/2	0.81	0.71	0.7	0.3	2.1	5.7	x	F	-
"	ClSSt	5GY 6/1	0.75	0.48	-	-	4.0	-	x	P	Text.in.
23581	SSt	5GY 8/1	0.84	0.78	-	-	1.3	-	-	P	Text.in.
"			0.71	0.50			2.9				
23582	SClSt	N9	-	-	-	-	x	x	x	P	-
23584	SClSt	1OR 4/2	0.84	0.68	0.7	0.5	2.1	5.0	x	P	-
"			0.72	0.48			3.1				
23586	SSt	N9	0.83	0.78	-	-	2.4	-	-	Ws	Sm
23588	"	"	0.81	0.80	-	-	2.4	-	-	Ws	Sm
			0.79	0.65	0.7	0.4					
Sandstones			0.80	0.72			* Beacon Heights Orthoquartzite				
Fine-grained liths.			0.78	0.59			23581 Two well sorted and well rounded modes				
						Section H6					
25138	SSt	5GY 6/1	-	-	-	-	1.3	-	-	Ws	Sm
25140	"	5Y 8/1	-	-	-	-	2.7	-	-	MWs	Sm
25144	"	N9	-	-	-	-	2.4	-	-	Ws	Sm

Appendix Table 2. Grain size data based on grain measurements in thin section. The graphic mean (M_z), and the inclusive graphic standard deviation (σ_I) (Folk, 1968) were determined from a cumulative curve, using a probability ordinate, based upon the below listed data. The M_z and σ_I values have been converted to sieve equivalents by the method of Adams (1974).

Sample No.	Cumulative percentages, with class boundaries in phi units												M_z	σ_I (φ units)
	-½	0	+½	+1	+1½	+2	+2½	+3	+3½	+4	+4½	+5		
*23575	-	-	-	95.0	71	38	13	5	2.5	0.6	0.1	-	2.22	0.49
23175	-	-	-	99.0	79	33	4	1	0.45	0.13	0.02	-	2.22	0.32
23183	-	-	-	-	-	-	96.5	75	36	9.0	2.5	1	3.72	0.40
23234	-	-	-	-	-	98.4	77	42	11	1.6	0.02	-	3.28	0.42
23241	-	-	-	-	99.99	97.0	76	44	16	3.2	0.2	0.03	3.32	0.46
23246	-	-	-	-	-	97.5	73	31	7.5	1.8	0.3	0.01	3.18	0.35
23301	99.1	96.0	90.0	76	52	22	7.5	0.65	-	-	-	-	1.89	0.60
23315	-	-	99.92	95.0	68	22	4	0.55	0.05	-	-	-	2.10	0.34
23414	-	-	-	-	-	97.0	68	16	0.4	-	-	-	3.06	0.28
23430	-	-	-	-	-	98.8	88	65	30	10	0.8	0.02	3.62	0.48
23581	99.6	98.8	97	93	83	75	57	37	7.5	0.5	-	-	2.87	0.73
23586	-	-	-	97.5	73	26	1.5	-	-	-	-	-	2.16	0.31

* Beacon Heights Orthoquartzite

Appendix Table 3.　Thickness variations in the fining-upwards
sequences of the Aztec Siltstone.

Section	Coarse Member (m)	Fine Member (m)	Total (m)
A4	4.7	2.0	6.7
A1	0.9	1.3	2.2
"	0.7	4.4	5.1
"	3.2	3.7	6.9
"	4.7	2.4	7.1
A2	3.4	0.8	4.2
M1	4.6	6.0	10.6
"	4.0	1.5	5.5
"	4.6	3.8	8.4
P1	7.5	1.6	9.1
"	6.0	0.6	6.6
"	3.3	5.8	9.1
L1	3.9	11.8	15.7
L2	7.6	3.7	11.3
"	3.0	3.8	6.8
"	3.9	5.1	9.0
"	10.4	10.3	20.7
S9	1.3	2.0	3.3
Means =	4.3	3.9	8.2

Appendix Table 4.   Field location of samples collected during the
                      1973-74 field season.   The locations are given with
                      reference to the section descriptions in Askin *et al.*
                      1971, and Barrett and Webb 1973.

Sample	Section	Location	Description
A1-05	A1	Unit 1	Red and green siltstone
A1-15	A1	Unit 16	Red siltstone
A1-16	A1	" "	Green siltstone
L1-12	L1	Unit 17	Red siltstone

Samples a to d were taken at 0.7 m vertical intervals, down the unit.

L1-13	L1	Unit 17	Red siltstone

A duplicate of the profile sampling done for L1-12, 2 m horizontal
distance from L1-12.

L1-19	L1	Unit 26 upper 2 m	Red and green siltstone
L2-13	L2	Unit 24	
L2-16	L2	Unit 3	
AZ-06	AZ Section 18	10 m from base of Aztec Siltstone	Red siltstone
AZ-07	" "	" "	Green siltstone
AZ-17,18,19,20	AZ Section 17	0.4 m from base of Aztec Siltstone	Red siltstone AZ-17 is green

Samples taken at 0.4 m vertical intervals down the unit.

REFERENCES

Adams, J. E. 1974: Empirical determination of sieve size
    statistics from grain measurement. Unpublished M.Sc.
    thesis, Victoria University of Wellington, N.Z. 155 p.

Adler, H. H. 1970: Interpretation of colour relations in
    sandstone as a guide to uranium exploration and ore
    genesis. Panel Proc. Int. At. Energ. Ag., Vienna,
    pp.331-344.

Alexander, C. S. and Prior, J. C. 1971: Holocene sedimen-
    tation rates in overbank deposits in the Black Bottom
    of the lower Ohio River, Southern Illinois. Am. J. Sci.
    270: 361-372.

Allen, A. D. 1962: Geological investigations in south
    Victoria Land. Part 7 - Formations of the Beacon Group
    in the Victoria Valley region. N.Z. J. Geol. Geophys.
    5 (2): 278-294.

Allen, J.R.L. 1962a: Intraformational conglomerates and
    scoured surfaces in the Lower Old Red Sandstone of the
    Anglo-Welsh Cuvette. Liverpool Manchester Geol. J.
    3: 1-20.

_____ 1962b: Petrology, origin and deposition of the
    highest Lower Old Red Sandstone of Shropshire, England.
    J. Sed. Pet. 32 (4): 657-697.

_____ 1963a: The classification of cross-stratified
    units, with notes on their origin. Sedimentology 2:
    93-114.

_____ 1963b: Depositional features of Dittonian rocks:
    Pembrokeshire compared with the Welsh Borderland.
    Geol. Mag. 100: 385-400.

_____ 1963c: Asymmetrical ripple marks. Liverpool
    Manchester Geol. J. 3 (2): 187-236.

_____ 1964a: Studies in fluviatile sedimentation: Six
    cyclothems from the Lower Old Red Sandstone, Anglo-Welsh
    Basin. Sedimentology 3: 163-198.

_____ 1964b: Primary current lineation in the Lower Old
    Red Sandstone (Devonian), Anglo-Welsh Basin.
    Sedimentology 3: 89-108.

Allen, J.R.L., 1964c: Sedimentation in the modern delta of the River Niger, West Africa. in L.M.J.U. Van Straaten (Ed.), "Deltaic and Shallow Marine Deposits". Elsevier, Amsterdam, 26-34.

_____ 1965a: A review of the origin and characteristics of recent alluvial sediments. Sedimentology, 5: 89-191.

_____ 1965b: Sedimentation and palaeogeography of the Old Red Sandstone of Anglesey, North Wales. Yorkshire Geol. Soc. Proc., 35: 139-185.

_____ 1965c: Fining-upwards cycles in alluvial successions. Liverpool Manchester Geol. J., 4: 229-246.

_____ 1965d: Late Quaternary Niger delta, and adjacent areas: sedimentary environments and lithofacies. Bull. Am. Assoc. Petrol. Geologists 49: 547-600.

_____ 1966: On bed forms and paleocurrents. Sedimentology 6: 153-190.

_____ 1970: Studies in fluviatile sedimentation: A comparison of fining upwards cyclothems, with special reference to coarse-member composition and interpretation. J. Sed. Pet., 40: 298-323.

_____ 1974a: Sedimentology of the Old Red Sandstone (Siluro-Devonian) in the Clee Hill Area, Shropshire, England. Sed. Geol. 12: 73-167.

_____ 1974b: Studies in fluviatile sedimentation: lateral variation in some fining-upwards cyclothems from the Red Marls, Pembrokeshire. Geol. J. 9 (1).

_____ 1974c: Studies in fluviatile sedimentation: implications of pedogenic carbonate units, Lower Old Red Sandstone, Anglo-Welsh outcrop. Geol. J. 9 (2): 181.

Allen, J.R.L. and Friend, P. F. 1968: Deposition of the Catskill Facies, Appalachian region: with notes on some other Old Red Sandstone basins. Geol. Soc. Amer. Special Paper 106, 21-74.

Allis, R., Cramp, J., Hunt, T., Keys, J.R. and Kyle, P. R. 1973: Immediate report of Victoria University of Wellington Antarctic Expedition, 1972-73. Victoria University of Wellington, N.Z. 39 p.

Arnborg, L. 1957: Erosion forms and processes on the bottom of the River Ångermanälven. Geogr. Annlr. 39: 32-47.

Askin, R. A., Barrett, P. J., Kohn, B. P. and McPherson, J. G. 1971: Stratigraphic sections of the Beacon Supergroup (Devonian and older (?) to Jurassic) in south Victoria Land. Victoria University of Wellington Antarctic Data Series No.2 (Ed. P. J. Barrett), 88 p.

Askin, R. A., Barrett, P. J., Kyle, P. R. and Laird, M. G. 1972: Immediate report of Victoria University of Wellington Antarctic Expedition 1971-72. Victoria University of Wellington, N.Z. 37 p.

Bailey, E. G. 1926: Subterranean penetration by a desert climate. Geol. Mag.,63: 276-280.

Balme, B. G. 1962: Upper Devonian (Frasnian) spores from the Carnarvon Basin, Western Australia. Palaeobotanist 9: 1-10.

Barnes, R. D. 1963: "Invertebrate Zoology" W. B. Saunders Company, Philadelphia-London. 632 p.

Barrell, Joseph,1908: Relations between climate and terrestrial deposits. J. Geol. 16: 159-190, 255-295, 363-384.

Barrett, P. J. 1972: Stratigraphy and paleogeography of the Beacon Supergroup in the Transantarctic Mountains, Antarctica. In Haughton, S. H. (Ed.) Second Gondwana Symposium, S. Africa, 1970, Proceedings and Papers, 249-256.

Barrett, P. J. and Kohn, B. P. 1971: Immediate report of Victoria University of Wellington Antarctic Expedition, 1970-71. Victoria University of Wellington, N.Z. 24 p.

_____ 1975: Changing sediment transport directions from Devonian to Triassic in the Beacon Supergroup of south Victoria Land, Antarctica. In Campbell, K.S.W. (Ed.) Third Gondwana Symposium, Canberra, Australia 1973, Papers, 15-35.

Barrett, P. J., Kohn, B. P., Askin, R. A. and McPherson, J. G. 1971: Preliminary report on Beacon Supergroup studies between the Hatherton and MacKay Glaciers, Antarctica. N.Z. J. Geol. Geophys. 14 (3): 605-614.

Barrett, P. J. and Kyle, R. A. 1975: The Early Permian glacial beds of south Victoria Land and the Darwin Mountains, Antarctica. In Campbell, K.S.W. (Ed.). Third Gondwana Symposium, Canberra, Australia 1973, Papers. 333-346.

Barrett, P. J. and Webb, P. N. 1973: Stratigraphic sections of the Beacon Supergroup (Devonian and older (?) to Jurassic) in south Victoria Land. Victoria University of Wellington Antarctic Data Series No.3. 165 p.

Beerbower, J. R. 1964: Cyclothems and cyclic depositional mechanisms in alluvial plain sedimentation. Kansas Geol. Surv. Bull. 169 (1): 31-42.

Berner, R. A. 1969: Goethite stability and the origin of red beds. Geochim. Cosmochim. Acta 33 (2): 267-273.

_____ 1971: "Principles of Chemical Sedimentology" McGraw Hill. 240 p.

Billingsley, P. 1961: Statistical methods in Markov chains. Ann. Math. Statist. 32: 12-40.

Biscaye, P. E. 1964: Distinction between kaolinite and chlorite in recent sediments of x-ray diffraction. Amer. Mineralogist, 49: 1287-1289.

Blackett, P.M.S. 1956: Lectures on rock magnetism. Jerusalem: Weizmann Science Press. 131 p.

Bosworth, T. O. 1907: The origin of the upper Keuper of Leicestershire. Geol. Mag., 44: 460-461.

_____ 1912: The Keuper Marl around Charnwood. Leicester: W. Thornby & Son.

Brewer, R. 1964: "Fabric and Mineral Analysis of Soils". John Wiley & Sons Inc., N.Y. 470 p.

Bruck, P. M., Dedman, R. E. and Wilson, R.C.L. 1967: The New Red Sandstone of Raasay and Scalpay, Inner Hebrides. Scot. J. Geol. 3 (2): 168-180.

Buol, S. W. 1965: Present soil-forming factors and processes in arid and semi-arid regions. Soil Sci. 99: 45-49.

Burgess, I. C. 1961: Fossil soils of the Upper Old Red Sandstone of south Ayrshire. Trans. Geol. Soc. Glas. 24: 138-153.

Burst, J. F. 1965: Subaqueously formed shrinkage cracks in clay. J. Sed. Pet. 35: 348-353.

Campbell, A. S. and Fyfe, W. S. 1965: Analcime-albite equilibria. Amer. J. Sci. 263: 807-816.

Chukhrov, F. V. 1973: On mineralogical and geochemical criteria in the genesis of red beds. Chem. Geol. 12: 67-75.

Clarke, F. W. 1924: Data of geochemistry. U.S.G.S. Bull. 770.

Clayton, R. N. and Degens, E. T. 1959: Use of carbon isotope analyses of carbonates for differentiating fresh-water and marine sediments. Bull. Amer. Assoc. Petrol. Geologists 43: 890-897.

Coleman, J. M. 1969: Brahmaputra river: channel processes and sedimentation. Sed. Geol. 3: 129-239.

Coombs, D. S. 1953: The pumpellyite mineral series. Min. Mag. 30: 113.

_____ 1971: Present status of the zeolite facies. In 'Advances in Chemistry Series' No.101 "Molecular Sieve Zeolites - I", 317-327.

Cosgrove, M. E. 1973: The geochemistry and mineralogy of the Permian Red Beds of S.W. England. Chem. Geol. 11: 31-47.

Craig, Harmon, 1957: Isotopic standards for carbon and oxygen and correction factors for mass-spectrometric analysis of carbon dioxide. Geochim. Cosmochim. Acta 12: 133.

Creer, K. M., Irving, E. and Runcorn, S. K. 1954: The direction of the geomagnetic field in remote epochs in Great Britain. J. Geomagn. Geoelect., Kyoto 6: 163-168.

Crump, J., Keys, J. R., Kyle, P. R., Kyle, R. A., Luckman, P., McPherson, J. G., Plume, R. and Rowe, G. Immediate report of Victoria University of Wellington Antarctic Expedition, 1973-74. Victoria University of Wellington, N.Z. 28 p.

Davidson, C. 1891: Work done by lob worms. Geol. Mag. 28: 489-493.

Dawson, J. W. 1848: On the colouring matter of red sandstones and of greyish and white beds associated with them. Quart. J. Geol. Soc. Lond. V: 29.

Debenham, F. 1921: The sandstone etc of the McMurdo Sound, Terra Nova Bay, and Beardmore Glacier regions. Nat. Hist. Rep. Brit. Antarct. (Terra Nova) Exped. 1910 Geology 1 (4a): 103-119.

272.

Deer, W. A., Howie, R. A. and Zussman, J. 1966:   An
    introduction to the rock-forming minerals.
    Longmans, Green & Co. Ltd. London. 528 p.

Degens, E. T. and Epstein, S. 1964:   Oxygen and carbon isotope
    ratios in coexisting calcites and dolomites from recent
    and ancient sediments. Geochim. Cosmochim. Acta 28:
    23-44.

Dennison, J. M. and Shea, J. H. 1966:   Reliability of visual
    estimates of grain abundance. J. Sed. Pet. 36: 81-89.

Dixon, E.E.L. 1921:   Geology of the South Wales Coalfield.
    Pt 13.   The country around Pembroke and Tenby.
    Geol. Surv. Gt Britain Mem., 220 p.

Dodd, J. Robert, and Stanton, Robert J. 1975:   Paleosalinities
    within a Pliocene Bay, Kettleman Hills, California:
    A study of the resolving power of isotopic and faunal
    techniques. Geol. Soc. Amer. Bull. 86: 51-64.

Doeglas, D. J. 1962:   The structure of sedimentary deposits
    of braided streams. Sedimentology 1: 167-190.

Donovan, R. N. and Foster, R. J. 1972:   Subaqueous shrinkage
    cracks from the Caithness Flagstone Series (Middle
    Devonian) of Northeast Scotland. J. Sed. Pet. 42:
    309-317.

Dontsova, E. I., Migdisov, A. A. and Ronov, A. B. 1972:
    On the causes of variation of oxygen isotopic composition
    in the carbonate strata of the sedimentary column.
    Geochem. Internat. (trans. from Geokhimiya 11: 1317-1324).

Dorsey, G. E. 1926:   The origin of the colour of red beds.
    J. Geol. 34: 131-143.

Dunbar, C. O. and Rodger, J. 1957: "Principles of Stratigraphy.
    John Wiley & Sons, New York. 356 p.

Echle, W. 1961:   Mineralogische Untersuchungen an Sedimenten
    des Steinmergelkeupers und der Roten Wand aus der
    Umgebung von Gottingen. Beitr. Mineral. Petrog. 8: 28.

Eichhoff, H. J. and Reineck, H. E. 1953:   Sekundäre
    verfärbungen durch herausläsen von hämatit aus
    geoteinen. Neues Jb. Miner. Mh. 11-12: 315-324.

Faure, G. and Barrett, P. J. 1973: Strontium isotope compositions of non-marine carbonate rocks from the Beacon Supergroup of the Transantarctic Mountains. J. Sed. Pet. 43: 447-457.

Ferrar, H. T. 1907: Report on the field geology of the region explored during the 'Discovery' Antarctic Expedition, 1901-04. Nat. Hist. Rep. Nat. Antarct. Exped. 1 (Geology): 1-100.

Fischer, W. R. and Schwertmann, U. 1975: The formation of hematite from amorphous iron(III) hydroxide. Clays and Clay Minerals 23: 33-37.

Fisk, H. N. 1944: Geological investigations of the alluvial valley of the lower Mississippi river. Mississippi River Commission, Vicksburg, Miss.

_____ 1947: Fine grained alluvial deposits and their effects on Mississippi River activity. Mississippi River Commission, Vicksburg, Miss.

Flanagan, F. J. 1969: U.S. Geological Survey standards - II. First compilation of data for the new U.S.G.S. rocks. Geochim. Cosmochim. Acta 33: 81-120.

Fletcher, F. W. and Woodrow, D. L. 1970: Geology and economic resources of the Pennsylvania portion of the Milford and Port Jervis fifteen-minute quadrangles. Penn. Geol. Surv. Atlas 223: 64 p.

Folk, R. L. 1960: Petrography and origin of the Tuscarora, Rose Hill, and Keefer formations, lower and middle Silurian of eastern West Virginia. J. Geol. Pet. 30: 1-58.

_____ 1962: Petrography and origin of the Silurian Rochester and McKenzie shales, Morgan County, West Virginia. J. Sed. Pet. 32: 539-578.

_____ 1968: "Petrology of Sedimentary Rocks". Hemphill's, Univ. of Texas. 170 p.

Folk, R. L. and Ward, W. C. 1957: Brazos River bar, a study in the significance of grain-size parameters. J. Sed. Pet. 27: 3-27.

Frass, E. 1899: Die Bildung des germanischen Trias, eine
    petrogenetische Studie. Jh. Ver. vaterl. Naturk.
    Württemb. 55: 37-100.

Freytet, P. 1973: Petrography and paleo-environments of
    continental carbonate deposits with particular reference
    to the Upper Cretaceous and Lower Eocene of Languedoc
    (S. France). Sed. Geol. 10: 25-60.

Friedman, G. M. 1958: Determination of sieve-size distribution
    from thin-section data for sedimentary petrological
    studies. J. Geol. 66: 394-416.

_____ 1962: Comparison of moment measures for sieving
    and thin section data in sedimentary petrological studies.
    J. Sed. Pet. 32 (1): 15-25.

Friend, P. F. 1965: Fluviatile sedimentary structures in the
    Wood Bay Series (Devonian) of Spitsbergen.
    Sedimentology 5: 39-68.

_____ 1966: Clay fractions and colours of some Devonian
    Red Beds in the Catskill Mountains. Geol. Soc. London
    Quart. J. 122: 273-292.

Friend, P. F. and Moody-Stuart, M. 1970: Carbonate deposition
    on the river floodplain of the Wood Bay Formation
    (Devonian) of Spitsbergen. Geol. Mag. 107: 181-195.

Garrels, R. M. and Christ, C. L. 1965: "Solutions, Minerals
    and Equilibria." Harper & Row Inc. N.Y. 450 p.

Gile, L. H. 1970: Soils of the Rio Grande Valley Border in
    southern New Nexico. Proc. Soil Sci. Soc. Am. 34:
    466-472.

Gile, L. H., Peterson, F. F. and Grossman, R. B. 1966:
    Morphologic and genetic sequences of carbonate
    accumulation in the desert soils. Soil Sci. 101: 347-360.

Gingerich, P. D. 1969: Markov analysis of cyclic alluvial
    sediments. J. Sed. Pet. 39: 330-332.

Glennie, K. W. 1970: Desert Sedimentary Environments from a
    series on "Developments in Sedimentology". 14. Elsevier
    Publishing Corp. Amsterdam, Lond., N.Y. 222 p.

Glennie, K. W. and Evamy. 1968: Dikaka: Plants and plant root structures associated with aeolian sands. Paleogr. Paleoclim. Paleoecol. 4: 77-87.

Goddard, E. N., Trask, P. D., DeFord, R. K., Rove, O. N., Singewald, J. T. and Overbeck, R. M. 1963: Rock-color chart. Geol. Soc. Amer., N.Y.

Goodchild, J. G. 1897: Desert conditions in Britain. Trans. Edinb. geol. Soc. 7: 203-222.

Griffiths, J. C. 1958: Petrography and porosity of the Cow Run sandstone, St Marys, W.Va. J. Sed.Pet. 28: 15-30.

_____ 1960: Modal analysis of sediments. Rev. Geogr. Phys. Geol. Dynamique 3: 29-48.

Grim, R. E. 1951: The deposition environment of red and green shales. J. Sed. Pet. 21: 226-232.

Gunn, B. M. and Warren, G. 1962: Geology of Victoria Land between the Mawson and Mulock Glaciers, Antarctica. N.Z. Geol. Surv. Bull. 71: 157 p.

Harder, H. 1970: Boron content of sediments as a tool in facies analysis. Sed. Geol. 4: 153-175.

Harms, J. C. and Fahnestock, R. K. 1965: Stratification, bed forms, and flow phenomena (with an example from the Rio Grande). in "Primary Sedimentary Structures and their Hydrodynamic Interpretation". Ed. G. V. Middleton. Soc. Econ. Paleont. Min. Special Pub. 12.

Harrington, H. J.1965: Geology and Morphology of Antarctica. in Van Oye, P. and Van Mieghem, J. (Eds) "Biogeography and Ecology of Antarctica 1. Junk, The Hague.1-71.

Hay, R. L. 1966: Zeolites and zeolitic reactions in sedimentary rocks. Geol. Soc. Amer. Spec. Paper No. 85: N.Y. 130 p.

Heath, G. R. 1966: Carbonate nodules formed in soil profiles: The nomenclature problem: Aust. J. Sci. 28: 395-396.

Helby, R. J. and McElroy, C. T. 1969: Microfloras from the Devonian and Triassic of the Beacon Group, Antarctica. N.Z. J. Geol. Geophys. 12 (2,3): 376-382.

Henson, M. R. 1973: Clay minerals from the Lower New Red Sandstone of south Devon. Proc. Geol. Assoc. 84 (4): 429-445.

Irving, E. 1957: The origin of the paleomagnetism of the Torridonian sandstones of north-west Scotland. Roy. Soc. Lond. Philos. Trans., ser. A, 250: 100-110.

Jaeger, J. C. 1957: The temperature in the neighbourhood of a cooling igneous sheet. Amer. J. Sci. 255: 306-318.

_____ 1959: Temperature outside a cooling intrusive sheet. Amer. J. Sci. 257: 44-54.

Jenny, H. 1941: Factors of soil formation. McGraw-Hill, N.Y. 221 p.

Jessup, R. W. 1961: A Tertiary-Quaternary pedological chronology for the south-eastern portion of the Australian arid zone. J. Soil Sci. 12: 199-213.

Jones, G. P. 1965: Red Beds in Northeastern Nigeria. Sedimentology 5: 235-247.

Joulia, F., Bonifas, M., Camez, T., Millot, G. and Weil, R. 1959: De'couverte d'un important niveau d'analcim-olite gresèuse dans le Continental intercalaire de l'ouest de l'Air (Sahara central). Dakar, Service de Géologie et de Prospection Minière, 40 p.

Jungst, H. 1934: Sur Geologischen Bedeutung der Synarese. Geol. Rundschau, 25: 312-325.

Kahle, C. F. 1974: Ooids from Great Salt Lake, Utah, as an analogue for the genesis and diagenesis of ooids in marine limestones. J. Sed. Pet. 44 (1): 30-39.

Keith, M. L., Anderson, G. M. and Eichler, R. 1964: Carbon and oxygen isotopic composition of mollusk shells from marine and fresh-water environments. Geochim. Cosmochim. Acta 28: 1757-1786.

Keith, M. L. and Degens, E. T. 1959: Geochemical indicators of marine and freshwater sediments. in P. H. Abelson (Ed.) Researches in Geochemistry. John Wiley & Sons Inc. N.Y. 38-61.

Keith, M. L. and Weber, J. N. 1964: Carbon and oxygen isotopic composition of selected limestones and fossils. Geochim. Cosmochim. Acta 28: 1787-1816.

Keller, W. D. 1929: Experimental work on red bed bleaching. Amer. J. Sci. 18 Fourth Series: 65-70.

_____ 1952: Analcime in the Popo Agie member of the Chugwater Fm. J. Sed. Pet. 22: 70-82.

_____ 1953: Illite and montmorillonite in green sedimentary rocks. J. Sed. Pet. 23: 3-9.

Kemeny, J. G. and Snell, J. L. 1960: Finite Markov chains. Van Nostrand, Princeton, N.J. 210 p.

Kindle, E. M. 1919: A neglected factor in the rounding of sand grains. Amer. J. Sci. 47: 431-434.

_____ 1924: Report by Committee on Sedimentation, Nat. Res. Council, 42 p.

Kleeman, A. W. 1967: Sampling error in the chemical analysis of rocks. J. Geol. Soc. Aust. 14 (1): 43-47.

Knowlton, F. H. 1919: Evolution of geological climates. Bull. Geol. Soc. Amer. 30: 499-565.

Krauskopf, K. B. 1956: Dissolution and precipitation of silica at low temperatures. Geochim. Cosmochim. Acta 10: 1-26.

_____ 1967: Introduction to Geochemistry. McGraw-Hill Inc. 721 p.

Krumbein, W. C. and Dacey, M. F. 1969: Markov chains and embedded chains in geology. J. int. Ass. Mathl. Geol. 1: 79-96.

Krumbein, W. C. and Garrels, R. M. 1952: Origin and classification of chemical sediments in terms of pH and oxidation-reduction potentials. J. Geol. 60: 1-33.

Krumbein, W. C. and Sloss, L. L. 1963: Stratigraphy and Sedimentation. W. H. Freeman & Co., San Francisco. 660 p.

Krumm, H. 1962: Mineralbestand und genese Fränkischer Keuper und Lias Tone. Geol. Rundschau. 51: 478.

Krynine, P. D. 1935: Formation and preservation of desiccation features in a humid climate. Amer. J. Sci. 30 Fifth Series, 96-97.

_____ 1949: The origin of Red Beds. N.Y. Acad. Sci. Trans. ser. II. 2 (11): 60-68.

Krynine, P. D. 1950: Petrology, stratigraphy, and origin of the Triassic sedimentary rocks of Connecticut. Conn. Geol. Nat. History Survey Bull. 73: 239 p.

Kubiena, W. L. 1963: Paleosoils as indicators of paleoclimates. in Changes of Climates, 202-207. UNESCO, Symp. XX. Rome. 488 p.

Kuenen, P. H. and Perdok, W. G. 1962: Experimental abrasion, 5. Frosting and defrosting of quartz grains. J. Geol. 70: 648-658.

Kyle, R. A. 1975: Paleobotanical studies of the Permian and Triassic Victoria Group, south Victoria Land, Antarctica. Unpublished Ph.D. thesis, Victoria University of Wellington.

Lajoie, J. and Chagnon, A. 1973: Origin of red beds in a Cambrian flysch sequence, Canadian Appalachians, Quebec. Sedimentology 20: 91-103.

Langmuir, D. 1970: The effect of particle size on the reaction: hematite + water → goethite. Geol. Soc. Amer. Abs of Ann. Meetings, 601-602.

_____ 1971: Particle size effect on the reaction: goethite = hematite + water. Amer. J. Sci. 271: 147-156.

Lattman, L. H. 1960: Cross-section of a floodplain in a moist region of moderate relief. J. Sed. Pet. 30: 275-282.

Leeder, M. R. 1973a: Fluviatile fining-upwards cycles and the magnitude of palaeochannels. Geol. Mag. 110 (3): 265-276.

_____ 1973b: Sedimentology and palaeography of the Upper Old Red Sandstone in the Scottish Border Basin. Scott. J. Geol. 9 (2): 117-144.

Leopold, L. B. and Wolman, M. G. 1960: River meanders. Bull. Geol. Soc. Amer. 71: 769-794.

Lepsersonne, J. 1960: Ann. soc. geol. Belg. Bull. 84: 21 [CA-55, 20814-d].

Levina, S. D. 1959: Sedimentary feldspathic rocks of the lower Permian red beds in the North Caucasus lower Permian deposits. Akad. Nauk SSSR, Izvestiya, Geol. series no. 11, 31-43; 1961, 27-38.

Lomas, Joseph, 1907: Desert conditions and the origin of the British Trias. Geol. Mag. 44: 511-514, 554-563.

_____ 1909: Desert formations, with reference to the origin of the Trias. Trans. Leicester lit. phil. Soc. 13: 105-110.

Lorens, P. J. and Thronson, R. C. 1955: Geology of the fine-grained alluvial deposits in Sacramento Valley and their relationship to seepage. in H. O. Banks (Ed.) "Seepage Conditions in Sacramento Valley"- Rept. Water Proj. Authority Calif. A1-A26.

Lumsden, D. N. 1971: Markov chain analysis of carbonate rocks: Applications, limitations and implications as exemplified by the Pennsylvanian system in S. Nevada. Geol. Soc. Amer. Bull. 82: 447-62.

MacKenzie, R. C. 1957: The oxides of iron, aluminium and manganese. Pp. 299-328 in "The Differential Thermal Investigation of Clays". Miner. Soc. London.

Marbut, C. F. 1951: Soils: Their Genesis and Classification. Soil Science Soc. of Amer. Madison. 134 p.

Mason, B. 1966: Principles of Geochemistry. John Wiley & Sons Inc. N.Y. 329 p.

Matz, D. B. and Hayes, M. O. 1966: Sedimentary petrology of Beacon sediments. Antarct. J. U.S. 1 (4): 134-135.

Matz, D. B., Pinet, P. R. and Hayes, M. O. 1972: Stratigraphy and petrology of the Beacon Supergroup, south Victoria Land. Pp. 353-358 in R. J. Adie (Ed.) Antarctic Geology and Geophysics, Symposium on Antarctic Geology and Solid Earth Geophysics, Oslo 1970. I.U.G.S., Universitetforlaget.

McBride, E. F. 1974: Significance of color in red, green, purple, olive, brown, and gray beds of Difunta Group, Northeastern Mexico. J. Sed. Pet. 44: 760-773.

McCrea, J. M. 1950: On the isotopic chemistry of carbonates and a paleotemperature scale. J. Chem. Phys. 18: 849-857.

McElroy, C. T. 1969: Comparative lithostratigraphy of Gondwana sequences, eastern Australia and Antarctica. I Simposio Internacional Sobre Estratigrafia y Paleontologia del Gondwana, Oct. 1967, Mar del Plata, Argentina.

McKelvey, B. C. and Webb, P. N. 1959: Geological
investigation in south Victoria Land, Antarctica.
Part II. Geology of Upper Taylor Glacier Region.
N.Z. J. Geol. Geophys. 2 (4): 718-728.
_____ 1961: Geological reconnaissance in Victoria
Land, Antarctica. Nature (Lond.) 189 (4764): 545-547.

McKelvey, B. C., Webb, P. N.,Gorton, M. P. and Kohn, B. P.
1970a: Stratigraphy of the Beacon Supergroup between
the Olympus and Boomerang Ranges, Victoria Land,
Antarctica. Nature, 227: 1126-1127.
_____ 1970b: Recent discoveries of Devonian fish in
Antarctica. Polar Records, 15 (95): 216-217.
_____ 1972: Stratigraphy of the Beacon Supergroup
between the Olympus and Boomerang Ranges, Victoria
Land. Antarctic Geology and Geophysics. (Ed.) R. J. Adie.
Universitetsforlaget, Oslo.

McPherson, J. G. 1973: Stratigraphy and petrology of the Aztec
Siltstone, south Victoria Land, Antarctica. Aust. & N.Z.
Assoc. for the Adv. of Sci. 45th Congr. Perth. Abs.

Meade, Jr R. H. 1960: Compaction and development of preferred
orientation in clayey sediments. Ph.D. thesis, Stanford
Univ. Stanford, Calif. 73 p.

Mehra, O. P. and Jackson, M. L. 1960: Iron oxide removal
from soils by a dithionite-citrate system buffered with
sodium bicarbonate. Proc. Seventh Natl. Conf. on Clays
and Clay Minerals, 1958: London, Pergamon Press, 317-327.

Melton, M. A. 1965: The geomorphic and paleoclimatic
significance of alluvial deposits in southern Arizona.
J. Geol. 73: 1-37.

Miall, A. D. 1973: Markov chain analysis applied to an ancient
alluvial plain succession. Sedimentology 20: 347-364.

Miller, W. J. 1910: Origin of the colour in the Vernon shales.
Bull. 140, N.Y. State Museum of Natural History (6th
Rept of Director for 1909), 150-156.

Miller, D. N. and Folk, R. L. 1955: Occurrence of detrital
magnetite and ilmenite in red sediments. Bull. Amer.
Assoc. Petrol. Geologists 39: 338-345.

Millot, G. 1970: Geology of clays. Trans. by Farrand,
    W. R. and Paquet, H. Springer-Verlag, N.Y. 429 p.

Mirsky, A., Treves, S. B. and Calkin, P. E. 1965:
    Stratigraphy and petrography, Mount Gran area, southern
    Victoria Land, Antarctica. Am. Geophys. Un., Antarctic
    Res. Ser. 6: 145-175.

Moody-Stuart, M. 1966: High and low sinuosity stream
    deposits, with examples from the Devonian of Spitsbergen.
    J. Sed. Pet. 36: 1102-1117.

Moore, C. A. 1968: Quantitative analysis of naturally occurring
    multi-component mineral systems by X-ray diffraction.
    Clays and Clay Minerals, 16: 325-336.

Moore, R. C., Lalicker, C. G. and Fisher, A. G. 1952:
    Invertebrate Fossils. McGraw-Hill Book Co. Inc. N.Y.
    766 p.

Morozova, T.D. 1964: The micromorphological method in
    paleopedology and paleogeography. Pp. 325-331 in
    A. Jongerius (Ed.) "Soil Micromorphology". Proc. 2nd
    Internat. Working Meeting on Soil Micromorphology.
    Arnhem, The Netherlands. 540 p.

Neal, J. T., Langer, A. M. and Kerr, P. F. 1968: Giant
    desiccation polygons of Great Basin playas. Geol. Soc.
    Amer. Bull., 79: 69-90.

Nordmeyer, H. 1959: Mineralogische Untersuchungen an drei
    Bodenprofilen: auf Zechsteinletten, unterem Buntsandstein,
    und Zechsteindolmit. Beitr. Min. Pet. 7: 1.

Norrish, K. and Chappell, B. W. 1967: X-ray fluorescence
    spectrography. in Zussman, J. (Ed.) "Physical Methods
    in Determinative Mineralogy". London. Academic Press.

Norrish, K. and Hutton, J. T. 1969: An accurate X-ray
    spectrographic method for the analysis of a wide range
    of geological samples. Geochim. Cosmochim. Acta 33 (4):
    431-453.

Oertel, A. C. 1974: The development of a typical red-brown
    earth. Aust. J. Soil Res. 12: 97-105.

Perry, E. C. and Tan, F. C. 1972: Significance of oxygen and carbon isotope variations in early Precambrian cherts and carbonate rocks of Southern Africa. Geol. Soc. Amer. Bull. 83: 647-664.

Pettijohn, F. J. 1957: Sedimentary Rocks. 2nd Ed. Harper & Row Publishers Incorp.

_____ 1963: Chemical composition of sandstones - excluding carbonate and volcanic sands. U.S. Geol. Surv. Prof. Paper 440-S: 19 p.

Pettijohn, F. J. and Lundahl, A. C. 1943: Shape and roundness of Lake Erie beach sands. J. Sed. Pet. 13: 69-78.

Picard, M. D. 1965: Iron oxides and fine-grained rocks of Red Peak and Crow Mt sandstone members, Chugwater (Triassic) Formation, Wyoming. J. Sed. Pet. 35 (2): 464-479.

_____ 1966: Oriented, linear-shrinkage cracks in Green River Formation (Eocene), Raven Ridge Area, Uinta Basin, Utah. J. Sed. Pet. 36: 1050-1057.

_____ 1971: Classification of fine-grained sedimentary rocks. J. Sed. Pet. 41 (1).

Plumstead, E. P. 1962: Fossil floras of Antarctica. Trans-Antarctic Exped. 1955-1958. Sci. Rep. 9. Geology. 154 p. (Published by the Trans-Antarctic Expedition Committee, London).

Rankama, K. 1963: Progress in isotope geology. Interscience Publishers, John Wiley & Sons, N.Y. and Lond. 705 p.

Raymond, P. E. 1927: The significance of red colour in sediments. Amer. J. Sci. 13: 234-251.

Reeves, C. C. Jr. 1970: Origin, classification and geologic history of caliche on the southern High Plains, Texas and eastern New Mexico. J. Geol. 78: 352-362.

Ritchie, A. 1969: Evidence from fossil fish distribution with special reference to recent discoveries in Australia and Antarctica. Abstr. 41st Congr. Aust. N.Z. Ass. Adv. Sci. Adelaide, Sect. 3, Geology.

_____ 1971: Fossil fish discoveries in Antarctica. Aust. Nat. Hist. 17: 65-71.

Ritchie, A. 1974: From Greenland's icy mountains.
    Aust. Nat. Hist. 18: 28-35.
_____ 1975: Groenlandaspis in Antarctica, Australia
    and Europe. Nature, 254: 569-573.
Robb, G. L. 1949: Red bed coloration. J. Sed. Pet. 19: 99-103.
Roubault, M., Roche, H. de la, and Govindaraju, K. 1968:
    Report (1966-1968) on geochemical standards: Granites
    GR, GA, GH; Basalt BR; Ferriferous Biotite Mica - Fe,
    Phlogopite Mica - Mg. Sciences de la Terre 13: 379-404.
Runcorn, S. K. 1959: Rock magnetism. Science 129: 1002-1012.
Russell, I. C. 1889: Subaerial decay of rocks and origin of
    the red colour of certain formations. U.S. Geol. Surv.
    Bull. 52: 25.
Russell, R. D. and Taylor, R. E. 1937: Roundness and shape
    of Mississippi River sands. J. Geol. 45: 225-267.
Salger, M. 1959: Der Mineralbestand von Tonen des
    fränkischen Keuper und Jura. Geol. Bavarica 39: 69.
Scheffer, F., Welte, E. and Ludwieg, F. 1957: Zur Frage
    der Eisenoxydhydrate im Boden. Chem. d. Erde 19: 51-64.
Schluger, P. R. 1971: Origin and environment of deposition
    of the red beds of the Perry Formation, Upper Devonian,
    of New Brunswick, Canada and Maine. Int. Sed. Congr.
    8th. Abstracts.
Schmidt, D. L. and Friedman, I. 1975: Continental deposition
    of Antarctic tillite indicated by carbon and oxygen
    isotopes. U.S.G.S. open report.
Schmitz, H. H. 1959: Über die mineralogische Zusammungsetzung
    des unteren Gipskeupers, nach einem Bohrprofil.
    Geol. Jahrb., 77: 59.
Schoen, R. 1964: Clay minerals of the Clinton Ironstone,
    New York State. J. Sed. Pet. 34: 855-863.
Schumm, S. A. 1960: The effects of sediment type on the
    shape and stratification of some modern fluvial deposits.
    Am. J. Sci. 258: 177-184.
_____ 1963: Sinuosity of alluvial rivers on the Great
    Plains. Geol. Soc. Amer. Bull. 74 (9): 1089-1100.

Schumm, S. A. 1968: Speculations concerning palaeohydrologic
    controls of terrestrial sedimentation. Geol. Soc. Amer.
    Bull. 79: 1573-1588.

_____ 1972: Fluvial paleochannels. Pp. 98-107 in
    Rigby, J. K. and Hamblin, W. K. (Eds.) "Recognition
    of Ancient Sedimentary Environments". Soc. Econ.
    Paleontologists and Mineralogists, Spec. Publ. No.16.

Seilacher, A. 1964: Biogenic sedimentary structures.
    Pp. 296-316. in Imbrie, J. and Newell, N. D. (Eds).
    Approaches to Paleoecology. Wiley, N.Y.

_____ 1967: Bathymetry of trace fossils. Marine Geol. 5:
    413-428.

Seki, Y. 1972: Lower grade stability limit of epidote in the
    light of natural occurrences. J. Geol. Soc. Japan 78:
    405-413.

Selley, R. C. 1970: Studies of sequence in sediments using
    a simple mathematical device. Quart. J. Geol. Soc. Lond.
    125: 557-581.

Shapiro, L. and Brannock, W. W. 1962: Rapid analysis of
    silicate, carbonate and phosphate rocks. Contr. to
    Geochem., U.S. Geol. Surv. Bull. 1144-A.

Sherbon-Hills, E. 1963: Elements of structural geology.
    Richard Clay (The Chaucer Press) Ltd, Bungay, Suffolk.
    483 p.

Slavin, W. 1968: Atomic Absorption Spectroscopy. Interscience
    N.Y. 307 p.

Smith, F. G. and Kidd, D. J. 1949: Hematite-goethite
    relations in neutral and alkaline solutions under
    pressure. Amer. Min., 34: 403-412.

Smith, N. D. 1970: The braided stream depositional environment:
    comparison of the Platte River with some Silurian clastic
    rocks north-central Appalachians. Geol. Soc. Amer. Bull.
    81: 2993-3014.

_____ 1971: Transverse bars and braiding in the Lower
    Platte River, Nebraska. Geol. Soc. Amer. Bull. 82:
    3407-3420.

Smith, N. D. 1972: Flume experiments on the durability of mud clasts. J. Sed. Pet. 42 (2): 378-383.

Smith, N. D. and Hein, F. J. 1971: Reworking and grain size inversions caused by Staphyinid Beetle (fluvial sediments). J. Sed. Pet. 41 (2): 598-602.

Smyth, C. H. 1913: The relative solubilities of the chemical constituents of rocks. J. Geol. 21: 105-120.

Stace, H.C.T., Hubble, G. D., Brewer, R. Northcote, K. H., Sleeman, J. R., Mulcahy, M. J. and Hallsworth, E. G. 1968: A Handbook of Australian Soils. Rellim Technical Publications, South Australia. 435 p.

Steel, R. J. 1974a: New Red Sandstone floodplain and piedmont sedimentation in the Hebridean Province, Scotland. J. Sed. Pet. 44: 336-357.

_____ 1974b: Cornstone (Fossil Caliche) its origin, stratigraphic and sedimentological importance in the New Red Standstone, W. Scotland. J. Geol. 82: 351-369.

Strakhov, N. M. 1957: Méthodes d'étude des roches sédimentaires. T II, Moscou. Trans. by Bureau Recherches Geol. Geophys. et Minières, Paris, 1959. 535p.

Sundborg, Å. 1956: The River Klarälven: a study of fluvial processes. Geograf. Ann. 38: 127-316.

Swineford, Ada. 1955: Petrology of upper Permian rocks in south-central Kansas. Bull. Kans. Geol. Surv. 111.

Tan, F. C. and Hudson, J. D. 1971: Carbon and oxygen isotopic relationships of dolomites and co-existing calcites, Great Estuarine Series (Jurassic), Scotland. Geochim. Cosmochim. Acta 35: 755-767.

Tanner, W. F. 1967: Ripple mark indices and their uses. Sedimentology 9: 89-104.

_____ 1971: Numerical estimates of ancient waves, water depth and fetch. Sedimentology, 16: 71-88.

Taylor, N. H. and Pohlen, I. J. 1962: Soil survey method. N.Z. Soil Bur. Bull. 25: D.S.I.R. Wellington.

Taylor, R. M. and Graley, A. M. 1967: The influence of ionic environment on the nature of iron oxides in soils. J. Soil Sci., 18: 341-348.

Taylor, R. M. and Schwertmann, U. 1974: The association of phosphorous with iron in ferruginous soil concretions. Aust. J. Soil Res., 12: 133-145.

Thomas, H. H. 1909: A contribution to the petrography of the New Red Sandstone in the west of England. Quart. J. Geol. Soc. Lond. 65: 229-244.

Thompson, A. B. 1971: Analcite-albite equilibria at low temperatures. Amer. J. Sci. 271: 79-92.

Thompson, A. M. 1970: Geochemistry of colour genesis in red-bed sequence, Juniata and Bald Eagle Formations, Pennsylvania. J. Sed. Pet. 40 (2): 599-615.

Tiller, K. G. 1958: The geochemistry of basaltic materials and associated soils of south-eastern South Australia. J. Soil Sci. 9: 225-241.

Tomlinson, C. W. 1916: The origin of the red beds. J. Geol. 24: 153-179, 238-253.

Twenhofel, W. H. 1932: Treatise on Sedimentation. Dover Publications Inc., N.Y. 1961 (reprinted from 1932 ed. by Williams & Wilkins Comp.). 926 p.

Usiglio, J. 1849: Analyse de l'eau de la Mediterranee sur la cote de France. Ann. chim. et Phys., ser. 3, 27: 92, 172. (see Clarke, 1924, 219-220).

Valastro, S., Davis, E. M. and Rightmire, C. T. 1968: University of Texas at Austin radiocarbon dates VI. Radiocarbon 10: 384-401.

Vanderstappen, R., and Verbeek. 1959: Présence d'analcime d'origine sédimentaire dans le Mésozoique du Bassin du Congo. Soc. Belge Géologie, Paleontologie et Hydrologie Bull., 68 (3): 417-421.

Van Houten, F. B. 1948: Origin of red-banded Early Cenozoic deposits in Rocky Mountain Region. Bull. Amer. Assoc. Petrol. Geol. 32: 2083-2126.

_____ 1961a: Ferric oxides in red beds as paleomagnetic data. J. Sed. Pet. 31: 296-300.

_____ 1961b: Climatic significance of red beds. Pp 89-139. In A.E.M. Nairn (Ed.) "Descriptive Palaeoclimatology" Interscience, N.Y. 380 p.

Van Houten, F. B. 1962: Cyclic sedimentation and the origin of analcime-rich upper Triassic Lockatong Fm, west-central N.J. and adjacent Pennsylvania. Amer. J. Sci. 260: 561-576.

_____ 1964a: Cyclic lacustrine sedimentation, Upper Triassic Lockatong Formation, central New Jersey and adjacent areas. Kansas Geol. Surv. Bull. 169: 497-531.

_____ 1964b: Origin of red-beds - some unsolved problems. Pp.647-659. In Nairn, A.E.M. (Ed.), "Problems in Palaeoclimatology", Wiley, N.Y. and London.

_____ 1965: Composition of Triassic Lockatong and associated formations of Newark Group, central New Jersey and adjacent Pennsylvania. Amer. J. Sci. 263: 825-863.

_____ 1968: Iron oxides in red beds. Geol. Soc. Amer. Bull. 79: 399-416.

_____ 1972: Iron and clay in tropical savanna alluvium, Northern Colombia: A contribution to the origin of red beds. Geol. Soc. Amer. Bull. 83: 2761-2772.

_____ 1973: Origin of red beds: A review - 1961-1972. Donath, Stehli and Wetherill (Eds.) Annual Review of Earth and Planetary Science, Vol. 1. Annual Reviews Inc. Palo Alto, California. 350 p.

Van Straaten, L.M.J.U. 1954: Composition and structure of Recent marine sediments in the Netherlands. Leidse Geol. Meded. 19: 1-110.

Vialov, O. S. 1962: Problematica of the Beacon Sandstone at Beacon Height West, Antarctica. N.Z. J. Geol. Geophys. 5: (5),718-732.

Vinogradov, A. P. 1959: The geochemistry of rare and dispersed chemical elements in soils. 2nd Ed. Translated from Russian. Consultants Bureau, Inc. N.Y. 209 p.

Visher, G. S. 1965a: Fluvial processes as interpreted from ancient and recent fluvial deposits. in Middleton, G. V. (Ed.) Primary Sedimentary Structures and their Hydrodynamic Interpretation, S.E.P.M. Spec. Publ. 12, 116-132.

_____ 1965b: Use of vertical profile in environmental reconstruction. Bull. Am. Ass. Petrol. Geol. 49: 41-61.

Walker, R. G. 1971: Non-deltaic depositional environments in the Catskill clastic wedge (Upper Devonian) of central Pennsylvania. Geol. Soc. Amer. Bull. 82: 1305-1326.

Walker, T. R. 1967a: Formation of red beds in modern and ancient deserts. Geol. Soc. Amer. Bull. 78: 353-368.

_____ 1967b: Colour of recent sediments in tropical Mexico: A contribution to the origin of red beds. Geol. Soc. Amer. Bull. 78: 917-920.

_____ 1973: Intrastratal alterations in the Fountain Formation (Pennsylvanian age), Denver area, Colorado. Geol. Soc. Amer., Abs. with Programs (Southeastern Sec). 5 (6): 521-522.

_____ 1974a: Red beds in the western interior. In U.S. Geol. Surv. paleotectonic folio of the Pennsylvania System, Washington, D.C.

_____ 1974b: Formation of red beds in moist tropical climates: A hypothesis. Geol. Soc. Amer. Bull. 85: 633-638.

Walker, T. R. and Honea, R. M. 1969: Iron content of modern deposits in the Sonoran Desert: A contribution to the origin of red beds. Geol. Soc. Amer. Bull. 80: 535-544.

Walther, Johannes, 1908: Geschichte der Erde und des Lebens. Leipzig: Veit & Co.

_____ 1909: 'Uber algonkische sedimente'. Z. dtsch. geol. Ges., 61: 283-305.

Weaver, C. E. 1958: Origin and significance of clay minerals in sedimentary rocks. Bull. Amer. Ass. Petrol. Geol. 42: 254-271.

_____ 1959: The clay petrology of sediments. Pp. 154-187. In Clays and Clay Minerals, Proc. 6th Nat. Conf. on Clays and Clay Minerals. Pergamon Press, N.Y. 411 p.

Webb, P. N. 1963: Geological investigations in southern Victoria Land, Antarctica. Part 4 - Beacon Group of the Wright Valley and Taylor Glacier region. N.Z. J. Geol. Geophys. 6 (3): 361-387.

_____ 1969: Immediate report of Victoria University of Wellington Antarctic Expedition 1968-69. Victoria Univ. of Wellington, N.Z. 33 p.

Webby, B. D. 1968: Devonian trace fossils from the Beacon
     Group of Antarctica. N.Z. J. Geol. Geophys. 11 (4):1001-1008.

White, E. I. 1968: Geology 5. Devonian fishes of the
     Mawson-Mulock area, Victoria Land, Antarctica.
     Trans-Antarctic Expedition 1955-58 Scientific
     Reports, No.16, 26 p.

White, E. M. 1972: Soil desiccation features in South Dakota
     depressions. J. Geol. 80: 106-111.

Williams, G. E. and Polach, H. A. 1971: Radiocarbon dating
     of arid-zone calcareous Paleosols. Geol. Soc. Amer. Bull.
     82: 3069-3086.

Williams, P. F. and Rust, B. R. 1969: The sedimentology of
     a braided river. J. Sed. Pet. 39: 649-679.

Williams, H., Turner, F. J. and Gilbert, C. M. 1954:
     Petrography. W. H. Freeman & Co., San Francisco, 406 p.

Wilson, M. J. 1971: Clay mineralogy of the Old Red Sandstone
     (Devonian) of Scotland. J. Sed. Pet. 41 (4): 995-1007.

Woodrow, D. L. 1968: Stratigraphy, structure and sedimentary
     patterns in the Upper Devonian of Bradford County,
     Pennsylvania. Penn. Geol. Surv. Gen. Geol. Rept. G54,
     78 p.

Woods, Henry 1926: Palaeontology (invertebrate). Cambridge.
     At the University Press, London. 424 p.

Woodward, A. S. 1921: Fish-remains from the Upper Old Red
     Sandstone of Granite Harbour, Antarctica. British
     Antarctic ("Terra Nova") Expedition, 1910, Nat. Hist.
     Rep. Geol. 1 (2): 51-62.

Wu, Dah Cheng, 1971: Origin of greenish-gray spots and layers
     in the Upper Flowerpot Shale (Perm.), N.W. Oklahoma.
     Oklahoma Geol. Notes, 31 (1): 3-10.

Young, G. C. 1974: Stratigraphic occurrence of Placodermi
     fishes in the Middle and Late Devonian. Newsletters on
     Stratigraphy 3 (4): 243-261.